Reaction-Diffusion Patterns on Growing Domains

Edmund John Crampin

Magdalen College
University of Oxford

A thesis submitted in partial fulfilment of the requirements for the degree of Doctor of Philosophy at the University of Oxford

Hilary Term 2000

Abstract

Edmund John Crampin
Magdalen College
Oxford

Thesis submitted for
the degree of D.Phil.
Hilary Term 2000

Reaction-Diffusion Patterns on Growing Domains

The reaction-diffusion (Turing) mechanism is one of the simplest and most elegant theories for biological pattern formation. The recent experimental realisation of Turing patterns in chemical systems has fostered renewed interest in reaction-diffusion theory, however, its relevance to many biological problems has been questioned because of the perceived failure of the mechanism to generate patterns reliably. A recent paper suggesting the involvement of reaction-diffusion in fish skin patterns has implicated domain growth as an important mechanism controlling pattern selection. In this thesis we present a systematic study of the effects of domain growth on reaction-diffusion patterns, and discuss the implications for reliable pattern generation.

Starting from the postulate that tissue growth rates are locally determined, we derive general evolution equations for reaction-diffusion on growing domains as a problem in kinematics. We argue that the biologically plausible scenario is to consider domain growth on a longer timescale than pattern formation. Then it is found that the solution goes through a sequence of recognisable (quasi-steady) patterns. Using symmetry arguments relating different pattern modes we show that for uniform domain growth the solution evolves by frequency-doubling, the regular splitting or insertion of peaks in the pattern. For pattern formation in two spatial dimensions domain growth is found to select rectangular lattices, rather than the hexagonal planform that is preferred on the fixed domain. For nonuniform growth the local tissue expansion rate varies across the domain and splitting or insertion may be restricted to regions of the domain where the growth is sufficiently fast.

The behaviour of solutions can be studied asymptotically and peak splitting and insertion are shown to occur according to the form of the reaction nullclines. We highlight a novel behaviour, frequency-tripling, where both mechanisms operate simultaneously, which is realised when quadratic terms are absent from the reaction kinetics. Any particular pattern in a sequence remains established until the domain is sufficiently large that a transition to a higher pattern mode occurs. This presents a degree of scale invariance. The pattern which persists finally is not strongly dependent on the final domain size, and hence domain growth can provide a mechanism for reliable pattern selection.

Acknowledgements

I express my sincere thanks to Professor Philip Maini for supervising the research leading to this thesis. The work presented here has been carried out at the Centre for Mathematical Biology in the Mathematical Institute, University of Oxford. I thank the current and former members of the Centre and the many visitors for providing a friendly and stimulating research environment.

More specifically, I thank Dr Eamonn Gaffney (Department of Mathematics and Statistics, University of Birmingham) for his interest in my research, and with whom many of the ideas in Chapters 4 and 5 were discussed and developed. I am grateful to Dr Bill Hackborn (Department of Mathematics and Computer Science, Augustana University College) for his interest and, during a visit to Oxford, collaboration on the numerical solution of the nonuniform and reactant-controlled domain growth problems (Chapter 6).

I am also grateful to Professor Hans Othmer (School of Mathematics, University of Minnesota) for the invitation to attend the IMA Workshop on Mathematics in Biology (Minnesota, 1998), and to the IMA for financial support. Finally, I express my deep gratitude to Professor Denis Noble (University Laboratory of Physiology, University of Oxford) and to Physiome Sciences, Inc. (Princeton, USA) for financial support during the final stages of the writing of this thesis.

This research was funded by a Research Committee Special Studentship from the BBSRC.

Contents

1. Introduction

Structural and functional ideas in developmental biology have been somewhat eclipsed by the recent advent of developmental genetics. The role of genetic information in determining the development of organised and differentiated structures from a single cell is commonly deduced by studying the effects of gene mutations, determining that a certain gene is *necessary* for the correct development of a particular structure. The revolution in molecular genetics has led to unprecedented discoveries and advances, however, there is a danger that something has been lost in the thrust of this research. While nobody would dispute that genes and gene products act in concert, our understanding of the mechanisms by which differentiated structures emerge from the interaction of genes and their products is at risk of being overlooked in the drive to identify (and label) the genetic components involved in the process. The implicit assumption that all growth and form of an organism can be explained in terms of gene instructions, that organisms are 'genetically programmed', is opposed by the alternative view that spatial organisation, illustrated by the adaptive and regulatory properties of developing organisms, must be explained otherwise.

The study of physical aspects of growth and form has a long and distinguished history. D'Arcy Thompson's celebrated book [125] draws parallels between biological forms and structures arising in physical systems. That physical laws constrain what is possible (in terms of morphology or pattern) is indisputable. However, to understand how morphology is determined and regulated it is necessary to postulate physical mechanisms that may plausibly coordinate the spatio-temporal emergence of structure.

This thesis is concerned with one such class of mechanism, based on simple physical principles, which can generate spatial pattern from initial homogeneity. In the context of morphogenesis, Alan Turing [126] proposed that a set of chemicals which react and diffuse within a substrate could lead to the spontaneous symmetry breaking of an initially homogeneous distribution of the chemical concentrations, and the generation of spatial patterns. Before discussing this model in more detail, we consider pattern formation in biological systems, and various alternative modelling approaches.

1.1 Models for Biological Pattern Formation

Any instance of a heterogeneous distribution of gene product or differentiated tissue constitutes a pattern, and any such scenario may be interrogated as to the mechanisms of organisation and regulation of the pattern. A multitude of different morphologies in many different areas of biology have been the subject of mathematical modelling. Several biological systems have attained status of paradigm in theoretical work in this field, including the segmentation of the insect embryo [58, 118], limb development [79, 26], the formation of animal coat markings [88] and the arrangement of hair follicles and feather primordia in skin [90, 89]. Certain unicellular organisms have also

been studied experimentally and theoretically in the context of pattern formation, for example the generation of whorls in the marine alga *Acetabularia* [44] and the branched and star-shaped morphologies of *Micrasterias* [66, 48, 50]. For these species (where each organism has only one nucleus) it is most apparent that structure must develop through spatially distributed physical processes occurring within the cell. At the other end of the scale, patterns in population density (often called 'patchiness') are studied in ecological settings [121, 83, 96, 80].

These examples raise an important theoretical consideration. For the patterning of animal skins, a greater or lesser degree of variation is often displayed between members of the same species and even between closely (genetically) related animals. However, the mechanisms regulating segmentation and limb development, for example, must be able to reliably generate the same number of pattern elements despite normal biological variation, for example in the size or geometry of the region in which the pattern develops. Models whose purpose it is to describe the mechanisms of spatial organisation must be able to account for whichever of these alternative features is observed in the biological system under scrutiny. We return to this crucial issue in the discussion of reaction-diffusion models below.

Two general categories for models of pattern formation may be described, which encompass most theoretical research to date, namely chemical prepattern and cell motility (or mechano-chemical) models. The latter consider the aggregation of cell populations subject to chemical signals and mechanical forces, where it is supposed that cell differentiation occurs in response to increased cell density (see the book by Murray [88] and references therein). In this thesis we are primarily concerned with models of the chemical prepattern type. Here it is argued that a pattern is first established in the concentration of certain chemicals (termed *morphogens*), and subsequent differentiation into different tissue types occurs according to whether or not the concentration exceeds some threshold locally. Thus it is implicitly assumed that the chemical pattern is established on a faster timescale than the response of the cellular machinery, so that the formation and interpretation of the pattern decouple.

The idea of threshold-mediated response to morphogen concentration gradients is developed in Wolpert's notion of positional information [134, 135]. Much of this work considers cellular response to (possibly multiple) simple gradients. Crick [20] established that gradients could form on realistic timescales over distances of a millimetre or less under the mechanism of passive or facilitated diffusion of morphogen from a localised source.

Theoretical approaches may also be divided into discrete (cellular) and continuum descriptions. Turing's original discussion of the reaction-diffusion mechanism considers both possibilities, however, the analysis is restricted to the case of diffusive coupling between cells (or through the tissue), which is by no means the only mechanism of cellular communication demonstrated in biology. Much is known at the molecular level about intercellular signalling. Cells can demonstrate active regulation of signals

and passage of substances, which are ignored in diffusion-based models. In some instances signalling molecules are held in the cell membrane and bind to receptors on adjacent cells only, a process known as juxtacrine signalling. Lateral inhibition, for which ligand binding down-regulates ligand and receptor expression, generates fine-grained patterns where the wavelength is two cell diameters (high and low expression levels of the ligand are found on alternate cells). This mechanism is observed in the *Delta-Notch* signalling pathway [17], and typically selects a subset of cells from an initially equivalent field which adopt a different cell fate. A recent model due to Owen *et al.* [104, 105] considers lateral induction, where signalling results in up-regulation of ligand and receptor expression (positive feedback), and has demonstrated that longer wavelength patterns may be generated in a mechanism with only nearest-neighbour cell communication. In two dimensions spot and stripe patterns may be generated by this model.

Before going on to discuss the reaction-diffusion mechanism in more detail, we briefly discuss the justification for such modelling, as well as some of the pitfalls. In this context it is useful to distinguish between *modelling* and *simulation* of a natural phenomenon. It would be a tall order (if not impossible) to describe all of the detailed processes involved in any single biological pattern forming event. However, such an all-encompassing mathematical description (or some approximation to it) would constitute a simulation of the system. This is not the intention of the sorts of models we have described above; rather the aim is to discover whether some smaller set of processes may in themselves be sufficient to account for the phenomenon. The model is built to encapsulate only those mechanisms of interest, and is analysed to determine qualitatively whether the phenomenon may be attributed to the interaction of these mechanisms. In this sense we are constructing and testing *theories* of pattern formation. Furthermore, a simple model, such as a reaction-diffusion system, may be considered to represent a caricature of some more complicated (and unidentified) system, which captures the dynamics of the higher dimensional system. In this sense different classes of model may be studied as paradigms for pattern formation, representing some level of mathematical abstraction from the physical reality. Clearly this is only satisfactory from the biological point of view if connections can be made from the mathematical analysis to physically measurable quantities. Of course a successful comparison between model behaviour and the natural phenomenon does not guarantee that the model constitutes the correct explanation. It may be the case that several models with different underlying assumptions generate similar behaviour. This is found to be the case for reaction-diffusion models and certain mechano-chemical models for pattern formation, where the underlying mathematical structure of the pattern forming bifurcation are similar, both mechanisms generating an intrinsic pattern wavelength. Hence it may be difficult to distinguish between the predictions of models describing very different mechanisms purely in terms of phenomenology.

1.2 Reaction-Diffusion Theory

In 1952, Turing proposed that pattern formation during morphogenesis might come about through an instability in systems of reacting chemicals, driven by diffusion. The resulting chemical prepatterns, states the hypothesis, are subsequently interpreted as positional information by competent cells and cell fates are determined via prepattern-dependent differentiation. As will be shown in the following chapter, a set of two or more chemicals is required to interact in a well defined manner in order that heterogeneous patterns may arise in their concentrations. Significantly, the diffusion-driven instability (DDI) requires disparity between the diffusivities of the chemicals.

This mechanism for spatial and spatio-temporal pattern formation is of great theoretical interest as it represents a spontaneous spatial symmetry-breaking phenomenon in a simple physical system. Any thermodynamically closed system, where there is no transfer of matter or heat into or out of the system, must evolve towards thermodynamic equilibrium. Pattern formation in such systems can be only transient. However, Prigogine and Nicolis [94] showed that if nonequilibrium (or far-from-equilibrium) thermodynamic conditions are maintained in an open reactor, e.g. by providing a constant supply of reactant, then heterogeneous patterns may be sustained. In the mechanism described by Turing these patterns have an intrinsic wavelength which does not depend on the physical size of the reactor, and patterns tend to demonstrate periodicity. Turing's theory has found application in fields far removed from developmental biology—see for example the book by Walgraef [130].

Turing's ideas have been applied to a wide variety of pattern formation problems in biology. However, the theory has received important criticism on several fronts. Firstly, although many molecules have been identified which appear to act as diffusive signals, some of which may act as morphogens in the Wolpertian sense, no set of chemicals has been demonstrated to operate in the manner that Turing described in a biological system. In fact, it is only relatively recently that Turing patterns have been demonstrated conclusively under controlled conditions in artificial chemical systems, discussed in the following section.

We have already hinted at the second major source of criticism of Turing's theory of pattern formation in biology. In many situations the number of pattern elements (for example the number of wavelengths generated in one dimension) is crucial. Turing patterns have been shown to display strong sensitivity to the size and geometry of the solution domain. This criticism, which has come to be known as the *robustness* problem, was first brought to light concerning the segmentation of *Drosophila*. Kauffman [59] suggested that periodic gene expression patterns observed during the early development of insects could be explained by a reaction-diffusion model, which appeared to give qualitatively similar patterns on regular and rather symmetric domains. Subsequent work [10] showed that patterns which do not resemble those occurring naturally are obtained for minor perturbations of the size and shape of the domain. In

fact it was subsequently discovered that the segmentation of the *Drosophila* embryo is achieved in a manner much closer to that described by Wolpert, where each individual element of the apparently periodic pattern is separately controlled and regulated, and the pattern is generated in a cascade of gene switching [2].

The root of this problem is in the fact that for domains of anything but very small aspect ratio (the ratio of domain size to intrinsic pattern wavelength) there are many different patterned solutions which may be generated, the number increasing as the domain size is increased, and the selection between these different patterns depends sensitively on initial data and domain geometry. Bard and Lauder [6] draw the same conclusion, finding in a series of numerical experiments that patterns in discrete cellular simulations are sensitive to the number of cells, concluding that only unpredictable *mosaic* patterns are possible. More recently Saunders and Ho [118] have considered segmentation of growing systems, concluding once again that reaction-diffusion does not constitute a reliable pattern generation mechanism. Dillon *et al.* [26] have shown that the multiplicity of solutions may be reduced by varying the boundary conditions. We will demonstrate that the consideration of domain growth during pattern formation may have important consequences for the robustness issue.

An alternative way of viewing the robustness issue is to argue that the reaction-diffusion mechanism fails to demonstrate the regulatory properties that we described earlier. While for given initial conditions it may be possible to select the desired pattern by judicious choice of domain size, in general biological systems are subject to natural variation in such parameters and reliable pattern generation requires a certain degree of scale invariance. To achieve this regulatory property, various modifications to the theory have been proposed, requiring some form of feedback from the domain size to the parameters in the function describing the reaction rates [100, 52]. We will discuss scale invariance later, in light of results we will present for pattern formation on growing domains. Before turning to consider domain growth we discuss the realisation of chemical patterns in laboratory experiments.

1.3 Chemical Pattern Formation

Travelling waves in chemical systems have been known for some time in the Belousov-Zhabotinsky reaction, however, reactions demonstrating the stationary patterns predicted by Turing have only been discovered within the last decade. General reviews of spatio-temporal phenomena in chemistry can be found in Epstein and Showalter [36] and Johnson and Scott [56] and, for spatial patterns, Maini *et al.* [78].

The experimental realisation of Turing patterns was precipitated by the development of gel reactors where reactants undergo diffusive transport through an aqueous gel, which serves to suppress any convective motion. First introduced by De Kepper and Boissonade in Bordeaux, the Gel Strip reactor has two reservoirs containing chemically inert sets of reactants which are allowed to diffuse into a thin rectangular ribbon of gel from opposite sides. In the middle of the ribbon both sets of chemicals are

present and may react. The concentrations in the two reservoirs can be held constant to maintain nonequilibrium conditions. The first unambiguous experimental observation of Turing patterns was reported by this group in the CIMA reaction[1] [13, 23]. Here the gel was loaded with starch primarily to aid visualisation. Starch, a large molecule with low mobility in the gel matrix, forms a complex with iodide, one of the reacting species, effectively reducing its diffusion coefficient to provide the necessary conditions for Turing patterns to form. Subsequent observations were reported by Ouyang and Swinney [103] using a variation on the design, the Gel Disk reactor, where patterns form in the plane perpendicular to the concentration gradients so that larger patterned domains can be observed. A vast amount of theoretical work has been done to develop analytical models of these complicated reactions, the aim being to reproduce the phenomena and to calculate phase and bifurcation diagrams describing the chemical systems.

Stationary patterns have also been recorded in the FIS reaction[2] when initiated with sufficiently large perturbation away from equilibrium. Here pattern formation is achieved by propagating chemical (redox) fronts which halt when they approach each other. In this case labyrinthine patterns [69] have been observed as well as self-replicating phenomena [70], where a localised spot grows, divides and separates, repeating to fill domain. Other phenomena include breathing spot patterns, where the spot radius oscillates [47]. Recently, similar structures have also been reported in the CIMA reaction [22]. However, these patterns are not of Turing type in the strict sense, as we shall see in the following chapter.

1.4 Domain Growth

The motivation for consideration of domain growth in developmental systems is apparent. Most pattern formation takes place during the growth of the organism. However, what may not be immediately clear is whether underlying growth, which is expected to take place over much longer timescales than the generation of pattern via reaction and diffusion, may be considered to decouple from the reaction-diffusion mechanism, as are other cellular processes. Furthermore, it is unclear how the incorporation of domain growth might influence pattern selection. The following is a quote from Cross and Hohenberg's comprehensive review of pattern formation in nonequilibrium systems [21, p.1052]:

'A natural procedure for biological systems is to consider the spatial domain Ω to be a function of time $\Omega(t)$. Then the dynamics of the [reaction-diffusion] equations will be supplemented by the stretching of the domain. In the simplest case one might assume that the timescale for variation of $\Omega(t)$ is slow, but never the less the final pattern obtained might be very different

[1] Chlorine-Iodide-Malonic Acid
[2] Ferrocyanide-Iodide-Sulfite

from the one which would be produced by specifying an initial condition on the fully grown domain $\Omega(t_{final})$.'

It is our intention in this thesis to present a systematic study of the influence of domain growth on pattern formation in reaction-diffusion systems.

Domain growth has previously been considered in reaction-diffusion models for the sequence of emergence of tooth primordia in the developing jaw [65] and for the branching morphology of growing *Micrasterias* [66]. New impetus was recently provided by Kondo and Asai [64], who suggested that a reaction-diffusion mechanism could be responsible for the dynamic changes in pigmentation patterns of the marine angelfish *Pomacanthus*. Unlike mammalian coat markings, the pattern in the skin of these fish changes dynamically during growth of the animal, rather than simply enlarging in proportion to the body size. Juvenile *P. imperator* display concentric stripes and *P. semicirculatus* have a regular array of vertical stripes which increase in number during growth. Juvenile *P. semicirculatus* of less than 2cm in length display three vertical stripes which separate until the length of the fish is approximately 4cm, at which point new stripes appear between the original ones. Similarly at around 8-9cm in length new stripes again appear between the existing ones. In this manner the pattern changes by insertion of new stripes as the animal roughly doubles in length, to preserve the wavelength of the pattern. In *P. imperator* this behaviour is maintained in the adult fish, where horizontal stripes maintain an average spacing. This dynamic regulation of the pattern is quite unlike the static pattern selection we have previously discussed.

In the following chapter we present a detailed discussion of the diffusion-driven instability, including further discussion of the robustness problem, and some mathematical properties of solutions to the model pertinent to pattern formation on growing domains. In Chapter 3 we derive the governing equations for reaction and diffusion processes on a growing domain as a problem in kinematics. Chapter 4 considers a simplified scenario in one spatial dimension where the domain growth is uniform in space. We investigate the effects on pattern formation of the rate at which the domain is growing, and on the reaction kinetics. This latter problem is taken up in Chapter 5 where we examine the dynamical transitions between patterns as the domain grows for different functional forms for the reaction term. Chapter 6 considers nonuniform domain growth and pattern formation in two spatial dimensions. Finally, in Chapter 7 we conclude the thesis with further discussion of reaction-diffusion pattern formation on growing domains.

2. Pattern Formation in Reaction-Diffusion Systems

Under the continuum hypothesis, the spatio-temporal state of a chemical system is described by partial differential equations derived from considerations of conservation of matter. We consider the net production rate of a chemical species, the reaction kinetics, within an elemental volume V and the flux of matter through the elemental volume boundary ∂V at fixed location within the reaction space Ω. The reaction space is a bounded region which will be called the *domain*, with boundary $\partial\Omega$. The rate of change of the amount of matter within the elemental volume is given by

$$\frac{\mathrm{d}}{\mathrm{d}t}\int_V c(\mathbf{x},t)\,\mathrm{d}\mathbf{x} = \int_{\partial V} -\mathbf{j}(\mathbf{x},t)\cdot\mathbf{dS} + \int_V R(c,p)\,\mathrm{d}\mathbf{x}, \tag{2.1}$$

where $c(\mathbf{x},t)$ is the concentration of a chemical species C at position $\mathbf{x}$ and time t. The flux $\mathbf{j}(\mathbf{x},t)$ is through the closed surface ∂V and $R(c,p)$ is the net rate of creation of concentration of species C. The reaction kinetics, R, are generally described by a polynomial or rational function in c and p represents interaction with other chemicals and external factors. Using the divergence theorem, (2.1) may be written

$$\frac{\mathrm{d}}{\mathrm{d}t}\int_V c(\mathbf{x},t)\,\mathrm{d}\mathbf{x} = \int_V \left[-\nabla\cdot\mathbf{j} + R(c,p)\right]\mathrm{d}\mathbf{x}. \tag{2.2}$$

The domain is fixed in time and so we may differentiate through the integral. Using the fact that the choice of elemental volume V was arbitrary within Ω, we have that at every point $(\mathbf{x},t)$ the following conservation equation holds

$$\frac{\partial c}{\partial t} = -\nabla\cdot\mathbf{j} + R(c,p). \tag{2.3}$$

If we suppose that the instantaneous flux $\mathbf{j}$ is due to (isotropic) Fickian diffusion then $\mathbf{j} = -D\nabla c$, where the diffusivity D is a constant, and we have the reaction-diffusion equation for species C on a fixed domain Ω

$$\frac{\partial c}{\partial t} = D\nabla^2 c + R(c,p). \tag{2.4}$$

Generally one is interested in the interaction of several chemical species, for example the set $\{C_1, C_2, \ldots, C_n\}$. Equation (2.4) is then replaced by a system of coupled equations which describe the evolution of a vector of concentrations $\mathbf{c} = (c_1, c_2, \ldots, c_n)$, and now $\mathbf{R}(\mathbf{c},p)$ describes the interaction of the species. Various kinetic schemes are presented in Appendix A, and will be introduced in the discussion of the behaviour of specific systems.

2.1 Nondimensionalisation and Boundary Conditions

To nondimensionalise the system of coupled equations we start, following Dillon *et al.* [26], by writing $\bar{c}_i = c_i/\mathcal{C}_i$ and $\bar{\mathbf{x}} = \mathbf{x}/L$. Here L is a length scale (usually taken to be the domain length for problems in one spatial dimension) and $\mathcal{C}_i$ is a reference

concentration for the chemical species C_i. A reaction rate ω, characteristic of the kinetic scheme, is used to nondimensionalise the reaction term which is represented in nondimensional form by $\bar{\mathbf{R}}(\bar{\mathbf{c}}, p)$. In general $\bar{\mathbf{R}}$ has the same functional form as $\mathbf{R}$, but generally has different coefficients.

To standardise the problem (and without loss of generality) we rewrite the system in order of decreasing diffusivity, D_i for the i^{th} species. We introduce a dimensionless scaling parameter

$$\gamma = \frac{\omega L^2}{D_1}, \tag{2.5}$$

where $D_1 = \max\{D_i\}$, which represents the ratio of diffusive T_D to kinetic T_R relaxation times, where

$$T_D = \frac{L^2}{D_1} \quad \text{and} \quad T_R = \frac{1}{\omega}. \tag{2.6}$$

Both of these timescales could be used to nondimensionalise the time variable. For reasons which will become evident later, we choose to nondimensionalise the equations using the kinetic relaxation timescale. Writing $\bar{t} = \omega t$, and dropping the overbars for notational convenience, we have the dimensionless equation

$$\frac{\partial \mathbf{c}}{\partial t} = \frac{1}{\gamma}\mathcal{D}\nabla^2\mathbf{c} + \mathbf{R}(\mathbf{c}, p), \quad \mathbf{x} \in \Omega \tag{2.7}$$

where $\mathcal{D} = \text{diag}[1, d_2, \ldots, d_n]$ is the diagonal matrix containing the ordered dimensionless diffusivities where $d_i = D_i/D_1 \leq 1$ and $d_i \leq d_{i-1}, i = 2, \ldots, n$.

The full specification of the reaction-diffusion system requires that conditions be imposed on the boundary of the solution domain, $\partial\Omega$, and that an initial condition is specified for the system of partial differential equations. If initial data is contained in the vector $\mathbf{c}_0(\mathbf{x})$, then a typical set of boundary conditions is given by

$$(\mathbf{n} \cdot \nabla)\,\mathbf{c} = \mathcal{P}(\mathbf{c}^* - \mathbf{c}), \quad \mathbf{x} \in \partial\Omega \tag{2.8}$$

$$\mathbf{c}(\mathbf{x}, 0) = \mathbf{c}_0(\mathbf{x}) \tag{2.9}$$

where the fixed concentration vector $\mathbf{c}^*$ is uniform over Ω and represents a constant external reference concentration for each species. The outward normal gradient operator $\mathbf{n} \cdot \nabla$ acts component-wise on $\mathbf{c}(\mathbf{x}, t)$, where $\mathbf{n}$ is the outward-pointing vector normal to the boundary. On $\partial\Omega$ we will restrict boundary conditions such that the matrix $\mathcal{P}$ is of the form $\mathcal{P} = \text{diag}[P_1, P_2, \ldots, P_n]$, where constants $0 \leq P_i \leq \infty$ define the type of condition imposed, specifying the rate of flux at the boundary for each species. For *scalar* conditions $\mathcal{P}_{ij} = \delta_{ij}P$ with constant P, where δ_{ij} is the Kronecker delta, and $P = 0$ gives zero flux (Neumann) data for each species while $P = \infty$ corresponds to Dirichlet conditions for which there is an instantaneous equilibrium with the external concentration, $\mathbf{c}^*$. The case for which $\mathbf{c}^* = \mathbf{c}_s$, where

$$\mathbf{R}(\mathbf{c}_s, p) = \mathbf{0} \tag{2.10}$$

is called *homogeneous* Dirichlet conditions. The concentration vector $\mathbf{c}_s$ is the *kinetic steady state* of the reaction scheme, the stability of which we discuss below. Another type of constraint often assumed on $\partial\Omega$ is a periodic boundary condition, taken to simulate a spatially unbounded system. On the one-dimensional domain, for $x \in [0,1]$, periodic conditions take the form $\mathbf{c}(0,t) = \mathbf{c}(1,t)$ for all t.

2.2 Diffusion-Driven Instability

The counterintuitive result of Turing's celebrated paper [126] is that a spatially homogeneous system of interacting chemicals which is stable to perturbation in the absence of diffusion may be driven to a persistent spatially heterogeneous state via a dynamic instability due to diffusion. This statement defines the diffusion-driven (Turing) instability (DDI), which is recognised as one example of a class of pattern forming instabilities in systems driven far from equilibrium. In otherwise similar patterning mechanisms (for example in fluid systems: thermal convection (buoyancy) driving the Rayleigh-Bénard instability or the rotation of concentric cylindrical walls in the Taylor-Couette flow system [21]) the spatial scale of pattern is determined by the geometry of the solution domain (i.e. by physical constraints). Patterns in Turing systems, however, are characterised by a wavelength which is determined by parameters intrinsic to the mechanism of the instability itself, as will be demonstrated in section 2.3.1. In this respect the Turing instability is set apart from other pattern forming systems. For a discussion of the differences between the Turing and Rayleigh-Bénard instabilities in finite systems see Chen and Cross [15]. Next we review the standard results for the onset of the instability in the linear regime (see, for example, Murray [88]), and go on to consider a nonlinear analysis for longer-time behaviour.

2.2.1 Linear Analysis. The defining requirement, stability of the homogeneous (spatially uniform) steady state $\mathbf{c}_s$ to perturbation in the absence of diffusion, is equivalent to requiring that $\mathbf{c}_s$ must be stable to homogeneous perturbations in the presence of the diffusion term. The diffusion-driven instability is the instability of such reaction-diffusion systems to heterogeneous perturbation. Near to onset we study the linear instabilities of the homogeneous steady state to classify the patterns which may grow in terms of their wavenumber (and frequency for spatio-temporal pattern formation).

The homogeneous steady state, positive solution of $\mathbf{R}(\mathbf{c}_s, p) = \mathbf{0}$ with no spatial variation, exists when compatible with the imposed boundary conditions. The analysis is thus restricted to the cases of homogeneous Dirichlet and Neumann (zero flux) conditions. We consider bifurcations from the steady state by examining the response of the system to an initially small perturbation $\mathbf{w}(\mathbf{x},t)$ where $|\mathbf{w}_i(\mathbf{x},0)| \ll 1$. Setting

$$\mathbf{c}(\mathbf{x},t) = \mathbf{c}_s + \mathbf{w}(\mathbf{x},t) \tag{2.11}$$

in the dimensionless reaction-diffusion equation (2.7) we linearise in the variable $\mathbf{w}$ giving

$$\frac{\partial \mathbf{w}}{\partial t} = \frac{1}{\gamma}\mathcal{D}\nabla^2\mathbf{w} + \mathcal{A}\mathbf{w} \tag{2.12}$$

where the Jacobian (stability) matrix $\mathcal{A}$ is evaluated at the homogeneous steady state

$$\mathcal{A}_{ij} = \left.\frac{\partial R_i}{\partial c_j}\right|_{c_s}. \tag{2.13}$$

We consider scalar boundary conditions

$$(\mathbf{n}\cdot\nabla)\,\mathbf{w} = -P\mathbf{w} \quad \text{on } \partial\Omega, \tag{2.14}$$

restricting ourselves to the homogeneous case, $\mathbf{c}^* = \mathbf{c}_s$. Solutions of system (2.12)–(2.14) take the general form $\mathbf{w}(\mathbf{x},t) = \exp(\lambda t)\,\Phi(\mathbf{x})$ where Φ is a vector and the growth rate may be complex, $\lambda = \alpha + i\beta$, allowing for temporal oscillation. Substituting this solution into equation (2.12) we obtain

$$\frac{1}{\gamma}\mathcal{D}\nabla^2\Phi + (\mathcal{A} - \lambda\mathcal{I})\Phi = 0 \tag{2.15}$$

where $\mathcal{I}$ is the identity.

Eigenfunctions of the spatial eigenvalue problem (2.15) can be written as $\Phi_m = \mathbf{y}_m\phi_m$, where $\mathbf{y}_m$ is a constant vector and $\phi_m(\mathbf{x})$ are (scalar) eigenfunctions of the Laplacian containing the spatial dependency of the solution, and are subject to the scalar boundary conditions

$$\begin{aligned} \nabla^2\phi_m &= -k_m^2\phi_m \quad \text{in } \Omega \\ \mathbf{n}\cdot\nabla\phi_m &= -P\phi_m \quad \text{on } \partial\Omega, \end{aligned} \tag{2.16}$$

where k_m is a dimensionless wavenumber associated with ϕ_m. The boundary conditions acting on Φ restrict the spatial dependency to a discrete set of eigenfunctions of the Laplacian, ϕ_m. Clearly, for the solution on an unbounded domain, the wavenumber k is a continuous variable. For nontrivial solutions of (2.15) we require

$$\det\left[\mathcal{A} - \frac{k_m^2}{\gamma}\mathcal{D} - \lambda(k_m^2)\mathcal{I}\right] = 0 \tag{2.17}$$

(the characteristic polynomial) which yields the *dispersion relation*, $\lambda = \lambda(k_m^2)$, an algebraic equation for the growth rate. The solution of the linear stability problem is then given by

$$\mathbf{w}(\mathbf{x},t) = \sum_{m=0}^{\infty} \exp\left(\lambda(k_m^2)t\right)\mathbf{y}_m\phi_m(\mathbf{x}) \tag{2.18}$$

where the vector $\mathbf{y}_m$ is determined by the initial data $\mathbf{w}_0(\mathbf{x}) = \mathbf{c}_0(\mathbf{x}) - \mathbf{c}_s$. The individual components making up the infinite sum (2.18) are *linear modes* and the label m is the relevant *mode number*. For certain nonlinearities in the reaction term

the amplitudes of growing modes are bounded to finite value. This is shown in the nonlinear analysis below. We distinguish between the eigenfunctions of the Laplacian (the linear modes) and the patterns which subsequently develop outside the linear regime, which we will call *pattern modes*.

The linear stability of the homogeneous steady state to spatially heterogeneous perturbation of mode m is determined by the sign of the real part of $\lambda(k_m^2)$. The kinetic steady state has neutral stability for $\mathcal{R}e\,\lambda = 0$, is (asymptotically) stable for $\mathcal{R}e\,\lambda < 0$ and is unstable (and hence a perturbing mode of appropriate wavenumber may grow) for $\mathcal{R}e\,\lambda > 0$. This latter possibility describes the onset of the diffusion-driven instability. We describe any mode for which the linear stability analysis predicts instability of the homogeneous steady state as a *growing* mode. Depending on the components of $\mathbf{y}_m$, determined by the initial conditions, all possible modes may not be available for growth. The question of which mode grows to become the final long term pattern, the *pattern selection* problem, will be discussed later. The requirement that the steady state is stable in the absence of diffusion is equivalent to there being no growing mode with wavenumber $k_0 = 0$, that is, $\mathcal{R}e\,\lambda(k_0 = 0) < 0$. This provides certain conditions on the components of the Jacobian matrix, $\mathcal{A}$, as will be demonstrated explicitly from the linear analysis in the simple case of a two-component reaction-diffusion system in one spatial dimension.

2.2.2 Two-Component Model System. We consider a reaction-diffusion model of two interacting species $\mathbf{c} = (u, v)$ in one spatial dimension, with external reference concentrations set at the homogeneous steady state of the kinetics, $\mathbf{R}(\mathbf{c}_s, p) = \big(f(u_s, v_s), g(u_s, v_s)\big) = \mathbf{0}$, and scalar boundary conditions. Linearising about the steady state and writing $\mathbf{w} = \mathbf{c} - \mathbf{c}_s$ we have

$$\frac{\partial \mathbf{w}}{\partial t} = \frac{1}{\gamma}\mathcal{D}\frac{\partial^2 \mathbf{w}}{\partial x^2} + \mathcal{A}\mathbf{w}, \quad x \in [0,1] \tag{2.19}$$

$$\frac{\partial \mathbf{w}}{\partial x} = P\mathbf{w}, \qquad\qquad x = 0, 1 \tag{2.20}$$

with

$$\mathcal{A} = \left[\begin{array}{cc} f_u & f_v \\ g_u & g_v \end{array}\right]_{(u_s, v_s)} \quad \text{and} \quad \mathcal{D} = \left[\begin{array}{cc} 1 & 0 \\ 0 & d \end{array}\right]. \tag{2.21}$$

Henceforth, the partial derivatives f_u, f_v, g_u and g_v will be assumed to be evaluated at the steady state (u_s, v_s). From (2.17) we have $\det\left(\mathcal{A} - k_m^2\mathcal{D}/\gamma - \lambda(k_m^2)\mathcal{I}\right) = 0$, which yields the dispersion relation for this problem

$$0 = \lambda^2 + \lambda\left(\frac{k_m^2}{\gamma}(1+d) - (f_u + g_v)\right) + h(k_m^2), \tag{2.22}$$

where

$$h(k_m^2) = \frac{d}{\gamma^2}k_m^4 - \frac{1}{\gamma}\left(df_u + g_v\right)k_m^2 + f_u g_v - f_v g_u. \tag{2.23}$$

Firstly, let us address the requirement of linear stability in the absence of diffusion. Substituting $k_m = 0$, in the absence of diffusion (or for homogeneous perturbation), into equations (2.22) and (2.23) we have $\lambda_{0,\pm}$ are the roots of

$$\lambda^2 - \lambda(f_u + g_v) + f_u g_v - f_v g_u = 0 \tag{2.24}$$

and so linear stability, $\mathcal{R}e\,\lambda_{0,\pm} < 0$, is guaranteed by the two constraints

$$\mathrm{tr}\mathcal{A} = f_u + g_v < 0, \quad \det\mathcal{A} = f_u g_v - f_v g_u > 0. \tag{2.25}$$

Next we consider spatially heterogeneous perturbations for which $k_m \neq 0$. In order to achieve the growth of some linear mode we require that there is at least one real k_m for which $\mathcal{R}e\,\lambda > 0$. From the dispersion relation we see that the first requirement of (2.25) precludes the coefficient of λ from taking a negative value, and so we must have $h(k_m^2) < 0$ for diffusion-driven instability. The second of (2.25) implies that this can only be the case if

$$df_u + g_v > 0, \tag{2.26}$$

which provides a third constraint on the system. Comparing with the first of (2.25), this implies that $d \neq 1$, which provides a necessary but not sufficient condition to ensure $\mathcal{R}e\,\lambda > 0$. The criterion for $h(k_m^2)$ to be negative, found by examining the minimum of the function, h_{min}, provides a fourth constraint for diffusion-driven instability,

$$h_{min} = \det\mathcal{A} - \frac{1}{4d}\left(df_u + g_v\right)^2 < 0. \tag{2.27}$$

Collecting together the four conditions that we have computed and which must be satisfied for the Turing instability we have:

- $f_u + g_v < 0$
- $f_u g_v - f_v g_u > 0$
- $df_u + g_v > 0$
- $f_u g_v - f_v g_u - \frac{1}{4d}\left(df_u + g_v\right)^2 < 0$

where the partial derivatives are evaluated at the kinetic steady state.

These four conditions may be employed to deduce parameter regimes for which specific kinetic schemes can undergo Turing bifurcation, or indeed whether such a bifurcation is possible for a particular reaction scheme. The region of the parameter space for a particular kinetic scheme within which the diffusion-driven instability may give rise to pattern is known as the *Turing space* [88]. For anything but the simplest form for $\mathbf{R}$ and hence $\mathcal{A}$ in (2.13), the direct algebraic calculation of the boundaries of the Turing space (given by the above conditions) is intractable. Murray [87] has described a parametric approach by which the problem is considerably simplified. The existence of a Turing space does not in itself guarantee that a pattern will arise from the dynamic instability in a *finite* system, where only a discrete set of linear modes is

consistent with the domain geometry and boundary conditions, at least one of which must have positive linear growth rate. This is discussed further in section 2.2.4

2.2.3 Configurations of the Jacobian. The two constraints (2.25), derived for the stability of homogeneous perturbations, lead to a restriction on the configuration of the signs of components for the Jacobian matrix $\mathcal{A}$. With $d \leq 1$, the constraints $f_u + g_v < 0$ and $df_u + g_v > 0$ require that $f_u < 0$ and $g_v > 0$, and $\det \mathcal{A} > 0$ implies that only the following configurations are compatible with diffusion-driven instability

$$\mathrm{sgn}(\mathcal{A}_p) \equiv \begin{bmatrix} - & + \\ - & + \end{bmatrix}, \quad \mathrm{sgn}(\mathcal{A}_c) \equiv \begin{bmatrix} - & - \\ + & + \end{bmatrix}. \tag{2.28}$$

The first of these is called a *pure* and the second a *cross activator-inhibitor* mechanism. The interpretation of these two possibilities in terms of activation and inhibition may be gleaned from an examination of the nullclines of systems with Jacobian matrix of these general forms. A pure system is one in which v is self-activating and also activates u, while u reciprocally inhibits v and is self-inhibiting. On the other hand, for a cross system v is self-activating but inhibits u, while u is still self-inhibiting, but now activates v. In both cases u is deemed to be the (self-) *inhibitor* and v the (self-) *activator*,[1] and with $d \leq 1$ the inhibitor diffuses faster than the activator.[2] This leads to the popular description [98, 88] of the mechanism as one of short range *local* activation with long range *lateral* inhibition. The constraint $\mathrm{tr}\mathcal{A} < 0$ implies that the self-inhibition is always stronger than the self-activation in reaction-diffusion systems of this type that are capable of forming pattern.

One important consequence of these sign configurations, and a feature distinguishing the two cases, is the relative polarity, or phase, of the patterns formed in the systems. Dillon *et al.* [26] show analytically that if the kinetic terms of a two-component reaction-diffusion system in one spatial dimension with zero flux boundary conditions are of the pure variety, then near to a primary bifurcation point the spatial gradients of the species' concentrations will be of the same sign (spatial oscillation in phase) at all points in the domain. For kinetics that are cross-type, the gradients are of opposite sign (spatial oscillation in antiphase) [111]. This result, it is conjectured, is maintained on primary bifurcating solutions away from the bifurcation point.

2.2.4 The Dispersion Relation. The quadratic form of the dispersion relation dictates that the values of k^2 for which the real part of $\lambda(k^2)$ is positive lie in a bounded range $k_-^2 < k^2 < k_+^2$ (of growing modes), given by the zeros of $h(k^2)$,

$$\frac{2d}{\gamma} k_\pm^2 \;=\; (df_u + g_v) \pm \sqrt{(df_u + g_v)^2 - 4d \,\det \mathcal{A}} \;=\; A \pm B \tag{2.29}$$

[1] Some authors reserve the term *activator-inhibitor* to refer to pure kinetics and call cross systems, where the (self-) inhibitor promotes the activator species, *activator-substrate* kinetics.

[2] If we had chosen the opposite ordering for the species, giving $d_i \geq 1$ and prompting $f_u > 0$, this would swap the roles of u and v, amounting only to a relabelling of the two species.

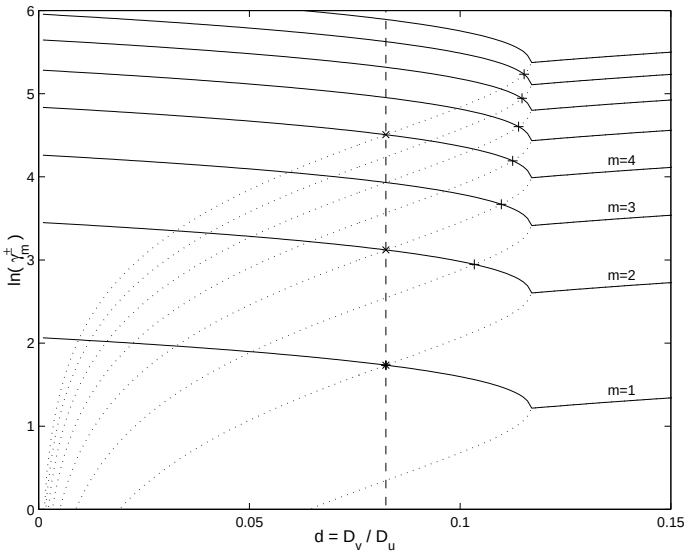

FIGURE 2.1 Intervals of instability of the homogeneous steady state to perturbation by spatial eigenfunctions of the Laplacian for Schnakenberg kinetics. We plot the natural logarithms of $\gamma_m^+(d)$ (solid) and $\gamma_m^-(d)$ (dotted) against the ratio of diffusivities d for modes $m = 1, \ldots, 8$, where $k_m = m\pi$. Points for which $\gamma_m^+ = \gamma_{m+1}^-$ are marked + and points where $\gamma_{m_n}^+ = \gamma_{m_{n+1}}^-$ where $m_n = m_0 2^n$ are marked by $\times$, which lie on a line of equal d (dashed). Note that for successively smaller d there is increasing overlap between the ranges of instability for different modes. The curves are calculated for Schnakenberg kinetics (see Appendix A.1) with kinetic parameters $a = 0.1$ and $b = 0.9$. Note that the bifurcation occurs at the same value $d = d_c$ independent of m (the bifurcation point is in fact independent of k - see equation (2.34).

where A and B depend on the kinetic parameters and d but not on γ.[3] For fixed kinetic parameters p this condition is satisfied when the scaling parameter falls in the interval $\gamma \in [\gamma_m^-, \gamma_m^+]$, where, making the dependence on d explicit,

$$\gamma_m^-(d) = \frac{2dk_m^2}{A(d) + B(d)} \quad \text{and} \quad \gamma_m^+(d) = \frac{2dk_m^2}{A(d) - B(d)}. \tag{2.30}$$

Successive ranges of instability overlap when $\gamma_m^+ > \gamma_{m+1}^-$ and there is an interval of stability of the homogeneous steady state when $\gamma_m^+ < \gamma_{m+1}^-$. For zero flux boundary conditions the spatial eigenfunctions are $\phi_m(x) = \cos(m\pi x)$. The instability intervals for $k_m = m\pi$ are plotted for a particular kinetic scheme in Figure 2.1 as d varies. In this case we have overlapping instability ranges (and intervals of stability) for, respectively,

$$1 + \frac{2m^2}{2m+1} \quad \geq \frac{A}{B} \quad \left(< \frac{A}{B} \right). \tag{2.31}$$

Points where the equality holds, that is where successive modes first become destabilising at the same value of d, are marked by '+'. We also indicate points at which

[3] For solutions on a bounded domain we also require that there is at least one discrete wavenumber k_m in the range of instability.

destabilising linear patterns of mode $m = m_0 2^n$ and $m = m_0 2^{n+1}$ first coincide, marked by '$\times$', and from (2.30) it can be shown that for $k_m = m\pi$ the corresponding value of d is independent of m_0 and n, shown by the dashed line in the figure. We discuss this result further later in this chapter.

When the ranges of instability for two or more wavenumbers overlap, there is competition between patterning modes. It is apparent from Figure 2.1 that there is increasing overlap further away from the bifurcation point (for example, as d decreases), and intervals of stability tend to disappear. The prediction from linear analysis that the mode with fastest linear growth rate, $\max_m \{\lambda(k_m^2)\}$, will be established proves to be of decreasing validity further from the bifurcation point, and of little use for problems in more than one spatial dimension where there is also increasing degeneracy for pattern orientation. The mechanism of pattern selection, by which one mode is chosen to grow to heterogeneous steady state from many admissible modes, is an important issue to which we will return later in this chapter.

Notably the linear solutions for zero flux conditions have an arbitrary phase shift of π, that is, the linear modes may be reflected about the homogeneous state and remain valid solutions. In fact linear solutions for any boundary conditions or geometry (or spatial dimension) have an arbitrary sign to the wavevector (only the magnitude is determined by the analysis). Thus for zero flux conditions patterns of the same spatial mode number may take one of two polarities, where we adopt the notation that mode $+m$, has positive polarity (high amplitude at the left-hand boundary) and mode $-m$ is of negative polarity. We also recall that pure kinetics will give the same polarity for both species while for cross kinetics the polarities will be opposites.

2.3 Instability and Characteristic Scales

By allowing λ to be complex in the previous analysis we admit the possibility of temporal or spatial oscillation, or both simultaneously. Following Cross and Hohenberg [21] we may in general characterise pattern-forming instabilities at the bifurcation point. For $\lambda = \alpha + i\beta$ and wavenumber k_c at this critical point, where $\alpha = 0$, instability is categorised according to which of k_c and β are non-zero:

1. $k_c \neq 0$ and $\beta = 0$: Spatial oscillation only. Long-time solutions are stationary and spatially heterogeneous structures.
2. $k_c = 0$ and $\beta \neq 0$: Temporal-oscillation only. At large times solutions remain spatially homogeneous.
3. $k_c \neq 0$ and $\beta \neq 0$: Spatio-temporal patterns. Long-time behaviour continues to evolve spatially and temporally.

General instabilities in systems driven far from equilibrium may be of any of the above types. The Turing bifurcation may give rise to instabilities of type (1) and (3). Type (2), corresponding to Hopf bifurcation in the kinetics, is excluded by the requirement that the homogeneous state is stable in the absence of diffusion. For the case of

two species interaction, the dispersion relation subject to the constraints for diffusion-driven instability precludes time-oscillating pattern solutions. We see from (2.22)–(2.23) that λ has an imaginary part when

$$\left(\frac{k_m^2}{\gamma}(1+d)-(f_u+g_v)\right)^2 - 4h(k_m^2) < 0. \tag{2.32}$$

However, for the homogeneous steady state to be unstable to heterogeneous perturbation (for a particular mode to grow to a heterogeneous pattern) we require that $h(k_m^2) < 0$. Hence, for any growing mode, λ must be purely real and so time-oscillatory diffusion-driven instability is not possible in a two-component system of this form. For three or more interacting species, however, the dispersion relation does in general admit such solutions, and we investigate a specific example with three species in Chapter 4.

At a primary bifurcation point the critical wavenumber is defined to be the wavenumber at which the dispersion relation first crosses the axis into the positive half-plane. A critical (maximum) value for the ratio of diffusivities is also determined at this point (see Figure 2.1). We may also recover a characteristic spatial scale from the critical wavelength, and a timescale from the growth rates predicted by the linear analysis.

In section 2.2.4 we have shown that the scaling parameter must lie in a given interval, $\gamma \in [\gamma_m^-, \gamma_m^+]$, for a particular linear mode m to grow. If we consider increasing γ from just greater than zero (there is a singular point where $\gamma = 0$) then we may define a critical value γ_c at which the homogeneous steady state first loses stability to a growing mode, the lowest mode available to the system. For γ below this value no pattern is possible. Hence for pattern we require

$$\gamma > \gamma_c = \gamma_{m_l}^- \tag{2.33}$$

where m_l labels the lowest mode. For the Neumann problem, in the absence of any reaction terms we have relaxation to an average homogeneous concentration vector, the value of which is set by the initial conditions. We might expect the system to relax to such a steady state whenever the relaxation time for diffusion is much smaller than the characteristic timescale of the kinetics. Indeed this intuition is borne out by the minimum requirement on γ. As pointed out by Arcuri and Murray [3], this condition may be interpreted in three ways:

1. $1/\gamma$ is proportional to the largest of the diffusivities, D_1, which must therefore be smaller than some threshold value.
2. The characteristic reaction rate for the kinetics, ω, which is proportional to γ, must be greater than a minimum reaction speed.
3. There is a minimum domain length, proportional to $\sqrt{\gamma_c}$.

Given that γ represents the relative strengths of the reaction and diffusion mechanisms, all of these conditions are equivalent. However, in the context of pattern formation on growing domains the last of these interpretations is the most relevant.

At the bifurcation point the critical wavenumber is determined by equation (2.29) when $k_c = k_+ = k_-$. Thus we must have $B(d) = 0$ which occurs at the critical diffusivity, $d = d_c$, given by the appropriate root, for $0 \leq d_c < 1$, of

$$d = d_\pm = \frac{\det \mathcal{A} - f_v g_u \pm 2\sqrt{-f_v g_u \det \mathcal{A}}}{f_u^2} \tag{2.34}$$

which is independent of k and γ. This imposes a maximum (fractional) value for d, the ratio of diffusivities, where we require $0 \leq d < d_c$ for diffusion-driven instability. However, as has been pointed out in the literature [51, 110, 26], for certain kinetic schemes the critical ratio of diffusivities may be arbitrarily close to unity.

2.3.1 A Spatial Scale: Critical Wavenumber k_c. At the bifurcation point the critical wavenumber is given by

$$k_c = \sqrt{\frac{\gamma(d_c f_u + g_v)}{2d_c}}, \tag{2.35}$$

from which we see that k_c varies as $\sqrt{\gamma}$. Therefore the corresponding dimensional critical wavenumber is independent of the domain length and constitutes a characteristic scale, intrinsic to the system. Turing defined the related wavelength, the *chemical wavelength*, at marginal instability. For a finite bounded system, the critical wavenumber may be defined as the closest admissible wavenumber to k_c.

2.3.2 A Temporal Scale: Maximum Growth Rate λ_{max}. From the dispersion relation we can show that the linear prediction for the maximum growth rate λ_{max} is independent of the scaling parameter γ. We note that the occurrence of γ in equations (2.22)–(2.23) is such that we may consider $\lambda = \lambda(k^2/\gamma)$ with γ appearing nowhere else explicitly. Thus the curve $\lambda(k^2, \gamma)$ as a function of γ for different k is simply scaled along the γ axis, and the maximum value of the function does not change (see Figure 2.2). Hence λ_{max} is a function only of the kinetic parameters and the ratio of diffusivities and we may take $T_\lambda = 1/\lambda_{max}$ to define a characteristic timescale for pattern development. The reaction-diffusion equation was nondimensionalised to have a unit timescale for reaction, hence we expect $T_\lambda \sim \mathcal{O}(1)$. In Table 2.1, values of T_λ (and equivalently, growth rates λ_{max}) calculated for different d for Schnakenberg kinetics are presented, showing that the timescale for pattern formation is reduced as d decreases from d_c. This timescale is intrinsic to the linearised equations and thus to the initial time evolution of the solution, while being independent of the scaling parameter.

d	0.1	0.05	0.01
λ_{max}	0.0572	0.263	0.547
T_λ	17.50	3.80	1.83

TABLE 2.1 Timescale for linear pattern growth $T_\lambda = 1/\lambda_{max}$ (in nondimensional units) for different values of d, the ratio of diffusivities, calculated from the dispersion relation for Schnakenberg kinetics (illustrated in Figure 2.2). Equivalently, λ_{max} represents a pattern growth *rate*.

2.4 Nonlinear Bifurcation Analysis

As we have shown, linear stability theory serves to analyse the response of the homogeneous steady state of a dissipative system to infinitesimal perturbations, allowing determination of the critical conditions for the onset of instability. Turing considered reaction-diffusion equations with linear kinetics. In his paper he sidesteps the issue of unbounded exponential growth by proposing that any such linear model is only applicable to the initial stages of patterning of a real chemical system, and that bounded steady amplitude will be achieved outside the range of applicability of the model. However, nonlinear terms in realistic kinetic schemes can be shown to bound the solution to finite values.

The analytical investigation of instabilities usually proceeds by identifying a control parameter in the system (here, for example, one of the kinetic parameters, the ratio of diffusion coefficients, d, or the scaling parameter, γ) which may be varied until the homogeneous steady state loses stability to a particular heterogeneous solution. The exchange of stability occurs at the bifurcation point, where the curve $\mathcal{R}e\,\lambda$ first moves into the positive half-plane. Close to bifurcation the structure of the long-time solutions may be determined by a nonlinear bifurcation analysis, which we describe here. Such analyses are described as *weakly nonlinear* as the perturbation procedure operates about the critical point of linear stability theory [133]. The method considers *primary* bifurcation branches: nontrivial solutions which bifurcate from the homogeneous steady state (the location of which does not depend on the bifurcation parameter). The approach that we take follows the discussion in the book by Grindrod [46] (see also [93, 5]).

2.4.1 Multiscale Expansion Method. We choose the ratio of diffusivities, d, as the bifurcation parameter and we wish to examine the dependence of solutions on γ. From section 2.3 we see that bifurcation to a spatially heterogeneous state occurs when d passes through the critical value $d = d_c$. As d decreases through d_c we anticipate a pitchfork-type bifurcation for the state variable $\mathbf{c}(x,t)$, with the homogeneous steady state $\mathbf{c}_s$ losing stability to two bifurcating branches corresponding to the two polarities available to the heterogeneous solution.

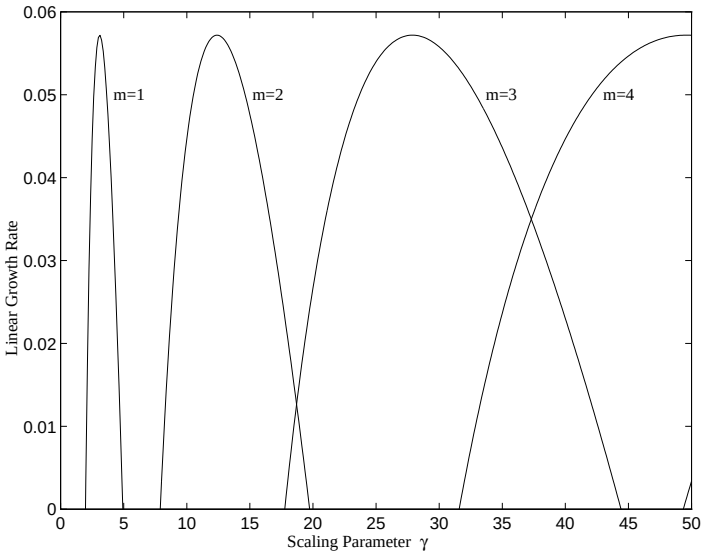

FIGURE 2.2 Real part of linear growth rate λ plotted as a function of scaling parameter γ for the first four linear modes, showing that the maximum growth rate is independent of mode m, where $k_m = m\pi$. We use Schnakenberg kinetics, with $a = 0.1$, $b = 0.9$ and ratio of diffusivities $d = 0.1$ such that an interval of stability is observed for $\gamma \in [5, 8]$.

The time evolution of the bifurcating solutions may be investigated by introducing a small parameter ϵ, where $0 < \epsilon \ll 1$. We set $d_c - d = \epsilon^2$ so that the system lies just inside the region of linear instability and then consider a multiscale expansion in time. Generally the control parameter d is expanded as a series in increasing powers of ϵ, but here we anticipate the pitchfork form for the bifurcation for which the second power is the natural choice. However, the analysis would seek out this expansion had the leading power been initially undetermined.

The Taylor expansion of $\lambda(k^2, d)$ about d_c gives

$$\lambda(d) = \lambda(d_c) - \epsilon^2 \frac{\partial \lambda}{\partial d}\bigg|_{d=d_c} + \mathcal{O}(\epsilon^4) \tag{2.36}$$

with λ a decreasing function of d. The first term on the right-hand side vanishes by the definition of the bifurcation point, giving linear growth $\exp(\lambda t) \sim \exp\left(\mathcal{O}\left(\epsilon^2\right) t\right)$. This suggests that there are three timescales for pattern formation in the static problem:

- $t = \mathcal{O}(1)$: the linear regime in which small amplitude linear modes grow from initial data,
- $t = \mathcal{O}(1/\epsilon^2)$: the nonlinear regime in which the modes interact through the nonlinearities, and
- $t \to \infty$: in which the long-time steady state pattern is achieved.

To investigate the nonlinear regime we introduce the long timescale $\tau = \epsilon^2 t$, and assume that t and τ are independent variables. Then $\partial \mathbf{c}/\partial t$ becomes $\partial \mathbf{c}/\partial t + \epsilon^2 \partial \mathbf{c}/\partial \tau$. Again, in the most general case, we could include a series of timescales, $t = t_0 + \epsilon t_1 +$

$\epsilon^2 t_2 + \ldots + \epsilon^n t_n + \ldots$, and determine which of those were relevant to the problem in the course of the analysis.

Confinement to the finite domain allows the system under investigation to be categorised as one of *small spatial extent*, i.e. the product $Lk \sim \mathcal{O}(1)$. The spectrum of allowed wavenumbers, k_m, is discrete and so for d close to d_c we may consider that only one mode (or a small number of modes at worst) will destabilise the homogeneous state. We will assume that the region of the dispersion relation for which $\mathcal{R}e\,\lambda > 0$ contains only one admissible mode. Therefore we suppose that the corresponding spatial eigenfunction $\phi_m(x)$ determines the spatial dependence in the dominant part of the solution in the nonlinear regime. For systems of large or infinite spatial extent one must consider initially undetermined spatial scalings which results in an envelope-type modulation of the spatial dependency through a *phase* equation [93]. We will assume that pattern evolution in the nonlinear regime is over the timescale of τ (so that we can consider t and τ to be independent) and seek solutions of the form

$$\mathbf{c} = \mathbf{c}_0 + \sum_{n=1}^{\infty} \epsilon^n \mathbf{c}_n(x, t, \tau) \tag{2.37}$$

for which the $\mathbf{c}_n = (u_n, v_n) \sim \mathcal{O}(1)$ are orthogonal. We expand the kinetic terms $\mathbf{R}(\mathbf{c}, p)$ as a Taylor series and, on rearranging, find that the $\mathcal{O}(1)$ solution (the homogeneous solution $\mathbf{c}_0 = \mathbf{c}_s$) drops out of both sides of the equation. We are left with linear equations in (u_n, v_n) for each order of ϵ^n

$$\mathcal{L} \cdot \begin{pmatrix} u_n \\ v_n \end{pmatrix} = \mathcal{Q}_n \tag{2.38}$$

in which $\mathcal{L}$ is the linear differential operator defined by

$$\mathcal{L} = \mathcal{I}\frac{\partial}{\partial t} - \frac{1}{\gamma}\mathcal{D}_c \frac{\partial^2}{\partial x^2} - \mathcal{A} \tag{2.39}$$

where $\mathcal{A}$ is the stability matrix given by equation (2.13) and contains the linear terms from the Taylor expansion of $\mathbf{R}$, and $\mathcal{D}_c = \mathrm{diag}[1, d_c]$. The $\mathcal{Q}_n$ contain the higher order (nonlinear) terms from $\mathbf{R}$ and the remaining terms from the expansion:

$$\mathcal{Q}_1 = \mathbf{0} \tag{2.40}$$

$$\mathcal{Q}_2 = \frac{1}{2}u_1^2 \mathbf{R}_{uu} + u_1 v_1 \mathbf{R}_{uv} + \frac{1}{2}v_1^2 \mathbf{R}_{vv} \tag{2.41}$$

$$\begin{aligned} \mathcal{Q}_3 = &- \begin{pmatrix} 0 \\ 1 \end{pmatrix} \frac{1}{\gamma}\frac{\partial^2 v_1}{\partial x^2} - \frac{\partial \mathbf{c}_1}{\partial \tau} \\ &+ u_1 u_2 \mathbf{R}_{uu} + (u_1 v_2 + u_2 v_1)\mathbf{R}_{uv} + v_1 v_2 \mathbf{R}_{vv} \\ &+ \frac{1}{6}u_1^3 \mathbf{R}_{uuu} + \frac{1}{2}u_1^2 v_1 \mathbf{R}_{uuv} + \frac{1}{2}u_1 v_1^2 \mathbf{R}_{uvv} + \frac{1}{6}v_1^3 \mathbf{R}_{vvv} \end{aligned} \tag{2.42}$$

$$\mathcal{Q}_4 = \ldots$$

where $\mathbf{R}_{uu}, \mathbf{R}_{uv}, \ldots$ denote component-wise partial differentiation of the reaction vector field $\mathbf{R}(\mathbf{c}, p)$ evaluated at the kinetic steady state $\mathbf{c}_s = (u_s, v_s)$. Such terms are functions of $(\mathbf{c}_s, p)$ only, and many of these terms will in fact be zero, for a particular kinetic scheme.

At $\mathcal{O}(\epsilon)$ we recover the linear approximation for the chosen boundary conditions, which is given by

$$\left[\mathcal{I}\frac{\partial}{\partial t} - \frac{1}{\gamma}\mathcal{D}_c\frac{\partial^2}{\partial x^2} - \mathcal{A}\right]\mathbf{c}_1 = \mathbf{0}. \tag{2.43}$$

Considering the linear analysis above, we have that the general solution of this equation takes the form

$$\mathbf{c}_1(x,t,\tau) = \sum_{m=0}^{\infty} \mathbf{a}_m(\tau)\ \exp\left(\lambda_m t\right)\cos\left(k_m x\right). \tag{2.44}$$

However, the condition of small spatial extent allows us to neglect all k_m except the destabilising mode, k_f say. The functions $\mathbf{a}_m(\tau)$ contain the dependence on the slow time τ. As t becomes large and for $\lambda(k_f^2) \sim 0$ for $d \sim d_c$, the solution to equation (2.43) becomes

$$\mathbf{c}_1(x,\tau) = a(\tau)\begin{pmatrix} \bar{u} \\ \bar{v} \end{pmatrix}\cos\left(k_f x\right) \tag{2.45}$$

where $\bar{\mathbf{c}} = (\bar{u}, \bar{v})$ is the nullvector, and $\lambda(k_f^2)$ the relevant eigenvalue, of the matrix

$$\mathcal{A} - \frac{k_f^2}{\gamma}\mathcal{D}_c. \tag{2.46}$$

The signs of $\bar{u}$ and $\bar{v}$ are the same for pure kinetics and are opposite for cross kinetics, consistent with the concentration profile polarities in the two cases. The solution amplitude to first order, $a(\tau)$, is yet to be determined in the analysis.

At $\mathcal{O}(\epsilon^2)$, after substituting the expressions calculated for u_1 and v_1, the components of $\mathcal{Q}_2$ will contain terms with spatial dependence $\cos^2(k_f x)$. The Fredholm Alternative Theorem [60] guarantees the existence and uniqueness of solutions of the linear equation $\mathcal{L}\mathbf{c}_2 = \mathcal{Q}_2$ if the vector $\mathcal{Q}_2$ is orthogonal to solutions $\mathbf{c}^*$ of the homogeneous adjoint equation

$$\mathcal{L}^*\mathbf{c}^* = \mathbf{0}. \tag{2.47}$$

The only solutions of the adjoint problem (with appropriate boundary conditions) have spatial dependence $\mathbf{c}^* = \mathbf{b}\cos(k_f x)$. Here we may employ the trigonometric identity $2\cos^2\theta = \cos 2\theta + 1$ to show that, under an appropriately defined inner product, $\mathcal{Q}_2$ is always orthogonal to $\mathbf{c}^*$. Hence, from the solution of the homogeneous equation, (u_2, v_2) will be determined only up to the addition of constant multiples of u_1 and v_1 respectively.

On substitution of the expressions for $\mathbf{c}_1$ and $\mathbf{c}_2$ into (2.42) for the linear equation (2.38) with $n = 3$, we arrive at the $\mathcal{O}(\epsilon^3)$ equation. On application of the Fredholm

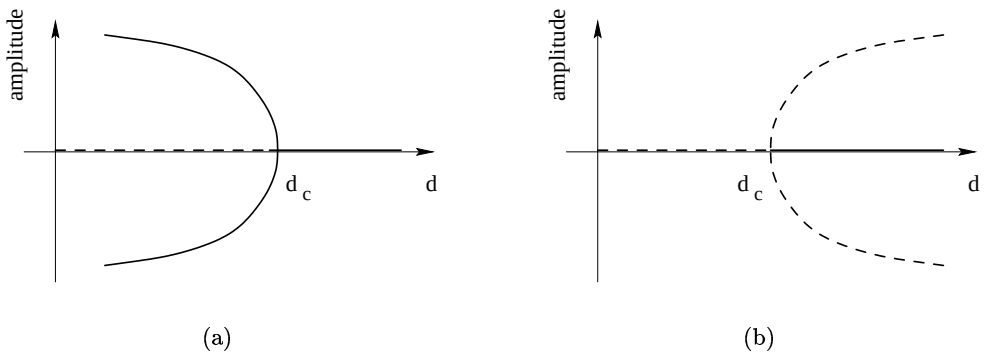

FIGURE 2.3 Schematic bifurcation diagrams for the pitchfork bifurcation (2.49) showing (a) supercritical and (b) subcritical bifurcations. Solid lines represent stable solutions and dotted lines unstable solution branches.

Alternative Theorem we find that the null vector of the adjoint $\mathbf{c}^*$ is no longer automatically orthogonal to $\mathcal{Q}_3$. We require orthogonality for solutions of the $\mathcal{O}(\epsilon^3)$ problem, giving a *solvability condition* by which secular terms (those with spatial dependence $\cos(k_f x)$) in $\mathcal{Q}_3$ are suppressed. The structure of this condition leads to an equation for the amplitude $a(\tau)$ of the form

$$\frac{da}{d\tau} = P_1\, a(\tau) + P_3\, a^3(\tau). \tag{2.48}$$

2.4.2 Amplitude Equation. Equation (2.48) is the *amplitude equation* for the pitchfork bifurcation. The absence of quadratic terms is due to symmetries in the spatial freedom of the system (see Nicolis [93]) and ensures that the two nontrivial steady state solutions are symmetric, corresponding to the two polarities identified for the linear problem. Writing in terms of the physical parameters, $\epsilon = \sqrt{d_c - d}$ and time $t = \tau/\epsilon^2$, the rescaled amplitude $z(t) = \epsilon a(t)$ satisfies

$$\frac{dz}{dt} = (d_c - d)\, P_1\, z(t) + P_3\, z^3(t) \tag{2.49}$$

with three fixed points

$$z_0 = 0 \tag{2.50}$$

$$z_\pm = \pm\sqrt{(d - d_c)\,\frac{P_1}{P_3}} \tag{2.51}$$

the first of which is identified with the homogeneous steady state of the reaction-diffusion equation. The stability of the branches is easily deduced from a linear stability analysis of the amplitude equation. The homogeneous steady state z_0 is stable for $d > d_c$ when $P_1 > 0$, which must therefore be the case for the Turing bifurcation. Then if $P_3 < 0$, solutions $z_\pm$ exist and are stable for $d < d_c$, giving a supercritical bifurcation as shown schematically in Figure 2.3(a), while for $P_3 > 0$ solutions $z_\pm$ exist for $d > d_c$ and are unstable, the subcritical case, shown in Figure 2.3(b). All of the

kinetic systems that are studied in this thesis give rise to supercritical bifurcations.

The asymptotic approximation to the long-time steady heterogeneous solution of the reaction-diffusion equation is given by

$$\mathbf{c}(x) = \begin{pmatrix} u(x) \\ v(x) \end{pmatrix} = \begin{pmatrix} u_s \\ u_s \end{pmatrix} \pm \sqrt{\left|(d_c - d)\frac{P_1}{P_3}\right|} \begin{pmatrix} \bar{u} \\ \bar{v} \end{pmatrix} \cos(k_f x) + \mathcal{O}(d_c - d). \quad (2.52)$$

We may deduce the influence of the scaling parameter γ in the nonlinear analysis without recourse to explicit calculation of P_1 and P_3 and the null vectors for a specific reaction scheme, all of which may depend on γ. One quickly sees that γ appears only in $\mathcal{L}$ and $\mathcal{Q}_3$ and hence will be present in the expression (2.52), and in particular the amplitude $z_\pm$, only as the quotient k_f^2/γ. Therefore γ will have the same influence as described in section 2.3.2 for the linear analysis. The maximum amplitude for all choices of mode k_f as γ is varied will be the same. Thus we expect all primary solution branches to have the same form, appropriately scaled along the γ axis for different k_f, and this is illustrated with concrete numerical examples below. Next we discuss the implications of this symmetry on the pattern modes.

2.4.3 Symmetries of the Steady State Patterns. Steady heterogeneous solutions to the reaction-diffusion equations exhibit a symmetry in the relationship between different primary bifurcation branches, and thus between patterns of different mode. This symmetry will prove to be a useful tool in examining patterns formed on the growing domain, where we show that the arguments may be extended to the full PDE system. To illustrate the symmetry we construct periodic solutions for the steady state equations from solutions of lower mode. To simplify notation we will consider a scalar reaction-diffusion equation, however, the result applies equally well to systems, where heterogeneous patterns form through the Turing instability. Recently this symmetry has also be noticed by Nishiura and Ueyama [95] and has previously been described for the steady state problem by Kevrekidis and Brown [63], who extend the arguments considerably to encompass the prediction of secondary ('mixed-mode') branches.

We consider solutions to the steady state problem

$$0 = \frac{1}{\gamma}\frac{\mathrm{d}^2 c}{\mathrm{d}x^2} + R(c), \quad x \in [0,1] \quad (2.53)$$

where $\gamma = \omega L^2/D$, with zero flux boundary conditions

$$\frac{\mathrm{d}c}{\mathrm{d}x} = 0, \quad x = 0, 1. \quad (2.54)$$

Let us suppose that for $\gamma = \gamma_1 > \gamma_c$ the solution consists of the primary mode m, where the linearised equations have solution with heterogeneity $\cos(m\pi x)$. We can construct new solutions by scaling, translating and reflecting this pattern. To obtain

a new pattern, $q_{2m}(x)$, of mode $2m$ we use the tent map transformation

$$p_2(x) = \begin{cases} 2x, & 0 \le x < \frac{1}{2} \\ 2\,(1-x)\,, & \frac{1}{2} \le x \le 1 \end{cases} \tag{2.55}$$

such that

$$q_2(x;\gamma_1) \equiv c(p_2(x);\gamma_1), \tag{2.56}$$

which satisfies the equation

$$0 = \frac{1}{4\gamma_1}\frac{\mathrm{d}^2 q_2}{\mathrm{d}x^2} + R(q_2). \tag{2.57}$$

The transformation $p_2(x)$ ensures that the zero flux conditions are satisfied at the boundaries of the unit interval, and so $q_2(x;\gamma)$ is a solution of the *same* equation as $c(x;\gamma_1)$ when $\gamma = 4\gamma_1$, i.e. when the domain length is doubled. The transformation has discontinuous derivative at the point $x = 1/2$, however, $q_2(x)$ has zero gradient here by construction and is, therefore, twice continuously differentiable. Patterns constructed under the transformation $p_2(x)$ from odd modes maintain the same polarity as the original pattern mode. Just as easily, patterns with the opposite polarity are constructed by the complementary transformation

$$\overline{p}_2(x) = \begin{cases} 1-2x, & 0 \le x < \frac{1}{2} \\ 2x-1, & \frac{1}{2} \le x \le 1 \end{cases} . \tag{2.58}$$

It is straightforward to see that a general transformation $p_m(x)$ can be defined in a similar manner to generate a pattern of mode m on the interval $[0,1]$ from the first mode $m = 1$, and to find the corresponding equation. In general $q_m(x;\gamma) \equiv c(p_m(x);\gamma)$ satisfies the same equation as $c(x;\gamma_1)$ when $\gamma = m^2\gamma_1$, or otherwise, when the domain length increases by a factor m. This explains the structure of Figure 2.2, where linear growth rates for different mode are simply scaled along the γ axis, and is similarly reflected in Figure 2.1 where the intersections of instability line up for modes related by these transformations.

2.5 Pattern Selection

As the control parameter, for example d or γ, is moved further past the bifurcation point, d_c or γ_c, an increasing range of solutions to the linear problem are admissible as growing linear modes. Furthermore, ranges of instability of the homogeneous steady state to different modes overlap increasingly as the system moves further from the critical point (see Figure 2.1 for the effect of decreasing d on the intervals in γ). The effect on pattern selection is illustrated in Figure 2.4. The conspicuous curves, which comprise sets of points from individual numerical simulations, represent steady state patterns of the same mode (we do not distinguish between the two polarities), with amplitude changing as γ increases. We draw attention to several notable features. Firstly, as predicted by linear and nonlinear analysis alike, the maximal amplitude

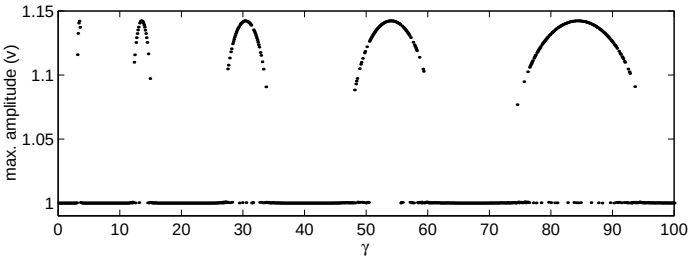

(a)

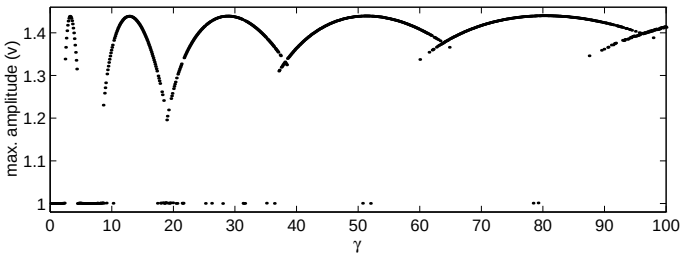

(b)

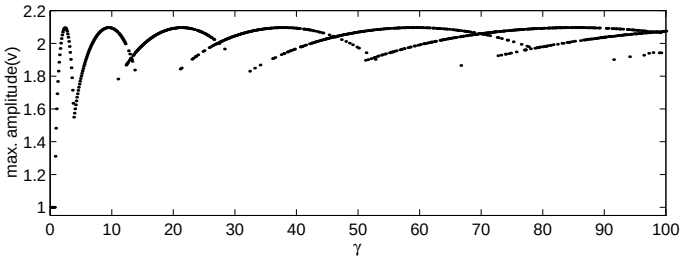

(c)

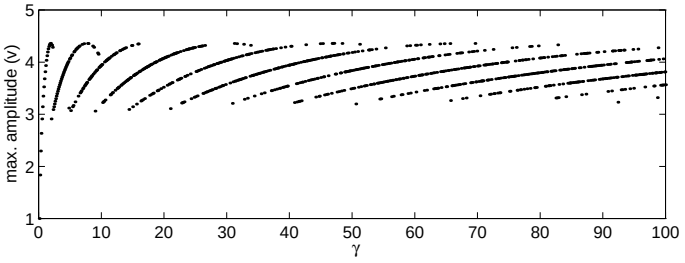

(d)

FIGURE 2.4 The disappearance of intervals of stability in γ and increase of multiplicity of solutions as d is decreased ($\epsilon = \sqrt{d_c - d}$ is increased), where (a) $d = 0.115$ ($\epsilon \approx 0.045$), (b) $d = 0.1$ ($\epsilon \approx 0.13$), (c) $d = 0.05$ ($\epsilon \approx 0.26$) and (d) $d = 0.01$ ($\epsilon \approx 0.38$). Each point shows the final steady amplitude for the activator v on a domain of fixed size, where the value of the scaling parameter γ is held constant during numerical simulation (the homogeneous steady state has amplitude $v = 1$). The initial conditions for each data point consist of random perturbations around the homogeneous steady state, of amplitude 1%. We have used Schnakenberg kinetics with $a = 0.1$, $b = 0.9$.

(as γ varies) for each mode is the same, independent of the wavenumber. Indeed the simple scaling of the branches for different modes can be discerned, illustrating the symmetry that we have described.

Close to the bifurcation point (when ϵ is smallest, in Figure 2.4(a)) there are intervals of stability of the homogeneous steady state between regions where a finite amplitude pattern is realised. These intervals rapidly disappear as d is decreased and are replaced by increasing overlap of solution branches. Where overlap occurs in the figure, two or more different steady solutions have been generated for domains of (approximately) the same size, but from different initial data. Here, in the competition between different growing modes, the initial data dominates the pattern selection (through the components of $\mathbf{y}_m$ in the linear analysis), rather than the linear growth rate. This dependence on the initial conditions clearly increases as d recedes from its critical value. In the nonlinear regime, competition between modes may be described using amplitude equations, as derived in the previous section. This approach is particularly appropriate for investigating the nonlinear interactions between modes in two-dimensional (and higher) spatially-distributed systems, where the selection between patterns of different planforms may be predicted. This is discussed further in Chapter 6.

2.5.1 Multiplicity of Solutions: the Robustness Problem. The distribution of steady patterns achieved for different sets of initial conditions on domains of fixed size, corresponding to fixed values of γ, is shown in Figure 2.5. From the dispersion relation we have calculated the value of γ for which different modes achieve maximum linear growth rate, calling these modes $m_\star$. We have performed repeated numerical simulations with these values of γ for different sets of random initial data and compiled tables of the relative frequency of occurrence of different steady pattern modes for two values of d, namely $d = 0.05$ in Figure 2.5(a) and $d = 0.01$ in Figure 2.5(b). Thus for (b) the distributions show the relative frequencies for the different solution branches found in Figure 2.4(d), at three different values of γ (and similarly (a) corresponds to Figure 2.4(c)). Two results are immediately apparent: firstly, the mean of the distributions tends towards lower modes than the linearly predicted fastest growing mode $m_\star$, becoming progressively lower for larger γ, and secondly the width of the distribution is smaller for d nearer d_c and increases with γ. Thus for different sets of initial data an increasingly wide range of pattern modes my be generated as the domain length increases. Put otherwise, for larger domain lengths the initial conditions must be controlled with increasing sensitivity to reliably pick out one particular mode.

This encapsulates the *robustness* problem for reaction-diffusion pattern formation. In order to generate patterns reliably, conditions such as the initial data and the size of the domain must be closely controlled. This has been a major source of criticism of the application of reaction-diffusion models to those biological situations in which a specific number of pattern units (spatial oscillations) must be reliably produced.

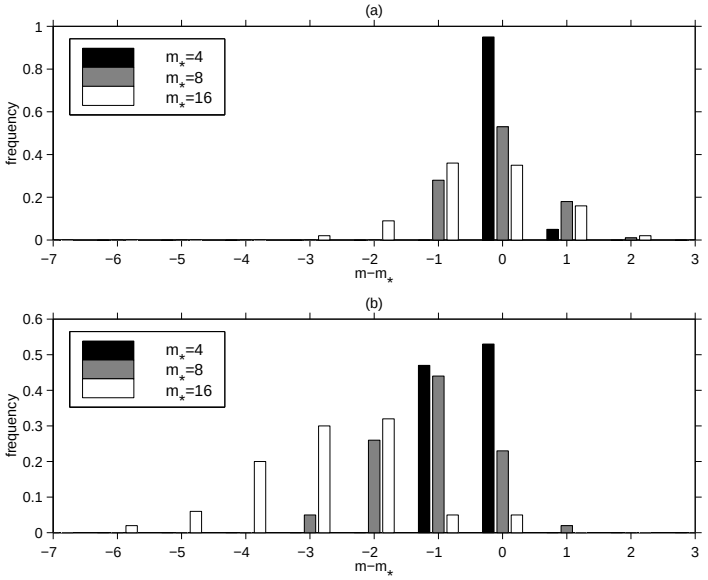

FIGURE 2.5 Relative frequency of occurrence of different modes m on domains of various fixed sizes from random initial data. Each figure shows frequency distributions corresponding to three values of γ, each chosen so that a particular mode $m_\star$ has maximal linear growth rate. These values of γ, calculated from the dispersion relation (for Schnakenberg kinetics), depend on d. In each case we plot the relative frequency (from a sample of 100) against $m - m_\star$, the distance in mode number of the steady pattern generated, m, from the linear prediction, $m_\star$. For (a) $d = 0.05$ and we take $\gamma = 33.4$ (black) where $m_\star = 4$ has fastest linear growth rate, $\gamma = 133.4$ (grey) for which $m_\star = 8$ is fastest growing and $\gamma = 533.4$ (white) for $m_\star = 16$. In (b) $d = 0.01$ and the values of γ are 13.3, 53.2 and 212.9 respectively. We note that the two pattern polarities were observed in roughly equal numbers (data not presented).

The problem is further compounded in higher spatial dimensions where the domain geometry must also be sensitively controlled, and where many more pattern modes tend to be admissible for any particular domain size and geometry.

2.5.2 Mechanisms of Pattern Selection. For equilibrium systems the pattern selection problem is solved by minimising a free energy functional and, at least in principle, solutions evolve towards the lowest energy state. No such general method is available for nonequilibrium systems. We have considered the role of domain size (and geometry) and of the initial data, which might be deemed *static* effectors of pattern selection. A full discussion and examples from other pattern forming instabilities is presented in the review article by Cross and Hohenberg [21]. Arcuri and Murray [3] report on a study of the influence of boundary conditions on the sensitivity of heterogeneous pattern to various initial conditions. Dillon *et al.* [26] investigate mixed scalar boundary conditions on a one-dimensional domain, and find that Dirichlet conditions for one but not both species at the boundaries reduces the sensitivity on domain scale and initial conditions. In general the boundaries are of greater importance in systems

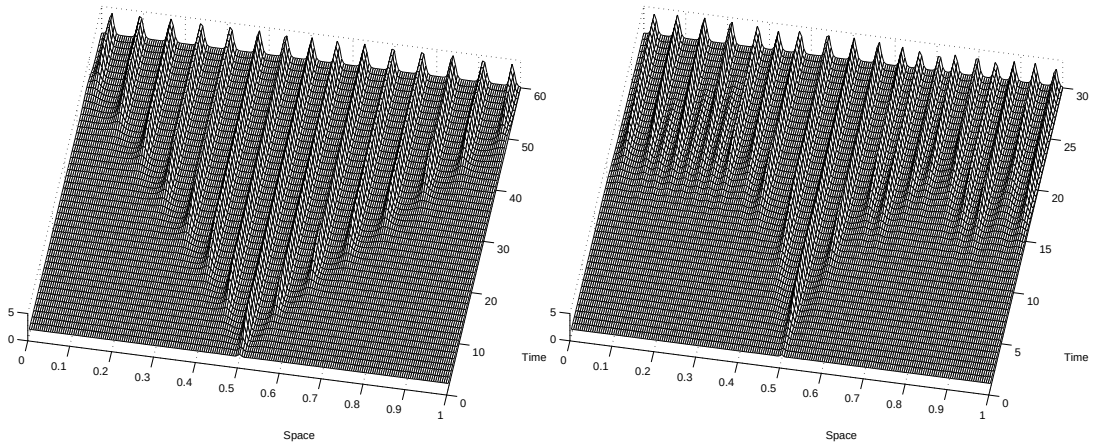

(a) (b)

FIGURE 2.6 Pattern selection behind a travelling front, initiated in the centre of the domain with (a) homogeneous conditions elsewhere and (b) random noise on the domain, $v_0(x) = \big(1+0.01\eta(x)\big)v_s$ where $\eta(x) \in [-1,1]$ is a random variable. For these simulations we use Schnakenberg kinetics with $a = 0.1$, $b = 0.9$, $d = 0.01$ and $\gamma = 1600$.

of small spatial extent and zero flux conditions are found to have the weakest influence on pattern selection.

Similarly there are *dynamic* processes which may determine the final steady pattern. For parameters that vary with time the trajectory taken through parameter space may contribute to pattern selection. For small variations in parameters the solution may be expected to adiabatically follow a stable solution branch of the steady state problem. Where the parameter variation is sufficiently great that the solution moves between solution branches the manner of transitions between the branches becomes important. The bifurcation structure will determine whether or not there is a continuous adiabatic connection between stable branches. These ideas are discussed below in light of results for pattern formation on growing domains.

Murray [88] suggests that the mechanism of initiation of pattern formation on the domain may determine the mode selected. From an initial disturbance at some location on an otherwise homogeneous domain, spatially periodic pattern spreads out to fill the domain behind a 'travelling wave of initiation'. This is demonstrated in Figure 2.6(a). The wavelength of the pattern may be calculated and lies within the linearly destabilising band. If the domain is bounded (and especially if the domain is small) then boundary effects will also affect the final wavelength, as the pattern relaxes to accommodate the conditions imposed there. However, this selection mechanism relies on the initial perturbation being restricted to some small region, and for even a low level of random noise elsewhere on the domain the wavelength of the final pattern cannot be reliably predicted, as demonstrated in Figure 2.6(b).

2.5.3 Reflection and Splitting of Travelling Pulses in the Gray-Scott Model. In general, reaction-diffusion systems can display a rich variety of spatio-temporal phenomena in response to *large amplitude* perturbations. The nature of the kinetic terms plays the major role in determining the solution behaviour. In this thesis we will consider only kinetic schemes which have a single steady state, such that $\mathbf{c}_s$ is the unique solution of $\mathbf{R}(\mathbf{c}_s, p) = \mathbf{0}$. However, for bistable systems an additional pair of solutions, one stable and the other linearly unstable, appear in a saddle-node bifurcation as some kinetic parameter varies. The Gray-Scott model [45] (see Appendix A.2) is an example of a kinetic scheme which, for suitably chosen parameters, demonstrates bistability, and has been extensively studied. In the vicinity of the bistable regime, several interesting spatio-temporal phenomena have been reported. Pearson [109] first identified self-replication of spot-like patterns in two-dimensional numerical simulations of the Gray-Scott model, amongst various other behaviours, some exhibiting spatio-temporal chaos (typically from the interaction of Turing and Hopf modes). This behaviour was observed for sufficiently large perturbation away from the trivial homogeneous steady state, and in a parameter regime in the vicinity of both a Hopf bifurcation in the kinetics, and a subcritical Turing bifurcation for the nontrivial steady state. Many of the patterns reported by Pearson had previously or were subsequently identified in chemical experiments on the FIS reaction by Lee, Swinney and co-workers [70, 71] (reviewed in [72]).

Corresponding phenomena in one-dimensional systems have been studied numerically by Petrov *et al.* [112], Reynolds *et al.* [115] and Rasmussen *et al.* [114]. Depending on the precise location in parameter space (while remaining in the vicinity of the curve bounding the bistable region) these authors have reported that finite initial perturbations may produce various behaviours. Travelling pulses which are reflected from zero flux boundaries are found in a region for which there is a unique steady state, reproduced in Figure 2.7(a). Also it is found that these pulses are reflected during collisions with other pulses [112]. Wave splitting (or self-replication of pulses), illustrated in Figure 2.7(b), is observed for small enough d in the bistable region and, for parameters for which there is a single stable branch, in the vicinity of the saddle-node bifurcation. For the latter case Petrov *et al.* have suggested that in this region the kinetics show excitable dynamics, where small perturbations decay exponentially to the globally stable steady state but sufficiently large perturbations result in long excursions through the phase space before returning to the fixed point. During this excursion the system is in a refractory (non-excitable) state (for a discussion see, for example, Murray [88]). They suggest that by decreasing d the wave back becomes decreasingly refractory, until finally it excites a secondary wave which moves off in the opposite direction. However, Nishiura and Ueyama [95] have shown that the splitting phenomena may be recovered for d near unity, by judicious choice of the kinetic parameters.

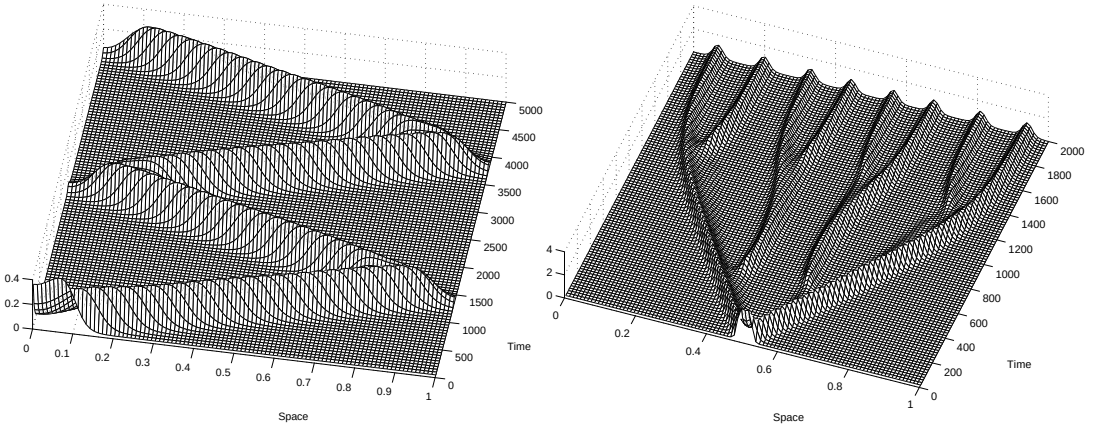

(a) (b)

FIGURE 2.7 Dynamic phenomena in the Gray-Scott model: (a) travelling wave reflection at zero flux boundaries (parameters from [95]), with $F = 0.025$, $k = 0.0544$ (monostable region) and $d = 0.5$ with $\gamma = 12500$. (b) wave-splitting (parameters from [115]) with $F = 0.059$, $k = 0.02$ (bistable region) and $d = 0.01$ with $\gamma = 3600$.

Several authors have investigated the pulse-splitting phenomenon in the Gray-Scott model analytically. Osipov and Severtsev [97] discuss splitting and periodic patterns on infinite domains. Reynolds *et al.* [116] present a heuristic explanation for self-replication of spots and analyse equations of motion for travelling pulses in the limit of small d. Nishiura and Ueyama provide an argument based on underlying 'hidden' symmetries in the bifurcation structure of such reaction-diffusion equations. The authors show that the transient dynamics from the initial perturbation move in the vicinity of saddle-node bifurcations for steady Turing structures, which is reflected in the splitting process observed. Finally we note that although there is no supercritical Turing bifurcation for either solution branch, the transient splitting of travelling pulses may lead to steady Turing-type structures, which appear in a saddle-node bifurcation rather than through DDI, as shown in Figure 2.8(a). However, long-time behaviour may also give oscillating 'mixed mode' behaviour, as in the example shown in Figure 2.8(b). In order to excite these spatio-temporal phenomena a sufficiently strong initial perturbation is required to escape exponential relaxation back to the trivial homogeneous state. Furthermore, these behaviours are restricted to narrow regions of parameter space (in the vicinity of the bistable region) for models such as the Gray-Scott system which have a highly complicated bifurcation structure. As we saw previously (Figure 2.6(a)), large initial perturbations for the simpler Schnakenberg system do not produce pulse splitting. Similar phenomena may, however, be generated for reaction-diffusion equations with Schnakenberg kinetics (and for other comparable systems) when pattern formation is driven by domain growth. In the following chapter we derive the governing equations for reaction and diffusion on a growing domain

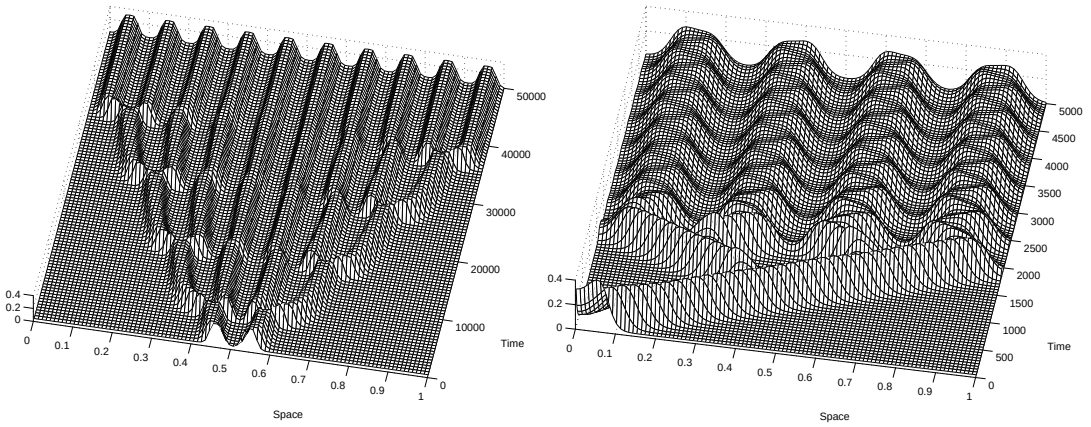

(a) (b)

FIGURE 2.8 Establishment of (a) steady and (b) oscillatory heterogeneous patterns for the Gray-Scott model with (a) $F = 0.04$, $k = 0.06075$ (parameters from [95]) and (b) $F = 0.025$, $k = 0.0542$, for both of which the kinetics have a unique steady state (but are close to the bistable region) and $d = 0.5$. In (a) $\gamma = 2 \times 10^5$ and in (b) $\gamma = 2.5 \times 10^4$.

and in the remainder of the thesis we go on to analyse pattern formation subject to underlying domain growth.

3. Incorporation of Domain Growth

In this chapter the evolution equations describing reaction and diffusion of chemicals within a growing domain are derived and developed to consider several different examples of domain growth. These examples are examined in detail in the remainder of this thesis.

Several assumptions will be made about the growing domain. The domain is not treated as a realistic biological tissue: rather, we consider a general framework which will allow for subsequent inclusion of a detailed description of the properties of any specific tissue. Consequently the derivation of the governing equation is considered as a problem in kinematics, and no constitutive equations are proposed. Specifically, it is assumed that the domain undergoes deformation and expansion with no accompanying change in density. Growth consists of local directional volume expansion (possibly nonuniform) resulting in convection of material. Firstly we look at previous attempts to investigate reaction and diffusion on growing domains.

3.1 Previous Models and Results

Previously several studies have incorporated some form of parameter time dependence into reaction-diffusion equations and their numerical simulation to model pattern formation on a growing domain. This has been done by a variety of *ad hoc* means. In their paper on fish skin patterns, Kondo and Asai [64] do not model growth as such but increase the numerical grid mesh spacing during a computation. Bunow *et al.* [10] investigate pattern formation on two-dimensional geometries for the imaginal wing disk of *Drosophila* using a similar technique in a finite element calculation. Several other authors have performed similar numerical computations. Varea *et al.* [127] argue that domain growth simply reduces the effective diffusion and assume $D(t) = D_0/(\alpha t)^2$, where domain length L is proportional to time t.

In their influential paper, which seems to be the standard reference for reaction-diffusion on growing domains, Arcuri and Murray [3] propose a similar approach, suggesting that the domain growth changes the relative strengths of reaction and diffusion, as described by the dimensionless scaling parameter γ (see also the book by Murray [88]). The authors choose to scale the time variable with γ so that it appears explicitly in the reaction-diffusion equation multiplying the reaction term. The scaling parameter is then assigned a specific time dependence and the equation subsequently studied is

$$\frac{\partial \mathbf{c}}{\partial t} = \mathcal{D}\frac{\partial^2 \mathbf{c}}{\partial x^2} + \gamma(t)\mathbf{R}(\mathbf{c}, p) \tag{3.1}$$

with appropriate boundary and initial conditions. Discussing the results of their simulations the authors note a 'strong tendency towards frequency-doubling', however,

this behaviour seems by no means universal in their model. Eilbeck [35] studied the same model, finding that it produced a succession of patterns with no missing modes. Jenkins [55] has also studied this equation for the two-species Schnakenberg kinetics, imposing time-dependence $\gamma(t) = \gamma_0(1+\rho t)$. He found that for small ρ (~ 0.005) with $d \sim 0.1$, and under various alternative growth functions (quadratic and exponential), a sequence of pattern modes was generated with no missing modes. Larger values for ρ (~ 100) served to delay the onset of patterning to large amplitude, after which the same incremental sequence was generated. No dependence of the sequence on the initial data was observed. However, Jenkins also found that moving d further from its critical value precipitated the omission of modes from the sequence of patterns. For extreme values an initial window of frequency-doubling behaviour was generated.

3.1.1 Domain Growth in a Model for Alligator Dentition. In a paper addressing the spatio-temporal positioning of teeth primordia in the alligator *Alligator mississippiensis*, Kulesa *et al.* [65] consider the problem of modelling an exponentially growing domain. The lower jaw of the alligator is modelled as a one-dimensional entity, with symmetry about the frontal midpoint (thus only half the jaw is considered), and with growth due to a constant strain rate σ. They argued as follows: for a domain of length $\ell(t)$ growing under constant strain,

$$\frac{\mathrm{d}\ell}{\mathrm{d}t} = \sigma\ell, \quad \ell(t) \propto \exp(\sigma t). \tag{3.2}$$

Kinetic terms are considered on a small segment of the domain of length y, ignoring the effects of diffusion. If Q is the quantity of reactant in length segment y then the concentration $c = Q/y$. The change in concentration at each location over a small time interval $(t, t+\Delta t)$, $\Delta t \ll 1$, is due to dilution from the growth ($y \to y + \Delta y$) and to the action of the kinetic terms over this time interval ($Q \to Q + \Delta Q$). Hence

$$\frac{\Delta Q}{y} = R(c)\Delta t \tag{3.3}$$

where $R(c)$ is the function describing production and degradation of the reactant. Growth at constant strain rate gives that $\Delta y = \sigma y \Delta t$ and so

$$\begin{aligned} \Delta c &= \frac{Q+\Delta Q}{y+\Delta y} - \frac{Q}{y} \\ &= \frac{1}{y}\left(\frac{Q + yR(c)\Delta t}{1+\sigma\Delta t} - Q\right). \end{aligned} \tag{3.4}$$

For $\sigma\Delta t \ll 1$ we have $(1+\sigma\Delta t)^{-1} = 1 - \sigma\Delta t + \mathcal{O}(\Delta t)^2$ and so

$$\begin{aligned} \Delta c &= \frac{1}{y}\left(yR(c)\Delta t - \sigma Q\Delta t + \mathcal{O}(\Delta t)^2\right) \\ &\approx (R(c) - \sigma c)\Delta t, \end{aligned} \tag{3.5}$$

which leads us, ignoring the diffusion term, to

$$\frac{\mathrm{d}c}{\mathrm{d}t} = \lim_{\Delta t \to 0} \frac{\Delta c}{\Delta t} = R(c) - \sigma c. \tag{3.6}$$

The diffusion coefficient, it is then supposed, scales with the square of the domain length, in the same manner as for Varea *et al.*, and the equation on the unit interval is then

$$\frac{\partial c}{\partial t} = \frac{d}{\gamma} \exp\left(-2\sigma t\right) \frac{\partial^2 c}{\partial x^2} + R(c) - \sigma c \tag{3.7}$$

Painter *et al.* [107] have used this approach to model the chemotactic response of cells to a reaction-diffusion prepattern on a growing domain.

Now we look at a general derivation for reaction and diffusion on a growing domain.

3.2 Kinematic Derivation

The equation for reaction and diffusion of a chemical C through a growing domain $\Omega(t)$ with boundary $\partial\Omega(t)$ may be derived from first principles. Considerations of conservation of matter in an elemental volume $V(t)$, which moves with the flow due to domain growth, give the equation for concentration $c(\mathbf{x}, t)$ at position $\mathbf{x}$ and time t as

$$\frac{\mathrm{d}}{\mathrm{d}t} \int_{V(t)} c(\mathbf{x}, t)\, \mathrm{d}\mathbf{x} = \int_{V(t)} \Big[-\nabla \cdot \mathbf{j} + R(c, p) \Big]\, \mathrm{d}\mathbf{x}. \tag{3.8}$$

where the integrals are over any (time-varying) elemental volume. The effect of other chemicals or factors in the tissue on the reaction rates are represented in the reaction term R by the variable $p(\mathbf{x}, t)$. Application of the divergence theorem is consistent, being instantaneously valid at all time. The Reynolds Transport theorem of elementary fluid mechanics (reproduced in Appendix B.1) gives

$$\frac{\mathrm{d}}{\mathrm{d}t} \int_{V(t)} c(\mathbf{x}, t)\, \mathrm{d}\mathbf{x} = \int_{V(t)} \left[\frac{\partial c}{\partial t} + \nabla \cdot (\mathbf{a}\, c) \right] \mathrm{d}\mathbf{x} \tag{3.9}$$

where $\mathbf{a}$ is the velocity field of the flow generated by the domain growth and

$$\frac{d\mathbf{x}}{dt} = \mathbf{a}(\mathbf{x}, t). \tag{3.10}$$

The usual argument as to the arbitrariness of the elemental volume requires that the equation hold everywhere on the growing domain $\Omega(t)$. The instantaneous flux $\mathbf{j}$ is taken to be due to Fickian diffusion, $\mathbf{j} = -D\nabla c$ where D is the diffusivity at constant density. The equations may be nondimensionalised as before, introducing no new dimensionless parameters. However, it is useful to point out that the incorporation of domain growth introduces (several) new timescales into the problem. This is discussed further below.

We introduce nondimensional variables $\bar{c}$ for the concentration and position $\bar{\mathbf{x}} = \mathbf{x}/L$, where L is a length scale. As before the reaction term is characterised by reaction rate ω and time is scaled according to $\bar{t} = \omega t$. Taking $\bar{\mathbf{a}} = \mathbf{a}/\omega L$, and dropping the

over-bars for notational convenience we recover the nondimensional evolution equation for $c(\mathbf{x}, t)$

$$\frac{\partial c}{\partial t} + \nabla \cdot (\mathbf{a}\, c) = \frac{d}{\gamma}\nabla^2 c + R(c, p) \tag{3.11}$$

$$\mathbf{x} \in \Omega(t), \quad t \in [0, \infty) \tag{3.12}$$

where $d = D/D_*$ for reference diffusivity D_* and $\gamma = \omega L^2/D_*$ is the dimensionless scaling parameter. For a system of reaction-diffusion equations D_* will be taken to be the diffusivity of the fastest diffusing species. Boundary conditions are imposed on

$$\mathbf{x} \in \partial\Omega(t) \tag{3.13}$$

and prescription of initial conditions on the domain closes the problem.

The derivation on the growing domain introduces two new terms to the standard reaction-diffusion equation. These terms will be discussed in more detail below, however, it will be intuitively clear that material is transported around the domain by the term $\mathbf{a} \cdot \nabla c$, and that $c\nabla \cdot \mathbf{a}$ represents a dilution due to local volume increase.

3.2.1 Determination of the Flow. The flow $\mathbf{a}$ may be specified directly for certain simple cases, however, in general it is expected that $\mathbf{a}(\mathbf{x}, t)$ will be determined by some extended system of constitutive equations describing the properties of the tissue. Here we will assume that growth properties are determined locally in the tissue, due to factors that are not modelled but which might include prepatterns in growth factors and cellular and sub-cellular structures influencing the direction of growth. Such properties will be specified on an initial domain and will be displaced, following the flow due to subsequent tissue growth.

The movement of tissue as a result of growth can be described in terms of the trajectories of elements of the tissue, i.e. the paths followed in time by elemental volumes. This Lagrangian description is particularly apt as the factors determining local growth characteristics move with the tissue as it grows. Therefore, a very natural coordinate system in which to work is Lagrangian coordinates, $(\mathbf{X}, t)$ where $\mathbf{X} = (X_1, X_2, X_3)$ is the initial position of a tissue element moving with the flow $\mathbf{a}$. The movement of tissue as a result of growth can be described in terms of the trajectories $\mathbf{\Gamma}$ of elements of the tissue such that

$$\mathbf{x} = \mathbf{\Gamma}(\mathbf{X}, t) = \big(\Gamma_1(\mathbf{X}, t), \Gamma_2(\mathbf{X}, t), \Gamma_3(\mathbf{X}, t)\big) \tag{3.14}$$

where $\mathbf{\Gamma}(\mathbf{X}, t)$ describes the trajectory[1] of a tissue element initially at position $\mathbf{X}$. The inverse of $\mathbf{\Gamma}$ is given by

$$\mathbf{X} = \mathbf{\Lambda}(\mathbf{x}, t) = \big(\Lambda_1(\mathbf{x}, t), \Lambda_2(\mathbf{x}, t), \Lambda_3(\mathbf{x}, t)\big) \tag{3.15}$$

which gives the initial location of a particle at position $\mathbf{x}$ at time t.

[1]Conventionally one writes $\mathbf{x} = \mathbf{x}(\mathbf{X}, t)$, representing the dependent variable and functional dependence by the same letter, but for clarity we will make the functional dependence explicit.

For the purposes of examining the effect of growth on pattern formation we will not be interested in solid body translations and rotations of the domain, which leave the pattern generated by reaction and diffusion within the tissue unaffected. The coordinates for the domain are chosen such that there is a reference point which is initially at the origin of the coordinate system and which remains at the origin. Some general conditions must then be observed for the components of $\mathbf{\Gamma}$. The initial condition is, by the definition of $\mathbf{\Gamma}$, that

$$\mathbf{\Gamma}(\mathbf{X}, 0) = \mathbf{X}. \tag{3.16}$$

In the absence of solid body translations we also have the boundary condition that for the reference point, $\mathbf{X}_r$, we require that $\mathbf{\Gamma}(\mathbf{X}_r, t) = \mathbf{X}_r$ and choosing the coordinate system such that $\mathbf{X}_r = \mathbf{0}$ leads to the condition

$$\mathbf{\Gamma}(\mathbf{0}, t) = \mathbf{0}. \tag{3.17}$$

Furthermore the domain is supposed to remain simply connected, which requires in one dimension (for example) that if

$$0 \leq X_p < X_q \leq 1, \tag{3.18}$$

then

$$\Gamma(X_p, t) < \Gamma(X_q, t), \qquad \forall t > 0. \tag{3.19}$$

This will be ensured by the approach taken here, where growth is specified locally and then integrated up to find the global form for the domain growth, as will be shown below.

3.2.2 Local Specification of the Growth. The deformation of the tissue due to growth is described by the rate-of-deformation tensor $\mathcal{L}_{ij}$ which can be decomposed into symmetric and antisymmetric parts $\mathcal{D}_{ij}$ and $\mathcal{W}_{ij}$ respectively. The antisymmetric part is associated with rigid body rotation, which is not relevant to pattern formation, and so in what follows we will consider only the symmetric component of $\mathcal{L}_{ij}$, the rate-of strain tensor $\mathcal{D}_{ij}$. Components of $\mathcal{D}_{ij}$ correspond to

- $\mathcal{D}_{ij}$ $(i = j)$: the rate of extension along the axis x_i
- $\mathcal{D}_{ij}$ $(i \neq j)$: the rate of (pure) shear along between axes x_i and x_j (with no accompanying volume change).

The trace of $\mathcal{D}_{ij}$

$$\mathcal{D}_{ii} = \nabla \cdot \mathbf{a} = S(\mathbf{X}, t) \tag{3.20}$$

(summation implied) gives the rate of volumetric change per unit volume (the rate of volume expansion) and so, for domain *growth*, $S(\mathbf{X}, t) > 0$. The antisymmetric part of $\mathcal{L}_{ij}$ corresponds to angular velocity $\frac{1}{2}\boldsymbol{\omega}$

$$\nabla \times \mathbf{a} = \boldsymbol{\omega} \tag{3.21}$$

for $\boldsymbol{\omega} = (\omega_1, \omega_2, \omega_3)$ and so we set $\boldsymbol{\omega} = \mathbf{0}$.

The components of the rate of strain tensor $\mathcal{D}_{ij}$ are determined by the local properties of the tissue, and thus we consider $\mathcal{D}_{ij}(\mathbf{X}, t)$, where

$$\mathcal{D}_{ij} = \frac{\partial a_i}{\partial x_j} \tag{3.22}$$

which is related to coordinates $(\mathbf{X}, t)$ via

$$\frac{\partial^2 \Gamma_i}{\partial t \, \partial X_k} = \frac{\partial a_i}{\partial x_j} \frac{\partial \Gamma_j}{\partial X_k} \tag{3.23}$$

(summation implied) from which in general we can calculate the function $\boldsymbol{\Gamma}(\mathbf{X}, t)$ and thus $\mathbf{a}$, the flow due to the domain growth.

Now we reconsider the terms introduced into the reaction-diffusion equation by the incorporation of domain growth. As $\nabla \cdot \mathbf{a} = S(\mathbf{X}, t)$ gives the local rate of volume expansion we recognise $c\nabla \cdot \mathbf{a} = Sc$ as a dilution term where (ignoring production terms in the kinetics) the local concentration is decreasing as the containing volume increases. The convection term $\mathbf{a} \cdot \nabla c$ represents the transport of chemical within the tissue as the tissue moves due to the growth (such that there is no movement of the chemical relative to the tissue). Then we can rewrite equation (3.11) as

$$\frac{\partial c}{\partial t} + \mathbf{a} \cdot \nabla c = \frac{d}{\gamma} \nabla^2 c + R(c, p) - Sc \tag{3.24}$$

In the following sections we consider several specific cases, where we assume the form of the components of $\mathcal{D}_{ij}$ and from them derive the trajectories, $\boldsymbol{\Gamma}$, and the flow, $\mathbf{a}$. Firstly we consider the general form taken for the evolution equation for one spatial dimension under a generalised local growth.

3.3 One-dimensional Growth

In one spatial dimension the specification of the local growth characteristics reduces to specifying the sole component of $\mathcal{D}_{ij}$. We wish to determine the trajectories given by

$$x = \Gamma(X, t) \tag{3.25}$$

with inverse $X = \Lambda(x, t)$. Equation (3.23) becomes

$$\frac{\partial^2 \Gamma}{\partial t \, \partial X} = S(X, t) \frac{\partial \Gamma}{\partial X} \tag{3.26}$$

where growth is now fully determined by the local expansion rate

$$\mathcal{D}_{11} = \frac{\partial a}{\partial x} = S(X, t) = S\big(\Lambda(x, t), t\big). \tag{3.27}$$

The boundary conditions on Γ are

$$\Gamma(0, t) = 0, \quad \Gamma(X, 0) = X \tag{3.28}$$

and then Γ may be computed directly by integrating (3.26) twice

$$\Gamma(X,t) = \int_0^X \left[\exp \int_0^t S\left(\bar{X},\bar{t}\right)\, \mathrm{d}\bar{t}\right] \mathrm{d}\bar{X}. \tag{3.29}$$

Then the flow is determined by

$$a = \frac{\mathrm{d}x}{\mathrm{d}t} = \frac{\partial \Gamma}{\partial t} \tag{3.30}$$

which fully determines the domain growth. In one dimension the evolution equation for $c(x,t)$ is

$$\frac{\partial c}{\partial t} + a\frac{\partial c}{\partial x} = \frac{d}{\gamma}\frac{\partial^2 c}{\partial x^2} + R(c) - Sc \tag{3.31}$$

where $S = S(\Lambda(x,t),t)$ and $a = a(\Lambda(x,t),t)$ so that each term in equation (3.31) is written in coordinates (x,t). The solution is defined on

$$x \in [0,\ell(t)]\,, \quad t \in [0,\infty) \tag{3.32}$$

where $\ell(t)$ is the time-dependent domain length. Following spatial nondimensionalisation using the initial domain length as reference lengthscale, such that $\ell(0) = 1$, then

$$\ell(t) = \Gamma(1,t). \tag{3.33}$$

3.3.1 Uniform Scaling. For the investigation of pattern formation phenomena it is natural to transform to a time-independent domain. Here we take a uniform spatial scaling to transform spatial coordinates to the unit interval, under

$$(x,t) \to (\xi,\tau) = \left(\frac{x}{\ell(t)}, t\right) \tag{3.34}$$

such that ξ is defined on

$$\xi \in [0,1]\,. \tag{3.35}$$

Under this transformation we have

$$\frac{\partial c}{\partial t} = -\xi\frac{\dot{\ell}}{\ell}\frac{\partial c}{\partial \xi} + \frac{\partial c}{\partial \tau}, \quad \frac{\partial c}{\partial x} = \frac{1}{\ell}\frac{\partial c}{\partial \xi} \tag{3.36}$$

and the transformed evolution equation is

$$\frac{\partial c}{\partial t} = \frac{d}{\gamma}\frac{1}{[\ell(t)]^2}\frac{\partial^2 c}{\partial \xi^2} + \left[\xi\frac{\dot{\ell}(t)}{\ell(t)} - \frac{a(\xi,t)}{\ell(t)}\right]\frac{\partial c}{\partial \xi} + R(c) - Sc \tag{3.37}$$

where the dot implies differentiation with respect to time.

3.4 Lagrangian Formulation

An inherent difficulty with the formulation for the evolution equation that we have derived for reaction and diffusion on the growing domain in coordinates $(\mathbf{x},t)$ is that for the purposes of numerical computation the form of $\mathbf{\Lambda}(\mathbf{x},t)$ must be known explicitly

(we are required to perform the inversion of $\mathbf{\Gamma}(\mathbf{X},t)$). This may not be possible for anything but simple functional forms for $\mathbf{\Gamma}$ (although of course the inversion may be computed numerically, this will prove computationally expensive) and will certainly not be possible if S is determined from some other data, or indeed if S has time and space dependence through the chemical species themselves,

$$S(\mathbf{x},t) = S\big(c_1(\mathbf{x},t),\dots c_n(\mathbf{x},t)\big). \tag{3.38}$$

which is called *reactant-controlled* domain growth. Thus it is useful to write the variables as functions of the Lagrangian position and to derive the evolution equation for $c(\mathbf{X},t)$. In one dimension this is done below. For the flow, and using subscripts to denote partial differentiation,

$$a(X,t) = \Gamma_t \tag{3.39}$$

$$a_x(X,t) = \frac{\Gamma_{Xt}}{\Gamma_X} = S(X,t) \tag{3.40}$$

and the derivatives in the evolution equation are transformed as

$$\frac{\partial c}{\partial t} = -\frac{\Gamma_t}{\Gamma_X}\frac{\partial c}{\partial X} + \frac{\partial c}{\partial t}, \quad \frac{\partial c}{\partial x} = \frac{1}{\Gamma_X}\frac{\partial c}{\partial X}, \quad \frac{\partial^2 c}{\partial x^2} = -\frac{\Gamma_{XX}}{{\Gamma_X}^3}\frac{\partial c}{\partial X} + \frac{1}{{\Gamma_X}^2}\frac{\partial^2 c}{\partial X^2}. \tag{3.41}$$

Hence equation (3.31) for $c(X,t)$ becomes

$$c_t = \frac{d}{\gamma}\left(\frac{1}{{\Gamma_X}^2}c_{XX} - \frac{\Gamma_{XX}}{{\Gamma_X}^3}c_X\right) + R(c) - Sc \tag{3.42}$$

$$\Gamma_{Xt} = S(X,t)\,\Gamma_X \tag{3.43}$$

where we have made the coupling to the equation for $\Gamma(X,t)$ explicit, and where of course Γ may be found explicitly by integrating as in equation (3.29). The coupled evolution equations for $c(X,t)$ and $\Gamma_X(X,t)$ are in a form which is much more amenable to numerical solution, and this is discussed later in Chapter 6. We have initial and boundary conditions for $c(X,t)$

$$c(X,0) = c_0(X) \tag{3.44}$$

$$c_X(0,t) = c_X(1,t) = 0 \tag{3.45}$$

and also for $\Gamma(X,t)$

$$\Gamma(X,0) = X \tag{3.46}$$

$$\Gamma(0,t) = 0. \tag{3.47}$$

To recover the form of the pattern on the dimensional domain (x,t) the solution must be scaled with the (time and space-dependent) trajectories $\Gamma(X,t)$ to determine $c(x,t)$. We have presented the Lagrangian formulation in one dimension, however, the analogous transformation to Lagrangian coordinates may be performed in higher spatial dimensions (W. W. Hackborn, *pers. comm.*).

3.5 Uniform Domain Growth in N-Dimensions

Now we turn to discussion of the simple case when the domain growth is determined by local expansion rates which are independent of spatial position,

$$\mathcal{D}_{ij} = \delta_{ij}\sigma(t) \tag{3.48}$$

where δ_{ij} is the Kronecker delta. Then the total volume expansion rate is

$$\mathcal{D}_{ii} = S(\mathbf{X}, t) = 3\sigma(t). \tag{3.49}$$

Direct integration with initial condition (3.16) and boundary condition (3.17) gives

$$\mathbf{\Gamma}(\mathbf{X}, t) = \mathbf{X} \exp\left[\int_0^t \sigma(\bar{t})\, \mathrm{d}\bar{t}\right] \equiv \mathbf{X} r(t) \tag{3.50}$$

which defines $r(t)$, and by differentiation the flow is easily determined as

$$\mathbf{a} = \mathbf{X} r(t)\sigma(t) = \mathbf{x}\sigma(t), \tag{3.51}$$

which is consistent with $S = \nabla \cdot \mathbf{a} = 3\sigma(t)$. The essential feature of uniform growth is that any two points move apart with a (relative) velocity which depends only on their separation. Thus for two points $\mathbf{x}_p$ and $\mathbf{x}_q$ with separation $\Delta\mathbf{x}$ then from the above we have that their relative velocity $\Delta\mathbf{a}$ is given by

$$\Delta\mathbf{a} = \mathbf{a}(\mathbf{x}_p, t) - \mathbf{a}(\mathbf{x}_q, t) = (\mathbf{x}_p - \mathbf{x}_q)\sigma(t) = \Delta\mathbf{x}\sigma(t). \tag{3.52}$$

Now we consider the evolution equation under uniform growth. The convection term in equation (3.24) corresponds only to uniform transport, and is expected to vanish under a uniform spatial scaling, as given for one dimension in section 3.3. In general the nondimensional domain length in the i^{th} direction is given by

$$\ell_i(t) = \Gamma_i(\mathbf{1}, t) = r(t) \tag{3.53}$$

and so we take the scaling

$$(\mathbf{x}, t) \to (\boldsymbol{\xi}, t) = \left(\frac{\mathbf{x}}{r(t)}, t\right) \tag{3.54}$$

where $\boldsymbol{\xi} = (\xi_1, \xi_2, \xi_3)$. Then the flow $\mathbf{a} = \mathbf{x}\dot{r}/r = \boldsymbol{\xi}\dot{r}(t)$ and the i^{th} component of the convection

$$\frac{1}{\ell(t)}\left[\xi_i \dot{\ell}(t) - a_i(\xi, t)\right] = 0. \tag{3.55}$$

It is straightforward to see that this is in fact the only possible domain growth for which the convection term disappears under uniform scaling. Using the definitions of $\boldsymbol{\xi}$, $\mathbf{a}$ and $\mathbf{\Gamma}$, and rearranging, the components of (3.55) can be written as

$$\frac{\partial \Gamma_i}{\partial t}(\mathbf{X}, t) - \frac{\dot{r}(t)}{r(t)}\Gamma_i(\mathbf{X}, t) = 0. \tag{3.56}$$

This implies that the components of $\mathbf{\Gamma}(\mathbf{X}, t)$ are separable functions of $\mathbf{X}$ and t, but the conditions (3.16) and (3.17) require that $\mathbf{\Gamma}$ take the form given in equation (3.50).

Another similar case considers anisotropic domain growth for which the axial expansion rates differ, but each are uniform (having no space dependence)

$$\mathcal{D}_{ij} = \delta_{ij}\sigma_i(t) \tag{3.57}$$

(no summation). Direct integration gives

$$\mathbf{\Gamma}(\mathbf{X},t) = \big(X_1 r_1(t), X_2 r_2(t), X_3 r_3(t)\big) \tag{3.58}$$

where the time dependences are given by

$$r_i(t) = \exp \int_0^t \sigma_i(\bar{t})\, d\bar{t}. \tag{3.59}$$

In this case the local rate of volume increase is given by

$$S = \nabla \cdot \mathbf{a} = \sigma_1(t) + \sigma_2(t) + \sigma_3(t). \tag{3.60}$$

For general non-uniform domain growth $\mathbf{\Gamma}(\mathbf{X},t)$ is a non-separable function of $\mathbf{X}$ and t. Thus in general the convection terms are not removed under a uniform transformation such as (3.54) and so may play a role in the formation of pattern in the system. In order to investigate pattern formation under non-uniform domain growth we must consider specific examples. In Chapter 6 we consider the one-dimensional problem comprising two sub-domains each with uniform but different growth rates, the *piece-wise uniform* case, to gain some insight into the complexities of pattern sequence generation under more general growth functions.

3.5.1 Slow Uniform Growth. The evolution equations in the previous section are derived for local expansion rates which are functions of time but not position. The introduction of domain growth necessarily introduces a new timescale to the problem. We denote this explicitly for the uniform case (see equation (3.49)) by writing

$$S(\mathbf{X},t) = 3\rho\sigma(t) \tag{3.61}$$

where $\sigma(t) \sim \mathcal{O}(1)$, which introduces the timescale $1/\rho$.[2] The effect of growth on pattern formation is expected to depend on the relative magnitudes of the timescales for domain growth and for pattern formation. One specific timescale for pattern formation that emerges from the linear analysis was presented in Chapter 2. Having nondimensionalised the equations appropriately, the spatial patterns are established on a time of $\mathcal{O}(1)$, and hence $1/\rho$ measures the timescale for domain growth relative to that for pattern formation.

In the following chapters we consider the effect of domain growth on pattern formation when the domain changes size and shape over a much longer timescale than that for pattern formation. This must be the relevant case for biological systems where

[2]The growth rate-determining parameter ρ introduces a timescale for domain growth, however, the rate at which the domain grows must be calculated from $\mathrm{d}\mathbf{\Gamma}(\mathbf{1},t)/\mathrm{d}t$ which is in general a function of ρ and time t.

reaction and diffusion of chemicals will be much faster than the timescales over which the cellular machinery involved in growth will operate. Thus we study slow domain growth, for which

$$0 < \rho \ll 1 \tag{3.62}$$

and initially we will concentrate on uniform growth on the one-dimensional domain. Then the evolution equation is given by

$$\frac{\partial c}{\partial t} = \frac{d}{\gamma(t)}\frac{\partial^2 c}{\partial \xi^2} + R(c) - \rho\sigma(t)c \tag{3.63}$$

where $\gamma(t)$ is the time-dependent scaling parameter defined by

$$\gamma(t) = \gamma_0 \big(r(t)\big)^2 = \gamma_0 \exp\left[2\rho \int_0^t \sigma\left(\bar{t}\right) \mathrm{d}\bar{t}\right] \tag{3.64}$$

and $\gamma_0 = \gamma(0)$ is the scaling parameter for the static domain problem when $\rho = 0$.

When $\rho \ll 1$ the dilution term is small, and in particular it is small compared to any $\mathcal{O}(1)$ linear terms in the kinetic function. Pattern formation in this nonautonomous equation is studied in the following chapter.

3.5.2 Modified Reaction Term. We examine the way in which the dilution term may modify the kinetics. The extra term is in general time and space-dependent. A modified reaction term $\hat{\mathbf{R}}$ may be defined for $S(\mathbf{x}, t)$, where

$$\hat{\mathbf{R}}\left(\mathbf{x}, t\right) = \mathbf{R}\left(\mathbf{c}\right) - S(\mathbf{x}, t)\,\mathbf{c}. \tag{3.65}$$

The obvious consequence is that there may be no *homogeneous* steady state for kinetics $\hat{\mathbf{R}}$, due to spatial dependence. The dilution term is independent of $\mathbf{x}$ when the local expansion is uniform. Furthermore, the dilution term is time-independent when the local expansion is constant (the domain grows under a constant strain rate) in each direction, $\sigma_i(t) = \rho_i$, for which

$$\Gamma_i(\mathbf{X}, t) = X_i \exp \rho_i t. \tag{3.66}$$

For uniform growth, where $\hat{\mathbf{R}}$ is independent of $\mathbf{x}$, at the initial time the kinetics do not have the same steady state as for the static problem. The new steady state must be calculated according to the form and parameters of the growth function, and perturbations taken about these values to produce the initial data.

The modification to the reaction kinetics necessarily changes the dispersion relation and the Turing space for the onset of the instability (although standard linear analysis cannot be performed for the nonautonomous problem). This raises the possibility that the dilution contribution will move the Turing space so as to allow the onset of instability where the original parameters on a static domain were incompatible, or indeed to move the system out of the Turing space.

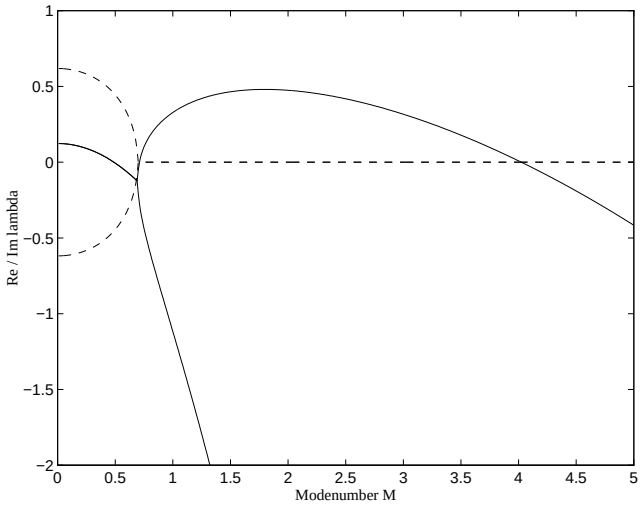

FIGURE 3.1 Dispersion relation for modified kinetic scheme, with $a = 0.1$, $b = 0.9$, $d = 0.05$, $\rho = 0.15$ and $\gamma = 10.0$ (remembering that γ scales the wavenumber). The real part of λ is shown as a solid line, and the imaginary part as a dashed line. The wavenumber is represented by a continuous mode number m where $k = m\pi$.

We now examine the modified kinetics for exponential growth, taking as an example Schnakenberg kinetics, for which, writing $\hat{\mathbf{R}} = (\hat{f}, \hat{g})$, we have

$$\hat{f}(u, v; \rho) = b - \rho u - uv^2 \tag{3.67}$$

$$\hat{g}(u, v; \rho) = a - (1 + \rho)v + uv^2. \tag{3.68}$$

The dispersion relation for these modified kinetics, for a particular parameter set, is shown in Figure 3.1. Here we see that the zeroth mode has $\mathcal{R}e\,\lambda > 0$ and also that $\mathcal{I}m\,\lambda \neq 0$, allowing temporal oscillation when the system is subject to spatially homogeneous perturbation, i.e. to perturbation in the absence of diffusion. Thus the modified kinetics are no longer in the Turing space, for which the steady state must be stable (and not oscillating) in the absence of diffusion. Numerical simulation has verified the presence of such a Hopf bifurcation for sufficiently large ρ. Using the numerical bifurcation and continuation package `AUTO97` [30, 31, 28, 29] we have performed a numerical bifurcation analysis on the ordinary differential equation system given by

$$\frac{\mathrm{d}u}{\mathrm{d}t} = \hat{f}\,(u, v; \rho) \tag{3.69}$$

$$\frac{\mathrm{d}u}{\mathrm{d}t} = \hat{g}\,(u, v; \rho)\,. \tag{3.70}$$

The bifurcation diagram is shown in Figure 3.2(a) and the waveforms for the variable u are shown in Figures 3.2(b) and 3.2(c). It should be noted, however, that the values of ρ at which these phenomena occur are large in relation to those for which the generation of interesting spatial pattern sequences are observed.

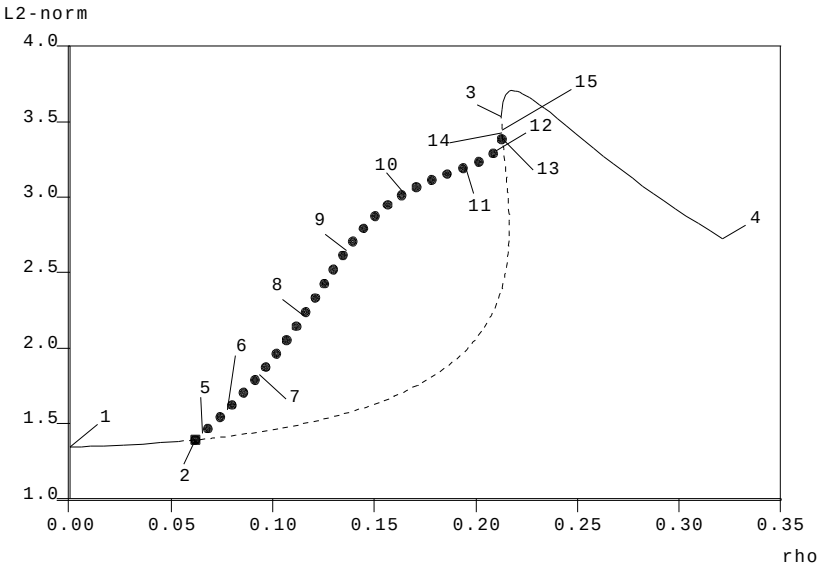

(a)

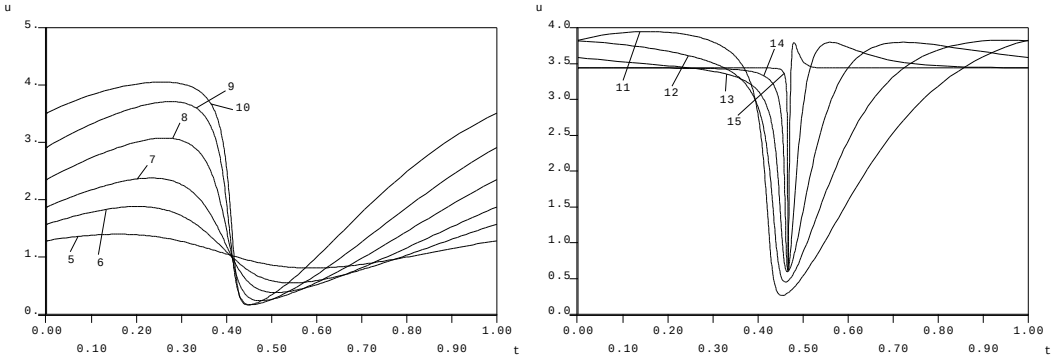

(b) (c)

FIGURE 3.2 Bifurcation diagram (a) and waveforms (b)–(c) for the modified kinetic scheme with no diffusion: equation (3.69) with $a = 0.1$, $b = 0.9$ and ρ as bifurcation parameter. In (a) the filled square represents a Hopf bifurcation point and the filled circles show stable periodic orbits. Stable (non-oscillatory) solutions for are shown by the solid line, and unstable solutions by the dashed line. Labels refer to the waveforms shown in (b) and (c) for the inhibitor u, where the periods of the waves are normalised to unit time. Similar waveforms are recovered for v.

3.6 Discussion

In this chapter we have considered the evolution equation derived for conservation of matter undergoing reaction and diffusion on a growing domain. The domain growth is specified in terms of local strain and shear rates, supposed to represent underlying tissue growth and movement. Several simplified cases have been identified and these 'reduced systems' will be studied in the remainder of this thesis.

We have considered only very simple geometries for the domain, the interval and the plane. Recently Varea *et al.* [128] have considered pattern formation on spherical surfaces, and Chaplain *et al.* [14] investigate patterns on the radially growing sphere. Clearly the formalism that we have described can be adapted to encompass these and other geometries.

Before we turn to investigate pattern formation in our equations, we briefly reconsider the previous attempts in the literature to model reaction-diffusion and growth. It is apparent from the equations derived from first principles that all of the models discussed earlier consider only the effects of *uniform* domain growth on pattern formation. The model we have derived is much more general and allows for the inclusion of *any* space and time dependence on the growth. The equation derived by Kulesa *et al.* [65] and by Painter *et al.* [107] corresponds to domain growth in one dimension under a constant strain rate and includes the dilution term. However, our equations for uniform growth differ significantly from the model studied by Arcuri and Murray [3] in that the time-dependent scaling parameter appears in a different position in their equation (also the dilution term is absent in Arcuri and Murray's work). The significance of this difference will be discussed in the following chapter in light of the pattern formation properties of our equation, however, it is apparent that the difference arises as Arcuri and Murray adopt a different procedure for nondimensionalisation, which fails to keep separate the timescales for the distinct processes of pattern formation and domain growth.

4. Slow Uniform Growth and Spatial Frequency-Doubling

In this chapter we investigate the patterning properties of the reaction-diffusion mechanism on a slow uniformly growing domain in one spatial dimension. In particular we are interested in how the behaviour of the solution depends on the new timescale that is introduced into the equation as a result of domain growth, and how this timescale interacts with the timescale for pattern formation in the static reaction-diffusion problem.

Spatial frequency-doubling has been reported by several authors [3, 64, 107]. The phenomenon consists of regular doubling of the spatial frequency of the standing wave pattern on the unit interval. On the dimensional domain this behaviour corresponds to regular doubling of the mode of spatial pattern. The period for frequency-doubling (hereafter FD) will be shown to be the time taken for the dimensional domain to double in length. In this chapter we examine this behaviour in detail, suggesting a symmetry of the governing equation which may underly the patterning behaviour, and we investigate dependence on parameters and the functional form describing the growth.

4.1 Slow and Fast Dynamics

The evolution equations describing reaction and diffusion in one spatial dimension[1] for two interacting species with concentrations $u(x,t)$ and $v(x,t)$, with uniform domain growth may be written as

$$u_t = \frac{1}{\gamma}u_{xx} + f(u,v) - \rho\sigma(t)u \tag{4.1}$$

$$v_t = \frac{d}{\gamma}v_{xx} + g(u,v) - \rho\sigma(t)v \tag{4.2}$$

$$\gamma_t = 2\rho\gamma_0\sigma(t)\exp\left[2\rho\int_0^t \sigma\left(\bar{t}\right)\mathrm{d}\bar{t}\right] \tag{4.3}$$

where v is the self-activator, which is defined on

$$x \in [0,1]\,, \quad t \in [0,\infty)\,. \tag{4.4}$$

We impose zero-flux boundary conditions

$$u_x = v_x = 0 \quad \text{on} \quad x = 0, 1. \tag{4.5}$$

[1] For convenience we adopt the notation x for the uniformly scaled position, such that $x \in [0,1]$.

Initial conditions are random perturbations about the homogeneous steady state of the kinetics, (u_s, v_s) where

$$f(u_s, v_s) - \rho\sigma(0)u_s = 0 \tag{4.6}$$

$$g(u_s, v_s) - \rho\sigma(0)v_s = 0. \tag{4.7}$$

For slow growth we have

$$0 < \rho \ll 1 \tag{4.8}$$

such that the growth timescale $1/\rho \gg 1$, and we recall that pattern formation is on an $\mathcal{O}(1)$ timescale. The separation of scales that this produces gives two regimes, with evolution on a slow and a fast timescale respectively. If we introduce a slow time variable, $\tau = \rho t$, then asymptotically as $\rho \to 0$ we have the slow subsystem (when $u_\tau, v_\tau \ll \mathcal{O}(1/\rho)$):

$$u_{xx} = -\gamma f \tag{4.9}$$

$$dv_{xx} = -\gamma g \tag{4.10}$$

$$\gamma_\tau = \gamma_0 \exp\left[2\rho \int_0^{\tau/\rho} \sigma\left(\bar{t}\right) \mathrm{d}\bar{t}\right] \tag{4.11}$$

for which the quasi-steady solutions are parameterised by γ. This adiabatic limit holds except where $u_\tau, v_\tau \sim \mathcal{O}(1/\rho)$ for which we have the fast system

$$u_t = \frac{1}{\gamma} u_{xx} + f \tag{4.12}$$

$$v_t = d\frac{1}{\gamma} v_{xx} + g \tag{4.13}$$

where γ is constant. The fast subsystem governs the reorganisation of patterns away from the quasi-steady regime. The extra terms in the kinetics (the dilution terms) are $\mathcal{O}(\rho)$ and so do not feature to leading order.

This scaling arises very naturally in the equations and for zero-flux boundary conditions may be verified by considering the function

$$\phi(\tau;\rho) \equiv \frac{\mathrm{d}}{\mathrm{d}\tau} \int_0^1 \left[u(x,\tau;\rho) + v(x,\tau;\rho)\right] \mathrm{d}x \tag{4.14}$$

$$= \frac{1}{\rho} \int_0^1 \left[f(u,v) + g(u,v)\right] \mathrm{d}x \tag{4.15}$$

which should stay close to zero during slow dynamics, and scale as $1/\rho$ in the fast dynamic regime. Numerically we find that $\phi(\tau;\rho)$ remains close to zero in the quasi-steady state and has a maximum during the reorganisation of pattern (reaching the same maximal value independent of the particular pattern mode) where

$$\phi_{max} = \max_{\tau \in [0,\infty)} \left(\phi\left(\tau;\rho\right)\right) \sim \frac{1}{\rho}. \tag{4.16}$$

We will present concrete examples below.

Thus for the slow growth limit, $\rho \ll 1$, the analysis suggests periods of quasi-steady behaviour interspersed with fast transitions corresponding to fast dynamical reorganisation to a different pattern. This does not tell us anything about which pattern modes are expected in the sequence, or whether the sequence of patterns is sensitive to initial conditions.

Heuristically we may describe the process of generation of a pattern sequence in the model, under these two timescales, as follows. The initial bifurcation from the homogeneous steady state is through a diffusion-driven instability near the critical point $\gamma = \gamma_c$ which may be derived from linear stability theory. Linear growth of the destabilising mode and subsequent saturation to a large amplitude pattern ensues. The pattern then evolves in two dynamical regimes. The amplitude of the pattern is gently modulated in the quasi-steady state as γ changes with time. A pattern persists until at some point the solution undergoes a transition to a new quasi-steady pattern; undergoing a fast dynamic reorganisation (activator peak *splitting* and separation for Schnakenberg kinetics). Subsequently a pattern of higher spatial frequency (for γ increasing) is established which in turn persists, with slow amplitude modulation, before the solution undergoes further transitions.

4.2 Spatial Frequency-Doubling for Exponential Domain Growth

Growth at a constant strain rate, $S(t) = \rho\sigma(t) = \rho$, corresponds to an exponential uniform domain growth

$$\Gamma(X,t) = X\exp(\rho t). \tag{4.17}$$

Under this growth, FD is observed within a parameter regime that is to be determined. We illustrate this with a concrete example using the Schnakenberg scheme for the nonlinear kinetics (see Appendix A.1)

$$f(u,v) = b - uv^2 \tag{4.18}$$

$$g(u,v) = a + uv^2 - v \tag{4.19}$$

where $g(u,v)$ is the kinetic function for the self-activating species v and $f(u,v)$ is the inhibitor kinetics.

Numerical Solution. We have computed numerical solutions of equation (4.1)–(4.3) with Schnakenberg kinetics, zero-flux boundary conditions (4.4) and exponential growth function (4.17) using a finite differences scheme which uses the method of lines for spatial discretisation and Gear's method for integration in time, as implemented in the NAG numerical routine `D03PCF`. The kinetic parameters here and in all other simulations with Schnakenberg kinetics are $a = 0.1$, $b = 0.9$ and we take the ratio of diffusivities $d = 0.01$, unless described otherwise. The initial conditions in each case are random fluctuations about the kinetic steady state concentrations, with a uniform distribution and maximum deviation of 0.5%. Typically we take 1001 spatial points in $[0,1]$, however, in all simulations we have at least 10 spatial points per wavelength

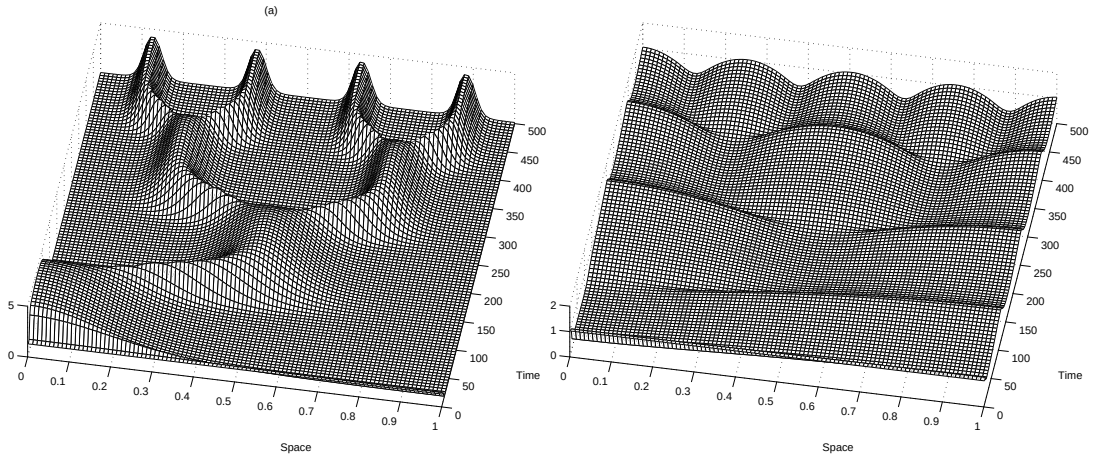

FIGURE 4.1 The spatial frequency-doubling sequence of patterns on an exponentially growing domain. We plot the evolution of (a) activator $v(x,t)$ and (b) inhibitor $u(x,t)$ concentrations for Schnakenberg kinetics, with $d = 0.01$ and $\rho = 0.005$. Pattern transitions are by activator peak splitting. The inhibitor profile is in spatial antiphase with the activator solution (the kinetics are of cross type). The accuracy in the time integration is 1.0×10^{-6}.

of pattern. Typical solutions are shown in Figure 4.1 for (a) activator and (b) inhibitor, and in Figure 4.2 the solution profile for the activator species is plotted on the dimensional growing domain.

In Figure 4.3(a) we plot the evolution of the maximum amplitude for each species (activator and inhibitor) given by

$$\eta_i(t) = \max_{x\in[0,1]} \left(c_i(x,t)\right), \quad i = 1,2 \tag{4.20}$$

which illustrates the periodic nature of the pattern sequence. The pattern changes at intervals corresponding to the time taken for the domain to double in length, which gives the period $\Delta t = (\ln 2)/\rho$, where $\Delta t \approx 693$ for the parameters in the simulation. Adding the equations for u and v written in the slow time variable $\tau = \rho t$ and integrating over the domain, we find

$$\phi(\tau) \equiv \frac{\mathrm{d}}{\mathrm{d}\tau}\int_0^1 (u+v)\,\mathrm{d}x = \frac{1}{\rho}\left[(a+b) - \int_0^1 v\,\mathrm{d}x\right], \tag{4.21}$$

where in the quasi-steady state $\phi \approx 0$, shown in Figure 4.3(b). Here ϕ is plotted against t for ease of comparison with previous figures. The evolution of ϕ illustrates the two dynamic regimes, with ϕ remaining close to zero except during the transition between quasi-steady patterns. The dependence on the strain rate ρ of the maximum value, ϕ_{max}, is presented in Figure 4.4.

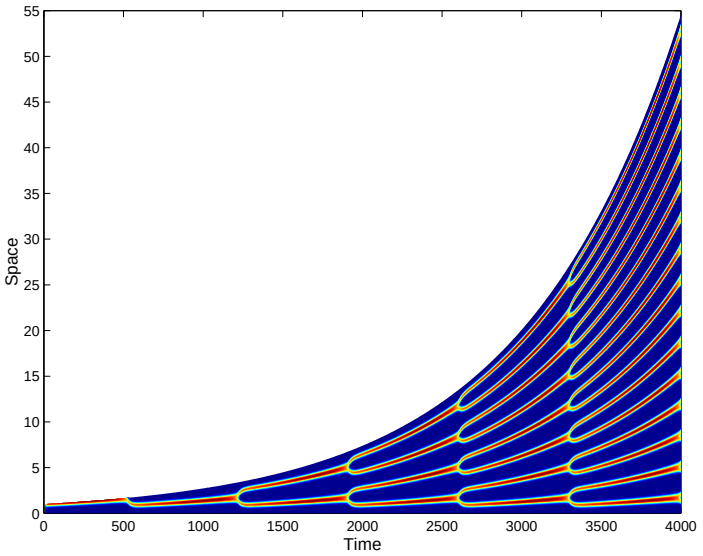

FIGURE 4.2 Spatial frequency-doubling on the dimensional domain—evolution of the activator $v(x,t)$ plotted on the exponentially growing domain showing periodic transitions as the domain length doubles. Kinetic parameters for the Schnakenberg scheme are as in Figure 4.1, with $\rho = 0.001$. Shading is from blue at zero concentration to red at high concentration ($v = 5$).

4.2.1 Symmetry Analysis. Frequency-doubling corresponds to a sequence in which the spatial frequency of the pattern regularly doubles, and no other pattern modes enter the sequence. Self-similarity of pattern modes can be used to predict necessary conditions under which this sequence is expected in our model. As $\gamma(t)$ is a monotonically increasing function we can eliminate t from the evolution equations (4.1) and (4.2) in favour of γ to give (for each species)

$$h(\gamma)\frac{\partial c}{\partial \gamma} = \frac{d}{\gamma}\frac{\partial^2 c}{\partial x^2} + R(c) - \frac{h(\gamma)}{2\gamma}c \tag{4.22}$$

where $h(\gamma) \equiv \mathrm{d}\gamma/\mathrm{d}t$, and for the final (dilution) term we have used $\mathrm{d}\gamma/\mathrm{d}t = 2\rho\sigma(t)\gamma(t)$. Let us assume that at $\gamma = \gamma^*$ the solution has spatial profile $c(x,\gamma^*)$. At any point in the sequence, in particular at $\gamma = \gamma^*$, a pattern of twice the spatial frequency $q_2(x,\gamma)$ may be constructed by applying the tent map $p_2(x)$ given in section 2.4.3, where

$$q_2(x,\gamma') \equiv c(p_2(x),\gamma'). \tag{4.23}$$

The transformed quantity q_2 in turn satisfies the evolution equation

$$h(\gamma')\frac{\partial q_2}{\partial \gamma'} = \frac{d}{4\gamma'}\frac{\partial^2 q_2}{\partial x^2} + R(q_2) - \frac{h(\gamma')}{2\gamma'}q_2. \tag{4.24}$$

Also, considering equation (4.22) we can see that the quantity $c(x,4\gamma')$ must satisfy the equation

$$\frac{1}{4}h(4\gamma')\frac{\partial c}{\partial \gamma'} = \frac{d}{4\gamma'}\frac{\partial^2 c}{\partial x^2} + R(c) - \frac{h(4\gamma')}{8\gamma'}c. \tag{4.25}$$

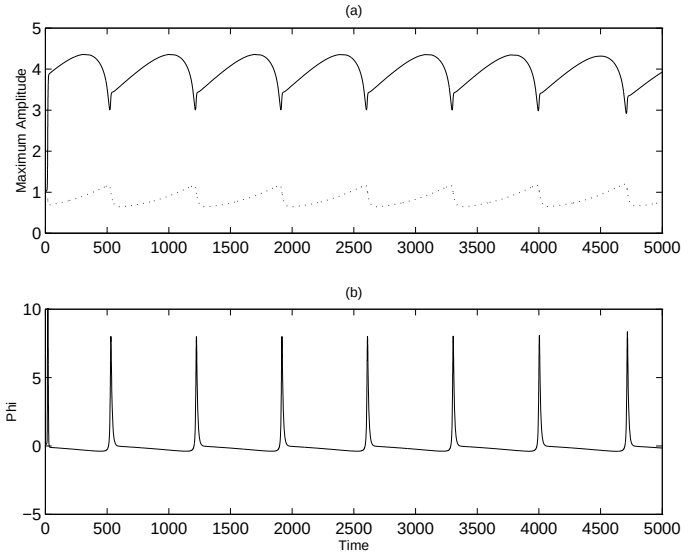

FIGURE 4.3 Periodicity in the transitions between quasi-steady patterns for exponential domain growth. We plot the evolution of (a) the maximum pattern amplitude for activator $\eta_2(t)$ (solid line) and inhibitor $\eta_1(t)$ (dotted line) species and (b) $\phi(t)$ (as defined in equation (4.21), here plotted against the fast time variable $t = \tau/\rho$ for ease of comparison), with parameters for the Schnakenberg kinetics as in Figure 4.1, and exponential domain growth with $\rho = 0.001$.

Now $c(x, 4\gamma')$ and $q_2(x, \gamma')$ satisfy the same equation if

$$h(4\gamma') = 4h(\gamma') \tag{4.26}$$

so that the left hand sides are the same and the final terms from the right hand side of the equations also match. Recalling that $h(\gamma) = \mathrm{d}\gamma/\mathrm{d}t$, this demands that the time dependence of γ, and hence the domain growth, is exponential,

$$\gamma(t) \propto \exp(2\rho t), \quad r(t) = \exp(\rho t) \tag{4.27}$$

so that the strain rate is constant in time. Furthermore, if at $\gamma = \gamma^*$ we find that in fact

$$q_2(x, \gamma^*) = c(x, 4\gamma^*), \quad \forall x \in [0, 1], \tag{4.28}$$

the *matching condition*, then the profiles are equivalent and, assuming uniqueness of solutions to the evolution equation for given initial and boundary conditions, they will continue to coincide for all time such that $\gamma > \gamma^*$. We have made no assumptions about γ^* or the spatial profile at γ^*: this observation holds in both quasi-steady and fast (transition) dynamical regimes.

We have shown that under exponential growth the quantities $q_2(x, \gamma) \equiv c(p_2(x), \gamma)$ and $c(x, 4\gamma)$ satisfy the same evolution equation. Below we investigate the consequences for FD. From the spatial profile $c(x, \gamma^*)$ we can construct $q_2(x, \gamma^*) \equiv c(p_2(x), \gamma^*)$ which by definition has twice the spatial frequency. Let us suppose that

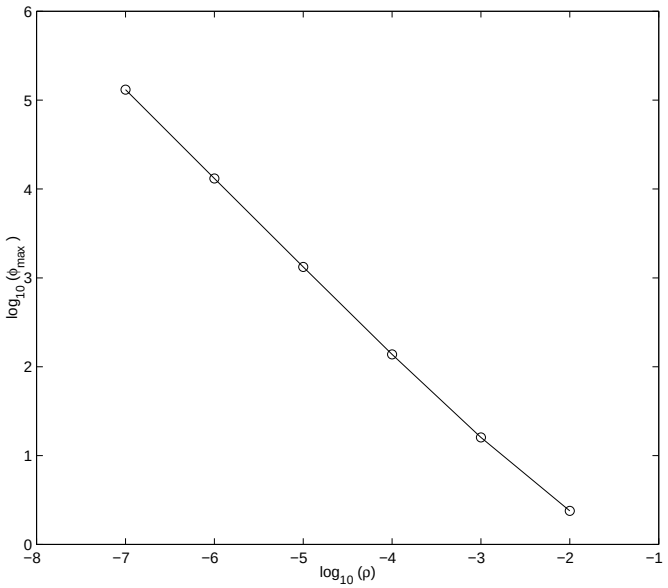

FIGURE 4.4 The reciprocal scaling of the maximum of $\phi(\tau)$ with the constant strain rate ρ, for Schnakenberg kinetics on the exponentially growing domain. The log-log plot shows that the maximum scales (approximately) as $1/\rho$.

for given initial conditions $c(x,\gamma)$ evolves such that for $\gamma \in [\gamma^*, 4\gamma^*]$ the solution is initially mode m and subsequently undergoes a transition to mode $2m$, such that the matching condition (4.28) is satisfied. Then the uniqueness of solutions of the evolution equation requires that $q_2(x,t)$ and $c(x,4\gamma)$ remain the same for $\gamma > \gamma^*$. But by construction $q_2(x,t)$ has twice the spatial frequency of $c(x,\gamma)$ and so, in the interval $\gamma \in [4\gamma^*, 16\gamma^*]$, the solution $c(x,\gamma)$ must consist of the sequence $2m$ and transition to $4m$, and so on.

In this way the pattern sequence for $\gamma > 4\gamma^*$ may be reduced to the behaviour on $\gamma \in [\gamma^*, 4\gamma^*]$. We now consider this initial interval. In particular, *if* $c(x,\gamma^*)$ consists of a pattern of mode $m = 1$ and we satisfy the matching condition to mode $m = 2$ at $\gamma = 4\gamma^*$ *then* our observations suggest that FD will naturally ensue in a self-similar cascade. Thus we need only consider the initial stages of the sequence to determine whether FD is realised—all subsequent behaviour is equivalent. Furthermore, this analysis predicts that such a sequence generated under exponential growth will undergo FD every time $\gamma \to 4\gamma$, and recalling that the scaling parameter $\gamma \propto L^2$ we see that this corresponds to doubling the length of the dimensional domain.

The stability of the solutions, for which we have shown existence, must be conjectured from the results of numerical simulations. Of course we should not need to have an exact matching (4.28) at any one instant and consequently we require some stability properties of the evolution equation. In particular we require that a solution $c(x,\gamma)$ perturbed at some point subsequent to the establishment of a large amplitude pattern remains in the vicinity of the unperturbed solution so that if $c(x,4\gamma)$ and

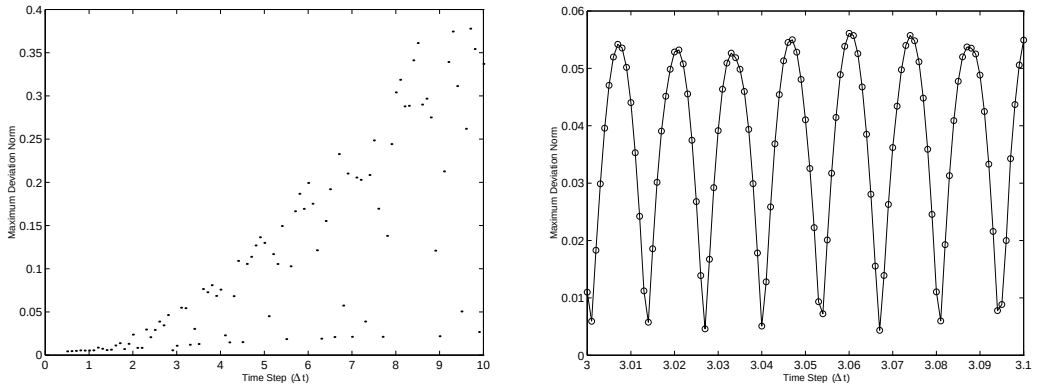

(a) (b)

FIGURE 4.5 The dependence of $\max_{x\in[0,1]} \left|c(x,\gamma) - q_2(x,\gamma/4)\right|$ during the transition between patterns as a function of the interpolation step size (see text for details). For comparison purposes the activator maximum amplitude $\eta_2 \approx 3$ during the transition. On closer inspection (b) the data are seen to oscillate. This is an artifact due to the sampling frequency and the sharpness of the transition.

$q_2(x,\gamma)$ are close at $\gamma = \gamma^*$ then they remain close during the interval $\gamma \in [\gamma^*, 4\gamma^*]$. We have performed numerical simulations of the evolution equations and have compared $c(x,4\gamma)$ and $q_2(x,\gamma)$ numerically, as described below (see also Figures 4.5(a) and 4.6), and conclude that this stability property is demonstrated by the system, at least in some range of the growth rate-determining parameter ρ. If the stability criterion is met then once some pattern is selected by the initial conditions the sequence is fully determined by the dynamics of the evolution equation and the initial conditions play no further part in determining the composition of the sequence. In this sense the patterns contained in the sequence are generated *robustly*.

We have computed $q_2(x,\gamma)$ for a solution $c(x,\gamma)$ in order to investigate the matching condition (4.28) during FD. A routine was implemented which compares the solution at time $t(\gamma)$ with the profile generated by the action of the tent map $p_2(x)$ on the solution at time $t(\gamma/4)$. To do this we use linear interpolation to approximate $c(x,\gamma/4)$, before applying the tent map to compute $q_2(x,\gamma/4) = c(p_2(x),\gamma/4)$. In Figure 4.5(a) we show how the maximum deviation over space for the activator (which is greater than the deviation for the inhibitor) depends on the time-step size. The maximum occurs during the transition between pattern modes. The time-step is simply the time interval between data records and hence the interval over which we interpolate—it does not reflect the accuracy in the time integration, which is kept constant. The figure shows that the deviation tends to zero with the step-size. This suggests that we do have $\left|c(x,\gamma) - q_2(x,\gamma/4)\right| \to 0$ during the transition, and hence the matching condition is satisfied. The transition between modes $m = 2$ and $m = 4$

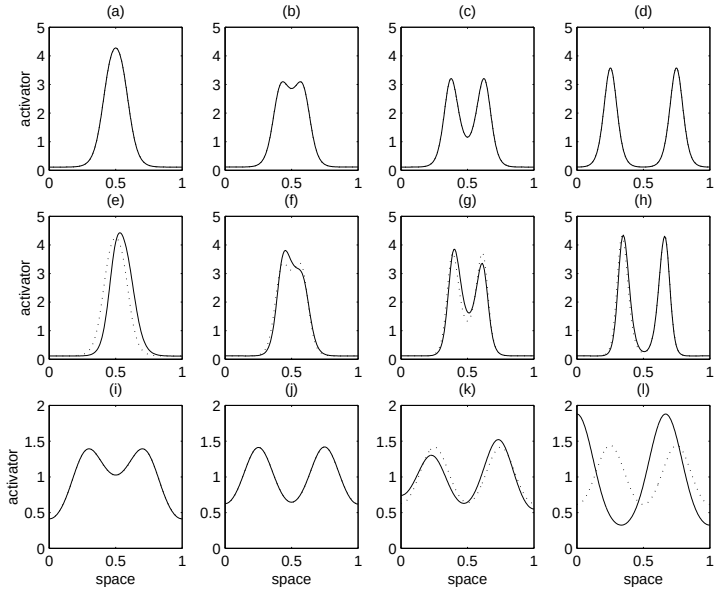

FIGURE 4.6 The peak splitting transition for three values of strain rate ρ. The transitions are from mode $m = 2$, for Schnakenberg kinetics with (a)–(d) the FD sequence for $\rho = 0.001$ and $d = 0.01$, (e)–(h) the onset of asymmetric splitting for $\rho = 0.02$ and $d = 0.01$ and (i)–(l) the breakdown in splitting behaviour for $\rho = 0.00001 < \rho_c$ with $d = 0.06$ (see text for details). The dotted trace shows the (symmetrical) tent map acting on the solution at $\gamma/4$, i.e. $q_2(x, \gamma) = c(x, \gamma/4)$ (which cannot be distinguished from the numerical solution (solid line) in (a)–(d)). At very small values of ρ correspondingly small timesteps are required numerically to investigate the solution behaviour during the transitions between patterns. Increasing d is found to raise ρ_c (see text), and in the figure we have taken $d = 0.06$ to allow a computationally reasonable timestep to be used.

is illustrated in Figure 4.6(a)–(d). Here $c(x, \gamma)$ and $q_2(x, \gamma/4)$ are plotted on the same axes and cannot be distinguished.

4.2.2 Parameter Dependence. We now look at the effect of varying parameters, and also changing various of the functional forms in the model, on the spatial frequency-doubling behaviour that we have described for exponential domain growth and Schnakenberg kinetics.

Constant Strain Rate. Numerically we find that the FD sequence is realised over several orders of magnitude of the strain rate ρ, the parameter that determines the growth rate. Here we examine the pattern sequence under exponential growth at the extremes of the range of validity of ρ. Our ability to numerically monitor FD into higher modes is severely limited by the mesh capacity that we can obtain computationally. In the current work, patterns up to mode $m = 256$ are considered in sequences of up to nine FD events. Frequency-doubling behaviour is observed under exponential growth with Schnakenberg kinetics for over four orders of magnitude in ρ for $d = 0.01$; approximately $10^{-6} < \rho < 10^{-2}$. The symmetry argument presented above would suggest that for exponential growth the sequence should persist indefinitely or fail,

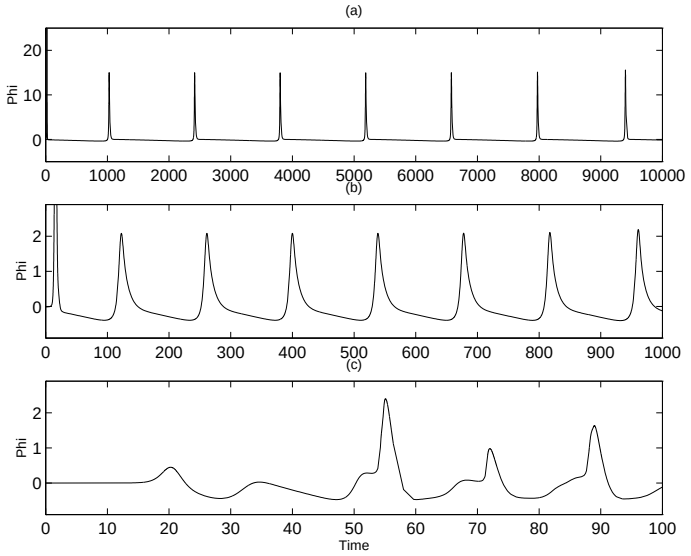

FIGURE 4.7 The departure from two characteristic dynamic regimes with increasing ρ. Timeseries for ϕ are plotted against the fast time variable t for exponential domain growth with (a) $\rho = 0.0005$, (b) $\rho = 0.005$ and (c) $\rho = 0.05$. (If plotted against the slow variable τ then all figures would have slow time (horizontal axis) on the interval $\tau \in [0, 5]$.) The early (high) peaks in (a) and (b) are initial transients.

according to whether the stability criterion is satisfied. Below we investigate this conjecture by varying the various parameters in numerical solutions of the equations.

As we let $\rho \to 1$ the timescale for domain growth converges to the timescale that was identified for pattern formation. Numerically we find that with increasing ρ an asymmetry is introduced during transition between modes of the FD sequence. For the example of Schnakenberg kinetics we find that peaks are no longer stationary before the transition to a higher mode and subsequent peak splitting is asymmetrical. The solution starts to undergo the transition before reaching a quasi-steady state. A comparison with the construction $q_2(x, \gamma/4)$, illustrated in Figure 4.6(e)–(h), shows that there is no longer matching for large ρ (as the tent map is by definition symmetrical).

The departure from the characteristic alternation between slow and fast dynamical regimes is demonstrated in the behaviour of $\phi(\tau)$, defined in section 4.1, which is shown in Figure 4.7 for three different values of ρ. The onset of the asymmetry is gradual and although the solution no longer enters a quasi-stationary state the strong tendency to peak splitting remains (for Schnakenberg kinetics), with the number of turning points on the domain continuing to double roughly periodically for some further range of ρ. When ρ becomes very large, $\rho \sim 1$, the solution is purely transient with no patterns recognisable as quasi-stationary modes. The changing form of the activator solutions with increasing ρ is shown in Figure 4.8.

Perhaps a more surprising result is that there is an also abrupt change in behaviour when ρ is decreased through a lower critical value, ρ_c. For ρ below this point the pattern sequence does not undergo FD and different sequences may be obtained for

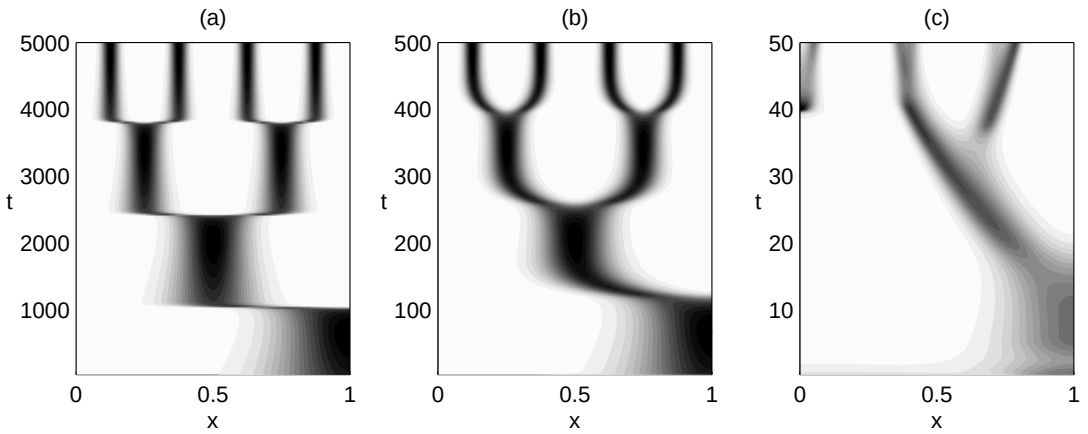

FIGURE 4.8 The loss of the FD sequence with increasing ρ. Activator solutions $v(x,t)$ are plotted for three values of the strain rate ρ for Schnakenberg kinetics and exponential domain growth. Parameters correspond to Figure 4.7 with (a) $\rho = 0.0005$, (b) $\rho = 0.005$ and (c) $\rho = 0.05$. The duration of the transitions is approximately the same in each case. In (c) the FD sequence is no longer observed. Shading is on a scale from white (0) to black (5).

different sets of initial conditions. Figure 4.6(i)–(l) illustrates the manner in which this breakdown occurs during a transition. This implies that there is a maximum timescale for domain growth beyond which the constraint imposed by the non-autonomy is not sufficient to generate the FD sequence. We note that for sequences for $\rho < \rho_c$, where the FD breaks down, $\phi(t)$ shows the same quasi-static and fast transition behaviour as for FD, however, the transitions no longer occur periodically in time.

Ratio of Diffusivities. It is of interest to see how the lower bound on ρ for FD and the onset of asymmetrical splitting as $\rho \to 1$ depend on d, the ratio of activator to inhibitor diffusivity. Numerically, we find that by increasing d (such that the diffusivities for activator and inhibitor move closer together) we also raise the lower bound, for example $\rho_c \approx 3 \times 10^{-4}$ for $d = 0.05$ compared to $\rho_c \approx 10^{-6}$ for $d = 0.01$. At the opposite end of the range of ρ for which FD is observed, as $\rho \to 1$, we find that as d is increased peaks move apart more quickly subsequent to splitting, thus delaying the onset of asymmetric transitions. This increased rate of peak separation is illustrated in Figure 4.9. We recall that d cannot be increased through the critical value d_c for the Turing bifurcation, as discussed in section 2.3. We also note that as d is increased towards d_c the peaks become wider, as can be seen in the figure.

4.2.3 Role of the Kinetics: Peak Splitting and Peak Insertion. The symmetry analysis presented above does not depend critically on the nonlinear part of the kinetic function. From this we might infer that FD is a generic property of reaction-diffusion equations provided that the linearised kinetics permit diffusion-driven instability, and that the FD pattern sequence will be realised given the initial matching of solution and construction and the stability properties as described. Numerical solution of a

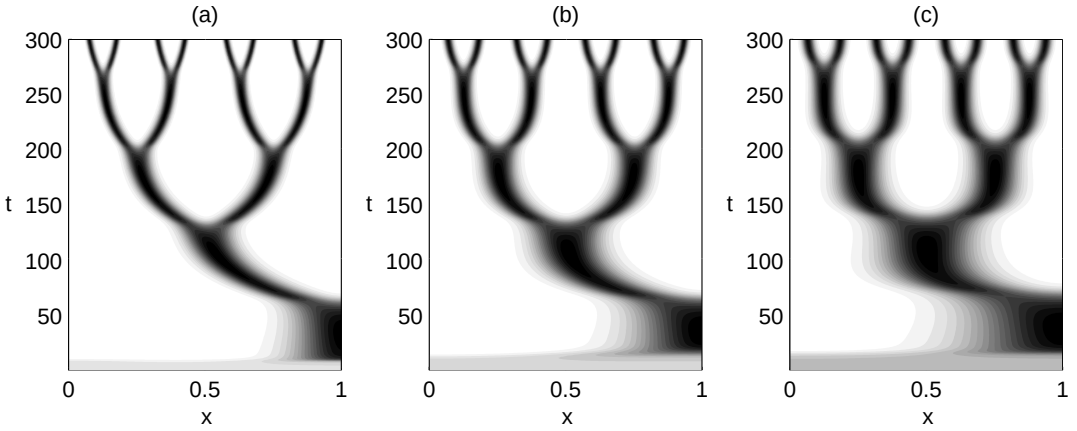

FIGURE 4.9 The dependence of the speed of peak separation on the ratio of diffusivities d, for peak separation subsequent to splitting in the FD sequence for Schnakenberg kinetics. Activator solutions $v(x,t)$ are plotted for $\rho = 0.01$ and three values of the ratio of diffusivities d on the exponentially growing domain, with (a) $d = 0.005$, (b) $d = 0.01$ and (c) $d = 0.02$. We recall that increasing d brings the diffusivities of the two species closer together. The shading scale is as for Figure 4.8.

variety of the kinetic models proposed in the literature has also produced FD sequences with either activator peak splitting, as was found for the Schnakenberg case, see Figure 4.1(a), or by activator peak *insertion*. This latter mechanism for transition between modes is demonstrated in Figure 4.10(a) for the model proposed by Gierer and Meinhardt (see Appendix A.3)

$$f(u,v) = \nu_1 v^2 - \mu_1 u \tag{4.29}$$

$$g(u,v) = \nu_2 \frac{v^2}{u} - \mu_2 v + \delta \tag{4.30}$$

and evolution equation (4.1)–(4.3). However, for this kinetic scheme we have found that when δ is identically zero the kinetics preclude FD by preventing either form of pattern reorganisation, as illustrated in Figure 4.10(b). The standard FD sequence is recovered for non-zero δ. We will investigate the mechanisms for peak splitting and peak insertion in the following chapter, and give an explanation for the singular behaviour found in the Gierer-Meinhardt model for $\delta = 0$. Also it will be shown that it is possible to generate a sequence of patterns in which activator peaks undergo splitting and insertion of new peaks *simultaneously*. This behaviour is observed for kinetic schemes which have purely cubic nonlinearity.

4.2.4 Influence of the Boundary Conditions. So far we have described pattern formation with zero-flux boundary conditions. The symmetry analysis that we have presented relies on the zero gradient at the boundary to produce solutions under the tent-mapping that are twice-continuously differentiable. However, numerical solutions show that the tendency for regular doubling of the number of peaks on the domain is not reliant on these boundary conditions. First we consider the case for periodic

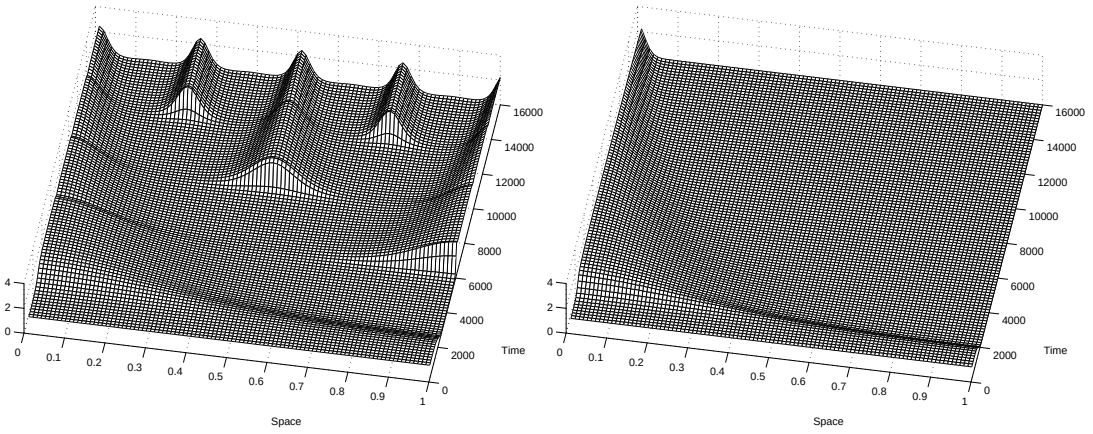

(a) (b)

FIGURE 4.10 Pattern sequence formation in the Gierer-Meinhardt model on the growing domain. Evolution of the activator species showing (a) frequency-doubling with peak insertion for with $\delta = 0.001$ and (b) the solution for $\delta = 0$ for which pattern reorganisation is precluded. Kinetic parameters $\nu_1 = \mu_1 = 0.02$ and $\nu_2 = \mu_2 = 0.01$,

boundaries, such that in one spatial dimension pattern formation is on the ring. In this case we remove boundary effects from the problem. It is clear that the half-peak pattern mode is not a solution on the periodic domain. Figure 4.11 shows the solution to equations (4.1)–(4.3) for the activator species on a periodic domain with exponential domain growth and Schnakenberg kinetics, from which we recover FD as usual. We have computed numerical solutions with periodic boundaries using an implicit differences scheme, which employs the Sherman-Morrison formula [113, p.68] to solve the sparse cyclic tridiagonal system (an augmented-tridiagonal matrix) generated by the discretisation.

Scalar boundary conditions (see section 2.1) may be written in the form

$$(\mathbf{n} \cdot \nabla)\, \mathbf{c} = P\,(\mathbf{c}^* - \mathbf{c}) \tag{4.31}$$

where $\mathbf{n}$ is the unit outward normal on the boundary. For different choices of the parameter $0 \leq P_i \leq 1$ and the external reference concentrations $\mathbf{c}^* \geq \mathbf{0}$ we move from zero flux ($P = 0$) to Dirichlet ($P = \infty$) conditions, which are homogeneous when $\mathbf{c}^* = \mathbf{c}_s$. For intermediate values of P we have inward or outward flux depending on whether the concentration at the boundary is lower or higher than the external concentration $\mathbf{c}^*$. This can be thought of as a leakage of chemical into or out of the domain.

Patterns generated on a domain of fixed size under flux-leakage boundary conditions are found by numerical simulation to be weakly perturbed from the zero flux

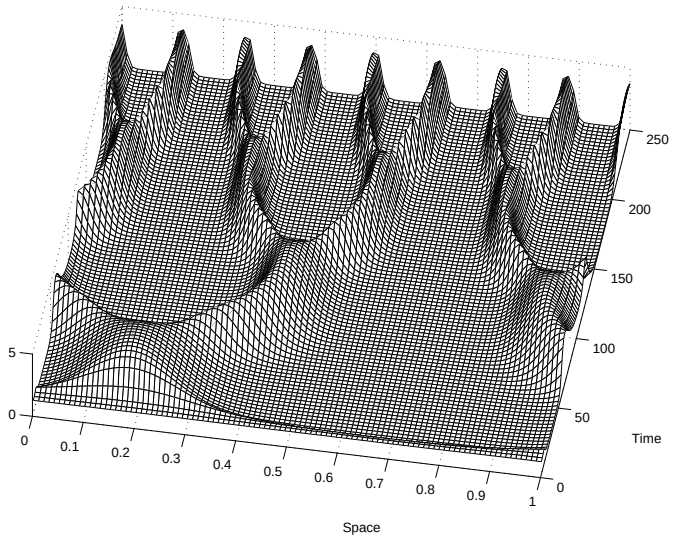

FIGURE 4.11 The FD sequence for periodic boundaries (solution on the ring). Evolution of the activator concentration profile $v(x,t)$ with exponential growth for $\rho = 0.01$ with Schnakenberg kinetics and $d = 0.01$. The initial domain size is such that $\gamma_0 = 5$.

patterns, with small lateral displacement of peaks and modification in the peak profile. Inward flux at the boundaries is found to displace peaks towards the centre of the domain, while outward flux pushes peaks towards the boundaries. This result for outward flux is observed for $\mathbf{c}^* = \mathbf{0}$ for which

$$(\mathbf{n} \cdot \nabla)\, \mathbf{c} = -P\mathbf{c} \tag{4.32}$$

where, for example, we might take $P = 1/2$ (and the concentrations $c_i > 0$ always). For inward flux conditions we choose $\mathbf{c}^* > \mathbf{0}$ and sufficiently large that $c_i^* - c_i > 0$ always. On the growing domain these boundary conditions give rise to regular doubling in the number of peaks on the domain, and cause only small quantitative perturbations to the FD sequence for zero flux conditions. Furthermore, for these boundary conditions the initial pattern to develop is found to be the centralised peak, rather than the boundary peak. For Dirichlet conditions, $P = \infty$, with values of $\mathbf{c}^*$ such that pattern modes are admitted as solutions of the evolution equation, the same strong tendency to frequency-doubling behaviour is observed.

4.3 Three-Species Models

In Turing's original paper, and in most of the subsequent discussion and application of the theory in biological and non-biological contexts alike, only two interacting species are considered.[2] In two-species models it is straightforward to show that temporal oscillations cannot occur with diffusion-driven instability. (The homogeneous steady

[2]For a single diffusing substance with nonlinear kinetics there can be no homogeneous state, stable to homogeneous disturbance, which is unstable to spatially heterogeneous perturbations. Heterogeneous

state may of course lose stability to spatially homogeneous oscillations through Hopf bifurcation in the kinetic term.) However, for three or more interacting species it is possible to induce spatio-temporal oscillations driven by diffusion.

Various authors have studied model systems with more than two components. Othmer and Scriven [101] consider the stability of the homogeneous state in n-component systems, allowing cross-diffusion (such that the off-diagonal elements in the matrix of diffusivities are non-zero). The authors find that for two-species systems with cross-diffusion then it is possible to excite oscillatory instabilities, however, there is no fastest growing wavenumber in this case (i.e. the complex solutions to the dispersion relation, $\lambda(k^2)$, have positive real part which is monotonically increasing with wavenumber). In general standard linear analysis becomes intractable for n-component systems where $n > 3$ due to the fact that stability is determined by eigenvalues which are the roots of an n^{th}-degree polynomial. It is interesting to consider what generalisations to the concepts of short-range activation and long range inhibition arise in these systems. Where three or more components interact it may be possible to divide the system into weakly-interacting subsystems of two or three components [101]. Furthermore it may be sufficient to consider the interaction of subsystems that behave collectively in an inhibitory or activatory manner to derive necessary and sufficient conditions for instability (R. Satnoianu, *pers. comm.*).

There is no *a priori* reasoning to suggest that models of putative biological interest should be restricted to two-species systems. Below we take from the literature a model describing the interaction of a three component system which gives rise to patterns through the Turing instability and which can give stationary spatial patterns and time-oscillating patterns as model parameters are varied. White and Gilligan [131] propose the model for the interaction of a host-parasite-hyperparasite system, such as a cereal root complex infested with a parasite into which a biological control agent (hyperparasite: fungi, bacteria or other microorganism) has been introduced, to account for spatial patchiness in population density. A brief derivation of the model is presented in Appendix A.4, however, here we are primarily interested in the solution behaviour, rather than in the biological details.

The population dynamics is described by local interaction terms and diffusion is assumed to model the spatial spread and dispersion of each species. The nondimensional equations for host (v), parasite (w) and hyperparasite (u) on the growing domain are

$$u_t = \frac{1}{\gamma(t)} u_{xx} - \delta\,(u - w) - \rho\sigma(t)u \tag{4.33}$$

$$v_t = \frac{d_v}{\gamma(t)} v_{xx} + v\left(1 - \frac{v}{\kappa}\right) - vw - \rho\sigma(t)v \tag{4.34}$$

solutions may, however, be admitted in scalar reaction-diffusion equations, but not through the Turing instability (see Grindrod [46]).

$$w_t = \frac{d_w}{\gamma(t)} w_{xx} + \mu \left(v \frac{w}{1+\beta} - u \frac{w}{1+\beta w} \right) - \rho\sigma(t) w \tag{4.35}$$

where δ, κ, μ and β are nondimensional kinetic parameters and for slow uniform growth γ changes, as before, according to equation (4.3). The boundary conditions are zero flux at $x = 0, 1$, and we impose random initial conditions. First we consider parameters such that on the static domain (where $\rho = 0$ so that $\gamma = \gamma_0$) a stationary pattern develops through the diffusion-driven instability. Considering the Jacobian (around the stable fixed point of the kinetic system) we find

$$\mathcal{A} = \begin{pmatrix} -\delta & 0 & \delta \\ 0 & -\dfrac{v_s}{\kappa} & -v_s \\ \dfrac{\mu v_s}{1+\beta} & \dfrac{\mu u_s}{1+\beta} & \dfrac{\mu\beta v_s^2}{(1+\beta)^2} \end{pmatrix} \tag{4.36}$$

where the kinetic steady state values u_s and v_s are positive. Thus the Jacobian has the sign structure

$$\operatorname{sgn}(\mathcal{A}) = \begin{pmatrix} - & 0 & + \\ 0 & \begin{bmatrix} - & - \\ + & + \end{bmatrix} & \end{pmatrix} \tag{4.37}$$

so that w is self-activating, and in particular the interactions between v and w are those required for DDI with cross-kinetics in the two species problem (highlighted in the square brackets). Hence we may expect that if the diffusivities of v and w are sufficiently different then this subsystem alone may be sufficient to give rise to stationary heterogeneous pattern, without any further destabilising influence of u. Indeed, if we take $d_w \ll d_v \approx 1$ then we can recover stationary patterns in the three species, as shown in Figure 4.12(a). Here w takes role of activator (and has the largest amplitude pattern) and v is the inhibitor (which is out of phase with w for the cross-kinetic system). We do not present any further analysis of DDI in this system here but refer the reader to White and Gilligan [131].

Considering the model on the growing domain, we find that in this regime the patterns evolve by peak splitting of species w (the activator) in an analogous manner to the two species examples studied in the previous section. A numerical solution for the activator species w is shown in Figure 4.12(b).

If the ratios of diffusivities are changed so that d_v and d_w are not significantly different in magnitude but are both small (in comparison to $d_u \equiv 1$), then we cannot make the above inferences. In fact it is possible to excite spatially heterogeneous instabilities which oscillate in time under such conditions. In this case, on the static domain the long-time behaviour of the system is oscillatory, with a timescale that is intrinsic to the equation parameters. The time-varying solution $w(x,t)$ for the model under these conditions is plotted in Figure 4.13(a). The oscillations for u and w are

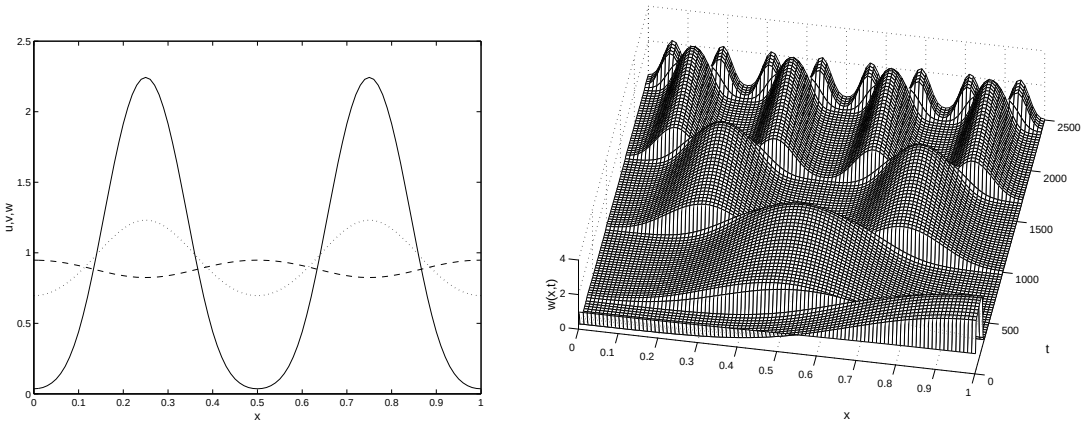

(a) (b)

FIGURE 4.12 Pattern formation for non-oscillatory solutions in the three-species model of White and Gilligan. In (a) we plot $u(x)$ (dotted), $v(x)$ (dashed) and $w(x)$ (solid) steady state patterns for the stationary domain with $\gamma_0 = 10$ and in (b) we plot the evolving profile $w(x,t)$ on the growing domain with $\rho = 0.001$ and $\gamma_0 = 1$. Kinetic parameters are $\kappa = 10$, $\mu = 15$, $\delta = 5$ and $\beta = 4$ with ratios of diffusivities $d_v = 1.0$ and $d_w = 0.05$.

out of phase with those of v. The frequency of oscillation is approximately 0.1 nondimensional units.[3] It is interesting to ask what effects the interaction of the timescale for domain growth has with the timescales for pattern oscillation and pattern formation linear growth. The timescale for slow domain growth is much longer than that for oscillation so that the patterns will not be quasi-stationary when transitions are initiated. Solutions for $\rho = 0.01$ are shown in Figure 4.13(b)–(d). We choose a value for ρ at the high end of 'slow' domain growth because the timestep required to compute the oscillation is correspondingly small. Similar behaviour is observed for lower values of ρ. The simulations show that the solution no longer undergoes the simple FD behaviour shown in the previous case. The solution becomes increasingly complicated, and pattern appears to move in an increasingly (oscillatory) wave-like manner from the centre outwards. At later times the behaviour becomes quite irregular and asymmetric. This increased complexity might be expected as the effect of introducing a third timescale into the problem.

There are no qualitatively new phenomena which can arise from the diffusion-driven instability when systems of more interacting components are considered. The three-species problem illustrates both stationary and oscillatory spatial patterns, which introduce a new timescale through the oscillation. On the growing domain, this third

[3]The ratios of diffusivities in Figure 4.13(a) are $d_v = 0.04$ and $d_w = 0.005$, however, similar results are recovered for $d_w = 0.02$, as used by White and Gilligan. The period of the oscillations is $T \approx 11$ nondimensional time units. This is contrary to the period of oscillation reported by White and Gilligan, which is on the order of 10^2 too large, probably due to under sampling arising from too large a timestep in their simulation.

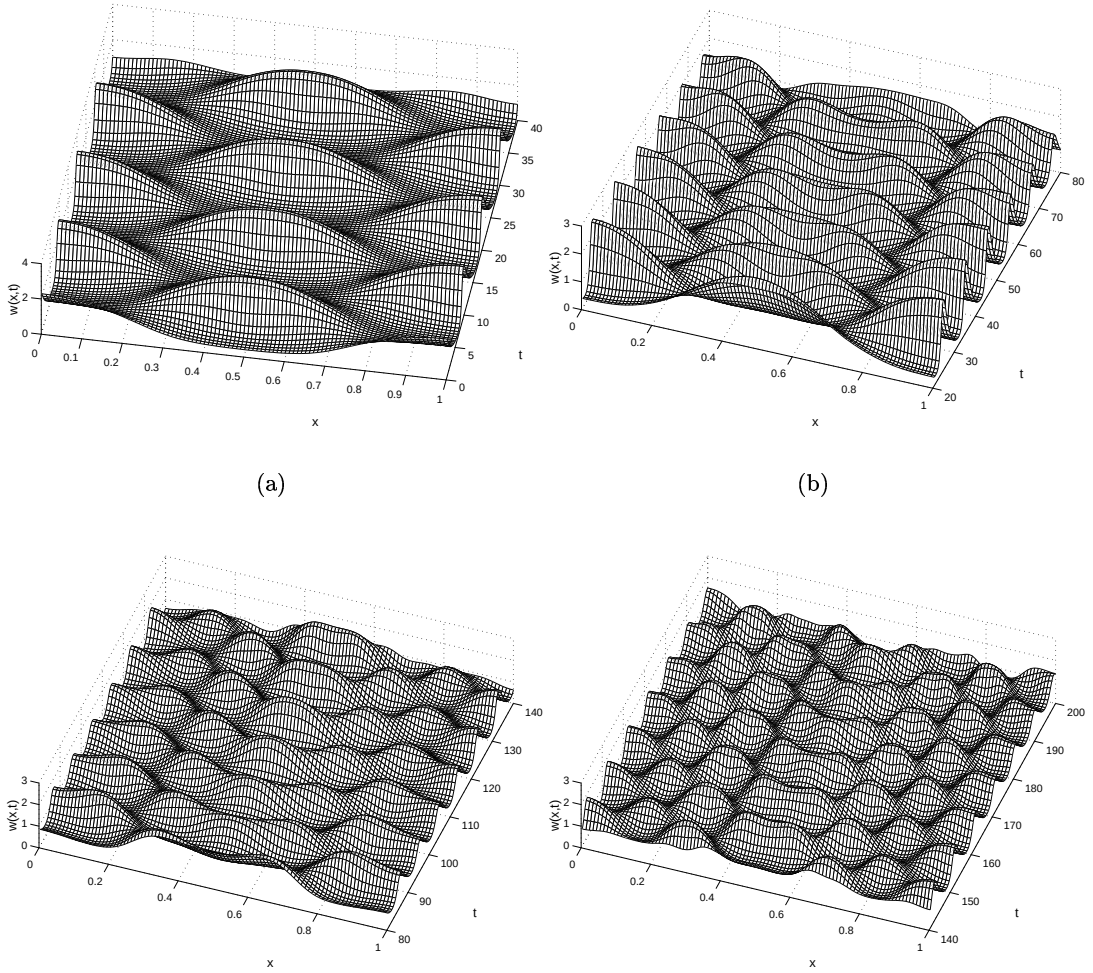

FIGURE 4.13 Oscillating patterns in the three-species model of White and Gilligan (a) on the static domain and (b)–(d) evolution of oscillating pattern on the growing domain, with (b) $t \in [20, 80]$, (c) $t \in [80, 140]$ and (c) $t \in [140, 200]$. Kinetic parameters are $\kappa = 500$, $\mu = 2$, $\delta = 2$ and $\beta = 4$ with ratios of diffusivities $d_v = 0.04$ and $d_w = 0.005$. In both cases $\gamma_0 = 25$ and for the growing domain $\rho = 0.01$.

timescale interacts with those already in the problem, the timescales for pattern growth and domain growth, and underlies the difference in behaviour between these two cases.

4.4 Other Domain Growth Functions

For a tissue expanding locally under constant strain rate the growth is exponential. This may be considered to model a population of cells dividing at a fixed rate which is independent of spatial or temporal coordinate. While this may be a reasonable model of the initial stages of an unconfined growth it is not realistic for many biological applications. We wish to know if the functional form of the domain growth has any bearing on the pattern sequence generated. We can use the symmetry analysis to investigate pattern formation under other functional forms for the domain growth. In previous studies various authors have considered linear growth. Although this may not have a strong biological motivation, studying this growth function gives further insight into the mechanism of pattern sequence formation. We also consider the biologically plausible scenario of logistic time dependence, where the final domain attained is limited to some finite size.

4.4.1 Linear Growth. Uniform linear domain growth, which we define by $r(t) = 1 + \rho t$, may be generated by the time-varying strain rate

$$S(t) = \rho\sigma(t) = \frac{\rho}{1+\rho t}. \tag{4.38}$$

We apply the previous analysis to the problem with explicit linear growth. Again t is eliminated, writing

$$\gamma(t) = \gamma_0(1+\rho t)^2, \quad h(\gamma) = \frac{d\gamma}{dt} = 2\rho\sqrt{\gamma_0\,\gamma} \tag{4.39}$$

so that $h(4\gamma) = 4\rho\sqrt{\gamma_0\gamma} = 2h(\gamma)$, which does not satisfy the condition (4.26). For convenience we will take $\gamma_0 = 1$. As before we examine the evolution of a pattern over some interval $[\gamma, 4\gamma]$. On eliminating t the governing equation for $c(x, 4\gamma'; \rho)$ is

$$\rho\sqrt{\gamma'}\frac{\partial c}{\partial \gamma'} = \frac{d}{4\gamma'}\frac{\partial^2 c}{\partial x^2} + R(c) - \frac{\rho c}{2\sqrt{\gamma'}}. \tag{4.40}$$

Again we consider the frequency-doubling construction, while this time allowing for a change in ρ to find the equivalent equation. Now $q_2(x, \gamma'; \rho') \equiv c(p_2(x), \gamma'; \rho')$ satisfies

$$2\rho'\sqrt{\gamma'}\frac{\partial q_2}{\partial \gamma'} = \frac{d}{4\gamma'}\frac{\partial^2 q_2}{\partial x^2} + R(q_2) - \frac{\rho' q_2}{\sqrt{\gamma'}} \tag{4.41}$$

so that $q_2(x, \gamma; \rho/2)$ and $c(x, 4\gamma; \rho)$ are shown to satisfy the same equation.

The implication of this result is that prolonged FD behaviour is not a natural consequence of this growth function. However, as before, if there exists a point $\gamma = \gamma^*$ such that

$$q_2(x, \gamma^*; \rho/2) = c(x, 4\gamma^*; \rho) \tag{4.42}$$

then $q_2(x, \gamma; \rho/2)$ and $c(x, 4\gamma; \rho)$ coincide for all $\gamma > \gamma^*$. This implies that if a sequence generated with linear growth rate ρ undergoes N frequency-doubling events before this sequence breaks up, then a sequence generated at growth rate 2ρ must complete $N + 1$ such events. Again we conjecture that stability properties are inherited from the results of numerical simulations. Numerical evidence confirming this prediction for one such regime is presented in Figure 4.14. Although the analysis does not give any information about the sequence after the breakdown of FD, numerical solutions suggest that the subsequent behaviour is not robust, and the sequence may be different for each set of initial conditions.

4.4.2 Comparisons with Exponential Domain Growth. For slow pattern evolution in the quasi-steady regime the timescale for pattern formation must be sufficiently faster than that for domain growth. We can predict the point of breakdown of the frequency-doubling sequence under linear growth conditions from knowledge of the lower limit in the rate-determining parameter, ρ_c, for the sequence under exponential growth. Comparison of growth rates then suggests that FD will occur for linear growth while

$$h_{lin}(\rho) \geq h_{exp}(\rho_c) \tag{4.43}$$

where $h_{exp} = 2\rho\gamma$ and $h_{lin} = 2\rho\sqrt{\gamma\gamma_0}$, which gives frequency-doubling for

$$\gamma \leq \gamma^* \equiv \gamma_0 \left(\frac{\rho}{\rho_c}\right)^2 \tag{4.44}$$

and the FD behaviour is expected to break down for γ above γ^*. This value is indicated by the vertical dashed line in Figure 4.15. Numerical simulations have confirmed that for linear domain growth the value of γ for breakdown varies approximately with the square of ρ. From equation (4.44) we see that higher pattern modes (for which we require large γ^*) may be admitted prior to the breakdown of the sequence only if ρ is sufficiently larger than ρ_c. Then from the first of (4.39) the sequence is expected to break down for times t where

$$t > t^* \equiv \frac{1}{\rho_c} - \frac{1}{\rho} \approx \frac{1}{\rho_c} \tag{4.45}$$

which, for $\rho_c \approx 10^{-6}$, gives the correct order of magnitude for the results of numerical simulations shown in Figure 4.14.

For large ρ, analogously to the exponential case, breakdown of FD occurs as $\rho \to 1$ through the introduction of an asymmetry during transitions between low modes. This happens as the timescales for pattern formation and domain growth coincide and the distinction between slow and fast dynamics regimes for the evolution is eroded.

4.4.3 Logistic Growth. If the sensitivity of the tissue to the patterning mechanism is confined to a phase of exponential growth, then the previous results are sufficient to predict the patterning behaviour. However, if pattern is organised during the period

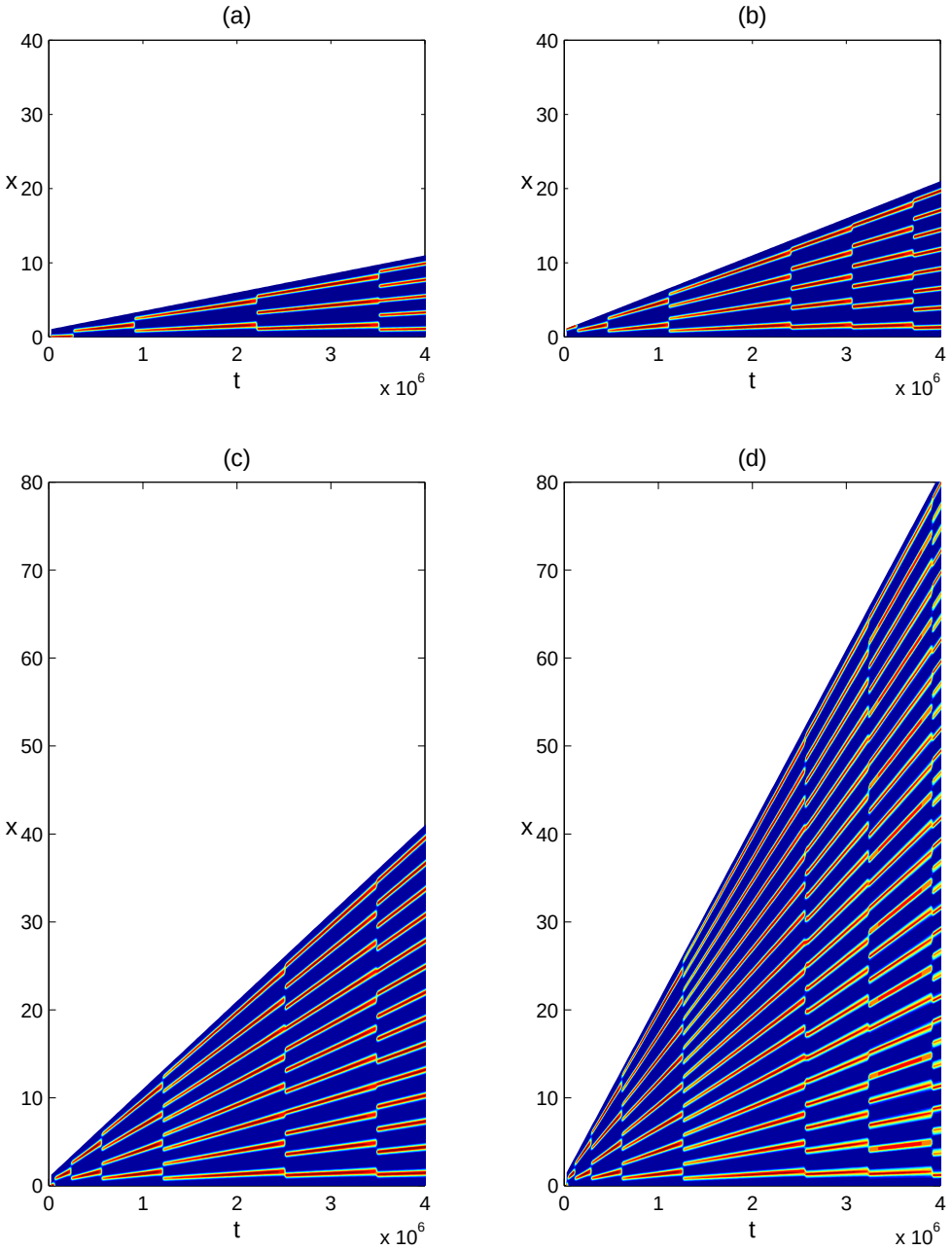

FIGURE 4.14 Pattern sequences under linear domain growth. The evolution of the activator concentration profile $v(x,t)$ with Schnakenberg kinetics for (a) $\rho = 2.5 \times 10^{-6}$, (b) $\rho = 5.0 \times 10^{-6}$, (c) $\rho = 1.0 \times 10^{-5}$ and (d) $\rho = 2.0 \times 10^{-5}$, with $\gamma_0 = 1.0$, showing 2, 3, 4 and 5 frequency-doubling transitions respectively before the sequence breaks down. Transitions appear discontinuous because they occur over a time interval much smaller than the total interval shown in the figures. Other simulations have shown that subsequent to breakdown of FD the pattern sequence is non-robust both as to the component modes in the sequence and as to when the transitions occur.

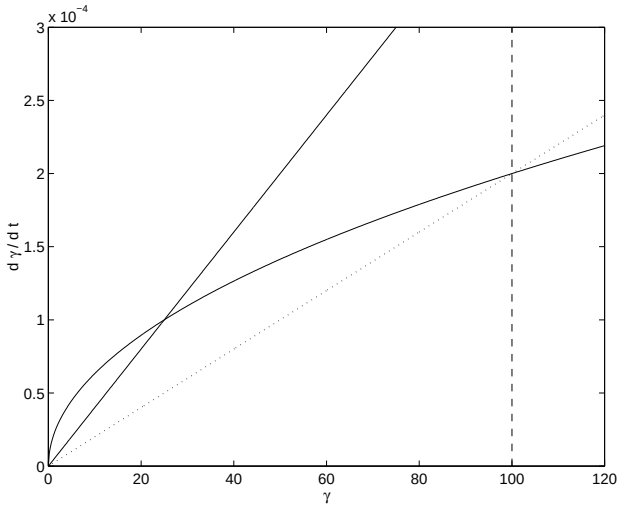

FIGURE 4.15 Illustration of the condition (4.44). The rate of change of γ is plotted against γ for exponential (straight line) and linear (curved line) growth functions. The intersection (marked with vertical dashes) between the linear growth curve and the line for exponential growth at the (lower) critical rate parameter ρ_c (dotted line) gives the approximate value of γ after which the FD sequence is expected to break down for linear growth. The straight solid line represents exponential growth for $\rho > \rho_c$ for which frequency-doubling is observed.

over which the domain growth slows and saturates to achieve some final domain size then we wish to see how this affects pattern formation, and in particular the robustness of the sequence and final pattern that is obtained. Therefore we consider pattern formation under a (spatially uniform) logistic growth function

$$r(t) = \frac{\zeta \exp(\rho t)}{\zeta + \exp(\rho t) - 1} \tag{4.46}$$

such that $\mathrm{d}r/\mathrm{d}t = \rho r(1 - r/\zeta)$, where ζ is the ratio of final to initial length. This may be generated from a local time varying strain rate with time dependence

$$S(t) = \rho\sigma(t) = \frac{\rho\,(\zeta - 1)}{\zeta + \exp\,(\rho t) - 1}. \tag{4.47}$$

In Figure 4.16(a) we show the results of a numerical simulation for logistic domain growth in which mode $m = 16$ persists at the final domain size. We have chosen the rate parameter ρ to be relatively large such that the transitions between patterns are shown to be smooth. The logistic growth is initially exponential in form, but slows to asymptotically approach the final domain length. If we are in the range for which exponential and linear growth functions give FD then we might expect, for a given ρ and for most ζ, that one constituent mode of the FD sequence will persist as the domain tends asymptotically to its final length. However, if ζ is such that the sequence begins to undergo reorganisation during the asymptotic approach to the final domain size, then some other mode may be admitted and non-robust pattern selection may occur. We will seek to ascertain the relative size of the interval in ζ in which another

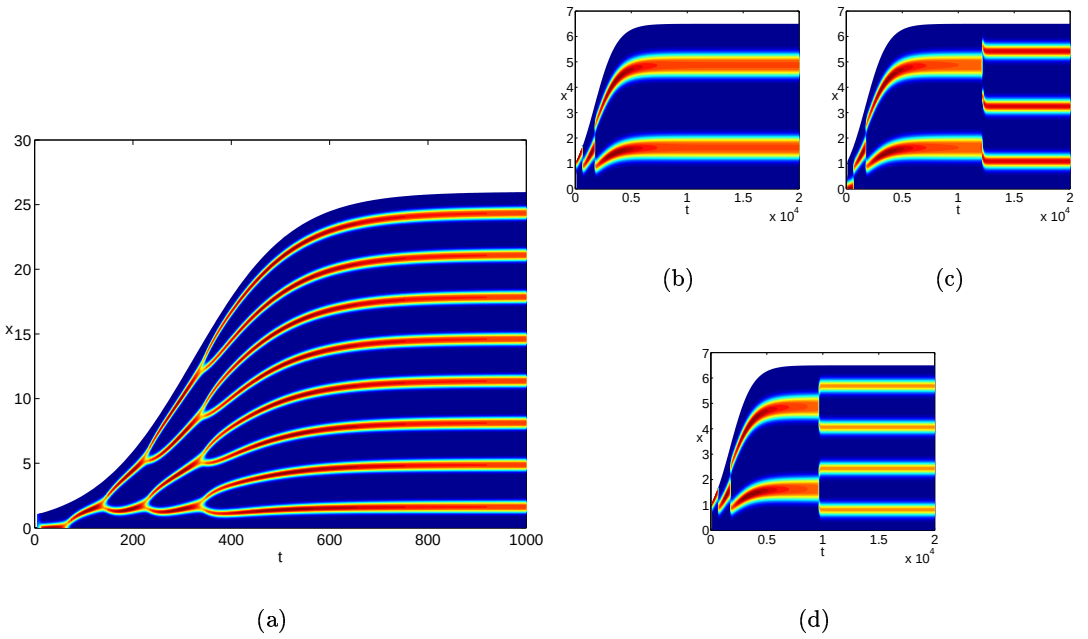

FIGURE 4.16 Pattern sequences under logistic growth. Evolution of activator concentration profile $v(x,t)$ with Schnakenberg kinetics for logistic growth with (a) $\rho = 0.01$ and $\zeta = 26.0$ showing selection of mode $m = 16$ from the FD sequence. The short interval in ζ for which other patterns are admitted is illustrated for $\rho = 0.001$ with (b) $\zeta = 6.50 \approx \zeta_4^{max}$ selecting $m = 4$, (c) $\zeta = 6.51$ for which the final pattern is $m = 6$, not in the FD sequence, and (d) selection of $m = 8$ for $\zeta = 6.52 \approx \zeta_8^{min}$. Solutions are for Schnakenberg kinetics.

mode, not an element of the foregoing FD sequence, is the final pattern mode selected as the domain tends to its final size.

If, for given ρ, a particular mode m of the FD sequence persists to the final domain length for the interval $\zeta \in [\zeta_m^{min}(\rho), \zeta_m^{max}(\rho)]$, then the existence of a window of non-robust behaviour implies that $\zeta_{2m}^{min} > \zeta_m^{max}$. The probability of observing a final pattern which is not of the FD sequence will depend on the relative sizes of $\mathcal{R}_m = \zeta_m^{max} - \zeta_m^{min}$ and $\mathcal{N}_{m,2m} = \zeta_{2m}^{min} - \zeta_m^{max}$, intervals of robust and non-robust pattern selection respectively, which will depend on m and ρ. Numerically we can estimate ζ^{max} and ζ^{min} for different modes through repeated simulations for different values of ζ and hence calculate estimates for $\mathcal{N}_{m,2m}$ and $\mathcal{R}_m$. Such estimates for $\rho = 0.001$ and $d = 0.01$, taken from a series of numerical simulations, are presented in Table 4.1. These data show that intervals of non-robust pattern selection $\mathcal{N}$ are over two orders of magnitude smaller than the intervals, $\mathcal{R}$, for which the final pattern is from the FD sequence. Figure 4.16(b)–(d) illustrates the final pattern selection over a small interval in ζ, with the final pattern moving from mode 4 to 8. The window of non-robust behaviour exists but is relatively very small. We find in the window $\mathcal{N}_{m,2m}$ that we get modes between m and $2m$, usually we see even modes (internalised peaks)

mode m	1	2	4	8	16	32	64
ζ_m^{min}	–	1.63	3.26	6.52	13.03	26.09	52.43
ζ_m^{max}	1.62	3.25	6.50	13.00	26.04	52.33	106.60
$\mathcal{R}_m = \zeta_m^{max} - \zeta_m^{min}$	–	1.62	3.24	6.48	13.01	26.24	54.17
$\mathcal{N}_{m,2m} = \zeta_{2m}^{min} - \zeta_m^{max}$	0.01	0.01	0.02	0.03	0.05	0.10	–

TABLE 4.1 Windows of non-robust pattern selection for logistic domain growth. The table contains numerical estimates (± 0.01) for the critical values of ζ (defined in the text) for various modes, under logistic growth with $\rho = 0.001$, $d = 0.01$ and Schnakenberg kinetics. Numerical solutions were computed to large time to reliably estimate ζ_{min}.

for Schnakenberg, although much less frequently we do observe odd mode patterns. Within the window it seems that for a given $\zeta \in [\zeta_m^{max}, \zeta_{2m}^{min}]$ one can get different final modes between m and $2m$ for different sets of initial conditions.

Numerical simulations also allow us to investigate how the windows of non-robustness depend on the parameters d and ρ. The numerical estimates of ζ_m^{max} and ζ_m^{min} for different combinations of these two parameters for the transition between modes 4 and 8 are shown in Table 4.2. These data suggest that the window $\mathcal{N}_{4,8}$ shrinks with increasing ρ (as the domain growth rate is increased) while the beginning of the window in ζ does not move as ρ is varied. However, when the ratio of diffusivities is increased towards d_c the window grows, while the onset is delayed by increasing d. Over the range of d and ρ tested, the window still remains much smaller than the range of ζ for which the pattern from the FD sequence is selected.

4.4.4 Hysteresis. The model (4.1)–(4.3) exhibits hysteretic behaviour, which appears to be generic and not dependent on the particular kinetic scheme, and which is manifest in two ways. Firstly the equations show the simple hysteretic effect of an S-shaped bifurcation curve, giving bistability over some range of the parameter (here γ). Secondly, the actual sequence of patterns generated changes for a shrinking as opposed to a growing domain, over some wider range of γ. We investigate these phenomena with a concrete example, by considering an explicit time dependence. An exponentially increasing and decreasing domain size is given by

$$\gamma(t) = \begin{cases} \gamma_0 \exp(2\rho t), & t < t' \\ \gamma_0 \exp\left(2\rho\,(2t' - t)\right), & t \geq t' \end{cases} \tag{4.48}$$

so that $\gamma(0) = \gamma(2t') = \gamma_0$. Firstly we show hysteresis in the transition between two modes. For this purpose we consider the transition between modes $m = 1$ and $m = 2$, which avoids the complication of intervening modes. The amplitude of the activator profile $v(x,t)$, $\eta_2(\gamma)$, while increasing and decreasing γ according to (4.48) through the transition between modes, is plotted in Figure 4.17. The beginning and end points are the same, but the onset of the down-mode transition is delayed on decreasing γ, showing the hysteretic effect.

ρ	d	ζ_4^{max}	ζ_8^{min}	$\mathcal{N}_{4,8}$
0.001	0.01	6.500	6.512	0.012
0.0001	0.01	6.499	6.559	0.060
0.01	0.01	6.500	6.507	0.007
0.001	0.005	6.335	6.338	0.003
0.001	0.02	6.789	6.852	0.063

TABLE 4.2 The dependence of the onset and interval length of windows of non-robust pattern selection on model parameters. The table shows numerical estimates for ζ_4^{max} and ζ_8^{min} under logistic domain growth with various ρ and d. The approximate error in the ζ values is ± 0.001, and in the calculated $\mathcal{N}$ is ± 0.002.

For transitions at higher mode, where intervening modes are skipped, there is no guarantee that on decreasing γ the same sequence will be followed. In fact we find that in general a different set of patterns is observed, with a tendency to include a greater number of modes sequentially. An example is presented in Figure 4.18. The reasons underlying these hysteretic effects will be discussed in the next chapter.

4.5 Domain Growth is a Mechanism for Reliable Pattern Selection

The FD sequence that we have studied for slow uniform domain growth in one spatial dimension provides a mechanism by which pattern modes may be selected robustly. Our numerical results suggest that the frequency-doubling behaviour (whether by splitting or insertion) is generic to reaction-diffusion systems which generate spatial pattern through the Turing instability, and that the sequence is not destroyed by varying the boundary conditions from zero-flux. The sense in which patterns in the sequence are robustly generated is that once initiated, the sequence of patterns unfolds with no dependence on the initial conditions. Once a large amplitude pattern is established the dynamics are governed by the change in γ. We have shown that logistic domain growth can reliably (although not perfectly) select one pattern from a sequence which persists as the domain tends asymptotically to its final size.

Semi-scale Invariance. On a domain of fixed size, pattern selection depends strongly on the domain length and multiple patterns may be admissible for a particular length for different sets of initial data. For the FD sequence the situation is quite different. The pattern sequences capture a degree of insensitivity to domain length, with each pattern element in the sequence persisting while the domain *doubles* in length. This *semi*-scale invariance is particularly significant in that it allows regulation, whereby a specific number of pattern elements is laid down despite significant variation in the domain size and without need to finely tune parameter values. Previous attempts to achieve scale invariance in reaction-diffusion systems have all required feedback from the domain size to the kinetic parameters in the model [100, 52]. The semi-scale invariance demonstrated on the growing domain arises as a natural consequence of the mechanism by which pattern sequences are formed.

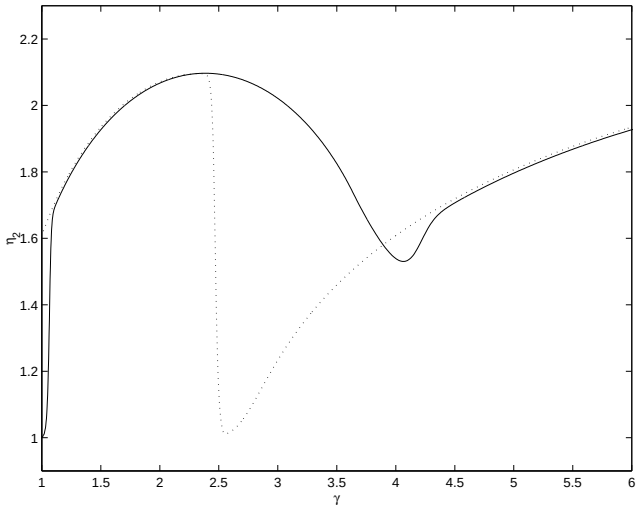

FIGURE 4.17 Hysteresis in a single transition for exponential domain growth and contraction. The maximum amplitude, $\eta_2(t)$, for the activator is plotted for increasing (solid) and decreasing (dotted) γ, both parameterised by time t. The domain growth and contraction has $\rho = 0.001$ for $\gamma(t)$ given by equation (4.48) with $\gamma_0 = 1$ and $t' = 1000$. We use Schnakenberg kinetics and $d = 0.01$.

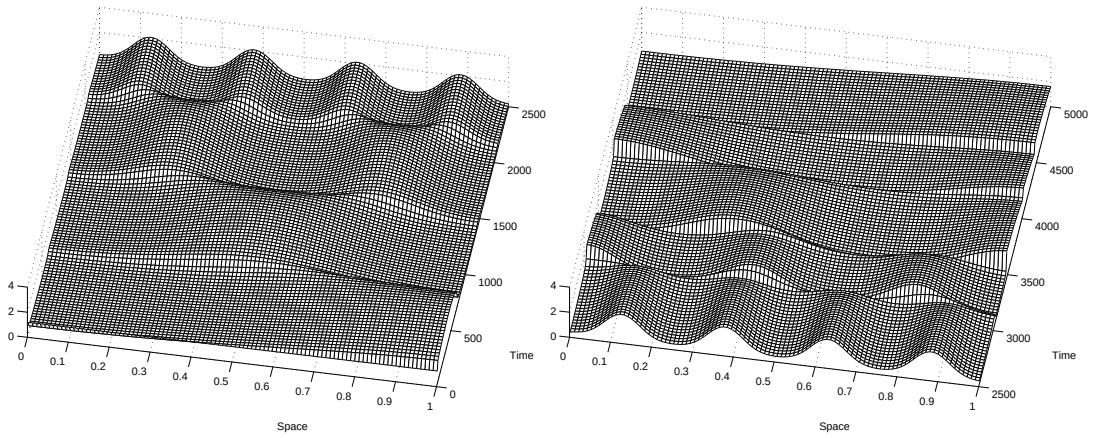

(a) (b)

FIGURE 4.18 Hysteresis in the pattern modes comprising the sequence for exponential domain growth and contraction, for the same initial and final domain size, γ_0. Activator $v(x,t)$ profiles are plotted for (a) increasing and (b) decreasing domain size (γ). The domain grows until time $t' = 2500$ from which point the domain is contracting. In the simulation we take $\rho = 0.001$ for $\gamma(t)$ given by equation (4.48) with $\gamma_0 = 1$, with Schnakenberg kinetics and $d = 0.05$.

4.6 Discussion

The slow growth limit that we have considered in this chapter seems reasonable in the context of biological pattern formation. When the spatial domain is changing length on a timescale which is commensurable with the time taken for pattern formation there is no quasi-steady behaviour, and the resulting evolving spatial profile appears to be quite disorganised. We have seen that the pattern sequence may depend on the rate and functional form of the change in γ with time. This indicates that the solution does not adiabatically follow steady solution branches during transitions between patterns. The dynamics which take the evolving spatial profile from the vicinity of one bifurcation branch to another is investigated in the following chapter. Under slow growth a dilution term appears which slightly modifies the kinetics. This term has a magnitude which is on the order of the slow rate of change of the domain size. In fact the symmetry argument and the conclusions that have been drawn are equally valid if this modification to the kinetics is neglected.

The symmetry analysis that allowed us to predict FD for exponential domain growth and conditions on the growth rate parameter ρ for linear domain growth reflects the symmetry in the underlying solutions to the steady state problem. Similar arguments have been proposed recently by Nishiura and Ueyama [95] for the bistable Gray-Scott model, to explain the closely related phenomenon of self-replicating patterns on the fixed domain. Numerically it is found that a pattern initiated in some region of a domain spreads to fill the domain by splitting of the outermost peaks (see Figure 2.7(b)). The authors suggest that the symmetry in the steady state equations that we have demonstrated in Chapter 2, which they call 'folding-up', causes related inhomogeneous solution branches to line up in the bifurcation diagram, so that the saddle-node bifurcation points at which they are created line up at the same value of the control parameter. The authors call this the 'edge of hierarchy structure of limiting points'. The trajectory of the PDE solution from suitably chosen initial data passes close to each of these limiting points of the branches so that transient patterns approximating the steady solutions are observed for the full PDE system. In the present work the situation is somewhat different in that we have a time dependent γ, which may be thought of as the control parameter. However, it seems that the symmetry identified in the steady state problem may be responsible for both results. Furthermore, we have been able to show that in our model the symmetry argument can be extended into the full PDE system.

Linear analysis identifies a minimum domain length (and hence a minimum γ) for each pattern mode. The critical domain length for solutions corresponding to patterns of the lowest mode (the half- or boundary-peak) gives a minimum domain length below which no Turing bifurcation is possible (however, for subcritical bifurcation, inhomogeneous solution branches may exist below this point). For the numerical computations in this chapter the initial domain length has been taken to be smaller

than the critical domain length. As the domain grows the first destabilising mode, the lowest admissible pattern, is excited as the domain length increases through the critical point ($\gamma = \gamma_c$). However, if the initial domain is sufficiently large that patterns of higher mode may be excited, then the FD sequence which ensues may be based on a different initial mode. In general, if the initial mode to be excited through the Turing bifurcation is mode $m = m_0$ then the sequence will comprise modes $m_0 \times 2^n$. However, we reiterate that pattern selection becomes increasingly unreliable as the domain length increases, and close control of initial data and domain length is required to select initial patterns of large mode number m_0. For this reason the mechanism that we have described in this chapter for uniform domain growth is not well suited to reliably generating patterns with an odd number of peaks, which require higher m_0. We will reconsider this later in the context of nonuniform domain growth.

We have demonstrated that a reaction-diffusion mechanism on a growing one-dimensional domain can reliably generate patterns with multiple periodic peaks. This is contrary to the conclusions of Saunders and Ho [118] which are based on the numerical simulations of the model by Arcuri and Murray [3] (AM). Here the authors nondimensionalise time using T_D, the diffusive relaxation time (see (2.6), by writing $\bar{t} = \omega t/\gamma$ and subsequently impose time dependence on γ where it appears explicitly in the evolution equation (3.1). The timescales for pattern formation and for domain growth, the importance of which we have emphasised, thus become conflated. This distorts the evolution of pattern sequences in the AM model, which fails to produce the robust sequences we have found. Neglecting the dilution term, one may transform the AM equations into our model by defining a new time variable $z = \int_0^t \mathrm{d}t/\gamma(t)$. The time dependence for γ in the AM equations which corresponds to an exponentially growing domain may then be found, namely $\gamma(z) = \gamma_0/(1 - 2\rho\gamma_0 z)$. Numerical solutions of equation (3.1) with this form for $\gamma(z)$ show that FD behaviour is observed in the AM model with the appropriate time dependence, for $z < 1/2\rho\gamma_0$ where $\gamma(z)$ becomes singular.

The strong tendency to splitting of activator peaks (and insertion for the Gierer-Meinhardt kinetics) is striking. Following breakdown of the FD sequence for linear growth, subsequent patterns still develop by splitting (for Schnakenberg kinetics) of a subset of the peaks on the domain, to give activator patterns with internalised peaks. In the following chapter we examine this tendency for splitting and insertion of new peaks in more detail.

5. Spikes and Transition-Layers: Piece-wise Linear Models

Two mechanisms for transition between quasi-steady patterns in sequences generated on the slowly growing domain are observed for the kinetic models in the literature admitting DDI. In the previous chapter these mechanisms were illustrated with Schnakenberg kinetics for activator peak splitting, shown in Figure 4.1(a), and by the Gierer-Meinhardt model for peak insertion, see Figure 4.10(a). In this chapter we seek to understand these properties of the equations and in particular establish what determines the mode of transition for a particular choice of kinetic scheme. To these ends we simplify the problem by introducing a piece-wise linear approximation to the reaction-diffusion system.

In Chapter 4 it was shown that for slow domain growth the evolution of solutions to the PDE separates into two distinct timescales. Here we make use of this separation of scales and consider the parameterisation by γ of quasi-steady patterns which evolve on the slow timescale. In the limit as ρ tends to zero these patterns are well approximated by the steady state patterns for the reaction-diffusion equation on the fixed domain. Furthermore, for small d the spatial behaviour of the reaction-diffusion system is separated into regions where the solution varies on two distinct spatial scales. It is convenient to write $d \equiv \epsilon^2$ where $\epsilon \ll 1$. Then in the limit $\epsilon \to 0$ the spatial variation of solutions in the steady state is determined by the *outer* equations

$$u_{xx} = -\gamma f(u,v) \tag{5.1}$$

$$0 = g(u,v) \tag{5.2}$$

suggesting that the solution must lie on the nullcline for v, except in the vicinity of large spatial gradients in v, where we expand the independent variable, $\xi = x/\epsilon$, to obtain the *inner* approximation

$$u_{\xi\xi} = 0 \tag{5.3}$$

$$v_{\xi\xi} = -\gamma g(u,v). \tag{5.4}$$

Our method is to exploit the ratio of diffusivities d as a small parameter in a singular perturbation expansion in which we look for solutions in the limit as d tends to zero. In particular we can find closed form approximate solutions of the system, showing that the slow dynamics carry the system to a point, which can be calculated, where a solution of a given mode ceases to exist and where reorganisation of the pattern ensues on the fast timescale. From this analysis we also identify a novel behaviour, *frequency-tripling*, which is characteristic of a symmetry in the kinetic equations.

The steady patterns arising from the Turing instability in reaction-diffusion equations may be grouped into two classes, according to the asymptotic behaviour as the

ratio of diffusivities tends to zero. *Spike* patterns, such as those generated by the Schnakenberg and Gierer-Meinhardt systems, consist of periodic peaks in the activator profile for which the amplitude increases (and becomes unbounded) and the width decreases as d is reduced to zero. Thus spike patterns approximate δ-functions in the limit. *Transition-layer* patterns develop discontinuous jumps between two activator levels, becoming step-functions as d tends to zero. The difference between these two pattern-types is determined by the manner in which the kinetics saturate the growth of destabilising modes, in particular by the shape of the nullcline for the activator kinetics (see, for example, Kerner and Osipov [62]—we take a similar approach to theirs below).

Reaction-diffusion models for spatial patchiness in population levels for predator-prey interactions have been proposed by Segel and Jackson [121] and Levin and Segel [73], in which the spatial distribution is generated by DDI. In many such ecological settings it is desirable that the subdivision of the domain into regions of high and low population density is maintained when the prey species is effectively stationary, such as herbivore-plant interactions (herbivorous copepods, zooplankton, and grazing phytoplankton [73]) or various host-parasite systems [121]. In this case the ratio of prey to predator diffusivity is reduced to zero. Mimura and Murray [83] showed that for these models the spatial extent of regions of high population tended to zero with the ratio of diffusivities (the kinetics are spike-type), and proposed that a cubic form is required for the nullclines for pattern which continues to subdivide the domain as d is decreased.

Much of the theory of large amplitude patterns of transition-layer type was developed by Fife [39, 40]. Kerner and Osipov discuss these patterns and their stability [62] and also discuss spike-type kinetics. Spike patterns, or point condensations, are the subject of much current interest (see Ni [92] for a recent review). Doelman and co-workers have used geometric singular perturbation theory to investigate the existence [33] and stability [32] of spike patterns in the Gray-Scott model, also studied by Muratov and Osipov [86]. Alternatively, Ward *et al.* [53, 54] consider the stability of spike solutions to the Gierer-Meinhardt system and the motion of spike solutions in two and three dimensions.

5.1 Transition-Layer Theory

Fife [38] showed the existence of large amplitude stationary solutions in a class of coupled reaction-diffusion equations, characterised by narrow transition regions which subdivide the domain into two phases (high and low activator concentrations), requiring one component to diffuse much faster that the other. Fife's discussion of these solutions depends on global properties of the system, rather than on the local behaviour of the system close to a bifurcation point, as do Turing's analysis and the weakly nonlinear bifurcation analysis presented in Chapter 2. Large amplitude weak solutions to the steady state problem may be constructed in the limiting case $\epsilon = 0$ by

allowing a jump discontinuity in the solution, which for $\epsilon \neq 0$ is smoothed out to give a continuously differentiable graph. In the singular limit solutions are deemed *weak* as they admit a jump discontinuity. In comparison to a bifurcation-type approach, here we are nowhere near a fixed point in phase space. In fact the conditions derived for Turing bifurcation from a homogeneous state, described in Chapter 2, are not necessary requirements. Large amplitude solutions may be formed where a sufficiently strong perturbation from a stable fixed point in the phase space takes the solution to a branch of stationary inhomogeneous solutions, so-called Turing branches, as discussed for the bistable Gray-Scott model in section 2.5.3.

The argument we present below is based in part on a discussion in the book by Grindrod [46], where a population model for ecological patchiness (predator-prey type interaction with diffusion) is considered. Conway [18] has a fuller discussion (see also Murray and Mimura [83]). In this chapter we use singular perturbation theory to construct heterogeneous solutions, showing existence of large amplitude patterns for a concrete example, and then examine the dependence of these solutions on γ. We will not pursue the analytical study of stability of the solutions, but rather refer to the arguments presented for transition-layer solutions by Fife [39] and also the work of Kerner and Osipov [62].

Transition-layer patterns may form in systems for which the activator nullcline takes a cubic form in the (u, v) phase plane, so that $g(u, v) = 0$ must have three solutions $v = k(u)$. The shape of the inhibitor nullcline $f = 0$ is not crucial for the existence of large amplitude patterns as long as the kinetics are monostable (such that the curves $f = 0$ and $g = 0$ intersect only at one point). We will discuss variations of this nullcline later. The two essential ingredients are the specific form of the activator nullcline and that the ratio of diffusivities is a small parameter. Below we illustrate the basic idea and show how it helps understand splitting and insertion. In a following section we pursue a specific example, where the analysis has been dramatically simplified by assuming a piece-wise linear form for the kinetics.

We study the coupled reaction-diffusion system for two species

$$u_t = \frac{1}{\gamma} u_{xx} + f(u, v) \tag{5.5}$$

$$v_t = \frac{\epsilon^2}{\gamma} v_{xx} + g(u, v) \tag{5.6}$$

with zero flux boundary conditions

$$u_x = v_x = 0 \quad \text{on} \quad x = 0, 1 \tag{5.7}$$

where the nullcline $g = 0$ has cubic form. The steady states of this equation are equivalent to the quasi-steady patterns for the problem on a growing domain, given by equations (4.9)–(4.10).

First we consider the possibility of solutions when $\epsilon = 0$. Consider the activator kinetics

$$v_t = g(u, v), \tag{5.8}$$

which has three stationary branches (the nullcline $g(u, v) = 0$) in the phase space, $v = k_i(u)$ where $i = 1, 2, 3$. In order to have transitions between two phases (corresponding to two branches of the nullcline) it must be the case that two of the branches, $i = 1$ and 3, are stable with respect to the dynamical system (5.8), for which we require $g_v < 0$. Following our ordering of the species in decreasing diffusivity, for DDI we must have $g_v > 0$ (self-activation of v) at the fixed point of the kinetics, which for consistency must lie on the unstable branch.[1] However, we note that the existence of the large amplitude transition-layer patterns does not depend on this condition, and below we discuss the implications of the kinetic steady state lying elsewhere. Simple considerations on the gradient of the nullcline at the fixed point (branch $i = 2$) dictate that for pure kinetics the nullcline is a negative cubic in v while for cross kinetics the nullcline has positive cubic form.

Firstly we consider the case of pure kinetics for which the nullcline is a negative cubic function of v, and so k_1 is defined on $u \in [u_{min}, \infty)$ while k_2 is defined on $u \in [u_{min}, u_{max}]$ and k_3 on $u \in (-\infty, u_{max}]$. Here u_{min} and u_{max} are the values of u at the turning points of the curve $g(u, v) = 0$ in the phase plane. From the phase plane it is straightforward to show that there are no nontrivial solutions with $v = k_i(u)$ satisfying both the conditions imposed at the boundaries. Next we consider solutions which are continuous in $u(x)$ and its derivative $u_x(x)$ but which allow a discontinuity in $v(x)$ at $x = x^* \in [0, 1]$ where $u = u^* \in [u_{min}, u_{max}]$ satisfying the reduced system

$$0 = u_{xx} + \gamma h(u) \tag{5.9}$$

where

$$h(u) = \begin{cases} f(u, k_1(u)), & u < u^* \\ f(u, k_3(u)), & u > u^* \end{cases} \tag{5.10}$$

and for a pure system $f(u, k_1(u)) < 0$ and $f(u, k_3(u)) > 0$ (for cross kinetics the signs are reversed). Assuming monostability, $h(u)$ has no roots ($f(u, k_2(u)) = 0$ at $u = u_s$ which is on branch $i = 2$). We look for orbits of this equation in the phase plane starting and finishing on $u_x = 0$. A schematic of a typical phase plane for equation (5.9) is shown in Figure 5.1. Here we construct a solution such that $v = k_1(u)$ for $0 \le x < x^*$ and $v = k_3(u)$ for $x^* < x \le 1$. Evidently we could reverse the polarity, and jump from branch $i = 3$ to branch $i = 1$ as x increases, for which we would have

[1] We note that the so-called 'unstable' branch ($i = 2$) is unstable *w.r.t.* equation (5.8), however, it is consistent that the fixed point of the kinetics (u_s, v_s) which lies on this branch is stable *w.r.t.* the dynamical system $u_t = f(u, v)$, $v_t = g(u, v)$, as required in the definition of the Turing bifurcation (and may be driven unstable by spatially heterogeneous perturbation for the full reaction-diffusion equation).

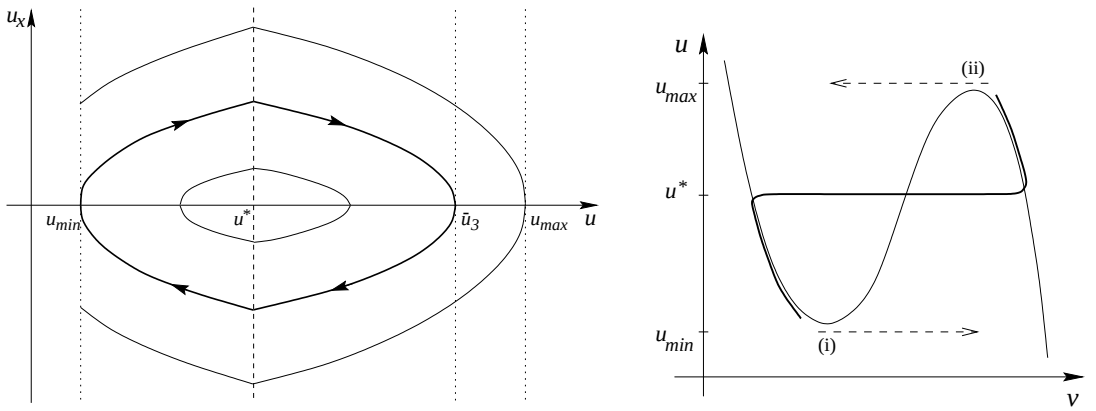

(a) (b)

FIGURE 5.1 Schematics of (a) the phase plane for equation (5.9), the outer problem for transition-layer patterns, and (b) the solution (bold) and the curve $g(u,v)=0$, showing the solution lying on the nullcline away from the jump in v at $u=u^*$ and the limiting points corresponding to case (i) and for case (ii) (see text for details).

$\tilde{h}(u)$ replacing $h(u)$ in equation (5.9) where

$$\tilde{h}(u) = \begin{cases} f(u,k_3(u)), & u < u^* \\ f(u,k_1(u)), & u > u^*. \end{cases} \tag{5.11}$$

Multiplying by u_x and integrating along orbits from 0 to x, we have the first integral

$$\frac{1}{2}{u_x}^2 + \gamma\Big[H\big(u(x)\big) - H\big(u(0)\big)\Big] = 0 \tag{5.12}$$

where

$$H\big(u(x)\big) \equiv \int_0^{u(x)} h(w)\,\mathrm{d}w \tag{5.13}$$

so that from (5.12) with boundary conditions (5.7)

$$H\big(u(1)\big) = H\big(u(0)\big). \tag{5.14}$$

We can find x from the so-called 'time-map'

$$x = \frac{1}{\sqrt{2\gamma}} \int_{u(0)}^{u(x)} \frac{\mathrm{d}w}{\sqrt{H\big(u(0)\big) - H(w)}} \tag{5.15}$$

where in particular for $x=1$

$$\gamma = \frac{1}{2}\left[\int_{u(0)}^{u(1)} \frac{\mathrm{d}w}{\sqrt{H\big(u(0)\big) - H(w)}}\right]^2 \tag{5.16}$$

and we see that γ parameterises the orbits in the (u,u_x) phase space. In fact it can be shown for a class of kinetic functions of the form we consider here that the time-map (5.16) is a monotonically decreasing function of $u(0)$. This is shown explicitly in a

result by Smoller and Wasserman [124]. Hence we can treat γ and $u(1)$ as functionals of $u(0)$.

There are three possibilities for the solution, depending on the precise form of the kinetics:

1. If $H(u_{min}) < H(u_{max})$ then for every $u(0) \in [u_{min}, u^*]$ there is a γ such that $u(1) \in [u^*, \bar{u}_3]$ exists satisfying (5.14), where $H(\bar{u}_3) = H(u_{min})$. This is the case shown in Figure 5.1(a).
2. If $H(u_{min}) > H(u_{max})$ then for every $u(0) \in [\bar{u}_1, u^*]$ there is a γ such that $u(1) \in [u^*, u_{max}]$ exists satisfying (5.14), where $H(\bar{u}_1) = H(u_{max})$.
3. If we have the symmetric case, where $H(u_{min}) = H(u_{max})$, then for every $u(0) \in [u_{min}, u^*]$ there is a γ such that $u(1) \in [u^*, u_{max}]$ exists satisfying (5.14).

In each case γ is determined by the time-map (5.16). In fact there is an infinite set of γ satisfying (5.16) for particular $u(0)$ and $u(1)$ corresponding to different numbers of cycles of the orbit, which give solutions of different mode.

Put otherwise, for a given γ one can find $u(0)$ and $u(1)$ satisfying the time map (5.16) along with equation (5.14) for a particular number of cycles, where valid solutions have $u(0), u(1) \in [u_{min}, u_{max}]$. Thus γ parameterises the quasi-steady solutions. Now $u(0)$ is a monotonically decreasing function of γ, and so as γ increases the solution may evolve towards a critical point $\gamma = \gamma^c$ at which the solution can no longer be constructed (the solution ceases to exist) and at which point reorganisation to a different mode must occur. For case (i) the critical point will occur at $u(0) = u_{min}$, shown in Figure 5.2(a), while for case (ii) the critical point is reached for $u(0) = \bar{u}_1$ (when $u(1) = u_{max}$), as in Figure 5.2(b) (see also Figure 5.1(b)). Both these conditions are reached simultaneously for case (iii). This analysis is pursued below with a concrete example.

For $\epsilon \neq 0$ these discontinuous solutions do not have sufficient smoothness to satisfy the equations. We treat the equations as a singular perturbation problem and expand about x^* in the stretched variable $\xi = (x - x^*)/\epsilon$ for which we have the inner problem for $U(\xi)$ and $V(\xi)$ describing the transition-layer,

$$0 = U_{\xi\xi} + \epsilon^2 \gamma f(U, V) \tag{5.17}$$

$$0 = V_{\xi\xi} + \gamma g(U, V) \tag{5.18}$$

and so as $|\xi| \to \infty$ we must have $U \to u^*$ and $V_\xi \to 0$ (and thus $V \to k_i(u^*)$ for $i = 1, 3$). Therefore we consider the reduced system where we let $\epsilon \to 0$ and take $U = u^*$ giving

$$0 = V_{\xi\xi} + \gamma g(u^*, V) \tag{5.19}$$

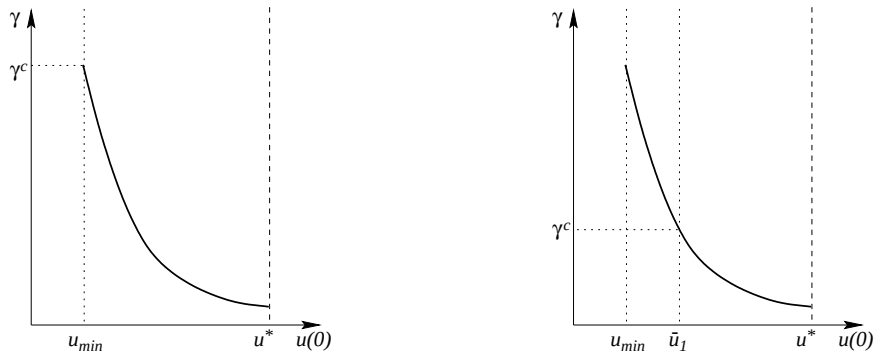

FIGURE 5.2 Evolution towards critical points as γ varies for solutions in the limit as $\epsilon \to 0$. In (a) $H(u_{min}) < H(u_{max})$ so that the solution can no longer be constructed as $u(0)$ decreases through u_{min} with increasing γ (case (i)), and in (b) $H(u_{min}) > H(u_{max})$ for which the solution ceases to exist when increasing γ causes $u(0)$ to decrease below $\bar{u}_1$, when $u(1) = u_{max}$ (case (ii)). When $H(u_{min}) = H(u_{max})$ these points coincide (case (iii)).

and we seek a heteroclinic orbit connecting $V = k_1(u^*)$ and $V = k_3(u^*)$. Multiplying equation (5.19) by V_ξ and integrating over $-\infty < \xi < \infty$ we have

$$G(u^*) \equiv \int_{k_1(u^*)}^{k_3(u^*)} g(u^*, w)\,\mathrm{d}w = 0 \tag{5.20}$$

and from considerations of the sign of g in different regions of the phase space we have for pure kinetics

$$G(u_{min}) > 0 \quad \text{and} \quad G(u_{max}) < 0 \tag{5.21}$$

while, for $g(u, v)$ a decreasing function of u,

$$\frac{\mathrm{d}G}{\mathrm{d}u^*} < 0 \tag{5.22}$$

so that the integral equation uniquely defines u^*, and hence x^*. For cross kinetics the inequalities in (5.21) are reversed and for $g(u, v)$ an increasing function of u then u^* is similarly uniquely determined.

Formally this analysis is equivalent to the leading order calculation in a matched asymptotic expansion. The leading order behaviour is sufficient to establish existence and the basic properties of the large amplitude solutions, including the location of the transition-layer (and dependence on γ). Similarly, periodic patterns may be constructed on the real line. We have said nothing about evolution from initial data or, other than of the outer problem, the stability of the solutions that we construct, and we will generally appeal to the results of numerical simulations for this purpose. However, in the literature various studies have been made of the stability of transition-layer problems. In a similar problem, Fife [39] considers a transition-layer as a travelling

wavefront with zero velocity and shows that a large spatial gradient may evolve from smooth initial data. Furthermore he shows that near the transition region ($x = x^*$) a perturbed wavefront may move back towards x^* under certain conditions.

Next we examine a specific and much simplified model and then investigate the mechanisms for transitions between patterns at the critical points identified above, determining how splitting and insertion are initiated.

5.2 Cubic Autocatalysis Model for Transition-Layer Patterns

Various schemes have been proposed in the literature as models of biochemical reactions with the prerequisites for the Turing bifurcation in a reaction-diffusion system. We consider reaction schemes of polynomial type, and seek to understand the influence of the nonlinearities on transitions between patterns on growing domains. Ermentrout [37] considered the role of quadratic and cubic nonlinearities in reaction terms in the generation of spotted and striped patterns on the two-dimensional domain. Following this example, we will consider the influence of cubic and quadratic nonlinearities in the transitions between patterns. It is informative to expand the kinetic function about the steady state so that the order of different terms is established. For concentration vector $\bar{\mathbf{c}} = \mathbf{c} - \mathbf{c}_s = (\bar{c}_1, \bar{c}_2, \ldots, \bar{c}_n)$ the transformed kinetics are

$$\bar{\mathbf{R}}(\bar{\mathbf{c}}) = \mathbf{R}(\bar{\mathbf{c}} + \mathbf{c}_s) = \mathcal{A}\bar{\mathbf{c}} + \mathcal{N}(\bar{\mathbf{c}}) \tag{5.23}$$

$$= \mathcal{A}\bar{\mathbf{c}} + \mathcal{N}_2(\bar{\mathbf{c}}, \bar{\mathbf{c}}) + \mathcal{N}_3(\bar{\mathbf{c}}, \bar{\mathbf{c}}, \bar{\mathbf{c}}) + \ldots \tag{5.24}$$

and we will assume that $\mathbf{R}$ can be expanded in this way. We note, however, that we no longer expect everywhere positive solutions for $\bar{\mathbf{c}}$, and the physically significant quantities $\mathbf{c}$ are recovered by the addition of the steady state concentrations $\mathbf{c}_s$. In this form the linearised equation contains simply the Jacobian $\mathcal{A}$, which should satisfy the conditions for Turing bifurcation, and the nonlinearities $\mathcal{N}_2$ and $\mathcal{N}_3$ are respectively quadratic and cubic combinations of the $\bar{c}_i$. Hereinafter for notational convenience we drop the over-bars, remembering that solutions may be negative legitimately. We will restrict discussion to include quadratic and cubic nonlinearities only, as these are the highest order terms associated with kinetics such as the Schnakenberg [119], glycolysis [122, 4] and Gray-Scott [45] models. The system may be further simplified by supposing that the nonlinear terms are in v and appear only in the activator equation (in $g(u, v)$). Then considerations in the phase plane on the orientation of the nullcline curve dictate that the cubic term in the kinetics must be negative (for both pure and cross kinetics). Below it is shown numerically that this kinetic model can give rise to Turing bifurcation to finite amplitude pattern, and that a sequence of patterns may form on the growing domain as normal. We will consider reaction terms which consist solely of odd powers of the dependent variables such that the reaction-diffusion system is invariant under the parity transformation

$$(u, v) \to (-u, -v) \tag{5.25}$$

and investigate the effect on pattern formation of quadratic perturbations which break the symmetry.

We can choose the linear part of the reaction term to admit the Turing bifurcation (although this is not required for the existence of large amplitude patterns of the form we have described) and specify the relative polarities of the spatial profiles for activator and inhibitor species according to the signs of the entries in the matrix $\mathcal{A}$. Initially we choose a pure kinetic system, in which the Fourier modes destabilising the spatially homogeneous state are spatially in phase for the activator and inhibitor. The nonlinear kinetics are given by f and g where

$$f(u,v) = -\sigma u + v \tag{5.26}$$

$$g(u,v) = -u + \mu v + \delta v^2 - v^3 \tag{5.27}$$

where the positive constants σ and μ are such that the linearised system,

$$\mathcal{A} = \begin{bmatrix} -\sigma & 1 \\ -1 & \mu \end{bmatrix}. \tag{5.28}$$

satisfies the conditions for DDI. The effect of quadratic terms on the behaviour of a system which is predominantly cubic is examined by introducing a small quadratic contribution, $|\delta| \ll 1$. In chemically oriented discussions of cubic autocatalysis the cubic term is usually given by uv^2. This form generates the same qualitative behaviour, while begin less easily studied analytically, and so to examine the role of the nonlinearities we proceed with the cubic in v.

In practice, even with this simple form, the nonlinearities in the equations are such that construction of the transition-layer solutions is a nontrivial exercise. The inner equations are easily integrated, but the $k_i(u)$ are the roots of a cubic and for the outer equations a simple closed form solution cannot be found. However, the essential features of the kinetic system are well approximated by a piece-wise linear version of the reaction term.

5.2.1 Piece-wise Linear Approximation. The use of a piece-wise linear approximation to a nonlinear function is a means of rendering a nonlinear system analytically tractable (see for example Rinzel and Keller [117] and Lane *et al.* [68]). We introduce a piece-wise linear scheme which retains the qualitative features of the nullclines of the nonlinear system (5.26)–(5.27), defined so that for $\delta = 0$ the turning points in the v-nullcline coincide with those for the full nonlinear problem. If we insist that the steady state of the kinetics is at the origin (so that the linearised system is simply the linear part of the kinetics) then it is desirable that the nullcline be continuous here. Therefore we approximate the nullcline by three linear regions. We will consider the effect of introducing a non-zero quadratic contribution by removing the symmetry of the nullcline, as will be shown in detail later. In general the gradient of the nullcline can be different in each of the linear regions, but to preserve the symmetry we

take equal gradients modulo their sign. For a pure kinetic system (5.26)–(5.27) the piece-wise linear reaction term is

$$f(u,v) = -\sigma u + v \tag{5.29}$$

$$g(u,v) = g_i = \begin{cases} g_1 \\ g_2 \\ g_3 \end{cases} = \begin{cases} -u - \eta(v + 2\theta_1), & v < -\theta_1 \\ -u + \eta v, & -\theta_1 \leq v \leq \theta_3 \\ -u - \eta(v - 2\theta_3), & v > \theta_3 \end{cases} \tag{5.30}$$

where $i = 1, 2, 3$ define the three branches of the v-nullcline, dividing (u, v) space into 3 regions at the turning points where $v = -\theta_1$ and $v = \theta_3$ respectively, where θ_1 and θ_3 are positive constants. We will use subscripts to refer to these three regions. The piece-wise linear kinetics are such that the reaction term is continuous at $v = -\theta_1$ and $v = \theta_3$ for all u, and exhibit a unique fixed point (at the origin) for $\eta\sigma < 1$. In order that the turning points for the v-nullcline with $\delta = 0$ are at the same locations as for the nonlinear kinetics, we modify one of the parameters in the linearised equations, defining the positive constant

$$\eta = \frac{2\mu}{3}. \tag{5.31}$$

This does not qualitatively change the behaviour of the equations. Furthermore, we approximate the turning points for $\delta \neq 0$ by

$$\theta_{1,3} = \frac{1}{3}\left(\sqrt{3\mu + \delta^2} \mp \delta\right) \tag{5.32}$$

which takes the appropriate values for v but not, therefore, for u.

We have chosen parameters such that the Turing bifurcation is still admitted in the linearised system with

$$\mathcal{A}' = \begin{bmatrix} -\sigma & 1 \\ -1 & \eta \end{bmatrix}. \tag{5.33}$$

Activator solutions on the slow uniformly growing domain for the full nonlinear kinetics (5.26)–(5.27) and for the piece-wise linear scheme (5.29)–(5.30) are compared in Figure 5.3. All three possible sequence types are illustrated: frequency-doubling by peak splitting in (a) and (b) and by peak insertion for (e) and (f), while (c) and (d) show frequency-tripling, where peak splitting and insertion occur simultaneously. The frequency-doubling sequences are recovered by the addition of small quadratic-like perturbations to the kinetics, the sign of which determines the method of transition between quasi-steady patterns. In these cases the parity symmetry is broken by moving one turning point for the v-nullcline relative to the other, according to equation (5.32). In each case the nonlinear and piece-wise linear kinetics are shown to give qualitatively similar results.

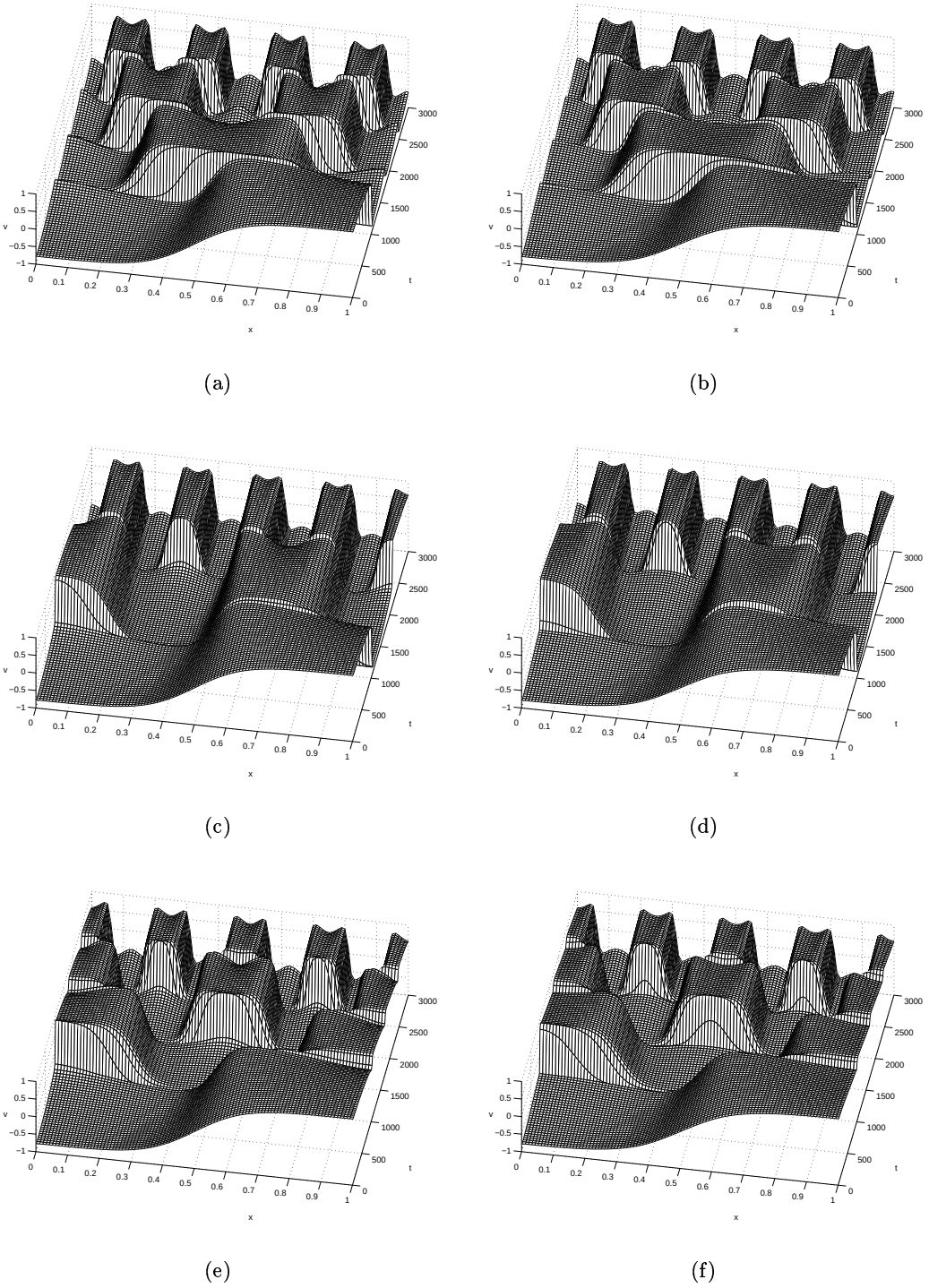

FIGURE 5.3 Comparison of activator pattern sequences generated with nonlinear kinetics (5.26)–(5.27), shown in the left-hand figures, and piece-wise linear kinetics (5.29-5.30), shown on the right-hand, with $\sigma = 1.0$ and $\mu = 0.8$ (so that $\eta = 2\mu/3 = 0.533$). For (a) and (b) $\delta = -0.01$ giving frequency-doubling by peak splitting, while for (e) and (f) $\delta = 0.01$ and the sequence is generated by peak insertion. For (c) and (d) $\delta = 0$ (the nonlinearities are cubic) and the sequence generated exhibits frequency-tripling.

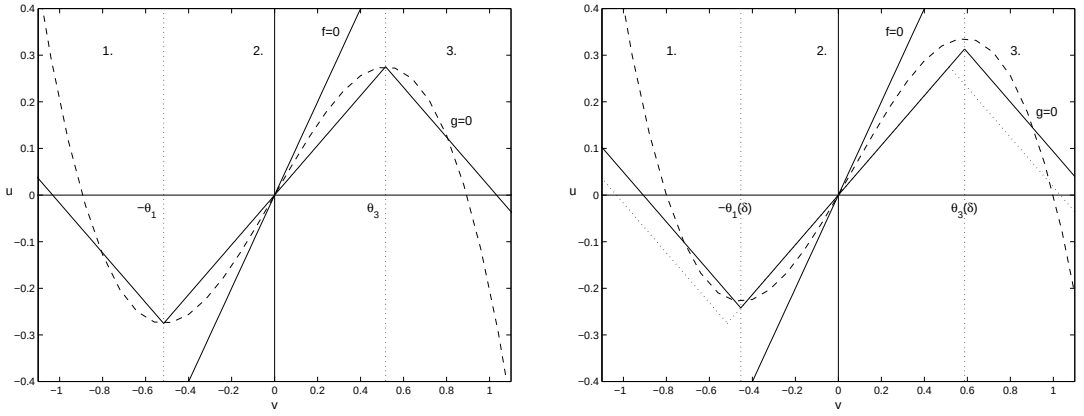

(a) (b)

FIGURE 5.4 Nullclines for piece-wise linear kinetics (5.34)–(5.35). Superimposed is the v-nullcline for the nonlinear cubic autocatalysis system (5.27) (dashed line), with $\sigma = 1.0$ and $\mu = 0.8$ ($\eta = 0.533$). In (a) we plot the symmetric case ($\delta = 0$) and in (b) we introduce a quadratic perturbation ($\delta = 0.2$) (the symmetric case is shown by the dotted line).

Nullclines for this system, given by

$$f(u,v) = 0, \qquad u = \frac{1}{\sigma} v \tag{5.34}$$

$$g(u,v) = 0, \qquad u = \begin{cases} -\eta(v + 2\theta_1), & v < -\theta_1 \\ \eta v, & -\theta_1 \leq v \leq \theta_3 \\ -\eta(v - 2\theta_3), & v > \theta_3 \end{cases} \tag{5.35}$$

are plotted in Figure 5.4, where we have superimposed the v-nullcline for the full nonlinear system (5.27).

The piece-wise linear reaction-diffusion system may, naturally, be solved exactly in each of the three regions of the reaction term, and the undetermined constants eliminated by matching solution segments together appropriately. However, such an undertaking is algebraically challenging, sufficiently so to obscure the insights to be gained from the approximation. Indeed we quickly find that the solution cannot be expressed in closed form. Therefore we pursue an asymptotic approximation where we will consider only the leading order terms in an expansion in ϵ.

5.3 Matched Asymptotic Analysis for the Piece-wise Linear System

Initially we will consider a solution with a single transition-layer on the domain (corresponding to a pattern of lowest mode) at

$$x = x^* \in [0,1]. \tag{5.36}$$

From our discussion of pattern symmetries in Chapter 2 we recognise this as the basic building block for steady state patterns of higher mode. Away from the transition-layer itself, solutions lie on the nullcline $g = 0$ in regions $i = 1$ and $i = 3$, the former corresponding to $v < 0$ and the latter to $v > 0$. Therefore we take $v = k_1(u)$ near $x = 0$, so that $h(u)$ is defined as in section 5.1, and the transition-layer is a step increase in v (corresponding to a pattern of negative polarity). Formally we assume an expansion in powers of ϵ

$$u(x,\epsilon) \sim \sum_{j=0}^{\infty} \epsilon^j u^{(j)}(x), \qquad v(x,\epsilon) \sim \sum_{j=0}^{\infty} \epsilon^j v^{(j)}(x). \tag{5.37}$$

For the leading order problem we will drop the superscripts. Substituting the expansions into the steady state equations and collecting leading order terms we recover equation (5.9), which determines the variation of u across the domain, where for region 1,

$$u_{xx} - \gamma\lambda^2 u = 2\gamma\theta_1, \qquad u_x(0) = 0 \tag{5.38}$$

with solution

$$u_1(x) = a_1 \cosh(\lambda\sqrt{\gamma}x) - \frac{2\theta_1}{\lambda^2} \tag{5.39}$$

where

$$\lambda \equiv \sqrt{\sigma + \frac{1}{\eta}}. \tag{5.40}$$

Similarly in region $i = 3$ of the phase plane

$$u_3(x) = a_3 \cosh\left(\lambda\sqrt{\gamma}\,(1-x)\right) + \frac{2\theta_3}{\lambda^2} \tag{5.41}$$

which satisfies the zero flux condition at $x = 1$. These equations also determine the activator profiles in the outer regime through the relations $v_i(x) = k_i\big(u_i(x)\big)$,

$$v_1(x) = -\frac{a_1}{\eta}\cosh(\lambda\sqrt{\gamma}x) - \frac{2\sigma\theta_1}{\lambda^2} \tag{5.42}$$

$$v_3(x) = -\frac{a_3}{\eta}\cosh\left(\lambda\sqrt{\gamma}\,(1-x)\right) + \frac{2\sigma\theta_3}{\lambda^2}. \tag{5.43}$$

Taking as the inner variable $\xi = (x - x^*)/\epsilon$, the solution, (U, V), in the vicinity of the transition-layer is written as a power series in ϵ

$$U(\xi,\epsilon) \sim \sum_{j=0}^{\infty} \epsilon^j U^{(j)}(\xi), \qquad V(\xi,\epsilon) \sim \sum_{j=0}^{\infty} \epsilon^j V^{(j)}(\xi) \tag{5.44}$$

(again, in the leading order calculation we will omit the superscript). The leading order term in U is determined by equation (5.3). Linear dependence on ξ will not match with the outer solution, as calculated above, and so in the inner region we

assume

$$U = u^*. \tag{5.45}$$

This constant is determined by the integral (5.20) which we can evaluate easily enough, giving

$$u^* = \frac{1}{2}\eta\left(\theta_3 - \theta_1\right). \tag{5.46}$$

Thus we find that the value of u in the transition-layer does not depend on γ.

Construction of the inner solution for V is complicated by the fact that we must piece together solutions for regions $i = 1, 2$ and 3, requiring continuity of the solution where the kinetics change abruptly for $V = -\theta_1$ at a spatial location we denote as ξ_{12} and again where $V = \theta_3$, at the point ξ_{23}. In region $i = 1$, for which $g = g_1(u^*, V)$, we have

$$V_{\xi\xi} - \gamma\eta V = \frac{1}{2}\gamma\eta\left(3\theta_1 + \theta_3\right) \tag{5.47}$$

and we take the solution which decays as $\xi \to -\infty$

$$V_1(\xi) = b_1 \exp\left(\sqrt{\gamma\eta}\xi\right) - \frac{1}{2}\left(3\theta_1 + \theta_3\right). \tag{5.48}$$

Similarly in region 3 we find

$$V_3(\xi) = b_3 \exp\left(-\sqrt{\gamma\eta}\xi\right) + \frac{1}{2}\left(\theta_1 + 3\theta_3\right) \tag{5.49}$$

which decays as $\xi \to \infty$. In region $i = 2$ the leading order term in V satisfies

$$V_{\xi\xi} + \gamma\eta V = \frac{1}{2}\gamma\eta\left(\theta_3 - \theta_1\right) \tag{5.50}$$

for which

$$V_2(\xi) = b_2 \sin\left(\sqrt{\gamma\eta}\xi + \beta\right) + \frac{1}{2}\left(\theta_3 - \theta_1\right). \tag{5.51}$$

For continuity we require

$$V_1(\xi_{12}) = V_2(\xi_{12}) = -\theta_1 \tag{5.52}$$

$$V_2(\xi_{23}) = V_3(\xi_{23}) = \ \theta_3 \tag{5.53}$$

$$\left[V_1\right]_\xi(\xi_{12}) = \left[V_2\right]_\xi(\xi_{12}), \qquad \left[V_2\right]_\xi(\xi_{23}) = \left[V_3\right]_\xi(\xi_{23}) \tag{5.54}$$

and we seek to determine the six unknowns b_i, for $i = 1, 2, 3$, ξ_{12}, ξ_{23} and β. However, solving these equations we find

$$\xi_{12} = \frac{1}{\sqrt{\gamma\eta}}\left(-\frac{\pi}{4} - \beta\right), \qquad \xi_{23} = \frac{1}{\sqrt{\gamma\eta}}\left(\frac{\pi}{4} - \beta\right) \tag{5.55}$$

so that the intersection locations are known up to undetermined phase β. This means that in the leading order calculation we cannot determine the points ξ_{12} and ξ_{23} *within*

the transition-layer.[2] However, for $\beta \sim \mathcal{O}(1)$ this introduces only $\mathcal{O}(\epsilon)$ error in the location of the transition layer $x = x^*$. Taking $\beta = 0$, which is reasonable in particular for $\theta_1 = \theta_3$ where the transition is symmetrical about $\xi = 0$, we find on substituting $U = u^*$

$$V_1(\xi) = \frac{1}{2}(\theta_1 + \theta_3)\exp\left[\sqrt{\gamma\eta}\,\xi + \frac{\pi}{4}\right] - \frac{1}{2}(3\theta_1 + \theta_3) \tag{5.56}$$

$$V_2(\xi) = \frac{1}{\sqrt{2}}(\theta_1 + \theta_3)\sin\left[\sqrt{\gamma\eta}\,\xi\right] + \frac{1}{2}(\theta_3 - \theta_1) \tag{5.57}$$

$$V_3(\xi) = -\frac{1}{2}(\theta_1 + \theta_3)\exp\left[-\sqrt{\gamma\eta}\,\xi + \frac{\pi}{4}\right] + \frac{1}{2}(\theta_1 + 3\theta_3) \tag{5.58}$$

and the inner solution is determined up to the unknown position x^*, which may vary with γ.

To find the constants a_1 and a_3 we match the leading order inner and outer solutions. Writing the outer solution for u in the inner variable, $x = \epsilon\xi + x^*$, and letting $\epsilon \to 0$ we find

$$a_1(x^*) = \frac{1}{\cosh(\lambda\sqrt{\gamma}x^*)}\left(u^* + \frac{2\theta_1}{\lambda^2}\right) \tag{5.59}$$

$$a_3(x^*) = \frac{1}{\cosh\left(\lambda\sqrt{\gamma}\,(1 - x^*)\right)}\left(u^* - \frac{2\theta_3}{\lambda^2}\right) \tag{5.60}$$

and matching in v follows automatically. Thus we obtain composite solutions, noting explicitly the dependence on γ (and hence dimensional domain length)

$$u(x) \sim a_1(\gamma)\cosh\left(\lambda\sqrt{\gamma}x\right) - \frac{2\theta_1}{\lambda^2}, \qquad 0 \le x < x^*(\gamma) \tag{5.61}$$

$$\sim a_3(\gamma)\cosh\left(\lambda\sqrt{\gamma}\,(1 - x)\right) + \frac{2\theta_3}{\lambda^2}, \qquad x^*(\gamma) \le x \le 1 \tag{5.62}$$

and

$$v(x) \sim -\frac{a_1(\gamma)}{\eta}\cosh\left(\lambda\sqrt{\gamma}x\right) + \frac{1}{2}(\theta_1 + \theta_3)\exp\left[\frac{\pi}{4} + \sqrt{\gamma\eta}\left(\frac{x - x^*(\gamma)}{\epsilon}\right)\right] - \frac{2\sigma\theta_1}{\lambda^2}, \qquad 0 \le x < x_{12}(\gamma) \tag{5.63}$$

$$\sim -\frac{a_1(\gamma)}{\eta}\cosh\left(\lambda\sqrt{\gamma}x\right) + (\theta_1 + \theta_3)\left[\frac{1}{\sqrt{2}}\sin\left[\sqrt{\gamma\eta}\left(\frac{x - x^*(\gamma)}{\epsilon}\right)\right] + 1\right] - \frac{2\sigma\theta_1}{\lambda^2}, \quad x_{12}(\gamma) \le x < x^*(\gamma) \tag{5.64}$$

[2] We could simplify the analysis somewhat, at the expense of introducing an error in the inner region which may not be $\mathcal{O}(\epsilon)$, by neglecting the inner solution in region 2 completely and matching solutions in regions 1 and 3. Then continuity at $\xi = 0$ determines the constants b_1 and b_3.

$$\sim -\frac{a_3(\gamma)}{\eta}\cosh\left(\lambda\sqrt{\gamma}(1-x)\right) + (\theta_1+\theta_3)\left[\frac{1}{\sqrt{2}}\sin\left[\sqrt{\gamma\eta}\left(\frac{x-x^*(\gamma)}{\epsilon}\right)\right]-1\right]+\frac{2\sigma\theta_3}{\lambda^2}, \quad x^*(\gamma)\le x < x_{23}(\gamma) \tag{5.65}$$

$$\sim -\frac{a_3(\gamma)}{\eta}\cosh\left(\lambda\sqrt{\gamma}(1-x)\right) - \frac{1}{2}(\theta_1+\theta_3)\exp\left[\frac{\pi}{4}-\sqrt{\gamma\eta}\left(\frac{x-x^*(\gamma)}{\epsilon}\right)\right]+\frac{2\sigma\theta_3}{\lambda^2}, \qquad x_{23}(\gamma)\le x\le 1 \tag{5.66}$$

where the points x_{12} and x_{23} correspond to the locations at which the kinetic term changes between regions 1 and 2, and 2 and 3 respectively, and are given by

$$x_{12}(\gamma) = x^*(\gamma) - \frac{\epsilon\pi}{4\sqrt{\gamma\eta}}, \qquad x_{23}(\gamma) = x^*(\gamma) + \frac{\epsilon\pi}{4\sqrt{\gamma\eta}}. \tag{5.67}$$

The final condition required to determine the location of the transition-layer comes from integrating equation (5.9). As $u(x)$ is continuous across the domain

$$\int_0^1 h(u)\,\mathrm{d}x = 0 \tag{5.68}$$

obtains for $h(u)$ defined as in equation (5.10). Evaluating to leading order gives

$$a_1\sinh\left(\lambda\sqrt{\gamma}x^*\right) = -a_3\sinh\left(\lambda\sqrt{\gamma}\left(1-x^*\right)\right) \tag{5.69}$$

which states, consistently, that the gradient of u is continuous across the transition-layer. Eliminating constants a_1 and a_3 using (5.59) and (5.60) we have for $x^*(\gamma)$

$$\bar{\theta}_1\tanh(\lambda\sqrt{\gamma}x^*) = \bar{\theta}_3\tanh(\lambda\sqrt{\gamma}(1-x^*)) \tag{5.70}$$

where we have defined

$$\bar{\theta}_1 \equiv \frac{2\theta_1}{\lambda^2}+u^*, \qquad \bar{\theta}_3 \equiv \frac{2\theta_3}{\lambda^2}-u^* \tag{5.71}$$

which are independent of γ. Clearly for the symmetric case, $\theta_1=\theta_3$, $x^*=1/2$ and the transition-layer does not move with γ (and hence changing domain length). For the general case we solve by writing $x^*=(\ln z)/2\lambda\sqrt{\gamma}$ and expanding (5.70) to obtain the quadratic in z

$$\left(\bar{\theta}_1+\bar{\theta}_3\right)z^2+\left(\bar{\theta}_1-\bar{\theta}_3\right)\left(\exp\left(2\lambda\sqrt{\gamma}\right)-1\right)z-\exp\left(2\lambda\sqrt{\gamma}\right)\left(\bar{\theta}_1+\bar{\theta}_3\right)=0 \tag{5.72}$$

for which we take the positive solution $z_+(\gamma)$. In order that $x^*(\gamma)\in[0,1]$ we must have $1\le z_+(\gamma)\le\exp\left(2\lambda\sqrt{\gamma}\right)$, for which we require

$$\left|\frac{\bar{\theta}_3-\bar{\theta}_1}{\bar{\theta}_3+\bar{\theta}_1}\right|\le 1 \tag{5.73}$$

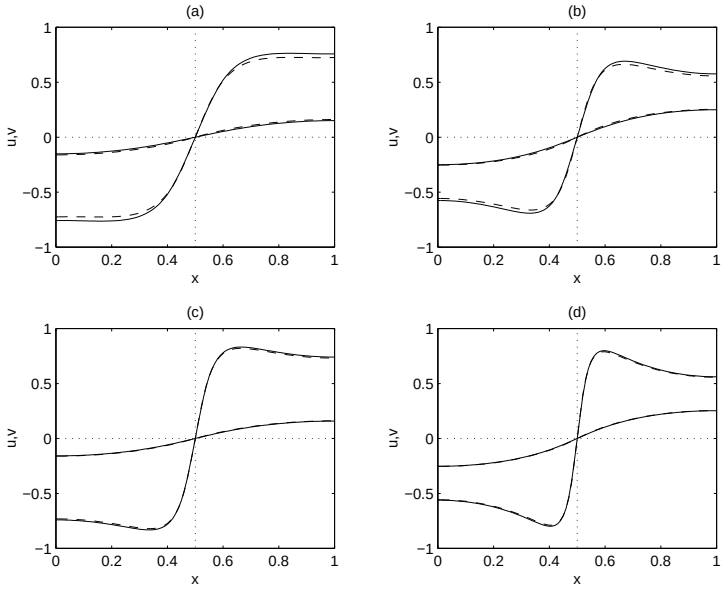

FIGURE 5.5 Numerical solution (solid) and asymptotic approximation (dashed) for piece-wise linear kinetics with $\sigma = 1.0$, $\mu = 0.8$ ($\eta = 0.533$) and $\delta = 0$ (the symmetric case) on the fixed domain. Activator solutions have larger amplitude than inhibitor solutions (both are shown). Figures (a) and (b) have $\epsilon = 0.1$ while (c) and (d) have $\epsilon = 0.05$. For the left-hand figures $\gamma = 2.0$; for the right-hand plots $\gamma = 6.0$. The analytical approximation improves as ϵ is decreased.

and this inequality holds always for $\theta_1, \theta_3 \geq 0$ along with the condition for monostability, $\eta\sigma < 1$. Also, it follows that when $\theta_3 \geq \theta_1$, $x^* \geq 1/2$, and similarly the reverse is also true.

This completes the construction of the solution to the steady state problem. In Figures 5.5 and 5.6 we plot steady state numerical solutions of equations (5.5)–(5.6) with piece-wise linear kinetics (5.29)–(5.30) and the analytical solutions given in equations (5.61)–(5.66). For the analytical solutions the location of the transition-layer $x^*(\gamma)$ is calculated as above, and we compare the solutions for two values of the small parameter ϵ. In Figure 5.5 we take $\delta = 0$ such that $\theta_1 = \theta_3$ and the location of the transition-layer is shown to be independent of γ, while comparing left- to right-hand plots we see that the transition becomes narrower (and increasingly steep) for larger γ. When $\delta > 0$ then $\theta_3 > \theta_1$ and the transition-layer moves to the right for increasing values of γ, as shown in Figure 5.6. These figures suggest that the analytical solution that we have constructed converges to the true solution as ϵ is decreased. In Figure 5.7 we plot the L^2 error for each of these δ and γ parameter combinations.

Using the symmetry argument for steady state solutions, presented in Chapter 2, patterns of higher spatial mode may be constructed by piecing together sections corresponding to the lowest mode pattern, appropriately reflected and scaled. Alternatively we can interpret this result to identify each half-wavelength section of a pattern of higher mode (with zero flux boundaries) with the lowest mode pattern (with γ scaled

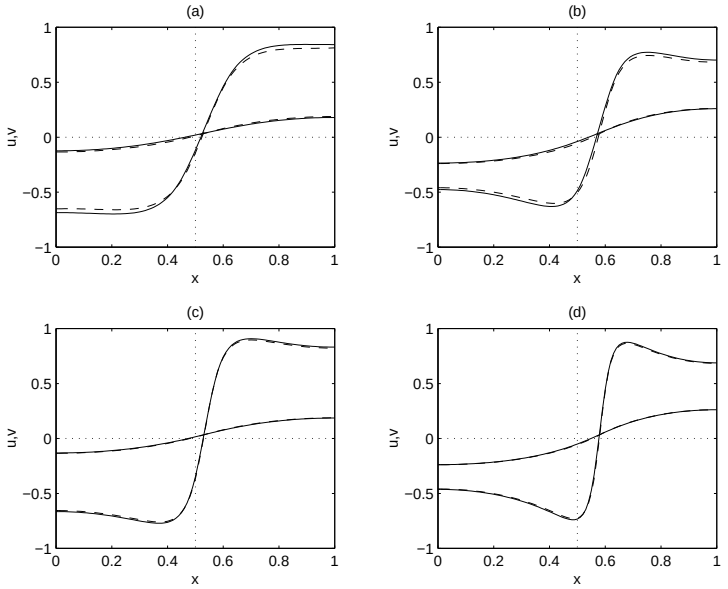

FIGURE 5.6 Numerical solution (solid) and asymptotic approximation (dashed) for piece-wise linear kinetics with $\delta = 0.2$ and other details as for Figure 5.5. In (a) and (b) we have $\epsilon = 0.1$ while for (c) and (d) $\epsilon = 0.05$. For the left-hand figures $\gamma = 2.0$; for the right-hand plots $\gamma = 5.0$.

appropriately). This may also be understood by considering the time-map (5.16) where patterns of higher mode correspond to multiple circuits of the orbit in the (u, u_x) plane for the lowest-mode pattern, so that a solution consisting of m circuits of the same orbit exists when γ is scaled by a factor m^2. Thus for the time-independent problem each half-wavelength section will vary with γ in the same manner. For slow uniform domain growth, the evolving PDE solution in the quasi-steady regime remains in the vicinity of these steady state solutions. Thus we may seek to understand the behaviour of higher pattern modes when γ increases with time by considering only the simplest pattern on the domain.

5.4 Transitions Between Patterns on the Growing Domain

We have constructed an approximate solution to the time-independent problem which is valid for γ less than a critical value, γ^c, which we calculate below. For γ greater than this value the steady solution of lowest pattern mode no longer exists. On the slowly growing domain, ρ small, this analytical solution approximates the quasi-steady pattern and is valid up to the point at which a pattern of higher spatial frequency is established for the PDE. The limiting feature for the construction of the analytical solution, as γ increases through the critical value, determines the mechanisms of breakdown for the full reaction-diffusion system. Furthermore, once the critical value γ^c is established for the lowest mode, the symmetry analysis tells us the values for breakdown for higher modes m through the scaling by the factor m^2.

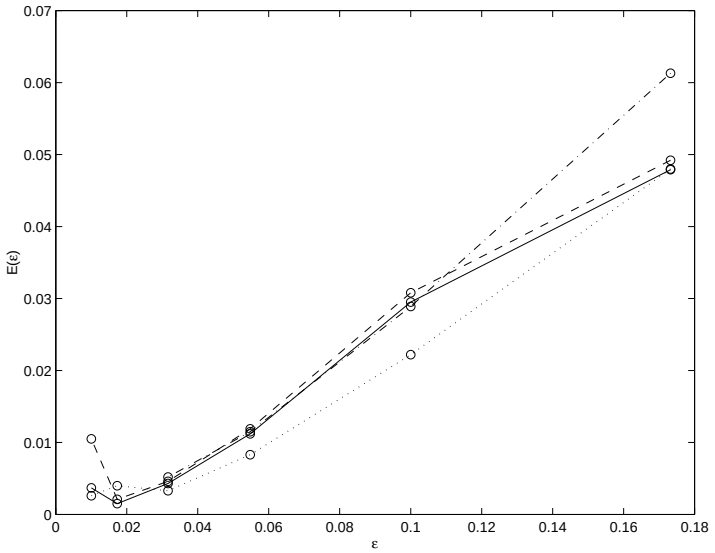

FIGURE 5.7 L^2 error, $E(\epsilon)$, for the analytical expressions for the activator solution v compared to numerical solutions with $\gamma = 2.0$, $\delta = 0.0$ (solid), $\gamma = 5.0$, $\delta = 0.0$ (dotted), $\gamma = 2.0$, $\delta = 0.2$ (dashed) and $\gamma = 5.0$, $\delta = 0.2$ (dot-dashed). Before calculating $E(\epsilon)$ it was verified that the numerical solutions were in the steady state.

5.4.1 Peak Splitting and Insertion. In the steady state the outer solution is constrained to lie on the v-nullcline. For slow uniform domain growth the quasi-steady solution evolves until this condition can no longer be satisfied. As γ increases the solutions are limited by the turning points of the v-nullcline,

$$u_{min} = -\eta\theta_1, \qquad u_{max} = \eta\theta_3. \tag{5.74}$$

For the lowest pattern mode $u(x)$ is monotonically increasing and the maximum and minimum occur at the domain boundaries. As γ is increased, one of these boundary values increases through one of the turning points. Activator peak splitting or peak insertion ensues, according to which of the points u_{min} or u_{max} is reached first. In the symmetric case, where $\theta_1 = \theta_3$, both points are reached for the same value of γ and simultaneous splitting and insertion follows, as demonstrated in the numerical simulations shown in Figures 5.3(c) and 5.3(d), described as frequency-tripling. For particular parameter sets we can use the values of u at the boundaries to predict the critical γ at which the transition between pattern modes occurs, and by which mechanism.

At the domain boundaries, from equations (5.61)–(5.62) we have $u(0)$ and $u(1)$ as functions of γ

$$u(0) = a_1(\gamma) - \frac{2\theta_1}{\lambda^2}, \qquad u(1) = a_3(\gamma) + \frac{2\theta_3}{\lambda^2}. \tag{5.75}$$

Now if $u(0) = u_{min}$ at $\gamma = \gamma_1^c$ then substituting for $a_1(\gamma)$ in the first of (5.75) we find

$$\lambda\sqrt{\gamma}x^*(\gamma) = \cosh^{-1}\left[\frac{\lambda^2\bar{\theta}_1}{2\theta_1 - \eta\lambda^2\theta_1}\right] \equiv \phi_1 \tag{5.76}$$

where ϕ_1 is independent of γ. Substituting this into equation (5.72) with $z = z_1 = \exp 2\phi_1$, after some algebra we find

$$\gamma_1^c = \left[\frac{1}{2\lambda}\ln\left(\frac{(\bar{\theta}_1 + \bar{\theta}_3)z_1^2 - (\bar{\theta}_1 - \bar{\theta}_3)z_1}{(\bar{\theta}_1 + \bar{\theta}_3) - (\bar{\theta}_1 - \bar{\theta}_3)z_1}\right)\right]^2. \tag{5.77}$$

Similarly, substituting into the second equation of (5.75),

$$\lambda\sqrt{\gamma}x^*(\gamma) = \cosh^{-1}\left[\frac{\lambda^2\bar{\theta}_3}{2\theta_3 - \eta\lambda^2\theta_3}\right] \equiv \phi_3 \tag{5.78}$$

where ϕ_3 is independent of γ, and we find that $u(1) = u_{max}$ at $\gamma = \gamma_3^c$ where

$$\gamma_3^c = \left[\frac{1}{2\lambda}\ln\left(\frac{(\bar{\theta}_1 + \bar{\theta}_3)z_3^2 + (\bar{\theta}_1 - \bar{\theta}_3)z_3}{(\bar{\theta}_1 + \bar{\theta}_3) + (\bar{\theta}_1 - \bar{\theta}_3)z_3}\right)\right]^2 \tag{5.79}$$

for $z_3 = \exp 2\phi_3$. From the discussion of the time-map (5.16) in section 5.1, if γ is a monotonically decreasing function of $u(0)$ (see Figure 5.2),

$$\frac{\mathrm{d}u(0)}{\mathrm{d}\gamma} < 0, \tag{5.80}$$

then the quasi-steady approximation breaks down as $u(0)$ decreases through u_{min} where the solution branch disappears. Then locally $g < 0$ and so from equation (5.8), which determines the dynamics in the outer part of the solution, we have $v_t < 0$ (in the fast timescale). For u below u_{min}, branch 3 of the nullcline $g = 0$ is attracting for this dynamical system and the v-solution relaxes to this branch on the fast timescale, giving a sudden growth of activator at the boundary (where there had been a minimum in the solution profile). This is pattern transition via insertion of a new activator peak (see the dashed arrow (i) in Figure 5.1(b)). By a similar argument on the time-map (5.16), γ may be shown to be an monotonic increasing function of $u(1)$ (see [124]) so that

$$\frac{\mathrm{d}u(1)}{\mathrm{d}\gamma} > 0 \tag{5.81}$$

and the solution ceases to exist if $u(1)$ increases through u_{max} before u_{min} is reached. Here $g > 0$ and $v_t > 0$ and so the v-solution relaxes to branch 1 of the nullcline on the fast timescale giving a sudden collapse at the activator peak, producing pattern change by activator peak splitting (see the dashed arrow (ii) in Figure 5.1(b)). When the boundary values pass through these critical points at the same value of γ, due to the symmetry of the kinetics, both splitting and insertion occur simultaneously.

These critical points are functions of the kinetic parameters and in particular θ_1 and θ_3. In Figure 5.8 we plot the analytical predictions as functions of δ, such that θ_1 and θ_3 vary according to equation (5.32), where $\theta_1 < \theta_3$ for $\delta > 0$ and correspondingly

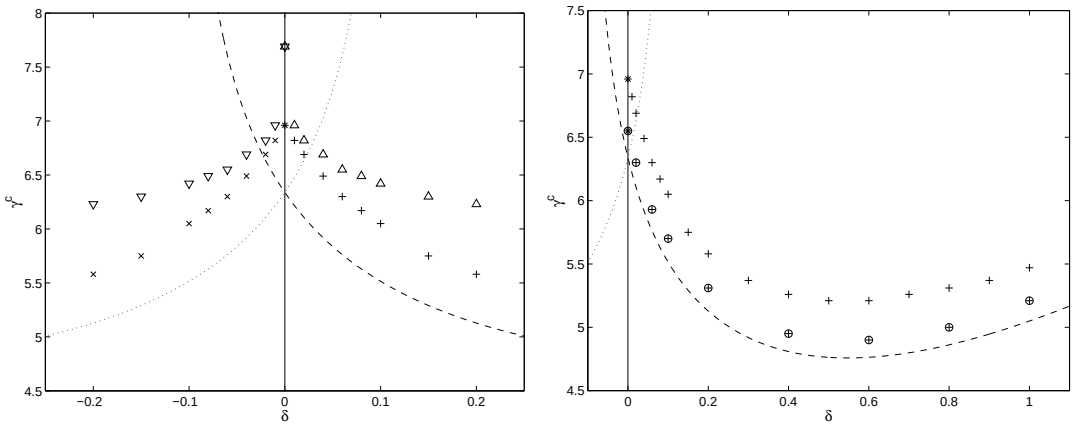

(a) (b)

FIGURE 5.8 Figures showing the analytical prediction of critical γ for pattern transitions by peak splitting, γ_3^c, (dotted) and insertion, γ_1^c, (dashed) given in equations (5.79) and (5.77) respectively, as functions of δ. Other kinetic parameters are as in Figure 5.5. In (a) points for splitting (marked $\times$) and insertion (+) and simultaneous splitting and insertion (marked $*$) are shown for numerical solutions with piece-wise linear kinetics on the growing domain with $\rho = 0.0001$. The darts indicate points for transitions in the full nonlinear system via splitting (marked $\triangledown$) and insertion ($\triangle$) (with both marks for simultaneous splitting and insertion). For both sets of data we have $\epsilon = 0.1$. In (b) we plot points for the onset of activator peak insertion for numerical solutions with the piece-wise linear scheme for $\epsilon = 0.1$ ($\times$) and $\epsilon = 0.05$ (circled symbols), showing convergence to the analytical predictions as $\epsilon \to 0$. There is an inherent error introduced in judging when the onset of the transition occurs for the numerical simulations. However, for small ρ the onset is very sudden, and we have taken a sufficiently small timestep for the numerical integration that γ^c can be identified to within ± 0.05.

we have insertion for $\delta > 0$ (dashed line) and activator peak splitting for $\delta < 0$ (dotted line). Both curves, $\gamma_1^c(\delta)$ and $\gamma_3^c(\delta)$, extend on either side of $\delta = 0$ and we expect to observe the behaviour which occurs at lower γ.[3] In Figure 5.8(a) we plot points for splitting and insertion obtained from numerical simulations for both piece-wise linear kinetics (crosses) and for the full nonlinear system (darts) on the slowly growing domain, showing qualitatively similar behaviour for small δ. Previously, in Figure 5.3, it was shown that the evolution of pattern sequences on the growing domain is similar for the nonlinear scheme and its piece-wise linear approximation, and this is reinforced here in the transition behaviour at the critical γ, from which we infer that the piece-wise linear approximation is a reasonable one. In Figure 5.8(b) we plot points obtained from numerical simulations for the onset of activator peak insertion for the piece-wise linear scheme for two values of ϵ, showing that the numerically derived values approach the analytical prediction as ϵ is decreased. For the growing domain

[3] In fact the curves do not extend very far on opposite sides of $\delta = 0$ as the curves tend to their asymptotes where the denominators in equations (5.77) and (5.79) go to zero.

we expect that there is also a contribution to the error from the rate of slow domain growth, and that as ϵ is decreased the numerical γ^c for onset of the transition will approach the analytically predicted value as $\rho \to 0$.

5.4.2 Spatial Frequency-Tripling. We have described a new phenomenon, spatial frequency-tripling, which is realised on the slowly growing domain when the reaction-diffusion equation is symmetric under the transformation $(u, v) \to (-u, -v)$.[4] We have shown previously that steady state solutions with three times the spatial frequency may be constructed from lower-mode solutions of the time-independent problem. However, it is also useful to show that the symmetry argument in the full PDE system, outlined in section 4.2.1 for spatial frequency-doubling, also accommodates this sequence. It is straightforward to show that the full reaction-diffusion equation (4.22) is invariant under the transformation $(x, \gamma) \to (\bar{p}_3(x), \gamma/9)$ where the map

$$\bar{p}_3(x) = \begin{cases} 1 - 3x, & 0 \leq x < \frac{1}{3} \\ 3x - 1, & \frac{1}{3} \leq x < \frac{2}{3} \\ 3(1 - x), & \frac{2}{3} \leq x \leq 1 \end{cases} \tag{5.82}$$

corresponds to frequency-tripling, and the factor of $\gamma/9$ for the transformation corresponds to the dimensional domain length changing by a factor of three. The same arguments may then be applied as previously, such that if the solution $c(x, 9\gamma^*)$ matches the construction at three times the spatial frequency, $q_3(x, \gamma^*) \equiv c(\bar{p}_3(x), \gamma^*)$, for some $\gamma = \gamma^*$ (rather than matching a construction with twice the spatial frequency at $4\gamma^*$) then the frequency-tripling sequence should ensue, subject to the same proviso concerning stability, which again we must conjecture from numerical results.

5.5 Discussion

Considering a piece-wise linear model of reaction and diffusion generating patterns of transition-layer type, we have been able to determine the method of pattern reorganisation on the growing domain and predict the onset of transitions by considering the existence of solutions to the associated steady-state problem. Thus far we have not considered the stability of these solutions (see the work of Kerner *et al.* for a lengthy discussion [62]). The heterogeneous solutions which we have constructed disappear when still at large amplitude (rather than with amplitude decaying to zero as γ increases through a bifurcation point of the homogeneous steady state). Furthermore, numerical simulations for the growing domain problem have shown that the quasi-steady solutions are stable as γ increases up to the value, γ^c, where the steady state solution branch ceases to exist, at which point transitions to higher pattern mode take place. This suggests that the branch of steady state heterogeneous solutions that

[4] It is interesting to note that the symmetry required for frequency-tripling is the same as that required for preferential selection of stripes over spots in two-dimensional pattern formation in reaction-diffusion systems [37, 74].

we have constructed is stable up to a point where the solution branch disappears in a saddle-node bifurcation, and that there is no earlier exchange of stability with a secondary bifurcating branch of solutions or otherwise. Thus from the construction of solutions to the steady state problem and the numerical simulations we are able to deduce features of the bifurcation structure of the underlying reaction-diffusion equation. Furthermore, in Chapter 4 we extended the symmetry argument to the full PDE system (rather than considering only the time-independent problem) and so we expect the same stability properties for solutions of higher pattern mode.

The bifurcation structure elaborated here explains the hysteretic behaviour reported in the previous chapter. On increasing γ the transition between solution branches occurs at the saddle-node point. However, on decreasing γ there is no reason why the reverse transition should take place at this same value of γ which does not correspond to a bifurcation point of the higher mode solution, or indeed that the downward transition should find the original primary bifurcation branch.

We have computed the critical values γ^c for the transition from lowest mode. The critical value of γ for any higher mode m is then determined from the symmetry analysis to be $m^2\gamma^c$. The analytical expressions that we have constructed are approximations to the lowest-mode pattern with negative polarity. Our arguments might just as easily be based on patterns of positive polarity, where the outer part of the lowest-mode solution would be determined by equation (5.9) with $h(u)$ given by the expression (5.11). Similarly, we have chosen a pure kinetic scheme such that solutions for activator and inhibitor are in phase, but could equally have chosen cross kinetics for the cubic autocatalysis model by swapping the signs of the two off-diagonal elements of the matrix $\mathcal{A}$ given in (5.28). The construction of solutions to the piece-wise linear problem in the limit of small d and the analyses for pattern transitions on the growing domain would follow with only minor modifications in this case.

For the kinetic scheme we have considered, heterogeneous solutions bifurcate from the homogeneous steady state as patterns of initially infinitesimal amplitude in a supercritical bifurcation. This was not required for the analysis. Transition-layer solutions with different behaviour on the growing domain can be generated by relaxing the condition that the kinetics admit the Turing bifurcation. In this case we no longer require the fixed point of the kinetics to lie on the middle (unstable) branch of the nullcline. When the kinetic steady state falls on one of the stable branches, either by changing g or shifting the u-nullcline ($f = 0$), sufficiently large amplitude perturbations of the homogeneous solution (now locally stable to small amplitude perturbation) are required to produce large amplitude patterns, which can be constructed in the limit as we have described. However, if the extremal point of the solution on the v-nullcline (at the domain boundary) reaches the fixed point then it will remain at this point, also fixing the value at the other boundary, even as γ increases with domain growth. Then pattern transition at *either* of the turning points is precluded and the pattern

mode will remain unchanged on the growing domain (although the transition-layer region may move and will get progressively narrower on the unit interval).

Many of the models in the literature for biological pattern formation, including the Schnakenberg and Gierer-Meinhardt models discussed in previous chapters, generate spike-type patterns. Some analysis has already been carried out on spike solutions to reaction-diffusion equations, where the form of the nullclines and accordingly the asymptotic structure is different and somewhat less transparent than for the transition-layer phenomena. In the following sections we consider some of the asymptotic properties of spike solutions, in particular the dependence of solutions on γ.

5.6 Analysis of Spike Patterns

Large amplitude patterns also exist as solutions in systems where the activator nullcline has only one stable branch. Such patterns are characterised by the behaviour of the width and height of the activator peak as $\epsilon \to 0$ where, in contrast to transition-layer patterns, the activator peak amplitude varies as some negative power of ϵ and the peak width is decreasing as ϵ tends to zero. In this section we consider the Schnakenberg kinetic scheme as a paradigm for spike patterns, and therefore we study kinetics of cross-type. However, similar results may be obtained for pure systems (for example the Gray-Scott model, see Doelman *et al.* [33]). Also we will consider a single activator peak located within the domain, rather than simply the transition from low to high concentration, as for the previous case.

Initially we consider the construction of solutions (existence) in the general setting. The outer (5.1)–(5.2) and inner (5.3)–(5.4) scalings follow as before. For the case $\epsilon = 0$ then as before the activator v is governed by

$$v_t = g(u, v) \tag{5.83}$$

where the nullcline $g(u, v) = 0$ has two branches; $v = k_i(u)$ for $i = 1, 2$, where only branch $i = 1$ is stable (in comparison with the transition-layer problem there is no stable branch $v = k_3(u)$). For cross kinetics, to generate spike solutions[5] we require that $k_1(u)$ is defined for $u \in (-\infty, u_{max}]$ and $k_2(u)$ is defined for $u \in (\infty, u_{max}]$. In fact for the Schnakenberg system (and many others) $k_2(u)$ is defined on $u \in [u_\infty, u_{max}]$ where, as $v \to \infty$, u tends to the asymptote $u \to u_\infty$, but this will not be important for existence arguments. Furthermore, under the conditions required for the kinetics to admit the Turing bifurcation, the kinetic steady state (u_s, v_s) must lie on the unstable branch $i = 2$. As for transition-layer patterns, the outer solution lies on the stable part of the v-nullcline $g(u, v) = 0$, here branch $i = 1$. The outer solution is governed by

$$0 = u_{xx} + \gamma f\big(u, k_1(u)\big) \tag{5.84}$$

[5] rather than inverted spikes, or *gullies*, see later discussion.

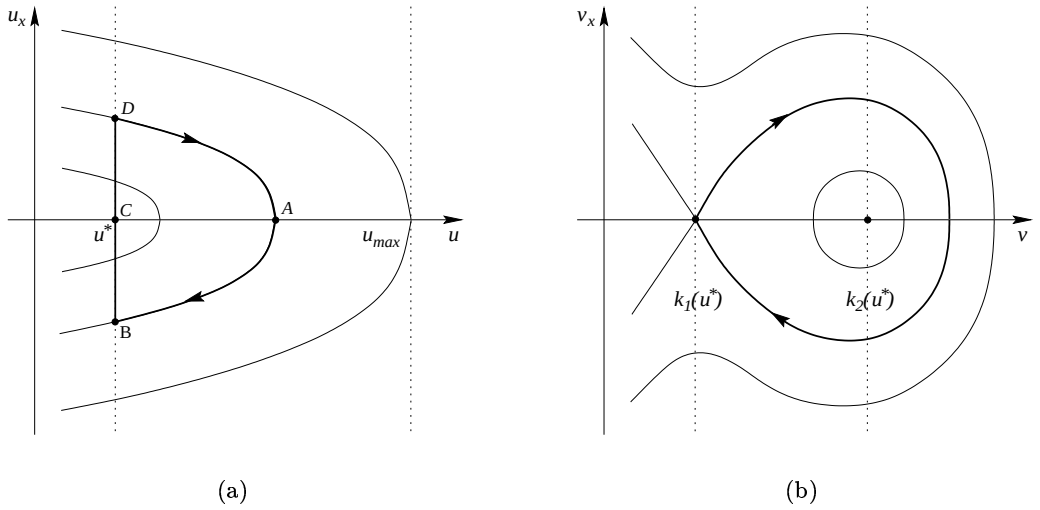

FIGURE 5.9 Schematic of the phase plane for the (a) outer and (b) inner problems for spikes with cross kinetics. In (a) the centralised peak corresponds to the trajectory A to B and then at $u = u^*$ a jump to D, returning to A where $u = u(0)$ at A ($\equiv u(1)$) for symmetric steady solutions. Increasing γ corresponds to larger orbits such that $u(0)$ is increasing with γ (for pure schemes the figure is effectively reflected in $u = 0$ and then $u(0)$ is decreasing with γ). The jump from B to D represents a discontinuity in u_x which corresponds to an excursion in the inner variable, shown in (b), where spikes are homoclinic orbits in (v, v_x).

which is valid away from the location of the spike, $x = x^*$, where $u = u^*$. The phase plane for equation (5.84) is shown schematically in Figure 5.9(a). The function $f(u, k_1(u))$ has no roots and, for cross kinetics, is everywhere positive so that trajectories in the (u, u_x) resemble the form shown in the figure.

In the limit $\epsilon \to 0$ there is a discontinuity in u_x across the spike (where u is continuous). Multiplying equation (5.84) by u_x and integrating we have

$$u_x = \pm\sqrt{2\gamma\big(H(u(0)) - H(u)\big)} \tag{5.85}$$

where $H(u)$ is defined, equivalently to equation (5.13), by

$$H(u) = \int_0^u f(w, k_1(w))\,\mathrm{d}w \tag{5.86}$$

and $u(0)$ is the inhibitor concentration at the left-hand boundary, where $u_x = 0$. Given that $f(u, k_1(u)) > 0$ (and is a monotonically decreasing function of u), $H(u)$ is positive and monotonically increasing and for real values of u_x we must have $u(0) \geq u(x)$ everywhere on the domain (and similarly for $u(1)$) so that u is maximised at the boundaries. Hence $|u_x|$ increases away from the boundaries and is greatest at the spike, where $u = u^*$. Thus u_x takes opposite signs on either side of the peak and the jump in the gradient across the spike is

$$\Delta u_x = 2\sqrt{2\gamma\big(H(u(0)) - H(u^*)\big)} \tag{5.87}$$

and hence u_x is discontinuous.

For $\epsilon \neq 0$ we require a connecting trajectory to smooth out the discontinuity, which is found by expanding in the inner variable $\xi = x/\epsilon$, giving

$$0 = V_{\xi\xi} + \gamma g\left(u^*, V\right) \tag{5.88}$$

which has two fixed points, a saddle point at $(V, V_\xi) = \left(k_1(u^*), 0\right)$ where $g_v < 0$ and a centre at $\left(k_2(u^*), 0\right)$ where $g_v > 0$. The centre is preserved for the nonlinear problem due to the symmetry about $V_\xi = 0$. We seek a solution which for periodic patterns takes us from, and returns us to, the vicinity of the point $\left(u^*, k_1\left(u^*\right)\right)$, which is an orbit in the (V, V_ξ) phaseplane homoclinic to the saddle at $V = k_1(u^*)$. The phase plane for the inner problem is shown schematically in Figure 5.9(b).

In this way, by matching solutions for the inner and outer problems, we can show the existence of large amplitude solutions in the form of spikes in the activator concentration. Next we construct such solutions for the Schnakenberg problem. The time-independent reaction-diffusion problem with Schnakenberg kinetics, where the kinetic parameter a is small,[6] is given by

$$0 = u_{xx} + \gamma\left(b - uv^2\right) \tag{5.89}$$

$$0 = \epsilon^2 v_{xx} + \gamma\left(\epsilon^\beta \hat{a} + uv^2 - v\right) \tag{5.90}$$

where $\beta > 0$. It is convenient to consider single spike solutions on the interval $[-1, 1]$, with zero flux conditions at the boundaries. The symmetry of the time-independent problem, as discussed in Chapter 2, and in particular the symmetry of these equations under $x \to -x$ suggests that we look for a spike centred at $x^* = 0$.[7] Half-peak solutions follow immediately by considering the interval $[0, 1]$.

Taking a regular series expansion for the outer region in variable x

$$u(x, \epsilon) = \sum_{j=0}^{\infty} \epsilon^j u^{(j)}(x), \qquad v(x, \epsilon) = \sum_{j=0}^{\infty} \epsilon^j v^{(j)}(x) \tag{5.91}$$

to leading order we have

$$u^0_{xx} = \gamma b \tag{5.92}$$

$$0 = u^0 (v^0)^2 - v^0 \tag{5.93}$$

with zero flux boundaries, which is solved to obtain

$$v^0 = 0 \tag{5.94}$$

$$u^0(x) = \gamma b\left(|x| - \frac{1}{2}x^2\right) + c \tag{5.95}$$

[6] The analysis follows with only minor modifications for $a \sim \mathcal{O}(1)$.

[7] Determination of the location of the *transition-layer* was found to be nontrivial, and is equivalent to finding the *width* of the activator peak. For spike patterns the width of the peak tends to zero with ϵ, and the location is assumed from symmetry arguments, thus no further assumptions are made here than were employed for the transition-layer problem.

where c is a constant.[8]

Expanding about the peak by introducing the inner variable $\xi = x/\epsilon$ (for $x^* = 0$), the inner region is governed by

$$0 = U_{\xi\xi} + \epsilon^2\gamma\left(b - UV^2\right) \tag{5.96}$$

$$0 = V_{\xi\xi} + \gamma\left(\epsilon^\beta \hat{a} + UV^2 - V\right) \tag{5.97}$$

and again seeking a regular expansion

$$U(\xi,\epsilon) = \sum_{j=0}^{\infty} \epsilon^j U^{(j)}(\xi), \qquad V(\xi,\epsilon) = \sum_{j=0}^{\infty} \epsilon^j V^{(j)}(\xi) \tag{5.98}$$

we find to leading order

$$U^0_{\xi\xi} = 0 \tag{5.99}$$

$$V^0_{\xi\xi} = \gamma(V^0 - U^0(V^0)^2). \tag{5.100}$$

Given that we do not want U^0 to blow up as $U \sim 1/\epsilon$ away from the spike, we choose U^0 to be constant,

$$U^0 = u^*, \tag{5.101}$$

which may depend on γ. Solving equation (5.100) for V^0 we find

$$V^0(\xi) = \frac{3}{2u^*}\operatorname{sech}^2\left(\frac{\xi\sqrt{\gamma}}{2}\right) \tag{5.102}$$

which is in the form of a spike, homoclinic to $(V, V_\xi) = (0,0)$ for $\xi \in [-\infty, \infty]$. Matching inner to outer solutions is automatic for v and for u we find $c = u^*$ so that the leading order composite solutions are

$$u(x) \sim u^* + \gamma b\left(|x| - \frac{1}{2}x^2\right) \tag{5.103}$$

$$v(x) \sim \frac{3}{2u^*}\operatorname{sech}^2\left(\frac{x\sqrt{\gamma}}{2\epsilon}\right). \tag{5.104}$$

Previously, for the transition-layer problem, we have evaluated the constant inhibitor concentration, u^*, for the inner solution with the integral condition (5.20), $G(u^*) = 0$, which requires that the gradient V_ξ tends to zero away from the inner region. However, we have effectively used this condition in the integration of equation (5.100), from which we deduce the form of the spike (5.102). For activator spike amplitude v_{pk} then the integral is

$$G(u^*) = \int_0^{v_{pk}} g(u^*, w)\, \mathrm{d}w = 0. \tag{5.105}$$

[8] Therefore we have $\mathrm{d}u(x)/\mathrm{d}\gamma \geq 0$ everywhere on the domain, and particularly at the boundaries, and hence $u(0)$ is an increasing function of γ here.

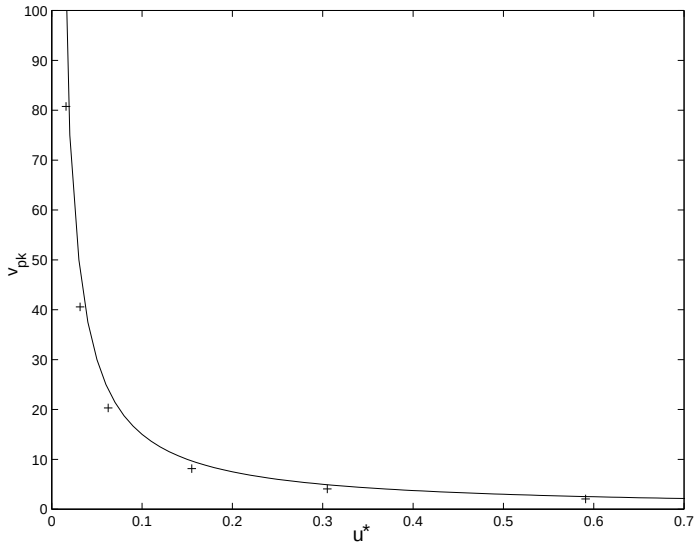

FIGURE 5.10 The relationship between activator amplitude v_{pk} and inhibitor concentration u^* in spikes for Schnakenberg kinetics. The solid line shows the analytical expression (5.106) and the crosses show values obtained from numerical simulations for different values of ϵ, with ϵ decreasing from right to left.

Evaluating the integral (for small a) we recover simply

$$v_{pk} = \frac{3}{2u^*} \tag{5.106}$$

which is consistent with our composite solutions. We plot this relation in Figure 5.10, along with data obtained from numerical simulations for different values of ϵ, showing close agreement to the analytical curve. However, thus far we have assumed uniform expansions for the dependent variables which, from this figure, are not $\mathcal{O}(1)$ in the inner region. This suggests that we rescale the equations to find variables which are $\mathcal{O}(1)$ before taking the expansion in ϵ. The following scaling of the equations is similar to one used in a recent paper by Doelman *et al.* [33] who consider the spike solutions in the Gray-Scott model.

We consider general scalings for the various terms in the inner equations, writing

$$u = \epsilon^{\alpha}\hat{u}, \quad \text{and} \quad v = \epsilon^{-r}\hat{v} \tag{5.107}$$

where $\alpha, r \geq 0$. The time independent activator equation (5.4) becomes

$$0 = \hat{v}_{\xi\xi} + \gamma\left(\epsilon^{(\beta+r)}\hat{a} + \epsilon^{(\alpha-r)}\hat{u}\hat{v}^2 - \hat{v}\right). \tag{5.108}$$

To obtain solution in the form of a homoclinic orbit of the saddle point we must have balance between the final two terms (otherwise the equation is linear and certainly will not admit such a solution). Thus we require $\alpha = r$, and we seek an inner solution

$(\hat{U}(\xi), \hat{V}(\xi))$ for the equations

$$0 = \hat{U}_{\xi\xi} + \epsilon^{2(1-\alpha)}\gamma\left(\epsilon^{\alpha} b - \hat{U}\hat{V}^2\right) \tag{5.109}$$

$$0 = \hat{V}_{\xi\xi} + \gamma\left(\epsilon^{(\alpha+\beta)}\hat{a} + \hat{U}\hat{V}^2 - \hat{V}\right). \tag{5.110}$$

For $0 \leq \alpha < 1$ we have $\epsilon^{2(1-\alpha)}$ is small and the equations decouple (giving distinguished subsystems describing inner and outer regimes). For $\alpha > 1$, then from (5.109) we must have $\hat{U} = 0$ for which there is no homoclinic solution for $\hat{V}$. If, however, $\alpha = 1$ then we recover a coupled second order ODE system for the inner region, so that in the asymptotic limit the problem does not simplify in the manner described above.

If we assume that $0 \leq \alpha < 1$, then expanding in powers of $\epsilon^{(1-\alpha)}$

$$\hat{U}(\xi, \epsilon) = \sum_{j=0}^{\infty} \epsilon^{(1-\alpha)j}\, \hat{U}^{(j)}(\xi), \qquad \hat{V}(\xi, \epsilon) = \sum_{j=0}^{\infty} \epsilon^{(1-\alpha)j}\, \hat{V}^{(j)}(\xi) \tag{5.111}$$

we recover the same leading order problem as was solved above, for which $\hat{U}^0$ is constant, as in (5.101), and $\hat{V}^0$ is given by (5.102). Matching to the leading order expressions for the outer problem, the composite solutions are

$$u(x) \sim \epsilon^{\alpha} u_0^* + \gamma b\left(|x| - \frac{1}{2}x^2\right) \tag{5.112}$$

$$v(x) \sim \epsilon^{-\alpha} \frac{3}{2u_0^*} \operatorname{sech}^2\left(\frac{x\sqrt{\gamma}}{2\epsilon}\right) \tag{5.113}$$

showing the scaling of the spike width and amplitude with ϵ.

From this analysis we are not able to evaluate the parameter α, which determines the scaling with ϵ. In fact for Schnakenberg kinetics numerical simulations suggest that the correct scaling in the inner region is $\alpha \approx 1$, the situation in which there is no simplification of the time-independent equations. Nevertheless, we can compare the form of our approximate analytical solutions to the results of numerical simulations by taking the numerical value of v_{pk} and calculating u^* accordingly. In Figure 5.11 we compare the analytical expressions (5.112) and (5.113) to numerical solutions for two values of ϵ. From these figures and from the part of the composite solutions on the unit interval $[0, 1]$ we may recover a mode $m = 1$ (half-peak) approximation. However, it is apparent that the composite solution is not uniformly valid in this case, as the zero-flux boundary condition for the inhibitor u is not satisfied at $x = 0$, where the half-spike is located, as the gradient in the inhibitor u_x is discontinuous (and hence ill-defined) here. It is for this reason that we chose to construct a centralised spike on $[-1, 1]$. For $\epsilon \neq 0$ the discontinuity in u_x is removed and the boundary condition can be satisfied, so that the half-peak is a valid solution of the steady state problem.

5.6.1 Splitting and Insertion. The mechanism described previously for transitions between quasi-steady patterns under slow uniform domain growth is sufficient to explain transitions via peak insertion for spike patterns, demonstrated for Gierer-Meinhardt kinetics in Figure 4.10(a). Here $u(0)$ (the boundary value of u) increases

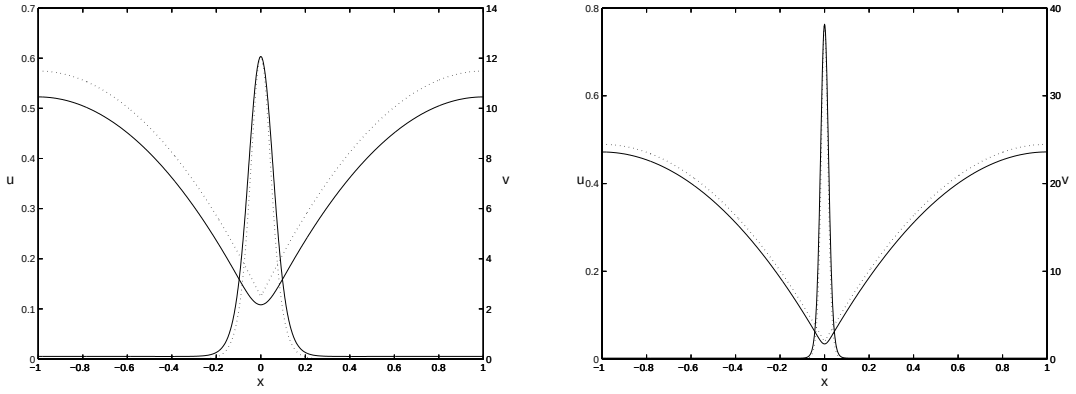

(a) (b)

FIGURE 5.11 Numerical solution (solid) and asymptotic approximation (5.103)–(5.104) (dotted) for spike solutions with Schnakenberg kinetics for two values of ϵ. We plot steady state solutions with $\gamma = 4.0$ and (a) $\epsilon \approx 0.0316$ ($d = 0.001$) while in (b) $\epsilon = 0.01$ ($d = 0.0001$). Note the different scales on the u and v axes.

with γ until reaching u_{max} at the critical value of γ. At this point v locally increases rapidly, giving a pattern transition on the fast timescale by activator peak insertion. Similarly, spike systems with pure kinetics for which the v-nullcline has a stable branch $v = k_1(u) \in [u_{min}, \infty)$ and an unstable branch $v = k_2(u) \in [u_{min}, \infty)$ undergo activator peak insertion when $u(0)$, now decreasing with γ, reaches u_{min}, beyond which the solution ceases to exist.

However, our numerical simulations have shown that spike-type patterns may demonstrate both peak insertion and peak splitting on the growing domain. Spike splitting is realised for Schnakenberg kinetics, shown in Figure 4.1(a). For transition-layer patterns the mechanisms for splitting and insertion are essentially equivalent. From the differences in the nullclines and, correspondingly, in the asymptotic behaviour of spike and transition-layer solutions, it is evident that an explanation of spike splitting must take a different form. This is due to the fact that spikes are homoclinic orbits in the (v, v_x) plane, and do not connect two distinct branches of the v-nullcline, as do transition-layers. However, a similar explanation in terms of the existence of solutions as γ increases might be expected. In fact, plotting spike solutions in the (u, v) plane one notices that the approximation of constant u in the spike region becomes less and less reasonable as γ increases. This suggests that the essential features responsible for spike splitting may not be captured in the leading order expansion. Various other authors have sought to understand spike splitting, following the observation of splitting phenomena in the Gray-Scott model, as discussed in Chapter 2. Doelman *et al.* [33] study two-pulse solutions to the Gray-Scott model and consider existence and stability results for pairs of pulses on the unbounded domain.

They identify the region of parameter space in which one-pulse solutions cease to exist and show numerically that the self-replication process may occur in the vicinity of the boundary of the stable one-pulse region. Further, they find that a pair of pulses will separate with decreasing velocity, and evolve towards one of the stable multi-peak solutions which act as attractors during the self-replication process. Reynolds *et al.* [116] consider the splitting of moving pulses in terms of the balances of flux into the spike region. However, at present we know of no transparent explanation of the splitting of static spikes.

5.6.2 Pattern Sequences in the Gierer-Meinhardt Model. In the previous chapter we noted that the kinetic model proposed by Gierer and Meinhardt, equations (4.29)–(4.30) (see Appendix A.3), can give a singular solution behaviour on the growing domain, where transition between pattern modes appears to be precluded, by setting the constant term in the activator kinetics, δ, to zero. For non-zero values, pattern sequences are formed as usual, via activator peak insertion. These two behaviours are illustrated in Figure 4.10.

For non-zero δ the v-nullcline is given by

$$u = \frac{\nu_2 v^2}{\mu_2 v - \delta} \tag{5.114}$$

where ν_2 and μ_2 are positive constants. Thus we have the standard arrangement in the phase plane for pure kinetics with stable $u = k_1(v)$ and unstable $u = k_2(v)$ branches defined on $u \in [u_{min}, \infty)$, where u_{min} is the minimum value of (5.114). Insertion of new peaks in the activator concentration profile occurs when $u(0)$, decreasing as γ increases (for pure kinetics) reaches this minimum value. However, when δ is identically zero, the v-nullcline becomes

$$v = 0 \tag{5.115}$$

$$u = k_2(v) = \frac{\nu_2}{\mu_2} v \tag{5.116}$$

where the former is the stable branch. Therefore, in the limit $\epsilon \to 0$, the outer part of the solution lies on $v = 0$ in the phase space, and as γ increases $u(0)$ decreases towards $u(0) = 0$. However, in the fast timescale, $u(x,t)$ is governed by the equation

$$u_t = \frac{1}{\gamma} u_{xx} + \nu_1 v^2 - \mu_1 u \tag{5.117}$$

where ν_1 and μ_1 are positive constants. In the outer regime v is exponentially small (and for $\epsilon = 0$ then $v = 0$). For zero flux conditions u is a minimum at the boundary and so the second spatial derivative near the boundary is positive. Therefore the time derivative at the boundary is bounded from below by

$$\frac{\mathrm{d}u(0)}{\mathrm{d}t} = -\mu_1 u(0) \tag{5.118}$$

and for finite time $u(0)$ is bounded away from zero. Thus the quasi-steady solutions never obtain the minimum value for u for any finite value of γ and the critical point for insertion is never reached. For any non-zero δ then the minimum point moves away from $u = 0$ and we recover insertion as γ increases through its critical value.

The somewhat surprising implication of this result is that the initial pattern mode established from random initial data must persist with slowly increasing γ. We have identified the critical point in γ as the point at which the solution ceases to exist and hence infer that for $\delta = 0$ the solution branch exists for all γ. Furthermore, for different choices of initial domain length and initial data, any pattern mode may be established initially and so this result holds for all pattern modes (this is also evident from the scaling of different solution branches with γ as discussed in Chapter 2). Finally, we have performed numerical simulations in which we added small amplitude random noise to the solution at each integration timestep and found that the pattern appears to remain stable with increasing γ. This singular property of the solutions when $\delta = 0$ may be important as several authors (see for example Ni [92]) ignore the constant terms when investigating the behaviour of solutions to the Gierer-Meinhardt equations.

5.6.3 Piece-wise Linear Spikes. The necessary ingredients for spike solutions presented at the start of this section suggest that spikes should be possible in a piece-wise linear kinetic scheme with the requisite features of the nullclines. To this end we investigate solutions of the piece-wise linear scheme introduced in section 5.2 when the gradient of activator nullcline in region $i = 3$ is varied.

To expedite comparison to the cross-kinetic Schnakenberg system, we study piece-wise linear kinetics of cross-type

$$f(u,v) = -\sigma u - v \tag{5.119}$$

$$g(u,v) = g_i = \left\{ \begin{array}{l} g_1 \\ g_2 \\ g_3 \end{array} \right. = \left\{ \begin{array}{ll} u - \eta(v + 2\theta_1), & v < -\theta_1 \\ u + \eta v, & -\theta_1 \leq v \leq \theta_3 \\ u - \phi\eta(v - \theta_3) + \eta\theta_3, & v > \theta_3 \end{array} \right. \tag{5.120}$$

where we have introduced the parameter ϕ which will be varied to change the gradient of the second stable branch of the v-nullcline, shown in Figure 5.12(a) for various choices of ϕ. The corresponding steady state numerical solutions for the half-peak located at the right-hand boundary are shown in Figure 5.12(b). As ϕ is changed from positive to zero and then to negative values, such that there are two and then only one stable branches, the asymptotic behaviour of the solutions changes from transition-layer to spike type, as expected.

The natural transition behaviour for this system on growing domains is to undergo transitions by insertion of new activator peaks, shown in Figure 5.13(a), resembling the pattern sequence in the Gierer-Meinhardt model. However, if θ_3 is also allowed to vary, the splitting of peaks may be recovered for the piece-wise linear problem when θ_3

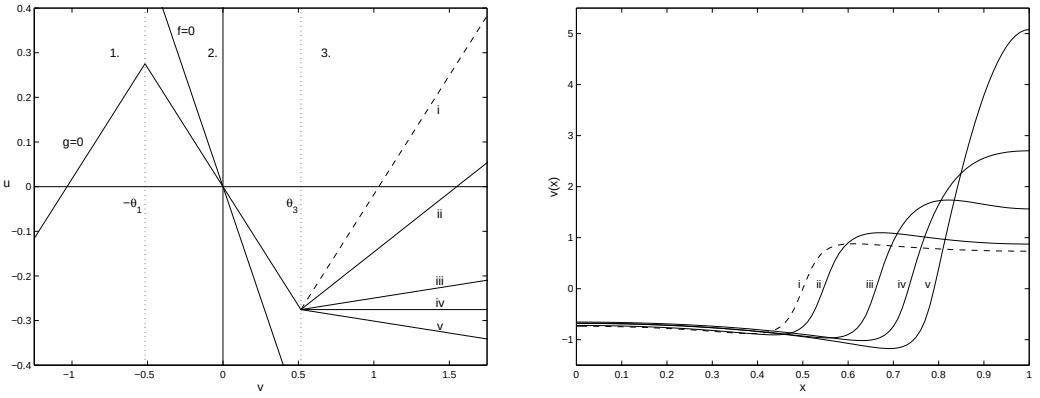

(a) (b)

FIGURE 5.12 Spike solutions in the piece-wise linear model (5.119)–(5.120): evolution from transition-layers to spikes as the second stable branch is removed. We use cross kinetics with $\sigma = 1.0$, $\mu = 0.8$ (so that $\eta = 2\mu/3 \approx 0.533$) and $\theta_{1,3} = \pm\sqrt{\mu/3}$. The nullclines are shown in (a) for (i) $\phi = 1.0$ (dashed line, as previously studied), (ii) $\phi = 0.5$, (iii) $\phi = 0.1$, (iv) $\phi = 0$ where the branch is no longer stable and (v) $\phi = -0.1$. The corresponding steady state solution profiles for the activator v are plotted in (b) with $d = 0.01$ and $\gamma = 1.0$, showing the transition to spike-type solutions as ϕ decreases through zero.

is reduced towards zero, illustrated in Figure 5.13(b). Further analysis of these pattern sequences has not been carried out, however, the simplification in the analysis of the equations engendered by the introduction of the piece-wise linear approximation may yield an understanding of the peak splitting phenomenon in spike solutions.

We have only considered the case when the homoclinic orbit in the (v, v_x) plane produces a spike increasing in v. If, however, the v-nullcline is the other way up in the phase space, so that for cross kinetics the unstable, $v = k_1(u)$, and stable, $v = k_2(u)$, branches are defined for $u \in [u_{min}, \infty)$, then inverted spikes or *gullies* are formed. Similarly, this is the case for pure kinetics where the two branches of the v-nullcline are defined on $u \in (-\infty, u_{max}]$. The results of a numerical simulation for such a kinetic scheme are shown in Figure 5.13(c), where for slow domain growth the solution undergoes splitting of the plateaus of high activator concentration (or, equivalently, insertion of new gullies). Similarly, it should be possible to vary the nullclines such that the gullies split as the domain grows (and new activator plateaus are inserted). We do not know of any nonlinear kinetic schemes proposed in the literature which generate these types of patterns, however, this behaviour is generic to the class of reaction terms with nullclines of the form that we have described.

5.6.4 Discussion. The investigation of spike solutions has raised several interesting questions. Firstly, during the construction of spike solutions to the Schnakenberg model in the asymptotic limit $\epsilon \to 0$ we found that the formal expansion was only

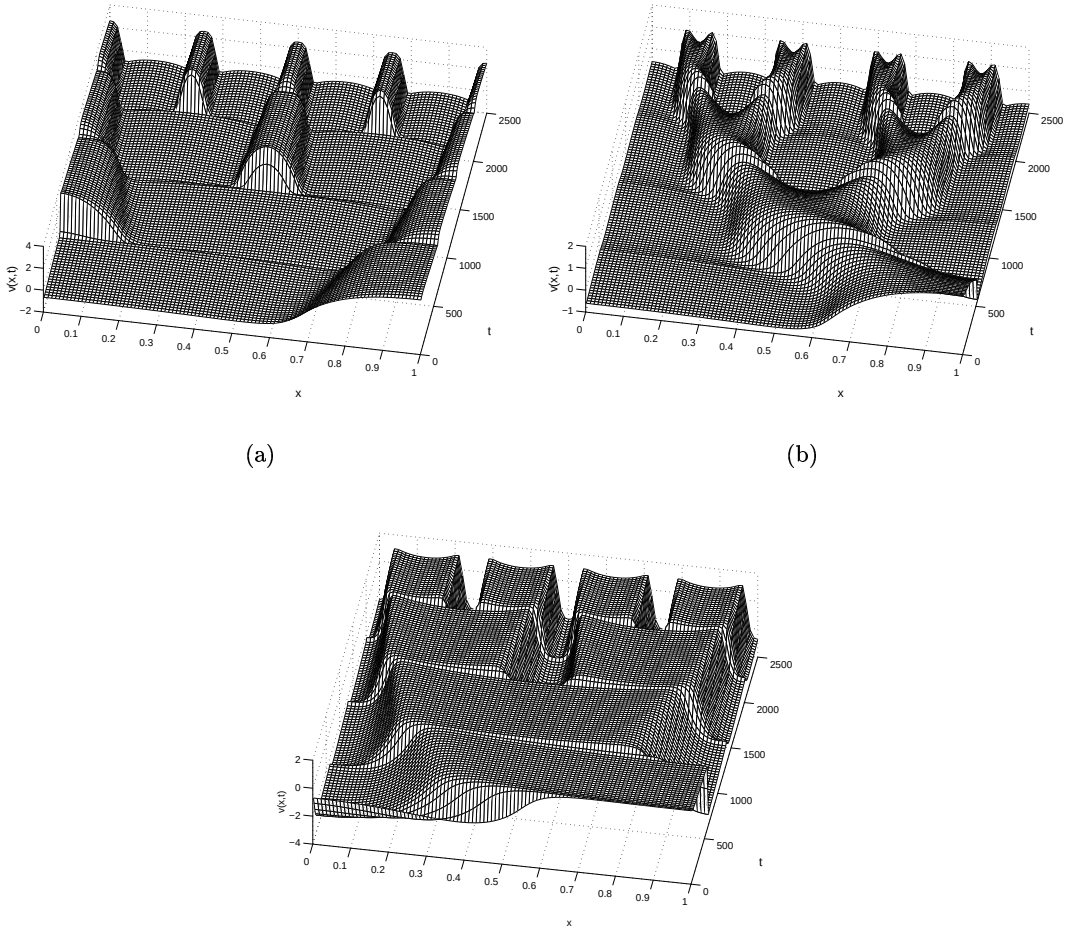

FIGURE 5.13 Spike splitting and insertion in the piece-wise linear kinetic model (5.119)–(5.120) with $\sigma = 1.0$ and $\mu = 0.8$ ($\eta = 2\mu/3 \approx 0.533$). We take $\phi = -0.01$ and (a) $\theta_3 = \theta_1 = \sqrt{\mu/3}$ while in (b) $\theta_3 = \theta_1/10$. In (c) the parameters are as for (a) but we have transformed the kinetics under $(u, v) \to (-u, -v)$.

valid for $0 \leq \alpha < 1$. This parameter cannot be found analytically, however, numerical simulations suggest $\alpha \approx 1$. Despite this apparent contradiction, the analytical solutions give a good approximation to numerical simulations (see Figure 5.11). Secondly, although insertion of activator peaks (and the failure to do so when $\delta = 0$) in the Gierer-Meinhardt model can be well understood, the analysis that we have presented does not give an explanation for spike splitting, as realised for Schnakenberg kinetics. Furthermore, numerical simulations suggest that the leading order inner approximation, where u is constant, is not sufficient to understand the phenomenon. The piece-wise linear model that we have described may prove useful as a simplified system in which to explore this behaviour.

6. Nonuniform Domain Growth and Higher Dimensions

6.1 Nonuniform Domain Growth

Thus far our investigation and analysis has been restricted to situations in which the domain growth is uniform, determined for the one-dimensional problem by the local strain rate which is independent of position (but may depend on time, as for the linear and logistic growth cases studied in Chapter 4). However, as was discussed during the derivation of the model, it is possible and generally desirable to consider a domain which is growing with different rates at different localities. For many biological systems growth is restricted to some region of a tissue, or does not occur at a uniform rate throughout the region of interest. We wish to investigate the formation of pattern sequences in the reaction-diffusion model under nonuniform conditions. In particular we would like to know whether introducing weak nonuniformity (where there is slow quantitative change in the growth across the domain) disrupts the FD sequence, or whether the sequence is robust to such changes. Furthermore, we are interested in whether suitably chosen and sufficiently strong nonuniformity (such that one section of the domain is growing in a quite different manner or rate to another part) can produce reliable sequences other than frequency-doubling.

Nonuniformity in the domain growth introduces terms with explicit spatial dependence into the evolution equation. In its original formulation, and in most subsequent development, the theory of pattern formation in reaction-diffusion equations assumes homogeneity in parameters throughout the domain, for the good reason that DDI generates inhomogeneity where before there was none. Indeed, this is the source of much of the theoretical interest in such pattern forming instabilities. One exception is the analytical study of a reaction term with explicit space-dependence by Auchmuty and Nicolis [5] (see also the numerical simulations of Herschkowitz-Kaufman [49]). Also, the recent interest in the modelling of chemical pattern formation in gel reactors leads to the study of spatial gradients in certain reaction terms. In the Gel Strip reactor the feed of the reactants, held at fixed concentrations at the boundaries, establishes steady gradients across the domain of pattern formation. Theoretical studies prior to the experimental realisation of Turing patterns in gel reactors are given by Dewel and Borckmans [25] and modelling of the structures experimentally observed in these ramped systems is presented by Borckmans *et al.* [9] and Dulos *et al.* [34].

In several applications of the theory to problems in biological pattern formation, authors have considered some underlying spatial dependence. For example, Gierer and Meinhardt [41] include a shallow source gradient in their model for morphogenesis and regeneration in Hydra to orient patterns (by removing degeneracy in the spatial modes). Benson [7] and coauthors have demonstrated that inhomogeneous reaction-diffusion equations may generate patterns with continuously varying amplitude [77]

(see also [81]) and wavelength [8] when one or both diffusion parameters are varying in space. In our equations for nonuniform domain growth the spatially-dependent terms are small, due to the small parameter arising from the different timescales, and so we do not expect strong influence on the amplitude or wavelength of patterns generated by the model.

Biologically there may be many underlying reasons for nonuniformity in domain growth. For example, signalling cues which determine the local growth rates (such as growth factors, or other chemicals) may not be uniformly distributed throughout the tissue. In such cases the local strain rate for the one-dimensional problem will depend on position (as well as time). In a simplified scenario for nonuniform growth, the domain comprises a number of subdomains each of which is undergoing growth at a different constant strain rate. Below we consider pattern formation for piece-wise uniform domain growth with two adjoining subdomains. Also, it is biological plausible that the reacting and diffusing chemicals may themselves be responsible for the local determination of the growth, so that the local expansion rate is a function of their concentrations, that is,

$$S(x,t) = S\big(\{c_i(x,t)\}\big), \quad i = 1, \ldots, n \tag{6.1}$$

a situation we call reactant-controlled growth.

The general reaction-diffusion model for nonuniform growth in one dimension is given by equation (3.31). Scaling the spatial dependence to the unit interval, writing $\xi = x/\ell(t) \in [0,1]$ for nondimensional domain length $\ell(t)$, we recover the evolution equations for two species $u(\xi,t)$ and $v(\xi,t)$

$$u_t = \frac{1}{\gamma(t)} u_{\xi\xi} + \chi(\xi,t)\, u_\xi + f(u,v) - S(\xi,t)\, u \tag{6.2}$$

$$v_t = \frac{d}{\gamma(t)} v_{\xi\xi} + \chi(\xi,t)\, v_\xi + g(u,v) - S(\xi,t)\, v \tag{6.3}$$

where $\gamma(t) = \gamma_0 \left[\ell\,(t)\right]^2$ and

$$\chi(\xi,t) = \frac{1}{\ell(t)} \Big[\xi\, \dot{\ell}(t) - a(\xi,t)\Big] \tag{6.4}$$

(where the dot represents a time derivative). Local growth $S(\xi,t)$ determines the local velocity field $a(\xi,t)$ via equation (3.27). Generally S is specified in terms of the Lagrangian variables (X,t). The position x of a particle at time t originally at position X at time $t = 0$ is given by $x = \Gamma(X,t)$, so that the uniformly scaled position $\xi = \Gamma(X,t)/\ell(t)$. To calculate S we must be able to compute the value of X corresponding to particular ξ and t (hence we are required to invert Γ).

6.1.1 Piece-wise Uniform Domain Growth. To investigate the role of nonuniformity in the domain growth we firstly consider the example of a one-dimensional domain comprising two subdomains undergoing slow uniform domain growth but with

different (slow) growth rates. This problem is studied in detail with the aim of gaining insight into the possibilities and complexities of pattern sequence formation under more general nonuniform growth conditions.

For slow uniform growth, from equation (3.61) we have $S(t) = \rho\sigma(t)$ giving the global growth function

$$x = \Gamma(X,t) = Xr(t) \tag{6.5}$$

where

$$r(t) = \exp\left[\rho\int_0^t \sigma(\bar{t})\,\mathrm{d}\bar{t}\right] \tag{6.6}$$

and for slow growth $0 < \rho \ll 1$. For the simplest example of piece-wise uniform domain growth we define S on the two subdomains by

$$S = S(t) = \begin{cases} S_1(t), & 0 \le X \le \Theta \\ S_2(t), & \Theta < X \le 1 \end{cases} \tag{6.7}$$

where Θ is the initial position of the interface between the two subdomains. For slow growth $S_i(t) = \rho\sigma_i(t)$, $i = 1,2$, and by straightforward calculation from equation (3.29) we recover

$$x = \Gamma(X,t) = \begin{cases} Xr_1(t), & 0 \le X \le \Theta \\ \Theta(r_1(t) - r_2(t)) + Xr_2(t), & \Theta < X \le 1 \end{cases} \tag{6.8}$$

where the r_i are calculated as in equation (6.6). Due to the growth of the left-hand subdomain ($i = 1$) the interface between the subdomains $\theta(t) \in [0, \ell(t)]$ moves as

$$\theta(t) = \Theta r_1(t) \tag{6.9}$$

and is a moving internal boundary. Similarly, from equation (3.33) along with the second of (6.8) the total domain length is given by

$$\ell(t) = \Theta r_1(t) + (1-\Theta)\, r_2(t) \tag{6.10}$$

and the rate of change $\dot{\ell}(t)$ follows accordingly. We may now calculate the flow, a, for the piece-wise uniform case from the expression for Γ, where $a = \partial\Gamma/\partial t$, giving

$$a(X,t) = \begin{cases} X\dot{r}_1(t), & 0 \le X \le \Theta \\ \Theta(\dot{r}_1(t) - \dot{r}_2(t)) + X\dot{r}_2(t), & \Theta < X \le 1 \end{cases}. \tag{6.11}$$

Writing as a function of x and t we have

$$a(x,t) = \begin{cases} x\dfrac{\dot{r}_1}{r_1}, & 0 \le x \le \theta(t) \\ \theta(t)\left(\dfrac{\dot{r}_1}{r_1} - \dfrac{\dot{r}_2}{r_2}\right) + x\dfrac{\dot{r}_2}{r_2}, & \theta(t) < x \le \ell(t) \end{cases} \tag{6.12}$$

and in the uniformly scaled coordinates (ξ, t)

$$\frac{a(\xi,t)}{\ell(t)} = \begin{cases} \xi\dfrac{\dot{r}_1}{r_1}, & 0 \le \xi \le \tilde{\theta}(t) \\ \tilde{\theta}(t)\left(\dfrac{\dot{r}_1}{r_1} - \dfrac{\dot{r}_2}{r_2}\right) + \xi\dfrac{\dot{r}_2}{r_2}, & \tilde{\theta}(t) < \xi \le 1 \end{cases} \tag{6.13}$$

where after the uniform scaling the interface between subdomains moves as $\tilde{\theta}(t) = \theta(t)/\ell(t) \in [0,1]$, which is easily written as a function of Θ, $r_1(t)$ and $r_2(t)$ only. Now we have all the components required to specify the evolution equations (6.2)–(6.2) for piece-wise uniform growth.[1]

We require the continuity of the solutions $u(\xi,t)$ and $v(\xi,t)$ and of their fluxes at the moving internal boundary $\xi = \tilde{\theta}(t)$ between the two subdomains. The diffusion constants are now effectively functions of time through $\gamma(t)$ but are independent of ξ and so continuity of flux requires that the first spatial derivative is continuous across $\xi = \tilde{\theta}(t)$ for each species. Thus we require at every time t

$$\Big[u(\xi,t)\Big]_{\tilde{\theta}^-(t)}^{\tilde{\theta}^+(t)} = 0, \qquad \Big[u_\xi(\xi,t)\Big]_{\tilde{\theta}^-(t)}^{\tilde{\theta}^+(t)} = 0 \tag{6.14}$$

and similarly for $v(\xi,t)$.

The advective terms in the equations arise despite the uniformity of growth for each subdomain because of the choice of spatial transformation, the differing growth rates necessitating the consideration of the internal moving boundary. A different approach to nondimensionalisation would consider two semi-domains, each transformed to the half-unit interval. Then there would be no moving boundary, the junction being fixed at $\xi = 1/2$, but the (time-dependent) diffusivities would be different on the two semi-domains. Clearly different spatial rescalings would be required for the two semi-domains in order to examine the form of the pattern on the dimensional domain, and these rescalings would change with time. This process would replace, and is equivalent to, the advective terms. The advective nature of the equations is thus rendered more transparent in the formulation chosen above which includes these terms explicitly.

For slow piece-wise uniform domain growth we must specify growth parameters $\rho \ll 1$ and Θ, and the initial domain size through γ_0 along with functions $\sigma_1(t)$ and $\sigma_2(t)$. We restrict discussion to the case where the σ_i are constant and to simplify notation we write

$$S_i = \rho_i, \quad i = 1,2 \tag{6.15}$$

where both ρ_1 and ρ_2 are of order ρ and hence are small parameters. Then $r_i(t)$ is given by the simple expression

$$r_i = \exp(\rho_i t), \quad i = 1,2 \tag{6.16}$$

[1] At each step in the discussion the equations reduce to the form derived for reaction-diffusion on a uniformly growing domain, equation (3.63), when the two subdomains have the same growth, i.e. when $\sigma_1(t) \equiv \sigma_2(t)$ such that $r_1(t) = r_2(t)$.

such that

$$\frac{a(\xi,t)}{\ell(t)} = \begin{cases} \rho_1 \xi, & 0 \le \xi \le \tilde{\theta}(t) \\ \tilde{\theta}(t)\,(\rho_1 - \rho_2) + \rho_2 \xi, & \tilde{\theta}(t) < \xi \le 1 \end{cases} . \tag{6.17}$$

For slow growth we notice that $a \sim \mathcal{O}(\rho)$ and, from equation (6.10) along with (6.16), that $\dot{\ell}(t) \sim \mathcal{O}(\rho)$. Given that $\ell(t) \ge 1$ and $\xi \in [0,1]$ we also find that $\chi \sim \mathcal{O}(\rho)$ or smaller, so that the advection component is small.

6.1.2 Numerical Solution for Slow Piece-wise Uniform Growth. Equations (6.2)–(6.4) along with (6.10) and (6.17) with initial data and boundary conditions at $\xi = 0, 1$ for both species, fully determine the problem to be solved numerically. The time-dependent internal boundary $\xi = \tilde{\theta}(t)$ introduces a further level of complexity into the numerical simulation of the system. We cannot simply reduce the problem to a set of ordinary differential equations by a naive spatial discretisation and standard central finite differences as the governing equations differ on the two subdomains. Therefore we must adapt the discretisation to incorporate the internal boundary.

The spatial interval is discretised with a uniform mesh, as for the uniform growth case, writing $U_i(t) \approx u(\xi_i, t)$ as the approximate values of the solution $u(\xi, t)$ at the mesh points ξ_i, $i = 1, 2, \ldots, N$, and similarly v is approximated by $V_i(t) \approx v(\xi_i, t)$. The first spatial derivative is taken as the standard central difference,

$$\frac{\partial u}{\partial \xi}(\xi_i, t) \approx \frac{U_{i+1}(t) - U_{i-1}(t)}{2h} \tag{6.18}$$

where h is the spatial mesh size. When this expression straddles the internal boundary the requirement of conservation of the first spatial derivative is invoked, and so the expression is universally valid on the interval. However, while central differences may also be used for the second spatial derivative within the two subdomains, the expression will not be valid across the internal boundary. Here we must adapt the expression when points in the central difference formula $\{\xi_{i-1}, \xi_i, \xi_{i+1}\}$ straddle the boundary $\tilde{\theta}(t)$. When this occurs we adopt the strategy often used to deal with conditions imposed on curved boundaries for finite differences (see Morton and Mayers [85]). We introduce an extra spatial mesh point, $\xi_\theta = \tilde{\theta}(t)$ at the internal boundary. When $\xi_i < \xi_\theta < \xi_{i+1}$ we proceed by calculating an approximation, U_θ, to the solution at position ξ_θ using linear interpolation between the approximations at points surrounding ξ_θ, given by U_i and U_{i+1}. Then we modify the central differences formula for the second derivative by foreshortening the range in the direction of the boundary

$$\begin{aligned} \left[\frac{\partial^2 u}{\partial \xi^2}\right]_{\xi_i} &\approx \frac{\left(\dfrac{U_\theta - U_i}{\xi_\theta - \xi_i}\right) - \left(\dfrac{U_i - U_{i-1}}{\xi_i - \xi_{i-1}}\right)}{\left(\dfrac{\xi_\theta - \xi_i}{2}\right) + \left(\dfrac{\xi_i - \xi_{i-1}}{2}\right)} \\ &= \frac{2}{\xi_\theta - \xi_{i-1}} \left[\left(\frac{U_\theta - U_i}{\xi_\theta - \xi_i}\right) - \left(\frac{U_i - U_{i-1}}{\xi_i - \xi_{i-1}}\right)\right] \end{aligned} \tag{6.19}$$

(omitting the time dependence for notational simplicity). A similar expression can be derived for the case $\xi_{i-1} < \xi_\theta < \xi_i$. Furthermore we approximate U_θ for $\xi_i < \xi_\theta < \xi_{i+1}$ by linear interpolation between the known points

$$\begin{aligned} U_\theta &\approx \frac{(\xi_{i+1} - \xi_\theta)}{h} U_i + \frac{(\xi_\theta - \xi_i)}{h} U_{i+1} \\ &= (1 - \lambda_+)\, U_i + \lambda_+ U_{i+1} \end{aligned} \tag{6.20}$$

where

$$\lambda_+ = \frac{\xi_\theta - \xi_i}{h}. \tag{6.21}$$

Then from the above we find the difference approximation for the second derivative

$$\left[\frac{\partial^2 u}{\partial \xi^2}\right]_{\xi_i} \approx \frac{2}{(1+\lambda)\, h^2} \left[U_{i+1} - 2U_i + U_{i-1}\right] \tag{6.22}$$

where $\lambda = \lambda_+$. The same expression is derived for the case $\xi_{i-1} < \xi_\theta < \xi_i$, where we have $\lambda = \lambda_-$ with

$$\lambda_- = \frac{\xi_i - \xi_\theta}{h}. \tag{6.23}$$

Using these expressions and similar expressions for v, and with appropriate conditions at the fixed boundaries $\xi = 0, 1$, we recover a system of ordinary differential equations in the U_i and V_i which may then be integrated in time with a suitable numerical routine, for example Gear's method, as employed for the uniform case.

Numerical Results. The results of numerical simulations under a variety of parameter regimes are presented below. Each of the two subdomains for piece-wise uniform growth undergoes spatially uniform exponential growth (at constant strain rate) such that if zero flux conditions were imposed at both ends of each subdomain then the frequency-doubling sequence would develop for both. However, the continuity of flux condition at the interface permits communication between the two regions. Pattern formation on each subdomain will influence the solution behaviour on the other. Thus we may expect that the pattern sequence will differ from the case of uniform exponential growth across the whole domain.

In Figure 6.1(a) we plot activator solutions for $\rho_1 = 0.01$, $\rho_2 = 0.02$ with $\gamma_0 = 1$, and with subdomains of initially equal length. In comparison to the pattern formed under uniform growth, as shown in Figure 6.1(b), the solution shows asymmetry in the temporal sequence of peak splitting and subsequently in the separation of peaks. The location of the interface between the uniformly growing subdomains is shown by the dashed line. In these and in subsequent figures the initial mode to form gives a boundary peak on the right hand boundary. Further numerical simulations have shown that the ensuing pattern sequence and asymmetry are the same for an initial peak located on the left-hand boundary. We have solved the uniform domain growth problem in Figure 6.1(b) using both the numerical scheme for the uniform equations (4.1)–(4.3) and for the piece-wise uniform growth formulation, and have found that the same

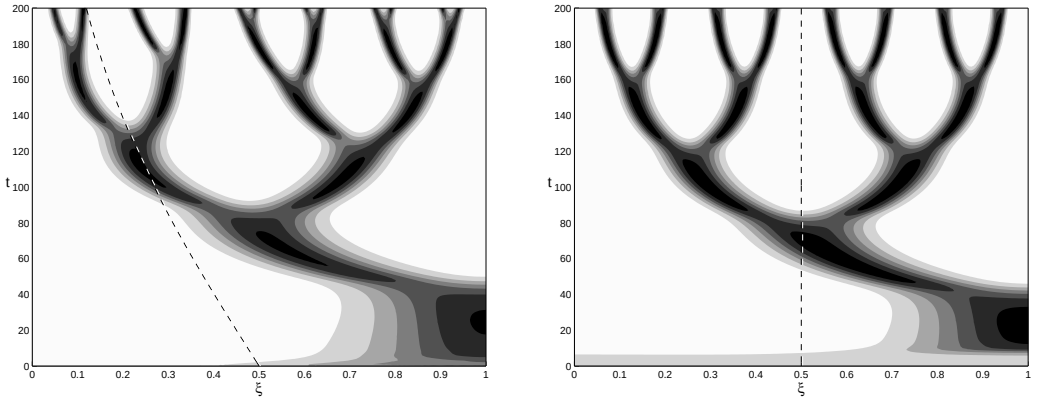

FIGURE 6.1 Asymmetric peak splitting for Schnakenberg kinetics on the piece-wise uniformly growing domain. Numerical solutions for the activator species $v(\xi, t)$ are shown for (a) piece-wise uniform domain growth with $\rho_1 = 0.01$, $\rho_2 = 0.02$ and $\gamma_0 = 1$ and (b) uniform domain growth with $\rho = 0.0172$ and $\gamma_0 = 1$ giving (approximately) the same dimensional domain length at time $t = 200$. The dashed line shows the interface $\tilde{\theta}(t)$ which is stationary for the uniform case. Shading is 0 (white) to 4 (black). In this and later figures we assume that the faster-growing subdomain is on the right hand side, however, this is for ease of comparison and is not required by the model formulation.

result is recovered in each case. The (stationary) location of the interface $\tilde{\theta} = 0.5$ is plotted for uniform growth as an aid to comparison. The activator concentration is plotted (in pseudo-colour, gray-scale) as a function of time and scaled spatial coordinate ξ, and therefore the relative separations of peaks on the dimensional domain at each time, found by uniform rescaling, are preserved.

At this relatively high value for the strain rate ρ the asymmetry in the peak splitting is reminiscent of the asymmetrical behaviour observed for the uniform growth case, described in section 4.2.2. Each peak in the activator concentration profile undergoes peak splitting and separation, and in this sense the evolving solution profile represents a perturbed frequency-doubling sequence. However, for slower domain growth peaks occasionally fail to undergo splitting, even when the growth rates on the two subdomains are in very close proximity. In Figure 6.2(a) the solution is plotted for $\rho_1 = 0.001$ and $\rho_2 = 0.0011$, for initially equal subdomain lengths. The solution follows closely the pattern for the uniform growth case, shown in Figure 6.2(b), until the 4-peak stage undergoes splitting at $t \approx 2500$, where the peak nearest the interface on the slower-growing subdomain fails to split. Subsequently the pattern reorganises so that the peak separation is again approximately equal across the whole domain. This defect in the peak splitting is reminiscent of the breakdown of the frequency doubling sequence for very slow uniform growth and for linear domain growth.

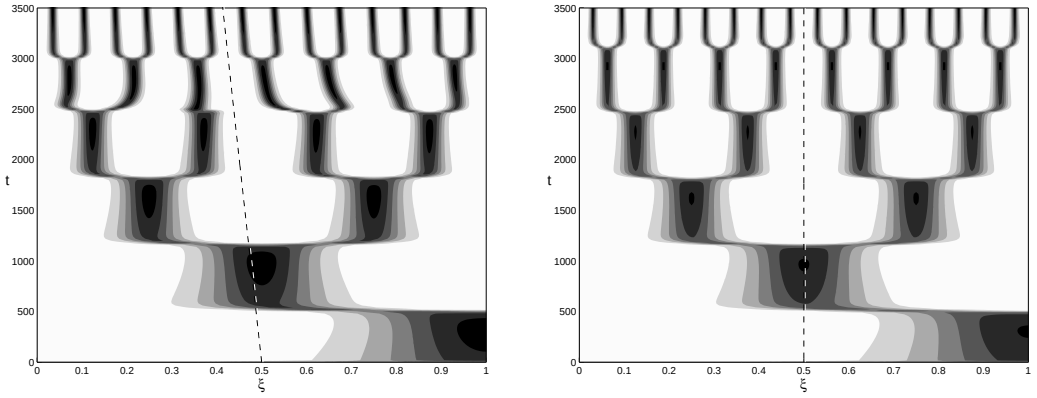

FIGURE 6.2 Missing peaks for piece-wise uniform domain growth. We plot numerical solutions for the activator $v(\xi, t)$ for (a) piece-wise uniform domain growth with $\rho_1 = 0.001$, $\rho_2 = 0.0011$ and $\gamma_0 = 1$ and (b) uniform domain growth with $\rho = 0.0010544$ and $\gamma_0 = 1$ giving (approximately) the same dimensional domain length at time $t = 3500$. Other remarks as for Figure 6.1.

When only one of the subdomains is growing, which may be considered to be an extreme case of the piece-wise uniform growth problem, then numerical simulations suggest that there is a strong tendency to peak splitting on the growing subdomain. This situation is illustrated in Figure 6.3(a), where $\rho_1 = 0$ and the initial domain size is such that the first pattern to form is the (right-hand) boundary peak. The FD-like pattern sequence which is generated has peaks restricted to the growing subdomain, and is asymmetric in a manner similar to the solution in Figure 6.1(a). For an initially left-hand boundary peak the same behaviour is found with all peaks moving into the growing region. If the initial domain size is increased so that patterns of higher mode are initially excited, then activator peaks may form simultaneously on the growing and non-growing subdomains, as shown in Figure 6.3(b) where the initial domain size was chosen to be $\gamma_0 = 20$. Here one can get different sequence behaviour. In the example, two peaks become three via splitting on the growing subdomain, and subsequently six peaks are formed, with peak splitting on the stationary subdomain close to the interface. However, the tendency for peaks to split on the growing part is retained.

When the growing subdomain has a slower growth rate the distinction between growing and non-growing regions appears even more distinct. In Figure 6.4(a) we plot the results of a repetition of the simulation in Figure 6.3(b), where we keep $\rho_1 = 0$ but take a smaller value for ρ_2. The transition from a two-peak pattern to three peaks is unambiguous and no peak splitting is observed on the non-growing part. However, the influence of the non-growing subdomain can be seen in the failure of peak splitting on the growing region later on. Similar results are found for an initial pattern of four peaks, shown for $\gamma_0 = 80$ in Figure 6.4(b).

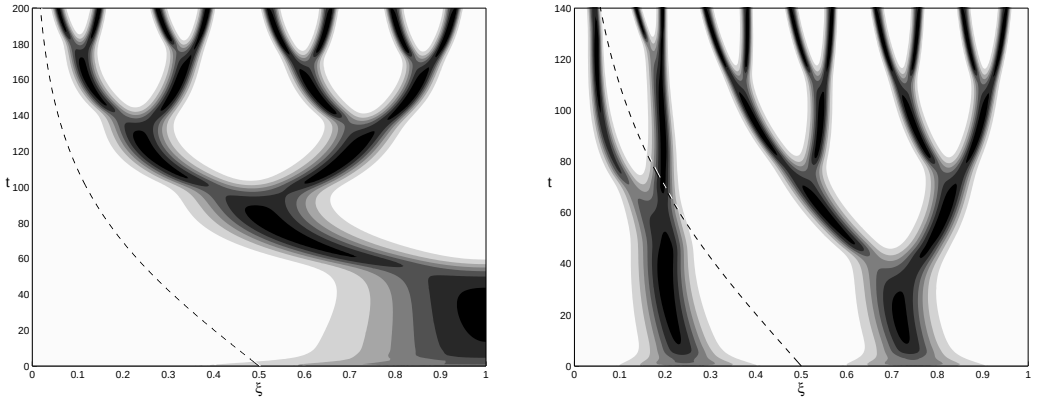

FIGURE 6.3 Pattern sequences generated from larger initial domains. We show the activator $v(\xi, t)$ for piece-wise uniform domain growth with $\rho_1 = 0.0$, $\rho_2 = 0.02$ and (a) $\gamma_0 = 1.0$ so that the initial mode $m = 1$ and (b) with $\gamma_0 = 20.0$ where the initial pattern is mode $m = 4$. Other remarks as for Figure 6.1.

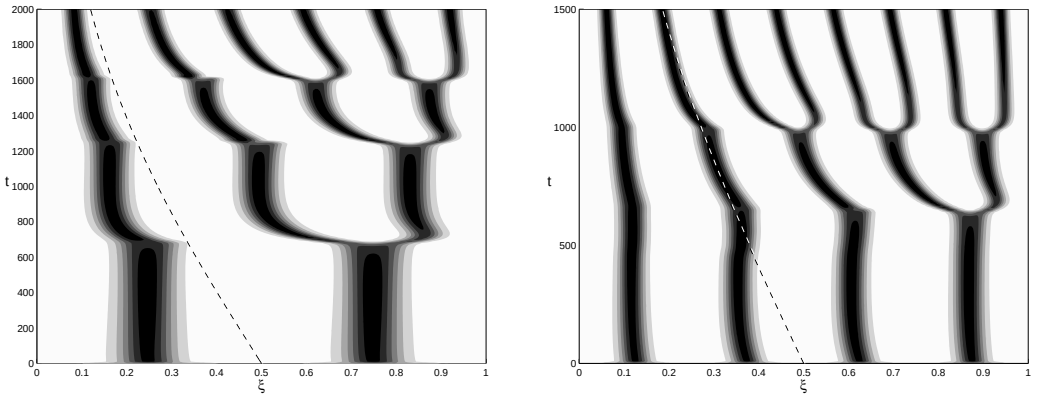

FIGURE 6.4 Pattern sequences generated from larger initial domains. Numerical solutions for activator $v(\xi, t)$ are shown for piece-wise uniform domain growth with $\rho_1 = 0.0$, $\rho_2 = 0.001$ and (a) $\gamma_0 = 20.0$ so that the initial mode to grow is mode $m = 4$ and (b) $\gamma_0 = 80.0$ where the initial pattern is $m = 8$. Other remarks as for Figure 6.1.

In this section we have considered only the example of Schnakenberg kinetics, and as a result we have discussed the consequences of piece-wise uniform domain growth for activator peak *splitting*. Similar results are found for kinetics which give rise to insertion of new activator peaks. In the following section we consider the problem for more general nonuniform domain growth which will provide a framework to validate the results we have presented for piece-wise uniform growth.

6.1.3 Lagrangian Formulation for Nonuniform Growth. The simple form of $\Gamma(X,t)$ for piece-wise uniform growth enabled us to invert Γ explicitly to find $X = \Lambda(x,t)$ and hence calculate a and S as functions of x and t. Λ can be found immediately for any uniform domain growth, where Γ is a separable function of X and t. For nonuniform growth the function Γ is not a separable function and it may not be possible to find Λ analytically. Therefore to compute numerical solutions for the evolution equations (6.2)–(6.3) it would be necessary to invert Γ numerically each time we require $a(\Lambda(x,t),t)$ and $S(\Lambda(x,t),t)$ during the computation. However, if the equations are recast in Lagrangian coordinates, (X,t), the inversion need only be performed when interpolating the results to find a solution at equally spaced ξ. In Lagrangian coordinates the evolution equation for $u(X,t)$ and $v(X,t)$ under nonuniform domain growth in one dimension with local growth $S(X,t)$ is given by

$$u_t = \frac{1}{\gamma_0}\frac{1}{\Gamma_X}\left[\frac{1}{\Gamma_X}u_X\right]_X + f(u,v) - Su \tag{6.24}$$

$$v_t = \frac{d}{\gamma_0}\frac{1}{\Gamma_X}\left[\frac{1}{\Gamma_X}v_X\right]_X + g(u,v) - Sv \tag{6.25}$$

$$[\Gamma_X]_t = S\,\Gamma_X \tag{6.26}$$

with zero flux boundary conditions for u and v and the zero translation boundary condition for Γ

$$u_X(X,t) = v_X(X,t) = 0, \quad X = 0,1 \tag{6.27}$$

$$\Gamma(0,t) = 0 \tag{6.28}$$

and initial conditions

$$u(X,0) = u_0(X), \qquad v(X,0) = v_0(X), \qquad \Gamma(X,0) = X. \tag{6.29}$$

These equations may be written as a system of first order PDEs in the variables $(u, u_X, v, v_X, \Gamma, \Gamma_X)$. Numerical solutions are found by discretising the first order system using the Keller box scheme [85], as implemented in the NAG library routine `D03PEF`. Solutions at equally spaced ξ or x may be calculated by interpolating from the solutions at equally spaced X, for example using routine `C05AZF` to invert Γ and `E01BFF` to interpolate.

We can use this more general formulation for solving the nonuniform domain growth equations to corroborate our results for piece-wise uniform domain growth. The function $S(X,t)$ we chose to approximate the step discontinuity in ρ across the

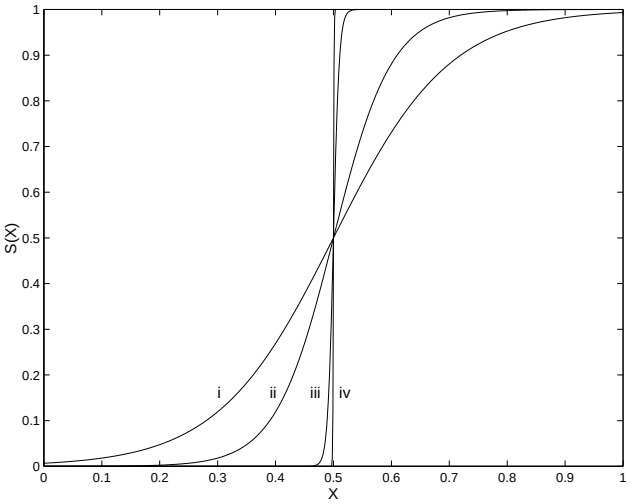

FIGURE 6.5 The *tanh* function, (6.30), illustrated for $S_1 = 0$ and $S_2 = 1$ with $\Theta = 0.5$ and (i) $\epsilon = 0.2$, (ii) $\epsilon = 0.1$, (iii) $\epsilon = 0.01$ and (iv) $\epsilon = 0.001$ showing successively closer approximations to a discontinuous step-function.

domain is the *tanh* function given by

$$S(X,t) = S_1(t) + \frac{S_2(t) - S_1(t)}{2}\left[1 + \tanh\left(\frac{X-\Theta}{\epsilon}\right)\right] \tag{6.30}$$

and shown in Figure 6.5, which as $\epsilon \to 0$ tends to a step-function between S_1 and S_2 (which may vary with time) centred on $X = \Theta$. In particular if we choose S_1 and S_2 to be constant, as in the previous case,

$$S_1(t) = \rho_1, \qquad S_2(t) = \rho_2 \tag{6.31}$$

then as $\epsilon \to 0$ we recover the piece-wise uniform S.

Numerical Results. Using the nonuniform equations with S given by (6.30) we can use the Lagrangian formulation to confirm our results for the piece-wise uniform case and to investigate the solution behaviour when there is a more gradual change of strain rate ρ over the domain.

For high values of the strain rate, i.e $\rho \sim 0.01$, there is little difference between the solutions for piece-wise uniform and nonuniform domain growth with smooth change in ρ across the domain, even when the change is very gradual ($\epsilon \sim 1$). As ρ is decreased we find that in the limit $\epsilon \to 0$ we recover the behaviour displayed on the piece-wise uniformly growing domain. Interestingly, it seems that certain of the features that we observed are dependent on the sharpness of the interface between subdomains for the piece-wise uniform case. In Figure 6.6 we plot activator solutions for decreasing ϵ corresponding to successively closer approximations to the piece-wise uniform problem, for which the corresponding solution is shown in Figure 6.2(a). When the change in S is gradual then all peaks undergo splitting (up to time $t = 3500$ at least), in a manner

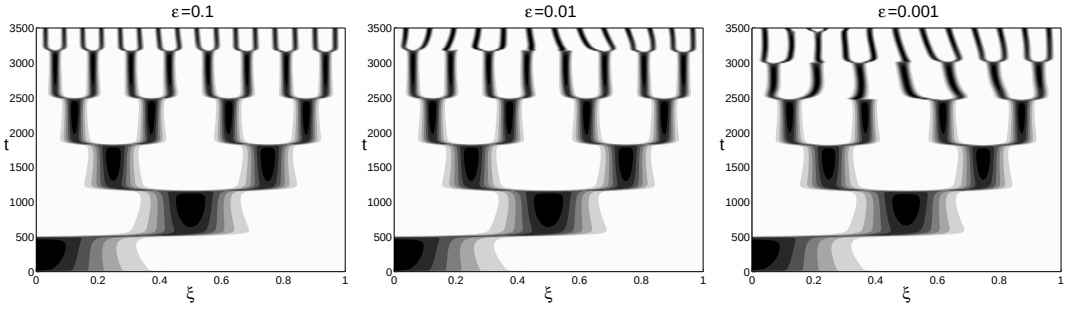

(a) (b) (c)

FIGURE 6.6 Pattern formation with nonuniform domain growth: as ϵ is reduced solutions resemble the piece-wise uniform case shown in Figure 6.2(a). Here we plot numerical solutions for the activator $v(\xi, t)$ with the *tanh* function for the domain growth and $\rho_1 = 0.001$, $\rho_2 = 0.0011$ and $\Theta = 0.5$. The initial domain length $\gamma_0 = 1$ and we plot solutions for (a) $\epsilon = 0.1$, (b) $\epsilon = 0.01$ and (c) $\epsilon = 0.001$ giving successively better approximations to the piece-wise uniform case.

similar to the uniform case (Figure 6.2(b)). As S becomes steeper then certain peaks fail to split at successively lower values of t (at correspondingly lower pattern modes).

Simulations for larger initial domains are shown in Figure 6.7, where we plot activator solutions for decreasing ϵ. We recover the piece-wise uniform behaviour, corresponding to Figure 6.4(a), as $\epsilon \to 0$. These results indicate that the transition from two activator peaks to three on the growing domain, when only the peak in the faster-growing region splits, is not strongly dependent on the exact nonuniformity. When $\epsilon \sim 1$, $S > 0$ on almost every part of the domain. We would expect splitting to be possible on the left-hand part of the domain except when ϵ is sufficiently small that $S \approx 0$ there. This is supported by the results in Figure 6.7 where it is only for very small ϵ that the splitting is restricted to the growing right-hand region, and not the left, as seen for the piece-wise uniform case.

Next we use the same model formulation to investigate reactant-controlled domain growth by choosing the local growth be a function of the local concentration of one or both of the reactants (the chemical species u or v).

6.1.4 Reactant-Controlled Growth. In this section we illustrate that the Lagrangian formalism may be used when explicit functional dependence for S on X and t is unknown, but rather S is a function of the dependent variables u and v. This will also be the appropriate formulation for numerical solution of the equations when S is determined by some extended system of constitutive laws describing the tissue growth. In the literature several models have been proposed in which domain growth is determined by reaction-diffusion variables. Dillon and Othmer [27] study pattern formation in the growing limb bud, modelled as an incompressible fluid with a distributed source term, S, which is a function of the local chemical composition. In their

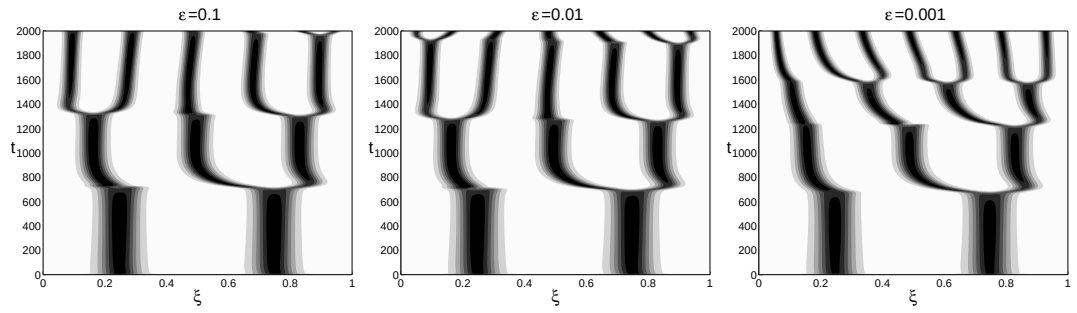

FIGURE 6.7 Pattern formation under nonuniform domain growth for larger initial domains. Numerical solutions are shown for the activator $v(\xi, t)$ with the *tanh* function for the domain growth and $\rho_1 = 0$, $\rho_2 = 0.001$ and $\Theta = 0.5$. The initial domain length is $\gamma_0 = 20$ and we plot (a) $\epsilon = 0.1$, (b) $\epsilon = 0.01$ and (c) $\epsilon = 0.001$.

model there are two chemical components which react and diffuse through the growing fluid region, however, their system is not of Turing-type and only simple gradients in the chemicals are formed. Modelling the morphogenesis of certain species of green algae, Harrison and coworkers [48, 50] couple a reaction-diffusion mechanism, which does generate Turing patterns, to domain growth. However, they also include a feedback mechanism to the kinetics such that DDI operates only within history-dependent boundaries separated by 'inert' regions for which there is no pattern formation.

The coupling of domain growth to the chemical kinetics provides a feedback between the pattern formation process and the mechanism that generates sequences of patterns. As an example, we consider a model for which domain growth is controlled by 'growth factor' v, the self-activating component, for which the reaction-diffusion dynamics are governed by

$$u_t = \frac{1}{\gamma_0}\frac{1}{\Gamma_X}\left[\frac{1}{\Gamma_X}u_X\right]_X + f(u,v) - u\,S(v) \tag{6.32}$$

$$v_t = \frac{d}{\gamma_0}\frac{1}{\Gamma_X}\left[\frac{1}{\Gamma_X}v_X\right]_X + g(u,v) - v\,S(v) - \Delta(v) \tag{6.33}$$

$$[\Gamma_X]_t = S(v)\,\Gamma_X \tag{6.34}$$

where $\Delta(v)$ is a function describing the uptake of the growth factor by the tissue and is a further modification to the reaction term for species v. We wish to consider reasonable forms for the uptake of v and the response function which determines the local growth $S(v)$. In biological systems such processes are governed by highly complicated biochemical pathways. We will not attempt to model these processes fully, rather we will assume a 'black box' type approach and assume functional forms which have reasonable properties.

The simplest approach is to assume that the uptake of growth factor by the tissue is proportional to its concentration. Then for constant tissue (cell) density the uptake will be a linear term in v. However, if the chemical binds to cell-surface receptors then the signal received by the cell will be saturating at high concentrations. If the inactive receptor R_i binds chemical C to form active receptor R_a then the rate equation for binding is

$$R_i + C \underset{k^-}{\overset{k^+}{\rightleftharpoons}} R_a \tag{6.35}$$

with rate constants k^+ and k^-. The Michaelis-Menten form for the fraction of bound (active) receptors F_b is given by

$$F_b = \frac{r_a}{r_a + r_i} = \frac{c}{\kappa + c} \tag{6.36}$$

where r_a and r_i are receptor concentrations (or densities) and $\kappa = k^-/k^+$ is the Michaelis-Menten constant. If binding of c to the receptors is cooperative then the sigmoidal expression for the bound fraction will contain the concentration c raised to the power m, reflecting the degree of cooperativity. In this case the uptake, with constant of proportionality α, is given by

$$\Delta(v) = \frac{\alpha v^m}{\kappa + v^m}. \tag{6.37}$$

The response of the cell to the fraction of bound receptors is far from trivial, involving complex signalling and intracellular machinery in the translation from chemical signal to cell growth and proliferation. A similar problem arises in the biological chemostat (or continuously-stirred tank reactor, CSTR, see for example Smith and Waltman [123]). In this experimental apparatus nutrient is supplied to a well-mixed tank containing a micro-organism population (with possibly several interacting species) and the run-off monitored to determine the rate of uptake of nutrient. This information, tallied with the population density increase, provides an empirical relationship between population growth and nutrient uptake. Here it has been noticed (Monod [84]) that the consumption of nutrient has the same sigmoidal relationship to the amount of nutrient supplied, and that the response of population growth is proportional to the uptake of the nutrient. The physiology of microbial uptake of nutrient and growth is a undoubtedly very complicated, however, the empirical sigmoid appears to be a remarkably good approximation, suggesting that the uptake is the limiting process involved. Similarly, in the absence of other detailed information, we suggest that the binding of the growth factor may in this respect be the important process for the tissue growth problem, and so we will assume a sigmoidal form for the local growth rate (in one spatial dimension) $S(v)$. Thus we suppose that the cellular interpretation of the number of bound receptors is proportional to the bound fraction.

The key features for this response function are the monotonicity and saturation of the sigmoid. In fact certain factors may produce non-monotonic response, for example

if a nutrient is essential at low concentration but inhibiting to growth (or toxic) at higher concentration. This is studied for the chemostat by Butler and Wolkowicz [11] and by Wolkowicz and Lu [132]. A similar biphasic response is observed in phototaxis for algae which are attracted toward sources of light but repelled by strong light [129]. The sigmoid dependence is also found in the chemotaxic response of certain organisms as the function that determines the bias in the random walk [61], the so-called receptor law [120, 102].

The assumption that tissue density remains constant implies that the result of tissue growth, increased cell size or proliferation, is expansion of the domain. The growth factor is removed sigmoidally (uptake) and the domain growth is then sigmoidal in response (proportional) with some delay, the time taken for the cellular response to produce new tissue, and the local growth S is given by

$$S(X,t) = S\big(v(X,t-\tau)\big) = \frac{\rho v(X,t-\tau)}{\kappa + v(X,t-\tau)}. \tag{6.38}$$

For simplicity we will assume that there is no delay, $\tau = 0$, so that tissue growth in response to the bound chemical is instantaneous. Although physically unrealistic, this approximation is reasonable in the context of reaction-diffusion patterns given that the solution is for the most part in quasi-steady state. Also we assume that ρ, which determines the ratio between the fraction of bound receptors and the growth rate (rather than biomass produced, as for the chemostat), will be small, so that domain growth remains *slow* in the sense that we have discussed. Furthermore, it is reasonable to assume that only a small amount of the growth factor is taken up by the receptors, so that the constant of proportionality α is also small. Finally, therefore, we consider the model

$$u_t = \frac{1}{\gamma_0}\frac{1}{\Gamma_X}\left[\frac{1}{\Gamma_X}u_X\right]_X + f(u,v) - \frac{\rho u v}{\kappa + v} \tag{6.39}$$

$$v_t = \frac{d}{\gamma_0}\frac{1}{\Gamma_X}\left[\frac{1}{\Gamma_X}v_X\right]_X + g(u,v) - \frac{(\rho v + \alpha)\, v}{\kappa + v} \tag{6.40}$$

$$[\Gamma_X]_t = \frac{\rho v}{\kappa + v}\,\Gamma_X. \tag{6.41}$$

We have solved this system numerically using the same computational routine as for the general nonuniform domain growth problem. The Lagrangian framework is preferred as it does not require explicit calculation of the local kinematic velocity for the domain, involving the inversion of Γ. A typical numerical solution for the activator species is shown in Figure 6.8(a), where the solution is interpolated to equally spaced points in ξ. The value of the local growth rate S is plotted as a function of time and scaled space in Figure 6.8(b), where those parts of the domain which are growing are shaded dark, and are seen to correspond closely to the evolving activator profile. The trajectories of particles embedded in the domain (flow lines) are plotted in Figure 6.9,

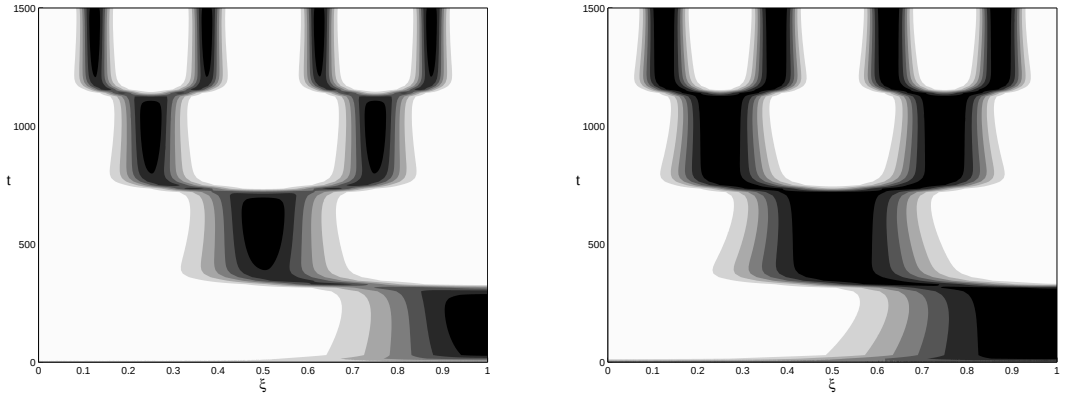

(a) (b)

FIGURE 6.8 Pattern formation with reactant-controlled domain growth. We plot (a) the activator (the 'growth factor') solution on the scaled domain and (b) the local strain rate (rate of volumetric change), for Schnakenberg kinetics and with $\gamma_0 = 1$, $d = 0.01$, $\rho = 0.005$ and $\kappa = 1$. We have taken $\alpha = 0$ although we have found no qualitative change to the results for small non-zero α. The numerical mesh has 1000 space points and no change to the solution is found by halving the mesh size.

uniformly scaled to the unit interval, given by

$$Z_X(t) = \Gamma(X,t)/\Gamma(1,t) \tag{6.42}$$

which we plot for different values of X. For clarity twice as many lines are plotted for $X \in [1/2, 1]$ as for $X \in [0, 1/2]$. In the figure the relative expansions of different regions of the domain are clearly seen. Numerical solutions were also computed with sigmoidal response functions for higher cooperativity, $m > 1$, giving qualitatively similar results.

The pattern sequence that is recovered is frequency-doubling in nature, through regular peak splitting (for the Schnakenberg kinetics). This result is perhaps unsurprising as the growth has the same symmetry as the pattern. However, this example illustrates that coupling between the domain growth and the reaction-diffusion pattern itself is sufficient to drive formation of the FD pattern sequence.

6.1.5 Discussion. The simulations presented in this section have all considered Schnakenberg kinetics, and pattern transitions have been through splitting of existing peaks in the solution profile. Naturally, similar results may be obtained for kinetic schemes for which transitions are through the insertion of new peaks. There is no significant effect on pattern amplitude or wavelength from the spatial dependence of terms in the equation for nonuniform growth. When domain growth is slow the advective term is correspondingly small, and peaks in the activator concentration reorganise continuously to maintain separation which is roughly independent of position. In Figures 6.1 and 6.3 the asymmetry in the pattern is due to the relatively high value of ρ. Here peaks do not reach their stationary positions during separation subsequent

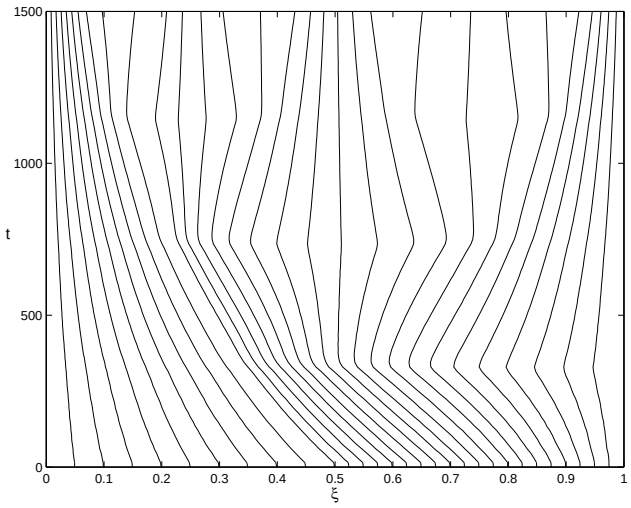

FIGURE 6.9 Flow lines, $Z_X(t)$, for reactant-controlled domain growth. The lines represent the trajectories of particles initially separated at regular intervals in X. For clarity twice as many points are taken in the second half as in the first half of the interval $X \in [0, 1]$. Parameters and other details as in Figure 6.8.

to splitting, before the domain is sufficiently large for the peaks to undergo the next transition. For slower domain growth (Figures 6.2 and 6.4) the nonuniformity of the domain growth is reflected in the failure of some peaks to split, giving an asymmetric sequence of patterns.

We have employed the Lagrangian formulation for nonuniform growth, and have described the numerical solution of the equations. However, the calculations proceed on a grid which is equally spaced in X, while patterns are approximately equally spaced in ξ. During growth of regions of the domain, any particular interval in X may expand to become a large interval in ξ. Hence in order to achieve reliable results a large number of grid points may be required. This is the trade-off against the computational effort saved in not being required to invert Γ during the calculation. In the simulations presented we have in each case performed computations with twice the number of grid points as shown, to ensure that the simulation has converged onto the true solution. A more sophisticated approach might be to periodically refine the computational mesh, to take the variable regional expansion into account.

We now reassess the two questions that were posed at the beginning of the chapter. We have shown that for small spatial perturbation, which we interpret as gentle gradients in the spatial dependence, we recover FD-type sequences (at least for the low modes that we have monitored). For more *strongly* nonuniform growth (for steeper change in S) at high ρ we have observed asymmetry, as for the uniform case, and for lower ρ selected peaks fail to undergo transitions, akin to the failure of FD for uniform linear growth. For highly nonuniform domain growth, and in particular when one region of the domain is not growing, other sequences may be formed by the failure of peak splitting (or insertion) at particular locations, specifically for those peaks on the

stationary part. This mechanism also appears to some degree robust, suggesting that it may be possible to choose the nonuniformity such that a specific pattern is selected during domain growth (as part of an evolving sequence) and furthermore, that the same pattern will be selected for some amount of variation of the nonuniformity.

6.2 Pattern Formation in Higher Dimensions

Much experimental research on biological and chemical pattern formation concerns patterning on surfaces or in relatively thin sheets. Correspondingly, in the literature concerned with biological problems as well as in chemical and physical systems there is a vast amount of work on theoretical aspects and modelling of pattern formation in higher spatial dimensions. Murray [88] considers reaction-diffusion as a model for animal coat markings and discusses linear stability and some effects of domain geometry on pattern formation. Meinhardt [82] discusses pattern formation in two dimensions in models for various aspects of embryology. Much of the work on pattern formation in chemical and physical systems centres around describing the detailed bifurcation structure near to the point of instability. The book by Walgraef [130] typifies this approach, discussing the use of amplitude equations to generate bifurcation diagrams near onset of instability in two spatial dimensions and in the investigation of the dynamics and properties of defects in the patterns. In a similar vein the article by Cross and Hohenberg [21] presents a wide review of pattern forming instabilities, including reaction-diffusion equations, as studied by amplitude and phase equations, including physically relevant aspects such as imperfections and issues related to pattern selection.

The major new feature for pattern formation in two dimensions is the influence of the geometry of the domain, and the conditions applied on the closed curve which bounds it. The increase in the number of spatial degrees of freedom gives rise to a corresponding escalation in the pattern selection problem, and hence pattern robustness. Kauffman *et al.* [59] considered pattern formation on the ellipse in reference to segmentation of the Drosophila embryo early in its development, and the sequential compartment formation in Drosophila wing disks, aiming to show that linear reaction-diffusion theory could account for the experimentally observed patterns in gene expression. Bunow *et al.* [10] have disputed these modelling results showing the strong sensitivity of the patterns to the precise geometry of the domain.

For reaction-diffusion systems, diffusion-driven instability may be studied in two dimensions with linear stability analysis of the homogeneous steady state, as for the one-dimensional case presented in section 2.2. The analysis proceeds as before, however the linear spatial modes are now eigenfunctions of the Laplacian in the higher spatial dimension, satisfying the conditions imposed on the domain boundary. The planforms of these patterns are discussed below (see also the book by Murray [88] for a full discussion).

There has been some work on pattern formation on curved surfaces. In his original paper on DDI, Turing discusses pattern formation on the sphere in the context of gastrulation. Recently Varea *et al.* [128] have studied pattern formation on the sphere and Chaplain *et al.* [14] have considered this problem in the context of solid tumour growth.

There are also some interesting results for three-dimensional chemical patterns (see Callahan and Knoblock [12] for a group theoretic analysis of pattern formation in three dimensions). Some general analytical results and concrete numerical simulations for three-dimensional patterns (and competition between modes) are presented by De Wit *et al.* [24]. So-called 'black-eye' patterns, which exhibit a hexagonal symmetry where the repeated element is a bright ring (surrounding a darker black-eye), have been observed in chemical reactors and it has been suggested by Gomes [42] that these apparently two-dimensional patterns in fact result from the projection of a three-dimensional lattice in a thin domain, viewed at the requisite orientation. Such patterns are observed elsewhere in nature and so these results may have implications for biological pattern formation.

In the present work we restrict discussion to the rectangular domain,

$$\Omega = [0, L_x] \times [0, L_y] \,, \tag{6.43}$$

and consider only growth in directions parallel to the axes of the rectangle. This is, of course, a great simplification but will serve to illustrate how the results we have obtained in one dimension extend to the higher dimensional problem. The nondimensionalised reaction-diffusion system on a domain of fixed size is given by

$$u_t = \frac{1}{\gamma}\nabla^2 u + f(u,v) \tag{6.44}$$

$$v_t = \frac{d}{\gamma}\nabla^2 v + g(u,v) \tag{6.45}$$

defined on

$$\overline{\Omega} = [0,1] \times [0,\alpha]$$

with zero flux boundary conditions imposed on the closed curve

$$\mathbf{x} \in \partial\overline{\Omega} \tag{6.46}$$

where $\gamma \propto L_x^2$ and $\alpha = L_y/L_x$ is the ratio of the sides of the rectangle.

Linear Analysis. The linear analysis presented in Chapter 2 may be extended to two-dimensional domains with boundary conditions prescribed on the bounding curve $\partial\overline{\Omega}$. We seek solutions to the spatial eigenvalue problem

$$\nabla^2\phi + k^2\phi = 0 \tag{6.47}$$

where $\phi(x,y)$ satisfies the boundary conditions on $\partial\overline{\Omega}$ and $k = |\mathbf{k}|$ is the magnitude of the wavevector of the linear mode (the dimensionless wavenumber). On the plane

the general form of solutions in which we are interested is

$$\phi_k(x,y) = \mathcal{R}e \sum_{j=1}^{M} A_j \exp\left(i\,\mathbf{k}_j \cdot \mathbf{x}\right) \tag{6.48}$$

to which solutions come in pairs for each j with wavenumbers $\pm k$, where $|\mathbf{k}_j| = k$. For $M = 1$ patterns are essentially one dimensional and we recover stripes (rolls) perpendicular to wavevector $\mathbf{k}$ and, for the isotropic case on the plane, with arbitrary orientation. For $M \geq 2$ periodic planforms may be generated, built on superposition of the pairs of wavevectors at angles which are multiples of π/M. Rhombic planforms may be produced, for which the wavevectors do not intersect perpendicularly.

When boundary conditions are imposed on the rectangular domain only a discrete set of wavenumbers is admissible. The exploration of the dispersion relation and determination of characteristic spatial scales in sections 2.2.4 and 2.3.1 may be extended similarly, i.e. k must lie in some interval $k \in [k_-, k_+]$ which may be determined from the dispersion relation, and a minimum domain size may be calculated for a particular linear mode. For $M = 1$ the directional degeneracy is eliminated, and we must have $\mathbf{k} \cdot \mathbf{x} = kx$ or ky, corresponding to stripes parallel to one or other axis. There are two cases of interest for $M = 2$, giving different planform orientations: firstly solutions that we will refer to as p-type, for which $A_1 = A_2 = a_k/2$ and

$$\mathbf{k}_1 \cdot \mathbf{x} = k_x x + k_y y, \quad \mathbf{k}_2 \cdot \mathbf{x} = k_x x - k_y y \tag{6.49}$$

such that the spatial eigenfunction may be written

$$\phi_k(x,y) = a_k \cos\left(k_x x\right) \cos\left(k_y y\right) \tag{6.50}$$

with $k_x = m_x \pi$, $k_y = m_y \pi/\alpha$ and $k^2 = k_x^2 + k_y^2$ giving a diagonal lattice of spots, and secondly s-type patterns,[2] where

$$\mathbf{k}_1 \cdot \mathbf{x} = k\,x, \quad \mathbf{k}_2 \cdot \mathbf{x} = k\,y \tag{6.51}$$

and from the boundary conditions $k = m_x \pi = m_y \pi/\alpha$, which gives a square planform which intersects the axes perpendicularly. The latter planform is admissible as a solution of the linearised problem when the domain may be tessellated by a square tile of appropriate size, for which a lower bound is determined by the minimum domain length calculated from the dispersion relation. For $M = 3$ the planform is hexagonal and corresponds to a hexagonal lattice of spots or a honeycomb structure. These structures cannot satisfy the zero flux boundary conditions on the rectangular domain. However, in the full nonlinear problem defects in the pattern allow distortion of the planform such that the boundary conditions may be satisfied. This is increasingly true for larger aspect ratio situations (the ratio of the domain size to the intrinsic pattern wavelength). Similarly, in the nonlinear regime the square planform may be distorted to give a rectangular lattice to satisfy the boundary conditions.

[2] We use the notation $m = [m_x, m_y]_p$ for p-type solutions and $m = [m_x, m_y]_s$ for s-type patterns.

Linear analysis does not give any insight into pattern selection between these different planforms. The relative stabilities of these bifurcating solutions are studied in the weakly nonlinear regime by amplitude equations that describe the evolution of the A_j as functions of time. These equations, derived by asymptotic expansion about the bifurcation point, are strictly valid only in the vicinity of the bifurcation. Nevertheless, good insight into the competition between different patterns can be gained by studying these equations and there is now a large literature concerning the bifurcation structures characterising different models and, more recently, in reproducing phenomena from the experimental Turing patterns. In two dimensions, consideration of solutions to the amplitude equations generated for one, two or three interacting destabilising modes allows one to find the relative stabilities of bifurcating stripe, square and hexagonal symmetric structures. Furthermore, amplitude equations may be used to examine the dynamics of defects in patterns and the transitions to more stable patterns (for example, Eckhaus and zigzag instabilities [21, 130]). A generic result for many reaction-diffusion systems, such as those studied here, is that hexagons appear first in a subcritical bifurcation, and then lose stability to squares or stripes depending on the relative size of the quadratic and cubic terms in the reaction kinetics.[3] It is now well documented that quadratic terms favour squares and hexagonal patterns over stripes. The competition between striped and spotted patterns (squares or hexagonal planform) has been investigated by Ermentrout [37] and Lyons and Harrison [74, 75] where it is shown that quadratic terms favour spots. Some numerical results supporting this conclusion are presented below. We will consider the Schnakenberg system, the quadratic nature of which becomes apparent after expanding the reaction terms around the kinetic steady state (see Appendix A.1), for which the solution on a fixed domain is shown in Figure 6.13(d), and we take the cubic autocatalysis model from Chapter 5 as a canonical stripe-generating system, showing the solution on a fixed domain in Figure 6.14(c).

6.2.1 Numerical Solution in Two Dimensions. The reaction-diffusion model in two dimensions can be solved numerically using standard methods for parabolic equations on rectangular grids (see Morton and Mayers [85]). The simplest finite difference method is the fully explicit Euler scheme which works well enough but, as in one spatial dimension, is subject to a prohibitively restrictive stability condition. In one dimension this restriction is circumvented by the semi-implicit Crank-Nicolson scheme, which gives a linear system of near-tridiagonal form which is easily (and inexpensively) solved. However the direct extension of this scheme to two dimensions results in the loss of the tridiagonality of the matrix equation to be solved, which greatly slows down the computation. The tridiagonal form is retained by the *Alternating-Direction Implicit* (ADI) scheme of Peaceman and Rachford [108] for which the integration is

[3] The relevant nonlinear terms here are those found by expanding the functions about the kinetic steady state concentration values—see section 5.2.

explicit in one direction and implicit in the other for one half-timestep, and for the second half-timestep the order is reversed.

We seek a numerical solution on the spatial grid (x_i, y_j) with $x_i = (i-1)\Delta x$, $i = 1, \ldots, N_x$ and $y_j = (j-1)\Delta y$, $j = 1, \ldots, N_y$, where $\Delta x = \Delta y$ for a uniform grid, and time $t_k = k\Delta t$, $k = 0, 1, 2, \ldots$ with timestep Δt. For numerical approximation $U_{i,j}^k \approx u(x_i, y_j, t_k)$ we have

$$\left[1 - \frac{\Delta t}{2\,(\Delta x)^2}\,\delta_x^2\right] U_{i,j}^{k+1/2} = \left[1 + \frac{\Delta t}{2\,(\Delta y)^2}\,\delta_y^2\right] U_{i,j}^k + \frac{\Delta t}{2} f\left(U_{i,j}^k, V_{i,j}^k\right) \tag{6.52}$$

$$\left[1 - \frac{\Delta t}{2\,(\Delta y)^2}\,\delta_y^2\right] U_{i,j}^{k+1} = \left[1 + \frac{\Delta t}{2\,(\Delta x)^2}\,\delta_x^2\right] U_{i,j}^{k+1/2} + \frac{\Delta t}{2} f\left(U_{i,j}^{k+1/2}, V_{i,j}^{k+1/2}\right) \tag{6.53}$$

where $\delta_x U_{i,j}^k = U_{i+1/2,j}^k - U_{i-1/2,j}^k$ is the central difference operator, and a similar expression holds for δ_y. An equivalent formula gives the numerical approximation $V_{i,j}^k \approx v(x_i, y_j, t_k)$.

The resulting scheme is unconditionally stable (as for the Crank-Nicolson scheme), although there is still a condition for convergence [85]. The tridiagonal linear system of equations is efficiently solved using LU decomposition (see Press *et al.* [113]).

6.3 Two-Dimensional Slow Uniform Domain Growth

We restrict our attention to uniform domain growth, where the strain rates are independent of position, although we may allow different rates along the two axes to give anisotropic domain growth, which is specified by

$$\mathcal{D}_{ij} = \delta_{ij}\sigma_i(t), \qquad i = 1, 2 \tag{6.54}$$

(no summation implied) where $\sigma_1 \neq \sigma_2$ for anisotropic uniform growth. Transforming the rectangular growing domain to the unit square,

$$(x, y) \to (\xi, \eta) = \left(\frac{x}{r_1(t)}, \frac{y}{r_2(t)}\right) \tag{6.55}$$

where

$$r_i(t) = \exp \int_0^t \sigma_i(\bar{t})\,\mathrm{d}\bar{t} \tag{6.56}$$

such that $\Omega = [0, 1] \times [0, 1]$, we recover the equations

$$u_t = \frac{1}{\gamma(t)}\left(u_{\xi\xi} + \frac{1}{[\alpha(t)]^2} u_{\eta\eta}\right) + f(u, v) - S(t)u \tag{6.57}$$

$$v_t = \frac{d}{\gamma(t)}\left(v_{\xi\xi} + \frac{1}{[\alpha(t)]^2} v_{\eta\eta}\right) + g(u, v) - S(t)v \tag{6.58}$$

where we define

$$\gamma(t) = \gamma_0\,[r_1(t)]^2 \quad \text{and} \quad \alpha(t) = \alpha_0 \frac{r_2(t)}{r_1(t)} \tag{6.59}$$

so that $\alpha(t)$ is the time-varying ratio of the sides, and $\alpha_0 = L_y/L_x$ is the initial ratio. The rate of volume expansion S is given by

$$S(t) = \sigma_1(t) + \sigma_2(t). \tag{6.60}$$

In light of the results presented in previous chapters for pattern sequences on the growing one-dimensional domain, two central issues must be resolved for the model in two dimensions:

1. Do the one-dimensional results hold for two-dimensional domains undergoing *uniaxial* domain growth: does the splitting and insertion of peaks observed in the one-dimensional study have an analogous behaviour for the two-dimensional problem, or does the higher dimensionality destroy the sequences of patterns?
2. What qualitative changes occur for *biaxial* growth in two-dimensions: what pattern sequences are formed and are the patterns robustly generated?

In the following section we present the results of numerical simulations of the model assuming various forms for the kinetics and with several choices of σ_1 and σ_2. The system is solved numerically using the ADI method described above, incorporating the relevant functional dependence for those parameters in the equations which change with time.

6.3.1 The Quasi-One-Dimensional Problem. Firstly we examine the pattern sequences generated on a narrow strip, with growth parallel to the long axis only (along the x-direction). Taking an initial domain with ratio of sides $\alpha < 1$ we set

$$\sigma_1(t) = \rho_1, \qquad \sigma_2(t) = 0 \tag{6.61}$$

where $\rho_1 \ll 1$ so that domain growth is slow. The numerical solution for the activator $v(x, y, t)$ is shown in Figure 6.10. The solution is plotted as a function of x and y at various times t, so that the changing shape of the domain with time is apparent. The reaction terms $f(u, v)$ and $g(u, v)$ in equations (6.57) and (6.58) were taken to be the spot-selecting Schnakenberg kinetics. The width of the strip (the y-extent) was taken to be half of the initial length. The solution shows the standard spatial frequency-doubling behaviour as was obtained for the one-dimensional studies presented above.

In this example the width of the domain is sufficiently small (and is unchanging) that the only admissible patterns are of zeroth mode in the y-direction: the patterns generated in the sequence are all of mode $m = [\,\cdot, 0]_p$. Thus there is no dependence of the solution on y, and the solution behaviour is truly one-dimensional.

6.3.2 Uniaxial Domain Growth. If we choose the initial domain geometry such that a genuinely two-dimensional pattern, one with spatial dependence on x and y, is established initially then we may examine how the pattern evolves under anisotropic growth (along one axis only). As in the previous case, we take $\sigma_1 = \rho$ and $\sigma_2 = 0$ such that the domain is growing parallel to the x-direction only, but here α is increased to give a wider elongating strip. In Figure 6.11 the domain is initially square, and

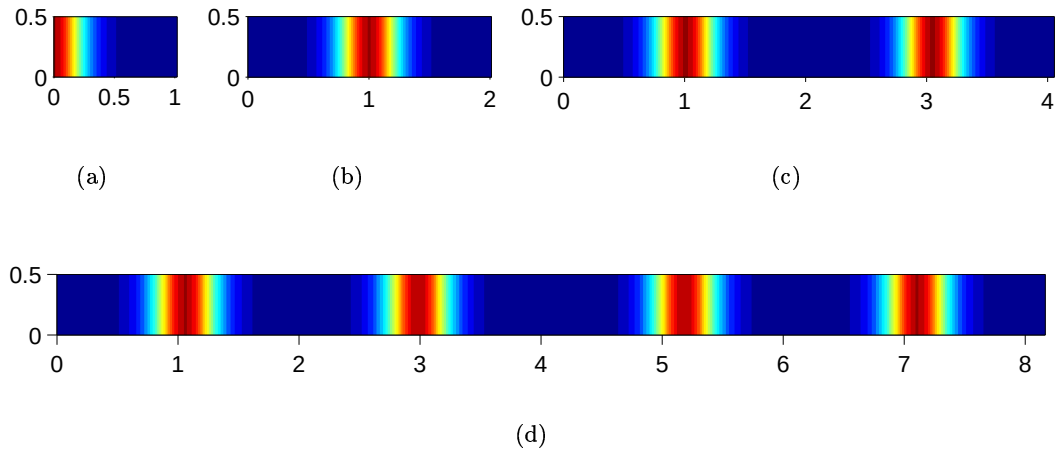

FIGURE 6.10 Spatial frequency-doubling via peak splitting for Schnakenberg kinetics on a thin elongating strip, with $\gamma_0 = 1$, $\alpha_0 = 0.5$ and $\rho_1 = 0.002$ ($\rho_2 = 0$). The activator solution $v(x, y, t)$ is shown at times (a) $t = 10$, (b) $t = 350$, (c) $t = 700$ and (d) $t = 1050$, corresponding to a doubling in x-extent at each step. Pseudo-colour scale is from 0 (blue) to 4 (red).

from random initial conditions with Schnakenberg kinetics the initial pattern to form is of mode $m = [+1, -2]_s$, equivalent to a half-spot, shown in 6.11(a). During the subsequent growth along the x-axis the solution evolves as a sequence of spot-patterns with rapid transitions between quasi-steady spatial profiles, comprising pattern modes $m = [+1, -2]_s$, $[-2, -2]_s$, $[-4, -2]_s$, $[-8, -2]_s, \ldots$. The sequence is generated in a similar manner to the pattern sequence in the one-dimensional case, with transitions by splitting and separation of the spots as the domain doubles in length in the x-direction.

The transition between two quasi-steady pattern modes is shown in detail in Figures 6.12(a)–(c). In Figures 6.12(d)–(h) the profile along the midpoint in y and parallel to the x-axis, $v(x, 1/2)$, is plotted for various times t corresponding to the full patterns in Figures 6.11(b), 6.12(a)–(c) and 6.11(c) respectfully. These graphs are strongly reminiscent of the peak-splitting phenomenon for solutions on the one-dimensional growing domain (Figure 4.6(a)–(d)), although it is interesting to note that the two-dimensional patterns have approximately twice the amplitude of the one-dimensional solutions.

In this example it is apparent that the domain remains too narrow to allow significant reorganisation of the arrangement of spots through relaxation into a different lattice type. Furthermore it is unclear whether the line of spots observed corresponds more closely to a narrow band along the axis of a square lattice or a similar thin strip along the vertices of a hexagonal planform. Further numerical simulations on domains of different initial size and geometry indicate that uni-directional growth favours the symmetry of the square lattice. In Figure 6.13(a) we have chosen the initial domain

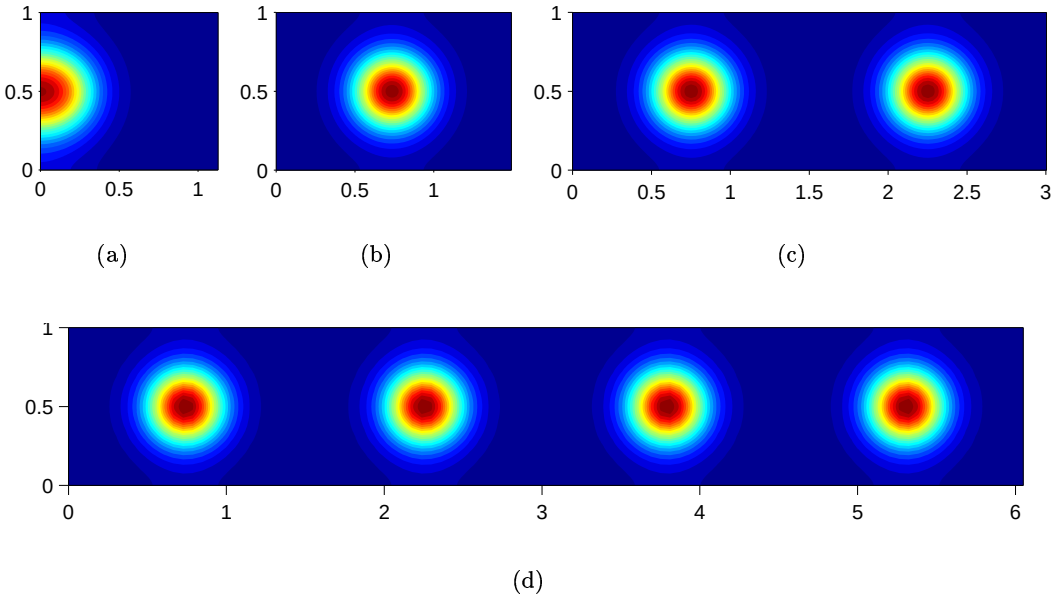

FIGURE 6.11 Spot splitting for Schnakenberg kinetics on an elongating strip, with $\gamma_0 = 1$, $\alpha_0 = 1$ and $\rho_1 = 0.002$ ($\rho_2 = 0$). We plot the activator pattern $v(x, y, t)$ at times (a) $t = 60$, (b) $t = 200$, (c) $t = 550$ and (d) $t = 900$, corresponding to doubling the strip length during the intervals between (b) and (d). In these and in subsequent spot-type patterns the pseudo-colour scale is from 0 (blue) to 8 (red).

length such that the destabilising pattern is mode $m = [-2, -6]_s$. For uniaxial domain growth along the x-axis the regular splitting of spots is found to occur, giving frequency-doubling in the x-direction, with the final pattern shown in Figure 6.13(b) after two such transitions. On this wider domain the arrangement of spots is not found to relax into a hexagonal lattice, the planform favoured on a static domain, which is shown in Figure 6.13(d). Here the fixed domain is of identical size and geometry to the growing domain at the time shown in the previous frame. The distortion of the hexagonal lattice is due to the relatively small aspect ratio, however, on larger fixed domains a truer hexagonal lattice is recovered, albeit with some defects to allow the boundary conditions to be satisfied.

Now we turn to examine pattern behaviour for kinetic schemes which select stripe patterns through dominance of the cubic terms in the expanded kinetics. As an example we take the system studied in detail in Chapter 5, with kinetics given by equation (5.26)–(5.27). Initially it will be our purpose to investigate whether, as in the previous example, domain growth can generate a pattern of greater symmetry than is generated on a static domain. For a small initial domain with $\alpha_0 > 1$ stripes preferentially align parallel to the shorter axis, as shown in Figure 6.14(a). Here the initial domain geometry is such that the first pattern to form is $m = [0, -6]_p$. During subsequent growth along the direction of the x-axis, such that at some later

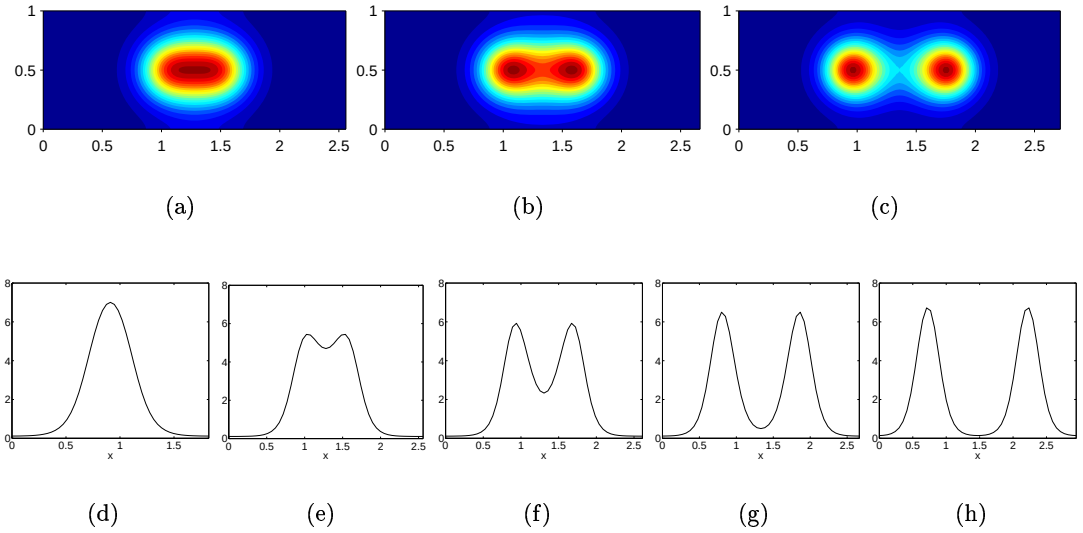

FIGURE 6.12 Detail of spot splitting for Schnakenberg kinetics, at times (a) $t = 470$, (b) $t = 480$ and (c) $t = 490$, and cross section profile, $v(x, 1/2, t)$, at times (d) $t = 200$, (e) $t = 470$, (f) $t = 480$, (g) $t = 490$, and (h) $t = 550$. Parameters as for Figure 6.11.

time the ratio of the sides $\alpha < 1$, the stripe pattern is essentially unchanged, shown in Figure 6.14(b). The pattern mode remains $m = [0, -6]_p$ although the size and geometry of the domain has changed significantly, as is reflected by the change of α where now $\alpha = 1/2$. In Figure 6.14(c) we show the activator solution generated from random initial data on a fixed domain of equal size and geometry to the previous frame. The intrinsic spatial scale (pattern wavelength) is clearly approximately the same, however, the simple symmetry of the pattern on the growing domain is not recaptured. Thus the effect of the uniaxial growth in this case is to stabilise a parallel stripe pattern. We have considered the kinetic system with small a positive quadratic term. Further simulations indicate that this behaviour is independent of the precise form of the kinetics, requiring only that stripes are strongly preferred. Variations on the kinetics with this proviso serve only to modify the cross-sectional profile of the stripes (which resemble the profiles for patterns on the one-dimensional domain).

6.3.3 Biaxial Domain Growth. In the previous section we examined the pattern sequences generated on a two-dimensional domain subject to growth along one axis only, and under various conditions on the domain geometry and reaction kinetics. Now we consider a two-dimensional rectangular domain with slow uniform domain growth along both axes, with

$$\sigma_1(t) = \rho_1, \qquad \sigma_2(t) = \rho_2 \tag{6.62}$$

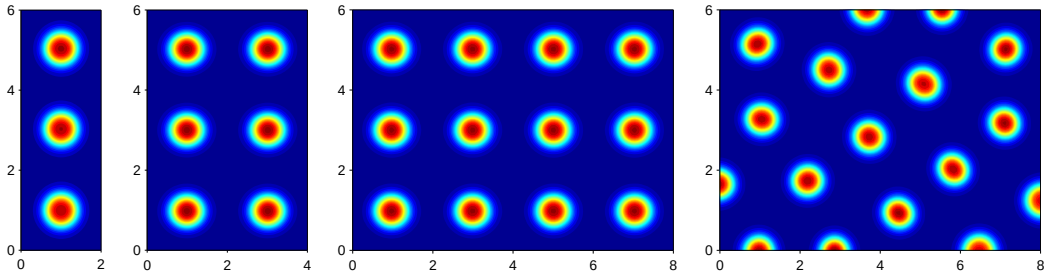

FIGURE 6.13 Selection of the square lattice through spot splitting on the uniaxially growing domain compared to the hexagonal lattice for pattern formation on a domain of fixed size. In (a)–(c) we plot activator solutions $v(x, y, t)$ for Schnakenberg kinetics on the growing domain with $\gamma_0 = 4$, $\alpha_0 = 3$ and $\rho_1 = 0.002$ at times (a) $t = 10$, (b) $t = 300$ and (c) $t = 650$. For (d) the domain is static ($\rho_1 = \rho_2 = 0$) and we plot a steady state pattern for $\gamma_0 = 64$ with $\alpha = 0.75$, giving the same domain size and geometry as (c).

where ρ_1 and ρ_2 are both small. When $\rho_1 = \rho_2$ the domain growth is isotropic. Within this same framework we could also assume some time dependence for the domain growth, as for several examples in Chapter 4.

Stripe Patterns. Firstly we reconsider stripe formation. Previously we found that stripes parallel to the direction of uniaxial growth remain aligned to the growth direction. However, of great interest is the stability of stripe patterns when domain growth is also in the direction perpendicular to the stripe orientation. Here elongation and separation of stripes occur simultaneously and, referring to the first question that we posed, the crucial issue is whether the stripes split in a manner similar to the one-dimensional problem (see Figure 5.3). The results of numerical simulations, presented in Figure 6.15, confirm this to be the case. In the figure the growth is isotropic, and so α retains its initial value, $\alpha_0 = 1$. Thus the vertices plotted are (ξ, η), showing the activator patterns $v(\xi, \eta, t)$ in the unit square, at various times t. The direction of a stripe pattern on a square domain will be parallel to one or other axis, the orientation determined by the initial data alone. In these simulations we use the cubic autocatalytic kinetic scheme (5.26)–(5.27) to study the subsequent evolution of striped pattern sequences under isotropic uniform domain growth.

In Chapter 5 it was shown that the perturbation of pure cubic kinetics with small quadratic terms determines whether evolving solution sequences on the one-dimensional domain gave rise to transitions through splitting or insertion of new peaks (or both simultaneously in the absence of the quadratic term). The same appears to be true for the transitions between pattern modes in two dimensions. In Figures 6.15(a)–(c) the sequence of patterns for the pure cubic case ($\delta = 0$) is shown. Here we see the

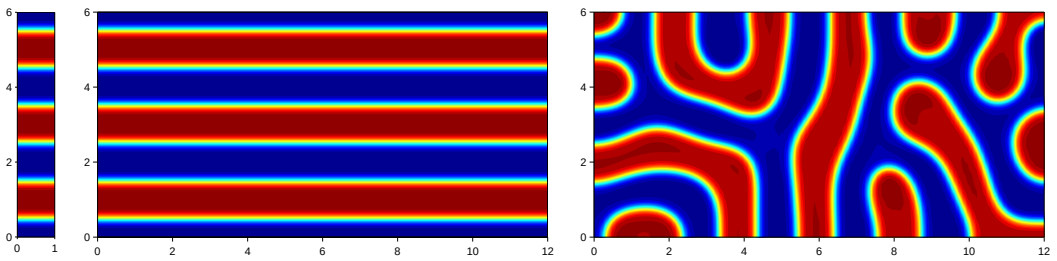

(a) (b) (c)

FIGURE 6.14 Domain growth parallel to stripes maintains the orientation of the striped pattern. Numerical solution for cubic autocatalysis kinetics with $\delta = 0.1$ on the uniaxially growing domain (a)–(b), compared with the steady state pattern generated on a fixed domain (c) of the same size as figure (b). Parameters for domain growth are $\gamma_0 = 1$, $\alpha_0 = 6$ and $\rho_1 = 0.005$ with final time (b) $t = 500$. In these and in subsequent stripe patterns the pseudo-colour scale is from -0.8 (blue) to 0.8 (red).

mode-tripling sequence that was described previously for the one-dimensional problem. The initial pattern is $m = [+1, 0]_p$, with subsequent patterns in the sequence $m = [-3, 0]_p$, $[+9, 0]_p, \ldots$, and with transitions each time the side perpendicular to the axis of the stripes triples in length. This sequence is the two-dimensional realisation of the frequency-tripling in the x-direction. In Figures 6.15(d)–(g) the kinetics are perturbed with a small positive quadratic term, such that stripes are selected but pattern transitions occur via insertion of new stripes each time the perpendicular side doubles in length, as for the one-dimensional case. Similar sequences are generated for anisotropic growth and for initially rectangular domains, where the ratio of the sides may bias the initial orientation of the stripe pattern. Painter [106] found, for one particular kinetic mechanism, that the parallel stripe structure may break down under domain growth, evolving to labyrinthine patterns. We have not observed similar behaviour here, and assume that the kinetic scheme that was used does not strongly select for stripes.

These results are simple two-dimensional extensions of the one-dimensional results discussed earlier. However, new phenomena emerge for the spot patterns under biaxial domain growth.

Spot Patterns. Using Schnakenberg kinetics we study the formation of spot patterns on isotropically growing domains, taking $\rho_1 = \rho_2$ for the domain growth rates (6.62). The pattern sequence for an initially square domain ($\alpha_0 = 1$) is shown in Figure 6.16. The novel feature demonstrated in this figure is the splitting of a single spot into four. As usual, spot splitting occurs when the axial length doubles. The symmetry of this sequence is certainly due to the square domain and the isotropic growth. If the domain is not square initially, or for anisotropic growth such that $\rho_1 \neq \rho_2$, then spot splitting events along the two perpendicular axes occur at different times. This

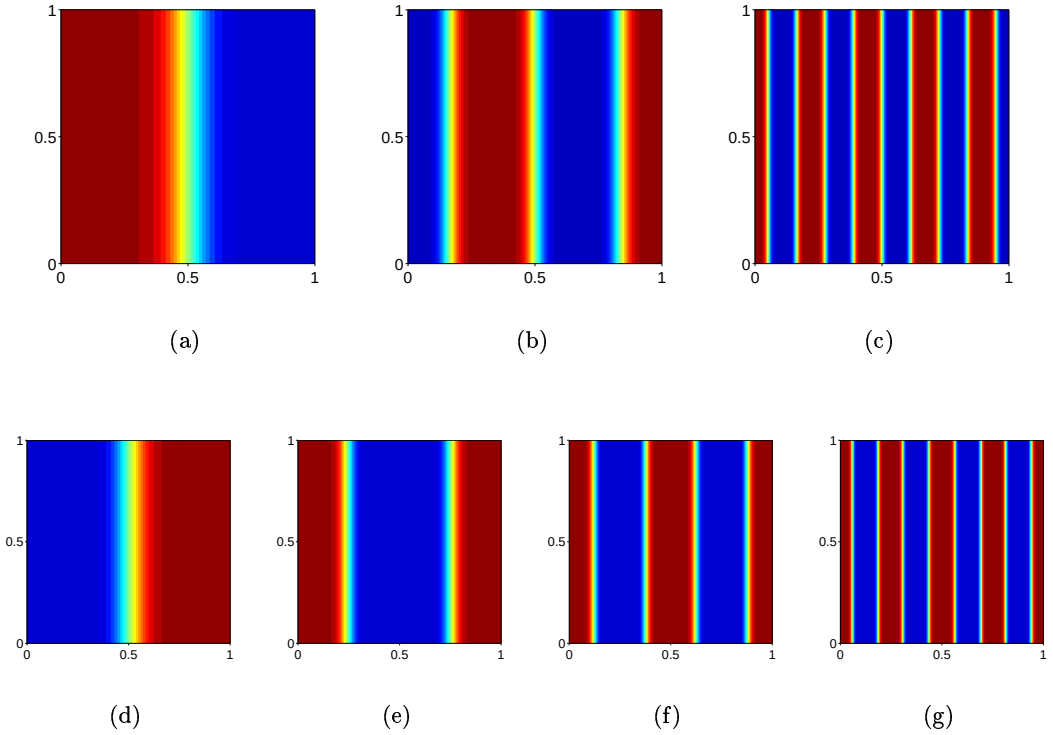

FIGURE 6.15 Sequences of stripe patterns generated under biaxial domain growth for cubic autocatalysis kinetics (5.26)–(5.27) showing (a)–(c) frequency-tripling of stripes for $\delta = 0$ and (d)–(g) frequency-doubling by stripe insertion for $\delta = 0.1$. The domain remains square as it grows, although this is not a requirement for the pattern sequences shown. The orientation of the stripes is in this case arbitrary, chosen by the random initial conditions. Similar behaviour is observed in the perpendicular orientation for stripes which are initially parallel to the x-axis. Parameters are $\gamma_0 = \alpha_0 = 1$ and growth rates $\rho_1 = \rho_2 = 0.002$ with solutions for the activator $v(\xi, \eta, t)$ shown on the scaled domain $[0, 1] \times [0, 1]$ at times (a) $t = 200$, (b) $t = 600$ and (c) $t = 1200$, and (d) $t = 250$, (e) $t = 600$, (f) $t = 950$ and (g) $t = 1300$. For plots (a)–(c) the domain sides triple and for (d)–(e) the sides double in length between each plot.

is because the axial length in one direction reaches its critical value before that of the other direction. The results of a numerical simulation for the latter of these two cases is shown in Figure 6.17. Here we plot $v(x, y)$ for various times t to show the changing shape of the domain. The domain is initially square but growth is faster parallel to the y-axis and spots separate more quickly in this direction. The figure illustrates that on removing the square symmetry the quadruple splitting is lost, however, the rectangular planform is retained.

Transitions between patterns for Schnakenberg kinetics are through splitting of peaks in one dimension, and spot splitting for two-dimensional patterns, the details of which depend on the symmetries in the domain and its growth. Details of the spot splitting are shown in Figure 6.12 and in Figure 6.16 for the square-symmetric domain. Alternative kinetic schemes which also select spot patterns were shown in one

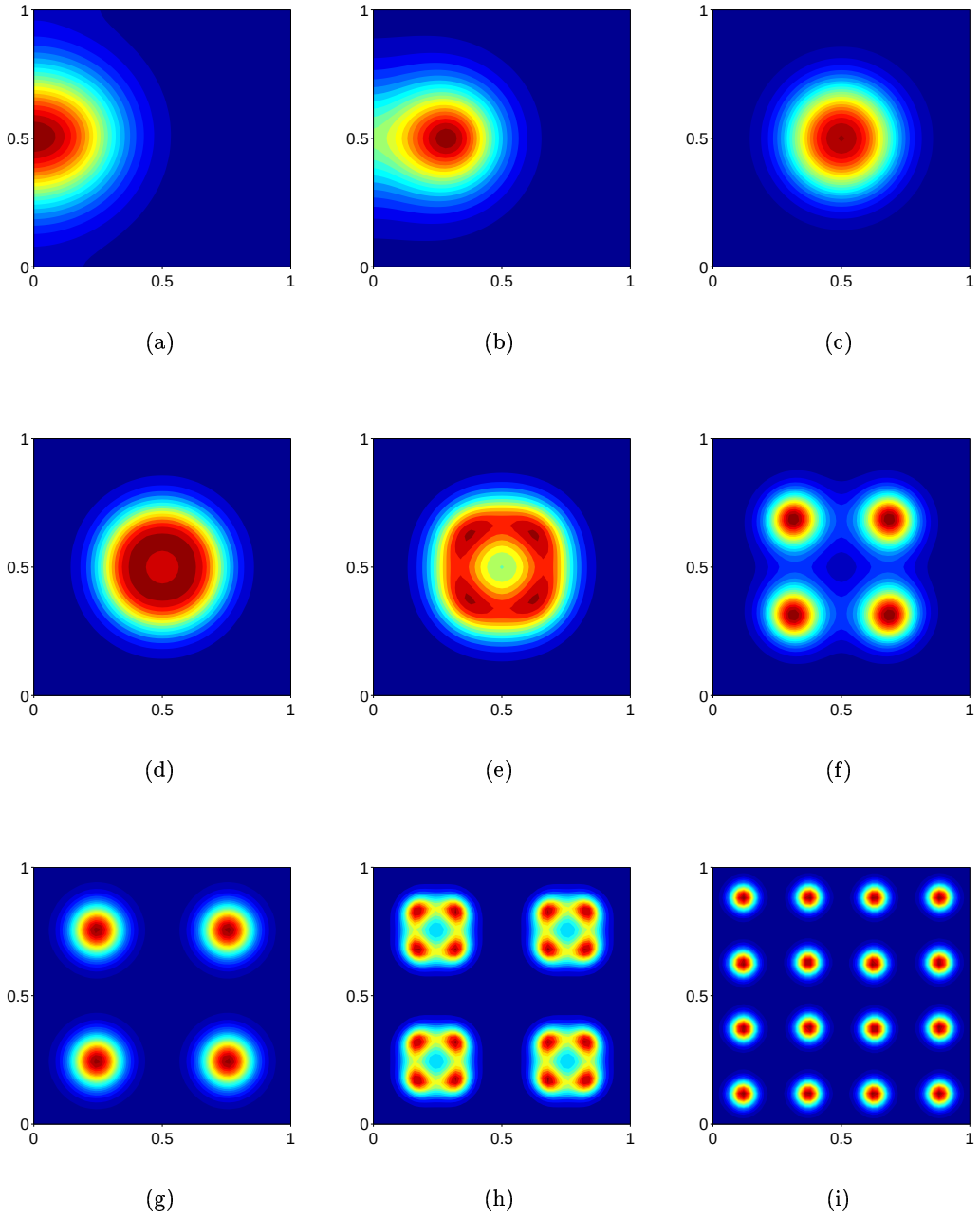

FIGURE 6.16 Symmetric splitting of spots generating a square lattice pattern for Schnakenberg kinetics on the isotropically growing domain. Parameters are $\gamma_0 = \alpha_0 = 1$ and growth rates $\rho_1 = \rho_2 = 0.002$ with solutions for the activator $v(\xi, \eta, t)$ shown at times (a) $t = 50$, (b) $t = 100$, (c) $t = 150$, (d) $t = 350$, (e) $t = 400$, (f) $t = 420$, (g) $t = 500$, (h) $t = 750$ and (i) $t = 850$. The domain length scale doubles between (c), (g) and (i).

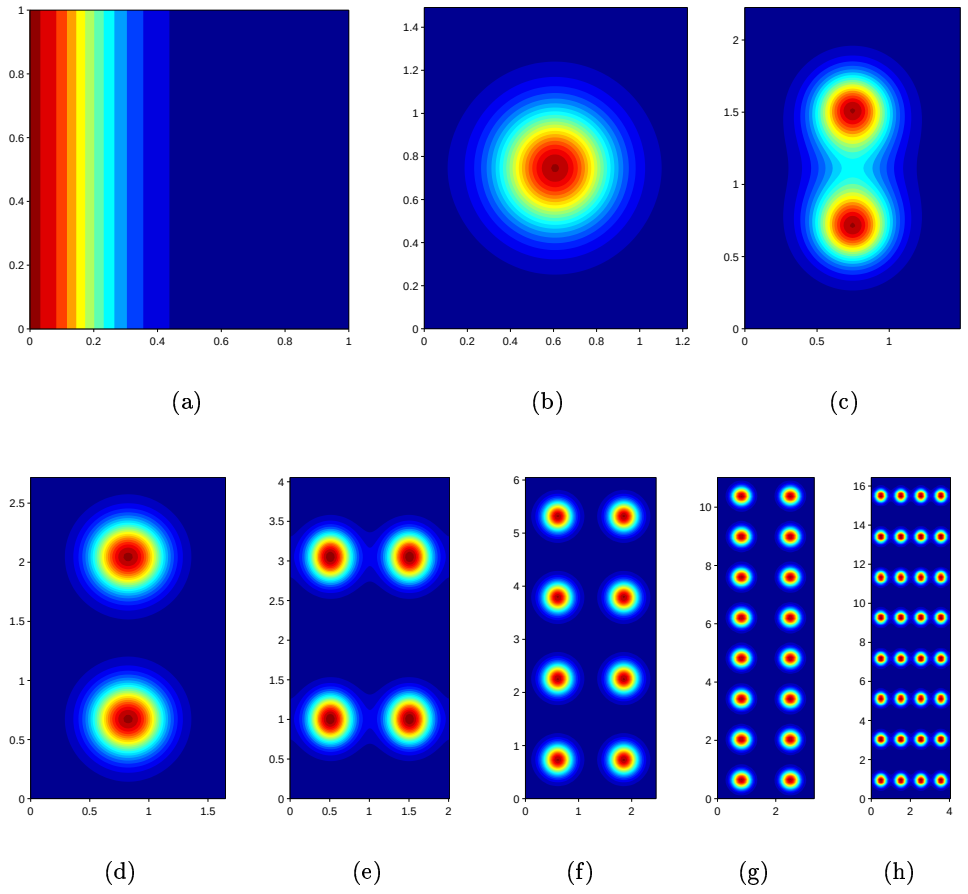

FIGURE 6.17 Generation of the rectangular lattice for Schnakenberg kinetics under anisotropic growth. Here $\rho_1 = 0.001$ and $\rho_y = 0.002$ while $\gamma_0 = \alpha_0 = 1$. The activator solution $v(x, y, t)$ is shown at times (a) $t = 10$, (b) $t = 200$, (c) $t = 400$, (d) $t = 500$, (e) $t = 700$, (f) $t = 900$, (g) $t = 1200$ and (h) $t = 1400$.

spatial dimension to undergo transitions via insertion of new peaks, the example we have used being the Gierer-Meinhardt equations (see Appendix A.3) with δ nonzero. In Figure 6.18 we plot the pattern sequence generated for Gierer-Meinhardt kinetics on an initially square, isotropically growing domain. Interestingly, a new phenomenon emerges for spot insertion. The patterns are found to alternate between two different orientations of the square lattice, what we have called p-type (diagonal) and s-type (square) planforms. For example in Figure 6.18(d) the pattern mode is $m = [+2, +2]_p$, which persists until the domain *side* is long enough to accommodate new peaks, at which point insertion of peaks generates mode $[+4, +4]_s$, shown in Figure 6.18(e). This mode, in turn, persists until the *diagonals* are long enough to accommodate insertion of new peaks, giving pattern mode $m = [+4, +4]_p$ (Figure 6.18(f)). This regular alternation takes place with time period corresponding an increase in the length of the domain side by a factor of $\sqrt{2}$. Thus between Figures 6.18(c) and 6.18(e), and

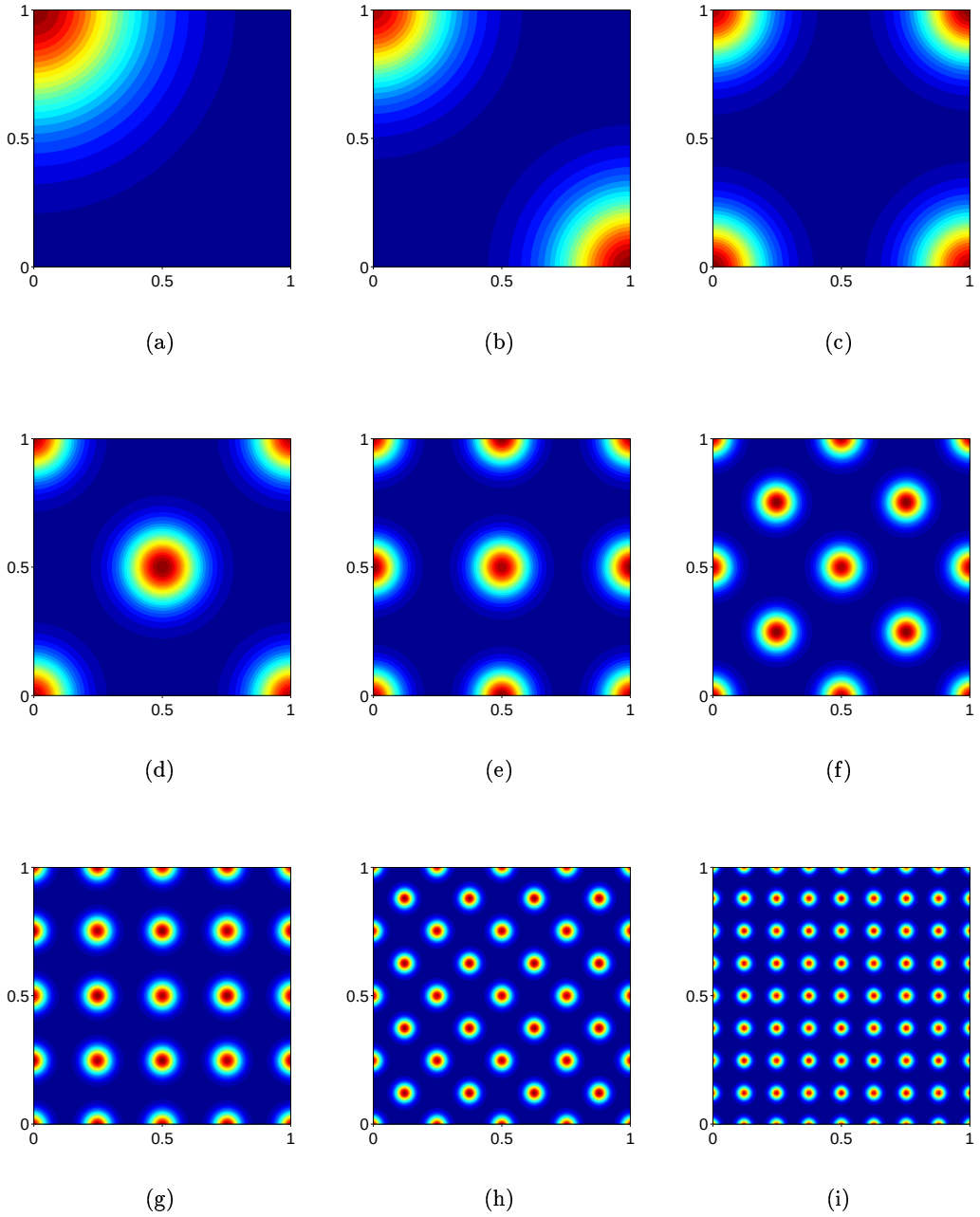

FIGURE 6.18 Spot insertion leading to alternation between orientations of the square lattice for Gierer-Meinhardt kinetics under isotropic domain growth. Between successive patterns the domain sides increase by a factor of $\sqrt{2}$. In this figure the ratio of diffusivities $d = 0.025$, and other parameters are $\gamma_0 = \alpha_0 = 1$ and $\rho_1 = \rho_2 = 0.005$. Numerical solutions for the activator $v(\xi, \eta, t)$ are shown at times (a) $t = 110$, (b) $t = 180$, (c) $t = 250$, (d) $t = 320$, (e) $t = 390$, (f) $t = 460$, (g) $t = 530$, (h) $t = 600$ and (i) $t = 670$.

between Figures 6.18(d) and 6.18(f) the domain sides and diagonals respectively double in length. Essentially there are two intercalating frequency-doubling sequences here, one sequence lagging the other. We have observed similar behaviour in numerical simulations on rectangular lattices, where the square symmetry and isotropic growth are relaxed (data not shown).

6.3.4 Discussion. These results indicate that pattern formation in two spatial dimensions can give rise to essentially one-dimensional pattern sequences, both for thin domains and for regular stripe patterns on squarer geometries. We have shown that domain growth may in fact stabilise parallel stripe patterns on domains of a size that would generate labyrinthine patterns for the static problem. Furthermore, we have shown that for spot-favouring kinetics the domain growth selects the square (or rectangular) lattice, rather than the hexagonal planform which is selected in the static case. An interesting observation for spike-type kinetics generating spot patterns is that the amplitude of the two-dimensional patterns is approximately twice that of one-dimensional structures. This is not the case for transition-layer systems where the amplitude is determined by the location of the two stable branches of the activator nullcline in the (u, v) plane.

The generation of patterns with increasing numbers of spots retaining the regular square symmetry is achieved when the initial domain is sufficiently small that regular patterns are generated initially. However, if the domain is initially large so that a disordered pattern forms initially (such as in Figure 6.13(d) or, for stripes, Figure 6.14(c)) then during subsequent domain growth the patterns do not relax to the regular lattice of spots (or to parallel stripe structures). In this sense the two-dimensional pattern sequences are unlike those observed in one dimension, where for exponential growth a frequency-doubling sequence will ensue from any initial pattern mode.

The preference for the square lattice seems to be generic for the different kinetic schemes and domain growth functions that we have considered. The higher symmetry afforded by square domains undergoing biaxial isotropic growth is certainly reflected in the pattern of peak splitting, viz. one peak splitting into four. This raises the interesting question of what patterns of peak splitting would be observed for other symmetries imposed on the domain geometry and growth. Lacalli [67] describes a numerical simulation of a reaction-diffusion equation on a circular disc with radially symmetric growth, where a central peak is found to split into six in a manner similar to the expanding ring which collapses into four peaks in Figure 6.16. However, the lattice generated under such symmetry is not reported. It is conceivable that the circular symmetry of radially symmetric growth will select the hexagonal planform. This is an interesting possibility which we have not yet explored, however, we would not expect the six-fold splitting to be recovered for perturbations of either the circular domain geometry or the radial symmetry of the growth.

The symmetry arguments presented in Chapter 2 for the steady state solutions and extended in Chapter 4 to the full PDE system hold equally well in two space dimensions. The transitions occur when the relevant spatial dimension doubles. However, for spot-inserting kinetics we have found a novel behaviour whereby two patterns exhibiting this symmetry intercalate. The pattern on the domain alternates between two different planforms as the domain grows. There are two important dimensions for the insertion mechanism due to the lattice structure, one parallel to the axes and the other the length of the diagonals. Insertions occur at the appropriate points, either midway between existing spots on lines parallel to the domain edges or on lines parallel to the diagonal, as these lengths double.

The results we have presented are confined to the highly restricted case of rectangular domains and growth out along one or both rectangular axes. Furthermore we have considered only growth at constant strain rate, and have not considered time dependence or indeed spatial nonuniformity in the growth. Time-dependence for the strain rates is easily incorporated into the numerical methods that we have discussed, and we would expect the results to be equivalent to those for the one-dimensional problem. In order to explore pattern formation on two-dimensional domains with more general geometries it is expedient to employ the finite element method for numerical solution of the equations, and this is currently under investigation [76]. Our formulation of the problem for numerical solution on rectangular domains may be extended to include nonuniform growth by writing the equations in Lagrangian form and modifying the numerical scheme to cope with convective terms, using an upwind method (see Morton and Mayers [85]).

7. Summary

It has been our aim in this thesis to characterise the effect of domain growth on pattern formation in reaction-diffusion systems. While motivated by the recent paper by Kondo and Asai concerning dynamic patterns in fish skin [64] (discussed in section 1.4) we have sought to explore general features of pattern formation on growing domains, rather than to discuss any specific patterning events from the biological realm. We have found, in particular for uniform domain growth, that the set of possible behaviours is severely limited. Such results may prove useful when trying to identify which biological pattern formation events might arise as a consequence of the reaction-diffusion mechanism, and where it may be more prudent to seek alternative explanations.

One key finding is the role of the various timescales in the problem. We have argued that slow domain growth (where growth is on a long timescale relative to pattern formation) is the appropriate model for biological scenarios, and this turns out to be the case for which a sequence of recognisable patterns is generated. For three-species reaction schemes exhibiting oscillatory patterns a third timescale is introduced and the evolution of solutions on the growing domain is found to be disorganised, even for slow domain growth. The interaction of the third timescale destroys the regular behaviour found previously.

Our investigation of the symmetry between different time-independent solutions on domains of fixed size found that a scaling law in the parameter γ (and hence in the domain length L) relates the different pattern modes. We have been able to extend this idea to the full time-dependent problem with domain growth to predict frequency-doubling and the novel frequency-tripling behaviour. Transitions between patterns are driven by the domain growth. Pearson's discovery of splitting and replication of structures in the bistable Gray-Scott model [109] (discussed in section 2.5.3) is all the more remarkable in that there is no such process driving the system. The kinetic schemes admitting the diffusion-driven instability that we have studied do not show this splitting behaviour without domain growth. However, the mechanism of peak (or spot) splitting in either class of kinetic schemes is not well understood and lacks satisfactory explanation.

One as yet unexplained feature of the simple two-species solutions on the uniformly growing domain is the effect of reducing the growth rate ρ through a lower critical value, below which the regular frequency-doubling breaks down. Corroborating evidence for this phenomenon is provided by the study of the linear growth case, where the breakdown of the regular sequence after several successful frequency-doubling events was shown to be consistent with the lower critical ρ. The implication of this result

is that if a domain grows too slowly then there is not sufficient coupling between domain growth and the pattern formation mechanism to produce the regular sequence. This runs counter to the intuitive idea that for slow domain growth the transitions between patterns are triggered simply by the peak separation exceeding some critical value. Nishiura *et al.* [95] have found that pattern for Gray-Scott kinetics close to the bistable regime develops, on a domain of fixed size, by splitting of the outermost peaks only (see Figure 2.8(a)) presumably for the reason that internal peaks do not achieve a minimum critical separation. For our system, however, peak separation is driven by the domain growth and it seems that the rate at which peaks move apart is important in determining the transitions between patterns, rather than just their instantaneous separation. For the uniform case all peaks on the domain separate at the same rate. With constant strain rate the time dependence is exponential and in one dimension the rate of expansion of any interval, $\mathrm{d}\,\Delta x/\mathrm{d}t = (X_2 - X_1)\rho\exp(\rho t) = \rho\,\Delta x$, is independent of time t. Evenly spaced peaks separate at the same rate, independent of time. Thus it seems that if peak separation is not fast enough then frequency-doubling does not result. For linear domain growth, peak separation $\mathrm{d}\,\Delta x/\mathrm{d}t = \rho\,\Delta x/(1+\rho t)$ is a decreasing function of t and frequency-doubling breaks down when peaks are separating at what was found to be the minimum separation rate for the exponential case.

In this thesis we have focused on patterns on one-dimensional growing domains. The extension of these results to higher dimensions is non-trivial. The two-dimensional patterns on the angelfish undergo transitions by insertion of stripes as the domain length perpendicular to the stripe orientation doubles, in a manner similar to the simulations shown in Figure 6.15(d)–(g). This is seemingly good circumstantial evidence that a mechanism such as reaction-diffusion is at work, however, the experimental observations may also be consistent with any other mechanism which has an intrinsic pattern wavelength. We have found that domain growth can stabilise parallel stripes in two dimensions, as well as giving rise to stripe splitting or insertion. Many more phenomena have been observed in the experimental system, including the formation and movement of Y-shaped branching points where one stripe divides into two. A wider range of behaviours may be possible in two dimensions under nonuniform domain growth. Frequency-doubling generates an even number of repeating elements and we found in one dimension that a low odd number of peaks could be generated with nonuniform growth, where peak splitting or insertion is restricted to one part of the domain. It would be of great interest to explore what further pattern behaviours are possible under nonuniform growth in two dimensions.

The rectangular lattice of spots would seem to be the only planform that can be selected by domain growth for kinetics containing quadratic terms. Thus hexagonal structures occurring in biology, for example the arrangement of feather primordia in the chick [57], are unlikely to be generated in this way. However, in many such

patterns robustness is not a requisite, and hexagonal patterns are favoured on the static domain.

One important feature of growth and form that we have overlooked in this thesis is curvature of the domain. The bowing and folding of sheets of tissue is as important in developmental systems as their migration and expansion. Translation without changing geometry (curvature or size) has no influence on the reaction-diffusion mechanism within a tissue, however, curved surfaces and in particular curvature changing with growth may be an important factor in pattern formation. To our knowledge there is, at present, little work discussing the interaction of curvature and domain growth in pattern formation. One notable exception is the paper by Chaplain *et al.* [14] in which the results of a simulation of reaction-diffusion on the surface of a radially growing sphere are reported, however, there are not sufficient data presented to ascertain whether or not similar phenomena are observed in their system.

We have been able to address the robustness problem, one of the major criticisms of reaction-diffusion theory [6, 10], having found that the incorporation of domain growth into the reaction-diffusion model drives the system to generate sequences of patterns [19]. Component patterns of the frequency-doubling sequence display semi-scale invariance, remaining established while the domain doubles in length, an important feature in the context of regulation. The frequency-doubling mechanism is an efficient manner in which to reliably generate patterns containing even numbers of elements.

The implication of this result is that arguments dismissing reaction-diffusion theory because of its perceived robustness failure must be reconsidered. Saunders and Ho [118] conclude that for reliable segmentation a sequential mechanism is required, in which the domain is successively divided into separate subdomains which are patterned independently. This relies on the result that small domains are patterned more reliably than large ones. We use this same result to select an initial pattern on a small domain, which then determines the modes in the ensuing frequency-doubling sequence. Pattern formation through frequency-doubling is a sequential process, whereby increasingly complicated patterns develop from simpler ones within a single dynamical system. This mechanism has already been proposed in the context of segmentation by Nagorka [91] for the early development of *Drosophila* (however, see earlier comments on current state of knowledge of molecular regulation in this system [2]). Our results support the view of Murray and coauthors [43], who have proposed that if several mechanisms are coupled together in hierarchical systems, whereby the steady state output of one pattern formation mechanism serves as the input or locally determines parameters for the next, then robustness with respect to initial data may be achieved.

Below we restate our results on the various ways in which pattern selection via domain growth can be said to be robust. Once an initial pattern is generated the

frequency-doubling sequence is insensitive to initial conditions. For exponential domain growth the mode composition of the sequence does not change over several orders of magnitude of the domain growth rate ρ, while for linear growth a number of frequency-doubling events is observed unless ρ is very much smaller than the characteristic linear growth rate of the patterns. Under logistic domain growth one of these patterns persists except when the final domain size lies in a small interval of values for which some other pattern mode is admitted. We have also shown that the precise form of the boundary conditions is unimportant (however, the symmetric choice of zero flux conditions greatly simplifies the analysis). These properties are due to the fact, shown in Chapter 5, that sequences are generated because of the dynamics of each element of the pattern, which for the exponential case are all equivalent. Transitions between patterns are dynamically driven and are not induced by fluctuations (as is the Turing bifurcation) and so the mechanism is robust to the presence of noise in the system. Finally, we have shown that the precise form of the kinetic functions for systems admitting the diffusion-driven instability determines the transition mechanism. The sequence, however, seems generic, except for some cases which we have highlighted.

This last point raises the question as to whether the behaviour we have described is particular to reaction-diffusion systems or is generic to all global pattern generation mechanisms, such as chemotaxis and mechanochemical models. In terms of the phenomenology of patterns generated on fixed domains, such mechanisms are difficult to distinguish, all having a range of destabilising modes which present the same pattern selection issues and similar robustness problems. As is discussed by Oster and Murray [99], the underlying mathematical structure of these biologically distinct models may be very similar indeed. If such mechanisms are found to differ then the predicted behaviour on the growing domain will provide a useful means to distinguish between them. Whether these other models exhibit qualitatively different behaviour in response to domain growth is the subject of current investigation.

A. Reaction Schemes: Chemical and Population Kinetics

In this appendix we briefly introduce the various reaction schemes used in this thesis. Employing the notation introduced in Chapter 2, the nondimensionalised concentrations are labelled $u, v, \ldots$ and written in order of decreasing diffusivity, so that for two-species models u represents the inhibitor and v the activator.

A.1 The Schnakenberg System

Schnakenberg [119] introduced a kinetic scheme derived from a hypothetical autocatalytic set of chemicals involving a trimolecular step:

$$X \rightleftharpoons A, \quad B \to Y, \quad 2X + Y \to 3X. \tag{A.1}$$

The quantities A and B are external reactants, assumed to be of constant concentration. Application of the law of mass action and definition of appropriate nondimensional quantities (see Murray's book [88]), with $u(t)$ and $v(t)$ representing the variation over time of the concentrations Y and X respectively, gives

$$\frac{\mathrm{d}u}{\mathrm{d}t} = b - uv^2 = f(u,v) \tag{A.2}$$

$$\frac{\mathrm{d}v}{\mathrm{d}t} = a + uv^2 - v = g(u,v) \tag{A.3}$$

where a and b are nondimensional parameters, and usually a is small ($\sim b/10$).

The Schnakenberg kinetic scheme is of *cross* activator-inhibitor type (see Section 2.2.3) and has a unique kinetic steady state, (u_s, v_s), for which

$$f(u_s, v_s) = g(u_s, v_s) = 0, \tag{A.4}$$

given here by

$$u_s = \frac{b}{(a+b)^2}, \quad v_s = a + b. \tag{A.5}$$

We can expand the kinetic functions in powers of u and v about this steady state, writing $\bar{u} = u - u_s$ and $\bar{v} = v - v_s$, and then, dropping the over-bars,

$$f(u,v) = -v_s^2 u - 2u_s v_s v - 2v_s uv - uv^2 \tag{A.6}$$

$$g(u,v) = v_s^2 u + (2u_s v_s - 1)\, v + 2v_s uv + u_s v^2 + uv^2 \tag{A.7}$$

showing the presence of quadratic as well as cubic terms for both f and g (see section 5.2).

A.2 The Gray-Scott Model

The Gray-Scott [45] model,[1] a variant of the autocatalytic model of glycolysis proposed by Sel'kov [122], considers the autocatalytic production of chemical B which decays to form product P in the irreversible reactions

$$A + 2B \to 3B, \quad B \to P. \tag{A.8}$$

Here B is self-activating (autocatalytic) while A is a substrate for which higher concentrations increase the rate of its own removal. In a closed reactor, for which initial concentrations of A and B are specified and no material is allowed to enter or leave the reactor, eventually all of the reactants would be converted to product. However, nonequilibrium conditions may be maintained by a constant feed of the reactant A and removal of the product P. After nondimensionalisation, under these nonequilibrium conditions, the (cross-) kinetics are given by

$$f(u,v) = F(1-u) - uv^2 \tag{A.9}$$

$$g(u,v) = -(F+k)v + uv^2 \tag{A.10}$$

where u is the nondimensional concentration of the substrate (A) and v of the activator (B). Here F is the (nondimensional) flow rate of substrate A into the reactor and k is effectively the rate constant for decay of B to form the product P. By varying these two parameters the kinetics may have a single (trivial) steady state

$$u_r = 1, \quad v_r = 0 \tag{A.11}$$

known as the the *red* state, or may exhibit bistability when the discriminant $\Delta = 1 - 4(F+k)^2/F > 0$, giving two additional steady states arising in a saddle-node bifurcation

$$u_b = \frac{1}{2}\left(1 - \sqrt{\Delta}\right), \qquad v_b = \frac{F}{2(F+k)}\left(1 + \sqrt{\Delta}\right) \tag{A.12}$$

$$u_i = \frac{1}{2}\left(1 + \sqrt{\Delta}\right), \qquad v_i = \frac{F}{2(F+k)}\left(1 - \sqrt{\Delta}\right) \tag{A.13}$$

where the *intermediate* state (u_i, v_i) is unstable and the *blue* state (u_b, v_b) is stable.

This model has been widely studied, both as the simplest chemically plausible model which gives oscillations in the continuously stirred reactor and also in the context of chemical pattern formation in reaction-diffusion equations. In the vicinity of the bistable regime the Gray-Scott model has been studied in the context of self-replicating phenomena, as is discussed in Chapter 2.

[1] Known by its originators as the cubic autocatalysis model

A.3 Gierer-Meinhardt Kinetics

Gierer and Meinhardt proposed several kinetic models based on biologically plausible arguments in their paper on biological pattern formation [41], including activator-inhibitor (pure) and activator-substrate (cross) kinetic schemes. The scheme which has come to be known in the literature as the Gierer-Meinhardt model[2] considers autocatalytic activation of A and self-inhibition of H

$$\frac{\partial A}{\partial t} = \rho_0 \rho + c\rho \frac{A^p}{H^q} - \mu A + D_A \frac{\partial^2 A}{\partial x^2} \tag{A.14}$$

$$\frac{\partial H}{\partial t} = c'\rho' \frac{A^r}{H^s} - \nu H + D_H \frac{\partial^2 H}{\partial x^2} \tag{A.15}$$

where $0 < (p-1)/q < r/(s+1)$, which is postulated to explain the regenerative properties of hydra observed in various transplantation experiments. Here the authors consider inhomogeneous distributed source terms $\rho(x)$ and $\rho'(x)$, usually taken to be simple gradients across the solution domain. However, for constant parameters these kinetics may admit the diffusion-driven instability. The standard values assumed for the powers in the quotients are $p = r = 2$, $q = 1$ and $s = 0$, and the nondimensionalised kinetics may be written as

$$f(u,v) = \nu_1 v^2 - \mu_1 u \tag{A.16}$$

$$g(u,v) = \nu_2 \frac{v^2}{u} - \mu_2 v + \delta \tag{A.17}$$

where u is the inhibitor (or substrate) and v the activator.

A.4 A Three-Species Model Arising in Population Dynamics

White and Gilligan [131] propose a model for the population dynamics of a host-parasite-hyperparasite system, to account for persistent spatio-temporal patterns in population densities in a homogeneous environment. The population dynamics is described by local interaction terms and diffusion is assumed to model the spatial spread and dispersion of each species. (Diffusion is commonly used as a model for the spatial spread of root systems and for the dispersal of spores.) In the field, patchiness has been observed for timescales much longer than those one would associate with stochastic heterogeneities (where eventually a uniform infestation of parasite would be expected). Phenomena monitored experimentally include drifting disease 'hot-spots' and periodic occurrence of disease at a particular spatial location.

[2] Denoted in their paper as *Activator-Inhibitor Model with Different Sources*

In dimensional form the local dynamics are governed for host (H), parasite (P) and hyperparasite (Q) by the system

$$\frac{\mathrm{d}H}{\mathrm{d}t} = rH\left(1 - \frac{H}{k}\right) - aPH \tag{A.18}$$

$$\frac{\mathrm{d}P}{\mathrm{d}t} = bPH - \frac{cP}{1+eP}Q \tag{A.19}$$

$$\frac{\mathrm{d}Q}{\mathrm{d}t} = lP - dQ \tag{A.20}$$

where the host plant H grows logistically and is removed by the parasite P at a rate a per unit parasite and has conversion factor b per unit host. Predation of the hyperparasite Q on the parasite is a saturating function of parasite population, with conversion at a rate l per unit parasite, and the hyperparasite has a natural decay rate d.

Nondimensionalising in the manner described in Chapter 2, we reorder the system with decreasing diffusivity. In their paper White and Gilligan assume $D_Q > D_H > D_P$, i.e. the hyperparasite is fastest dispersing and the parasite is the slowest. Following the authors we scale the population densities with their steady state values when $k = \infty$, namely $(Q_s^\infty, H_s^\infty, P_s^\infty)$, such that $u = Q/Q_s^\infty$, $v = H/H_s^\infty$ and $w = P/P_s^\infty$ and then for $d_v = D_H/D_Q$ and $d_w = D_P/D_Q$ we have

$$u_t = \frac{1}{\gamma}u_{xx} - \delta(u - w) \tag{A.21}$$

$$v_t = \frac{d_v}{\gamma}v_{xx} + v\left(1 - \frac{v}{\kappa}\right) - vw \tag{A.22}$$

$$w_t = \frac{d_w}{\gamma}w_{xx} + \mu\left(v\frac{w}{1+\beta} - u\frac{w}{1+\beta w}\right) \tag{A.23}$$

where the rescaled variables $\delta = d/r$, $\kappa = k/H_s$, $\mu = cQ_s/r$ and $\beta = bP_s$. Time is nondimensionalised with the rate parameter r. Here, as elsewhere, γ is the dimensionless scaling parameter which uniformly transforms the one-dimensional solution domain to the unit interval. Labelling the kinetic functions f, g and h we find that for this model $f = f(u, w)$, $g = g(v, w)$ and $h = h(u, v, w)$. Naturally, in general for the interaction of three species each kinetic function may depend on u, v and w.

B. Some Results from Fluid Mechanics

The results we reproduce below may be found in many elementary texts on fluid mechanics (see, for example, Acheson [1] or Chorin and Marsden [16]) and are employed in Chapter 3 to derive a reaction-diffusion-advection equation.

Firstly we recall the definition of the material derivative. If for some scalar quantity of interest, $G = G(\mathbf{x}, t) = G(x_1, x_2, x_3, t)$, then $\partial G/\partial t$ is the rate of change of G at constant $\mathbf{x} = (x_1, x_2, x_3)$ and the material derivative, $\mathrm{D}G/\mathrm{D}t$, is the rate of change of G following a fluid element

$$\frac{\mathrm{d}}{\mathrm{d}t} G\big(x_1(t), x_2(t), x_3(t), t\big) = \frac{\partial G}{\partial t} + \mathbf{a} \cdot \nabla G = \frac{\mathrm{D}G}{\mathrm{D}t}, \tag{B.1}$$

with $x_1(t)$, $x_2(t)$, $x_3(t)$ changing with time due to a flow velocity field $\mathbf{a}(\mathbf{x}, t)$.

B.1 Reynolds Transport Theorem

This theorem concerns the rate of change of volume integrals over the finite but time varying fluid element $V(t)$.

$$\frac{\mathrm{d}}{\mathrm{d}t} \int_{V(t)} G(\mathbf{x}, t)\, \mathrm{d}\mathbf{x} = \int_{V(t)} \left[\frac{\mathrm{D}G}{\mathrm{D}t} + G \nabla \cdot \mathbf{a} \right] \mathrm{d}\mathbf{x} \tag{B.2}$$

where $G(\mathbf{x}, t)$ is any scalar or vector function, and $V(t)$ is a region of space occupied by a finite deforming fluid element. The range of integration implies 'following the fluid' as the fluid element $V(t)$ is moving with the flow. The theorem may be proved by considering a change of variables to the Lagrangian description of the flow, in which spatial position $\mathbf{x}$, with respect to some Cartesian coordinates, is parameterised by position at time $t = 0$, $\mathbf{X} = (X_1, X_2, X_3)$, giving $\mathbf{x} = \mathbf{x}(\mathbf{X}, t)$. Then the range of integration is no longer a function of time, and the differential operator can be brought inside the integral as a rate of change following the flow, giving

$$\begin{aligned} \frac{\mathrm{d}}{\mathrm{d}t} \int_{V(t)} G(\mathbf{x}, t)\, \mathrm{d}x_1\, \mathrm{d}x_2\, \mathrm{d}x_3 &= \frac{\mathrm{d}}{\mathrm{d}t} \int_{V(0)} G(\mathbf{X}, t) J(\mathbf{X}, t)\, \mathrm{d}X_1\, \mathrm{d}X_2\, \mathrm{d}X_3 \\ &= \int_{V(0)} \left[\frac{\mathrm{D}G}{\mathrm{D}t} J + G \frac{\mathrm{D}J}{\mathrm{D}t} \right] \mathrm{d}X_1\, \mathrm{d}X_2\, \mathrm{d}X_3 \end{aligned} \tag{B.3}$$

where $J(\mathbf{X}, t)$ is the Jacobian for the transformation

$$J = \begin{vmatrix} \frac{\partial x_1}{\partial X_1} & \frac{\partial x_1}{\partial X_2} & \frac{\partial x_1}{\partial X_3} \\ \frac{\partial x_2}{\partial X_1} & \frac{\partial x_2}{\partial X_2} & \frac{\partial x_2}{\partial X_3} \\ \frac{\partial x_3}{\partial X_1} & \frac{\partial x_3}{\partial X_2} & \frac{\partial x_3}{\partial X_3} \end{vmatrix}$$

and $V(0)$ is the volume of the flowing fluid element at time $t = 0$. The computation of the derivative $\mathrm{D}J/\mathrm{D}t$ is achieved using Euler's identity

$$\frac{\mathrm{D}J}{\mathrm{D}t} = J(\nabla \cdot \mathbf{a}) \tag{B.4}$$

which is proved in the following section. This allows us to write

$$\frac{\mathrm{D}G}{\mathrm{D}t}\,J + G\,\frac{\mathrm{D}J}{\mathrm{D}t} = \left[\frac{\mathrm{D}G}{\mathrm{D}t} + G\,(\nabla\cdot\mathbf{a})\right]\,J \tag{B.5}$$

which on substitution into equation (B.3) and transforming back into coordinates $(\mathbf{x},t)$ gives the transport theorem (B.2). Using the definition of the material derivative (B.1) this may be written as

$$\frac{\mathrm{d}}{\mathrm{d}t}\int_{V(t)} G(\mathbf{x},t)\,\mathrm{d}\mathbf{x} = \int_{V(t)}\left[\frac{\partial G}{\partial t} + \nabla\cdot\mathbf{a}\,G\right]\,\mathrm{d}\mathbf{x}. \tag{B.6}$$

B.2 Euler's Identity

The material derivative of the Jacobian determinant $J(\mathbf{X},t)$ may be reduced to a simple form by the following considerations. Starting from the definition of the material derivative, we have

$$\frac{\mathrm{D}J}{\mathrm{D}t} = \left(\frac{\partial J}{\partial t}\right). \tag{B.7}$$

We use the multilinearity of the determinant to write

$$\begin{aligned}\frac{\partial J}{\partial t} &= \begin{vmatrix} \frac{\partial^2 x_1}{\partial t\partial X_1} & \frac{\partial^2 x_1}{\partial t\partial X_2} & \frac{\partial^2 x_1}{\partial t\partial X_3} \\ \frac{\partial x_2}{\partial X_1} & \frac{\partial x_2}{\partial X_2} & \frac{\partial x_2}{\partial X_3} \\ \frac{\partial x_3}{\partial X_1} & \frac{\partial x_3}{\partial X_2} & \frac{\partial x_3}{\partial X_3} \end{vmatrix} + \begin{vmatrix} \frac{\partial x_1}{\partial X_1} & \frac{\partial x_1}{\partial X_2} & \frac{\partial x_1}{\partial X_3} \\ \frac{\partial^2 x_2}{\partial t\partial X_1} & \frac{\partial^2 x_2}{\partial t\partial X_2} & \frac{\partial^2 x_2}{\partial t\partial X_3} \\ \frac{\partial x_3}{\partial X_1} & \frac{\partial x_3}{\partial X_2} & \frac{\partial x_3}{\partial X_3} \end{vmatrix} + \begin{vmatrix} \frac{\partial x_1}{\partial X_1} & \frac{\partial x_1}{\partial X_2} & \frac{\partial x_1}{\partial X_3} \\ \frac{\partial x_2}{\partial X_1} & \frac{\partial x_2}{\partial X_2} & \frac{\partial x_2}{\partial X_3} \\ \frac{\partial^2 x_3}{\partial t\partial X_1} & \frac{\partial^2 x_3}{\partial t\partial X_2} & \frac{\partial^2 x_3}{\partial t\partial X_3} \end{vmatrix} \\ &= \begin{vmatrix} \frac{\partial a_1}{\partial X_1} & \frac{\partial a_1}{\partial X_2} & \frac{\partial a_1}{\partial X_3} \\ \frac{\partial x_2}{\partial X_1} & \frac{\partial x_2}{\partial X_2} & \frac{\partial x_2}{\partial X_3} \\ \frac{\partial x_3}{\partial X_1} & \frac{\partial x_3}{\partial X_2} & \frac{\partial x_3}{\partial X_3} \end{vmatrix} + \begin{vmatrix} \frac{\partial x_1}{\partial X_1} & \frac{\partial x_1}{\partial X_2} & \frac{\partial x_1}{\partial X_3} \\ \frac{\partial a_2}{\partial X_1} & \frac{\partial a_2}{\partial X_2} & \frac{\partial a_2}{\partial X_3} \\ \frac{\partial x_3}{\partial X_1} & \frac{\partial x_3}{\partial X_2} & \frac{\partial x_3}{\partial X_3} \end{vmatrix} + \begin{vmatrix} \frac{\partial x_1}{\partial X_1} & \frac{\partial x_1}{\partial X_2} & \frac{\partial x_1}{\partial X_3} \\ \frac{\partial x_2}{\partial X_1} & \frac{\partial x_2}{\partial X_2} & \frac{\partial x_2}{\partial X_3} \\ \frac{\partial a_3}{\partial X_1} & \frac{\partial a_3}{\partial X_2} & \frac{\partial a_3}{\partial X_3} \end{vmatrix}. \end{aligned} \tag{B.8}$$

Now $a_i = a_i(x_1,x_2,x_3)$ and by the chain rule

$$\frac{\partial a_i}{\partial X_j} = \frac{\partial a_i}{\partial x_1}\frac{\partial x_1}{\partial X_j} + \frac{\partial a_i}{\partial x_2}\frac{\partial x_2}{\partial X_j} + \frac{\partial a_i}{\partial x_3}\frac{\partial x_3}{\partial X_j}. \tag{B.9}$$

Hence we may write the first term of (B.8) as

$$\frac{\partial a_1}{\partial x_1}\begin{vmatrix} \frac{\partial x_1}{\partial X_1} & \frac{\partial x_1}{\partial X_2} & \frac{\partial x_1}{\partial X_3} \\ \frac{\partial x_2}{\partial X_1} & \frac{\partial x_2}{\partial X_2} & \frac{\partial x_2}{\partial X_3} \\ \frac{\partial x_3}{\partial X_1} & \frac{\partial x_3}{\partial X_2} & \frac{\partial x_3}{\partial X_3} \end{vmatrix} + \frac{\partial a_1}{\partial x_2}\begin{vmatrix} \frac{\partial x_2}{\partial X_1} & \frac{\partial x_2}{\partial X_2} & \frac{\partial x_2}{\partial X_3} \\ \frac{\partial x_2}{\partial X_1} & \frac{\partial x_2}{\partial X_2} & \frac{\partial x_2}{\partial X_3} \\ \frac{\partial x_3}{\partial X_1} & \frac{\partial x_3}{\partial X_2} & \frac{\partial x_3}{\partial X_3} \end{vmatrix} + \frac{\partial a_1}{\partial x_3}\begin{vmatrix} \frac{\partial x_3}{\partial X_1} & \frac{\partial x_3}{\partial X_2} & \frac{\partial x_3}{\partial X_3} \\ \frac{\partial x_2}{\partial X_1} & \frac{\partial x_2}{\partial X_2} & \frac{\partial x_2}{\partial X_3} \\ \frac{\partial x_3}{\partial X_1} & \frac{\partial x_3}{\partial X_2} & \frac{\partial x_3}{\partial X_3} \end{vmatrix} \tag{B.10}$$

for which the second and third terms are identically zero as two rows of the determinant are repeated. Similarly computing the other terms of (B.8) we find

$$\begin{aligned}\frac{\mathrm{D}J}{\mathrm{D}t} &= \left(\frac{\partial J}{\partial t}\right) \\ &= \frac{\partial a_1}{\partial x_1}J + \frac{\partial a_2}{\partial x_2}J + \frac{\partial a_3}{\partial x_3}J \\ &= (\nabla\cdot\mathbf{a})J \end{aligned} \tag{B.11}$$

which is Euler's identity.

Bibliography

[1] D. J. Acheson, *Elementary Fluid Dynamics*, Clarendon Press, Oxford, 1990.

[2] M. Akam, *Making stripes inelegantly*, Nature, 341 (1989), pp. 282–283.

[3] P. Arcuri and J. D. Murray, *Pattern sensitivity to boundary and initial conditions in reaction-diffusion models*, J. Math. Biol., 24 (1986), pp. 141–165.

[4] M. Ashkenazi and H. G. Othmer, *Spatial patterns in coupled biochemical oscillators*, J. Math. Biol., 5 (1978), pp. 305–350.

[5] J. F. G. Auchmuty and G. Nicolis, *Bifurcation analysis of nonlinear reaction-diffusion equations—I. Evolution equations and the steady state solutions*, Bull. Math. Biol, 37 (1975), pp. 323–365.

[6] J. Bard and I. Lauder, *How well does Turing's theory of morphogenesis work?*, J. theor. Biol., 45 (1974), pp. 501–531.

[7] D. L. Benson, *Reaction Diffusion Models with Spatially Inhomogeneous Diffusion Coefficients*, D. Phil. Thesis, University of Oxford, 1994.

[8] D. L. Benson, P. K. Maini, and J. A. Sherratt, *Analysis of pattern formation in reaction diffusion models with spatially inhomogeneous diffusion coefficients*, Mathl. Comput. Modelling, 17 (1993), pp. 29–34.

[9] P. Borckmans, A. De Wit, and G. Dewel, *Competition in ramped Turing structures*, Physica A, 188 (1992), pp. 137–157.

[10] B. Bunow, J.-P. Kernevez, G. Joly, and D. Thomas, *Pattern formation by reaction-diffusion instabilities: Applications to morphogenesis in* Drosophila, J. theor. Biol., 84 (1980), pp. 629–649.

[11] G. J. Butler and G. S. K. Wolkowicz, *A mathematical model of the chemostat with a general class of functions describing nutrient uptake*, SIAM J. Appl. Math., 45 (1985), pp. 138–151.

[12] T. K. Callahan and E. Knobloch, *Pattern formation in three-dimensional reaction-diffusion systems*, Physica D, 132 (1999), pp. 339–362.

[13] V. Castets, E. Dulos, J. Boissonade, and P. De Kepper, *Experimental evidence of a sustained Turing-type nonequilibrium chemical pattern*, Phys. Rev. Lett., 64 (1990), pp. 2953–2956.

[14] M. A. J. Chaplain, M. Ganesh, and I. G. Graham, *Spatio-temporal pattern formation on spherical surfaces: Numerical simulation and application to solid tumour growth.* University of Bath Preprint 99/12, June 1999.

[15] Y. Y. Chen and M. C. Cross, *Pattern formation in finite-size nonequilibrium systems and models of morphogenesis*, Nonlinearity, 7 (1994), pp. 1125–1132.

[16] A. J. Chorin and J. E. Marsden, *A Mathematical Introduction to Fluid Mechanics*, Springer-Verlag, Berlin, 3rd ed., 1993.

[17] J. R. Collier, N. A. M. Monk, P. K. Maini, and J. H. Lewis, *Pattern formation by lateral inhibition with feedback: A mathematical model of Delta-Notch intercellular signalling*, J. theor. Biol., 183 (1996), pp. 429–446.

[18] E. D. Conway, *Diffusion and predator-prey interaction: Pattern in closed systems*, in Partial Differential Equations and Dynamical Systems, W. E. Fitzgibbon III, ed., no. 101 in Research Notes in Mathematics, Pitman, London, 1984, pp. 85–133.

[19] E. J. Crampin, E. A. Gaffney, and P. K. Maini, *Pattern formation through reaction and diffusion on growing domains: Scenarios for robust pattern formation*, Bull. Math. Biol., 61 (1999), pp. 1093–1120.

[20] F. Crick, *Diffusion in embryogenesis*, Nature, 225 (1970), pp. 420–422.

[21] M. C. Cross and P. C. Hohenberg, *Pattern formation outside of equilibrium*, Rev. Mod. Phys., 65 (1993), pp. 851–1112.

[22] P. W. Davies, P. Blanchedeau, E. Dulos, and P. De Kepper, *Dividing blobs, chemical flowers and patterned islands in a reaction-diffusion system*, J. Phys. Chem. A, 102 (1998), pp. 8236–8244.

[23] P. De Kepper, V. Castets, E. Dulos, and J. Boissonade, *Turing-type chemical patterns in the chlorite-iodide-malonic acid reaction*, Physica D, 49 (1991), pp. 161–169.

[24] A. De Wit, G. Dewel, P. Borckmans, and D. Walgraef, *Three-dimensional dissipative structures in reaction-diffusion systems*, Physica D, 61 (1992), pp. 289–296.

[25] G. Dewel and P. Borckmans, *Effects of slow spatial gradients on dissipative structures*, Phys. Lett. A, 138 (1989), pp. 189–192.

[26] R. Dillon, P. K. Maini, and H. G. Othmer, *Pattern formation in generalized Turing systems I: Steady-state patterns in systems with mixed boundary conditions*, J. Math. Biol., 32 (1994), pp. 345–393.

[27] R. Dillon and H. G. Othmer, *A mathematical model for outgrowth and spatial patterning of the vertebrate limb bud*, J. theor. Biol., 197 (1999), pp. 295–330.

[28] E. J. Doedel, *Lecture notes on numerical analysis of bifurcation problems*. Short Course on Numerical Bifurcation Analysis with AUTO, 1997. Montreal 97 Summer School.

[29] E. J. Doedel, A. R. Champneys, T. F. Fairgrieve, Y. A. Kuznetsov, B. Sandstede, and X. Wang, *AUTO97: Continuation and Bifurcation for Ordinary Differential Equations*, 1997. FTP from `pub/doedel/auto` at `ftp.cs.concordia.ca`.

[30] E. J. Doedel, H. B. Keller, and J.-P. Kernevez, *Numerical analysis and control of bifurcation problems I: Bifurcation in finite dimensions*, Int. J. Bifurcation and Chaos, 1 (1991), pp. 493–520.

[31] ———, *Numerical analysis and control of bifurcation problems II: Bifurcation in infinite dimensions*, Int. J. Bifurcation and Chaos, 1 (1991), pp. 745–772.

[32] A. Doelman, R. A. Gardner, and T. J. Kaper, *Stability analysis of singular patterns in the 1D Gray-Scott model: A matched asymptotics approach*, Physica D, (1998), pp. 1–36.

[33] A. Doelman, T. J. Kaper, and P. A. Zegeling, *Pattern formation in the one-dimensional Gray-Scott model*, Nonlinearity, 10 (1997), pp. 523–563.

[34] E. Dulos, P. Davies, B. Rudovics, and P. De Kepper, *From quasi-2D to 3D Turing structures in ramped systems*, Physica D, 98 (1996), pp. 53–66.

[35] J. C. Eilbeck, *Pattern formation and pattern selection in reaction-diffusion systems*, in Theoretical Biology: Epigenetic and Evolutionary Order from Complex Systems, B. C. Goodwin and P. T. Saunders, eds., Johns Hopkins, London, 1992, pp. 31–41.

[36] I. R. Epstein and K. Showalter, *Nonlinear chemical dynamics: Oscillations, patterns and chaos*, J. Phys. Chem., 100 (1996), pp. 13132–13147.

[37] B. Ermentrout, *Spots or stripes? Nonlinear effects in bifurcation of reaction-diffusion equations on the square*, Proc. R. Soc. Lond. A, 434 (1991), pp. 413–417.

[38] P. C. Fife, *Boundary and interior transition layer phenomena for pairs of second order differential equations*, J. Math. Anal. Appl., 54 (1976), pp. 497–521.

[39] ———, *Pattern formation in reacting and diffusing systems*, J. Chem. Phys., 64 (1976), pp. 554–564.

[40] ———, *Stationary patterns for reaction-diffusion equations*, in Nonlinear Diffusion, W. E. Fitzgibbon III and H. F. Walker, eds., no. 14 in Research Notes in Mathematics, Pitman, London, 1977, pp. 81–121.

[41] A. Gierer and H. Meinhardt, *A theory of biological pattern formation*, Kybernetik, 12 (1972), pp. 30–39.

[42] M. G. M. Gomes, *Black-eye patterns: A representation of three-dimensional symmetries in thin domains*, Phys. Rev. E, 60 (1999), pp. 3741–3747.

[43] B. C. Goodwin, S. A. Kauffman, and J. D. Murray, *Is morphogenesis an intrinsically robust process?*, J. theor. Biol., 163 (1993), pp. 135–144.

[44] B. C. Goodwin and L. E. H. Trainor, *Tip and whorl morphogenesis in* Acetabularia *by calcium-regulated strain fields*, J. theor. Biol., 117 (1985).

[45] P. Gray and S. K. Scott, *Autocatalytic reactions in the isothermal, continuous stirred tank reactor: Oscillations and instabilities in the system* $A + 2B \to 3B$, $B \to C$, Chem. Eng. Sci, 39 (1984), pp. 1087–1097.

[46] P. Grindrod, *The Theory and Applications of Reaction-Diffusion Equations: Patterns and Waves*, Oxford University Press, 2nd ed., 1996.

[47] D. Haim, G. Li, Q. Ouyang, W. D. McCormick, H. L. Swinney, A. Hagberg, and E. Meron, *Breathing spots in a reaction-diffusion system*, Phys. Rev. Lett., 77 (1996), pp. 190–193.

[48] L. G. Harrison and M. Kolář, *Coupling between reaction-diffusion prepattern and expressed morphogenesis, applied to desmids and dasyclads*, J. theor. Biol., 130 (1988), pp. 493–515.

[49] M. Herschkowitz-Kaufman, *Bifurcation anaylsis of nonlinear reaction-diffusion equations—II. Steady state solutions and comparison with numerical simulations*, Bull. Math. Biol., 37 (1975), pp. 589–636.

[50] D. M. Holloway and L. G. Harrison, *Algal morphogenesis: modelling interspecific variation in* Micrasteras *with reaction-diffusion patterned catalysis of cell surface growth*, Phil. Trans. R. Soc. Lond. B, 354 (1999), pp. 417–433.

[51] A. Hunding and R. Engelhardt, *Early biological morphogenesis and nonlinear dynamics*, J. theor. Biol., 173 (1995), pp. 401–413.

[52] A. Hunding and P. G. Sørensen, *Size adaptation in Turing prepatterns*, J. Math. Biol., 26 (1988), pp. 27–39.

[53] D. Iron and M. J. Ward, *The dynamics of boundary spikes for a nonlocal reaction-diffusion model.* submitted, 1999.

[54] D. Iron, M. J. Ward, and J. Wei, *The stability of spike solutions to the one-dimensional Gierer-Meinhardt model.* to be submitted, 1999.

[55] M. J. Jenkins, *Pattern Formation Through Self-Organisation in Diffusion-Driven Mechanisms*, D. Phil. Thesis, University of Oxford, 1990.

[56] B. R. Johnson and S. K. Scott, *New approaches to chemical patterns*, Chem. Soc. Rev., 25 (1996), pp. 265–273.

[57] H.-S. Jung, P. H. Francis-West, R. B. Widelitz, T.-X. Jiang, S. Ting-Berreth, C. Tickle, L. Wolpert, and C.-M. Chuong, *Local inhibitory action of BMPs and their relationships with activators in feather formation: Implications for periodic patterning*, Dev. Biol., 196 (1998), pp. 11–23.

[58] S. A. Kauffman, *Pattern formation in the* Drosophila *embryo*, Phil. Trans. R. Soc. Lond. B, 295 (1981), pp. 567–594.

[59] S. A. Kauffman, R. M. Shymko, and K. Trabert, *Control of sequential compartment formation in* Drosophila, Science, 199 (1978), pp. 259–270.

[60] J. P. Keener, *Principles of Applied Mathematics: Transformation and Approximation*, Addison-Wesley, Reading, Massachusetts, 1988.

[61] E. F. Keller and L. A. Segel, *Initiation of slime mold aggregation viewed as an instability*, J. theor. Biol., 26 (1970), pp. 399–415.

[62] B. S. Kerner and V. V. Osipov, *Autosolitons: A New Approach to the Problem of Self-Organisation and Turbulence*, Kluwer, Dordrecht, 1994.

[63] I. G. Kevrekidis and H. S. Brown, *Predicting pattern formation in coupled reaction-diffusion systems*, Chem. Eng. Sci., 44 (1989), pp. 1893–1901.

[64] S. Kondo and R. Asai, *A reaction-diffusion wave on the skin of the marine angelfish* Pomacanthus, Nature, 376 (1995), pp. 765–768.

[65] P. M. Kulesa, G. C. Cruywagen, S. R. Lubkin, P. K. Maini, J. Sneyd, M. W. J. Ferguson, and J. D. Murray, *On a model mechanism for the spatial pattering of teeth primordia in the alligator*, J. theor. Biol., 180 (1996), pp. 287–296.

[66] T. C. Lacalli, *Dissipative structures and morphogenetic pattern in unicellular algae*, Phil. Trans. R. Soc. Lond. B, 294 (1981), pp. 547–588.

[67] T. C. Lacalli, D. A. Wilkinson, and L. G. Harrison, *Theoretical aspects of stripe formation in relation to* Drosophila *segmentation*, Development, 103 (1988), pp. 105–113.

[68] D. C. Lane, J. D. Murray, and V. S. Manoranjan, *Analysis of wave phenomena in a morphogenetic mechanochemical model and an application to post-fertilisation waves on eggs*, IMA J. Math. Appl. Med. and Biol., 4 (1987), pp. 309–331.

[69] K. J. Lee, W. D. McCormick, Q. Ouyang, and H. L. Swinney, *Pattern-formation by interacting chemical fronts*, Science, 261 (1993), pp. 192–194.

[70] K. J. Lee, W. D. McCormick, J. E. Pearson, and H. L. Swinney, *Experimental observation of self-replicating spots in a reaction-diffusion system*, Nature, 369 (1994), pp. 215–218.

[71] K. J. Lee and H. L. Swinney, *Lamellar structures and self-replicating spots in a reaction-diffusion system*, Phys. Rev. E, 51 (1995), pp. 1899–1915.

[72] ———, *Replicating spots in reaction-diffusion systems*, Int. J. Bifurcation and Chaos, 7 (1997), pp. 1149–1158.

[73] S. A. Levin and L. A. Segel, *Hypothesis for origin of planktonic patchiness*, Nature, 259 (1976), p. 659.

[74] M. J. Lyons and L. G. Harrison, *A class of reaction-diffusion mechanisms which preferentially select striped patterns*, Chem. Phys. Lett, 183 (1991), pp. 158–164.

[75] ———, *Stripe selection: An intrinsic property of some pattern-forming models with nonlinear dynamics*, Dev. Dynam., 195 (1992), pp. 201–215.

[76] A. Madsvamuse, *Numerical Solution of Reaction-Diffusion Systems on Growing Domains*, P.R.S. Dissertation, University of Oxford, 1999.

[77] P. K. Maini, D. L. Benson, and J. A. Sherratt, *Pattern formation in reaction-diffusion models with spatially inhomogeneous diffusion coefficients*, IMA J. Math. Appl. Med. and Biol., 9 (1992), pp. 197–213.

[78] P. K. Maini and M. R. Myerscough, *Boundary-driven instability*, Appl. Math. Lett., 10 (1997), pp. 1–4.

[79] P. K. Maini and M. Solursh, *Cellular mechanisms of pattern formation in the developing limb*, Int. Rev. Cytol., 129 (1991), pp. 91–133.

[80] L. Matthews and J. Brindley, *Patchiness in plankton populations*, Dynam. Stabil. Syst., 12 (1997), pp. 39–59.

[81] A. May, P. A. Firby, and A. P. Bassom, *Diffusion driven instability in an inhomogeneous circular domain*, Mathl. Comput. Modelling, 29 (1999), pp. 53–66.

[82] H. Meinhardt, *Models of Biological Pattern Formation*, Academic Press, London, 1982.

[83] M. Mimura and J. D. Murray, *On a diffusive prey-predator model which exhibits patchiness*, J. theor. Biol., (1978).

[84] J. Monod, *Recherches sur la Croissance des Cultures Bacteriennes*, Herman, Paris, 1942.

[85] K. W. Morton and D. F. Mayers, *Numerical Solution of Partial Differential Equations*, Cambridge University Press, 1994.

[86] C. B. Muratov and V. V. Osipov, *Spike autosolitons in the Gray-Scott model.* submitted, October 1998.

[87] J. D. Murray, *Parameter space for Turing instability in reaction diffusion mechanisms: A comparison of models*, J. theor. Biol., 98 (1982), pp. 143–163.

[88] ———, *Mathematical Biology*, Springer-Verlag, Berlin, 2nd ed., 1993.

[89] B. N. Nagorcka, V. S. Manoranjan, and J. D. Murray, *Complex spatial patterns from tissue interactions—an illustrative model*, J. theor. Biol., 128 (1987), pp. 359–374.

[90] B. N. Nagorcka and J. R. Mooney, *The role of a reaction-diffusion system in the initiation of primary hair follicles*, J. theor. Biol., 114 (1985), pp. 243–272.

[91] B. N. Nagorka, *A pattern formation mechanism to control spatial organization in the embryo of* Drosophila melanogaster, J. theor. Biol., 132 (1988), pp. 277–306.

[92] W.-M. Ni, *Diffusion, cross-diffusion, and their spike-layer steady states*, Notices of the AMS, 45 (1998), pp. 9–18.

[93] G. Nicolis, *Introduction to Nonlinear Science*, Cambridge University Press, 1995.

[94] G. Nicolis and I. Prigogine, *Self-Organization in Nonequilibrium Systems*, Wiley-Interscience, New York, 1977.

[95] Y. Nishiura and D. Ueyama, *A skeleton structure of self-replicating dynamics*, Physica D, 130 (1999), pp. 73–104.

[96] A. Okubo, *Diffusion and Ecological Problems: Mathematical Models*, Springer-Verlag, Berlin, 1980.

[97] V. V. Osipov and A. V. Severtsev, *Theory of self-replication and granulation of spike autosolitons*, Phys. Lett. A, 222 (1996), pp. 400–404.

[98] G. F. Oster, *Lateral inhibition models of developmental processes*, Math. Biosci., 90 (1988), pp. 265–286.

[99] G. F. Oster and J. D. Murray, *Pattern formation models and developmental constraints*, J. exp. Zool., 251 (1989), pp. 186–202.

[100] H. G. Othmer and E. Pate, *Scale-invariance in reaction-diffusion models of spatial pattern formation*, Proc. Natl. Acad. Sci. USA, 77 (1980), pp. 4180–4184.

[101] H. G. Othmer and L. E. Scriven, *Interactions of reaction and diffusion in open systems*, I & EC Fundamentals, 8 (1969), pp. 302–313.

[102] H. G. Othmer and A. Stevens, *Aggregation, blowup, and collapse: The ABC's of taxis in reinforced random walks*, SIAM J. Appl. Math., 57 (1997), pp. 1044–1081.

[103] Q. Ouyang and H. L. Swinney, *Transition from a uniform state to hexagonal and striped Turing patterns*, Nature, 352 (1991), pp. 610–612.

[104] M. R. Owen and J. A. Sherratt, *Mathematical modelling of juxtacrine cell signalling*, Math. Biosci., 153 (1998), pp. 125–150.

[105] M. R. Owen, J. A. Sherratt, and H. J. Wearing, *Lateral inhibition by juxtacrine signaling is a new mechanism for pattern formation*, Dev. Biol., 217 (2000), pp. 54–61.

[106] K. J. Painter, *Chemotaxis as a Mechanism for Morphogenesis*, D. Phil. Thesis, University of Oxford, 1998.

[107] K. J. Painter, P. K. Maini, and H. G. Othmer, *Stripe formation in juvenile* Pomacanthus *explained by a generalised Turing mechanism with chemotaxis*, Proc. Natl. Acad. Sci. USA, 96 (1999), pp. 5549–5554.

[108] D. W. Peaceman and H. H. J. Rachford, *The numerical solution of parabolic and elliptic differential equations*, J. Soc. Indust. Appl. Math., 3 (1955), p. 28.

[109] J. E. Pearson, *Complex patterns in a simple system*, Science, 261 (1993), pp. 189–192.

[110] J. E. Pearson and W. Horsthemke, *Turing instabilities with nearly equal diffusion coefficients*, J. Chem. Phys., 90 (1989), pp. 1588–1599.

[111] A. J. Perumpanani, *Phase Differences in Morphogenesis*, P.R.S. Dissertation, University of Oxford, 1993.

[112] V. Petrov, S. K. Scott, and K. Showalter, *Excitability, wave reflection, and wave splitting in a cubic autocatalysis reaction-diffusion system*, Phil. Trans. R. Soc. Lond., A 347 (1994), pp. 631–642.

[113] W. H. Press, S. A. Teukolsky, W. T. Vetterling, and B. P. Flannery, *Numerical Recipies in FORTRAN*, Cambridge University Press, 2nd ed., 1994.

[114] K. E. Rasmussen, W. Mazin, and E. Mosekilde, *Wave-splitting in the bistable Gray-Scott model*, Int. J. Bifurcation and Chaos, 6 (1996), pp. 1077–1092.

[115] W. N. Reynolds, J. E. Pearson, and S. Ponce-Dawson, *Dynamics of self-replicating patterns in reaction diffusion systems*, Phys. Rev. Lett., 72 (1994), pp. 2797–2800.

[116] W. N. Reynolds, S. Ponce-Dawson, and J. E. Pearson, *Self-replicating spots in reaction-diffusion systems*, Phys. Rev. E, 56 (1997), pp. 185–198.

[117] J. Rinzel and J. B. Keller, *Travelling wave solutions of a nerve conduction equation*, Biophys. J., 13 (1973), pp. 1313–1337.

[118] P. T. Saunders and M. W. Ho, *Reliable segmentation by successive bifurcation*, Bull. Math. Biol., 57 (1995), pp. 539–556.

[119] J. Schnakenberg, *Simple chemical reaction systems with limit cycle behaviour*, J. theor. Biol., 81 (1979), pp. 389–400.

[120] L. A. Segel, *A theoretical study of receptor mechanisms in bacterial chemotaxis*, SIAM J. Appl. Math., 32 (1977), pp. 653–665.

[121] L. A. Segel and J. L. Jackson, *Dissipative structure: An explanation and an ecological example*, J. theor. Biol., 37 (1972), pp. 545–559.

[122] E. E. Sel'kov, *Self-oscillations in glycolysis: 1. A simple kinetic model*, Eur. J. Biochem., 4 (1968), pp. 79–86.

[123] H. L. Smith and P. Waltman, *The Theory of the Chemostat: Dynamics of Microbial Competition*, Cambridge University Press, 1995.

[124] J. Smoller and A. Wasserman, *Global bifurcation of steady-state solutions*, J. Differ. Equations, 39 (1981), pp. 269–290.

[125] D. W. Thompson, *On Growth and Form (Abridged—John Tyler Bonner)*, Cambridge University Press, 1961.

[126] A. M. Turing, *The chemical basis of morphogenesis*, Phil. Trans. R. Soc. Lond. B, 237 (1952), pp. 37–72.

[127] C. Varea, J. L. Aragón, and R. A. Barrio, *Confined Turing patterns in growing systems*, Phys. Rev. E, 56 (1997), pp. 1250–1253.

[128] ———, *Turing patterns on a sphere*, Phys. Rev. E, 60 (1999), pp. 4588–4592.

[129] R. V. Vincent and N. A. Hill, *Bioconvection in a suspension of phototactic algae*, J. Fluid Mech., 327 (1996), pp. 343–371.

[130] D. Walgraef, *Spatio-Temporal Pattern Formation*, Springer-Verlag, New York, 1997.

[131] K. A. J. White and C. A. Gilligan, *Spatial heterogeneity in three-species, plant-parasite-hyperparasite, systems*, Phil. Trans. R. Soc. Lond. B, 353 (1998), pp. 543–557.

[132] G. S. Wolkowicz and Z. Lu, *Global dynamics of a mathematical model for competition in the chemostat: General response functions and differential death rates*, SIAM J. Appl. Math., 52 (1992), pp. 222–233.

[133] D. J. Wollkind, V. S. Manoranjan, and L. Zhang, *Weakly nonlinear stability analyses of prototype reaction-diffusion model equations*, SIAM Review, 36 (1994), pp. 176–214.

[134] L. WOLPERT, *Positional information and the spatial pattern of cellular differentiation*, J. theor. Biol, 25 (1969), pp. 1–47.

[135] ———, *Positional information and pattern-formation in development*, Dev. Genet., 15 (1994), pp. 485–490.